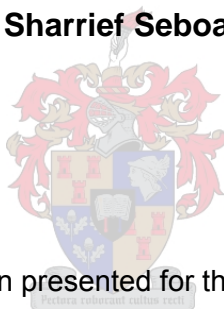


SYNTHESIS AND CHARACTERIZATION OF TAILORED POLYURETHANE COATINGS

By

Sharrief Seboa



Dissertation presented for the degree of

Doctor of Natural Sciences (Polymer Science)

at the

University of Stellenbosch

Promoter: Prof. R.D. Sanderson

Stellenbosch

December 2005

DECLARATION

I, the undersigned, hereby declare that the work contained in this dissertation is my own original work and that I have not previously in its entirety or in part submitted it at any university for a degree.

Signature: _____

Date: _____

ABSTRACT

Aqueous polyurethane (PU) dispersions were synthesized for use in paper coatings. These PUs contained a polyester polyol soft segment (content of between 65 to 75%) and a urethane hard segment (content of between 30 to 35%). Triethylamine (TEA) was used as the neutralizing agent. The polyester polyol segment consisted of neopentyl glycol (NPG), adipic acid, 1,4-cyclohexane dicarboxylic acid (1,4-CHDCA) and 2-phosphonobutane-1,2,4-tricarboxylic acid (PBTCA), while the urethane hard segment consisted of toluene diisocyanate (TDI), dimethylolproponic acid (DMPA) and ethylene glycol (EG) as a chain extender for increasing the hard segment content.

Waxes and fillers were incorporated into the PU coating mixtures to investigate their effect on the barrier properties of the PU. Two types of fillers were used: nano-fillers and micro-fillers. The nano-fillers used included the Cloisite nano-clays NC15A, NC93A and NC30B, and the micro-fillers used included talc, kaolin clay and barium sulfate.

Two different polyester polyols were synthesized: one containing a phosphate and the other containing no phosphate. The polyols were characterized in terms of their acid value, hydroxyl value and molecular mass. The PUs synthesized from the polyol containing no phosphate showed unfavourable barrier properties compared to results achieved with the phosphate-containing PU.

The PU dispersions were applied to paperboard, and then dried at a maximum temperature of 130°C for 15 to 60 seconds, depending on the coating volume. The PU-coated paperboard was characterized primarily by determining the moisture vapour transmission rate (MVTR), and by scanning electron microscopy (SEM).

PU films (stand alone, not supported by paper) were prepared by heating the concurrent PU dispersion in Teflon holders over three different temperature stages (60, 90 and 120°C) for about 2 days. The dried films were then characterized by thermogravimetric analysis (TGA), differential scanning calorimetry (DSC), dynamic mechanical analysis (DMA), Fourier transform infrared (FTIR) and nuclear magnetic resonance (NMR) spectroscopy.

The PU coatings showed self-assembly properties, which were affected primarily by the ionic content (comprising of DMPA, PBTCA and excess TEA) and emulsion viscosity. These self-assembly properties were analyzed by static contact angle (SCA) and MVTR

measurements. It was found that the final coating properties were affected by the self-assembly mechanism of the PU.

Generally, the phosphated PU coatings had lower MVTR values than the non-phosphated PU coatings. SEM analysis showed that the phosphated PU coatings had no pinholes, while the non-phosphated PU coatings had pinholes. DMA analysis showed that the phosphated PUs had higher T_g values than the non-phosphated PUs. Further, the inclusion of the phosphate monomer increased the emulsion stability and the compatibility between the hard and soft segments of the PU.

Also, the exfoliated PU nanocomposites at 1% filler loading gave much better MVTR results compared to the PU microcomposites. It also rendered the coating to be non-blocking, with minimal change in MVTR.

OPSOMMING

Waterige poli-uretaan (PU) dispersies is gesintetiseer vir gebruik as papierbedekkings. Hierdie poli-uretane het 'n poliester poli-ol sagte segment (tussen 65 en 75% inhoud) en 'n uretaan harde segment (tussen 30 en 35% inhoud) bevat. Die poli-uretane is met vier verskillende ent-middels geëent. Tri-etielamien (TEA) is as neutraliseermiddel gebruik. Die poli-ester poli-ol segment het bestaan uit: neopentielglikol (NPG), adipiensuur, 1,4-sikloheksaandikarboksielsuur (1,4-CHDCA) en 2-fosfonobutaan-1,2,4-trikarboksielsuur (PBTCA). Die uretaan harde segment het bestaan uit: toluendiisosianaat (TDI), dimetielpropioonsuur (DMPA) en etileenglikol (EG).

Wasse en vulstowwe is in die PU bedekkings geïnkorporeer. Twee tipes vulstowwe is gebruik, naamlik nano-vullers and mikro-vullers. Die nano-vulstowwe wat gebruik was sluit in die Cloisite nano-vulstowwe NC15A, NC93A en NC30B, en die mikro-vulstowwe wat gebruik was sluit in talk, kaolin klei and bariumsulfaat.

Twee verskillende poli-ester polihidroksie verbindings is gesintetiseer: een met fosfaat en een sonder fosfaat, en gekarakteriseer in terme van hulle suurwaardes, hidroksiwaardes en molekulêre massas. Die PUs wat vanaf die fosfaat-bevattende poli-ol gesintetiseer is, het baie beter as die nie fosfaat-bevattende PUs gevaar.

Papierbord (Eng. paperboard) is met die gesintetiseerde PU dispersies bedek en by 130 °C vir omtrent 15 tot 120 sekondes gedroog, afhangende die bedekkingsvolume. Die PU-bedekte papier is gekarakteriseer in terme van vogdeurlaatbaarheidstransmissietempo (Eng: MVTR – moisture vapour transmission rate), en skandeerelektronmikroskopie (SEM).

PU films wat nie deur papier gestut is nie, is ook voorberei deur die verhitting van die ooreenkomstige PU dispersies in Teflon houers by drie temperature (60, 90 and 120°C) vir omtrent 2 tot 3 dae. Die droë films is daarna gekarakteriseer deur middel van termogravimetriese analise (TGA), differensiële skandeerkalorimetrie (DSC), dinamiese meganiese analise (DMA), en Fourier-transformasie infrarooi (FTIR) spektroskopie en kern magnetiese resonansie (KMR) spektroskopie.

Die PU-dekkings het eienskappe van self-organisasie gewys, wat deur die ioniese inhoud (bestaande uit DMPA, PBTCA en oormaat TEA) en emulsie viskositeit beïnvloed was. Hierdie self-organisasie is deur SCA en MVTR gevolg. Dit is gevind dat die finale eienskappe deur die self-organisasie meganisme van die PU geaffekteer is.

Die MVTR analises het getoon dat die fosfaat-bevattende PU bedekkings in die algemeen baie beter as die nie-fosfaatbevattende bedekkings is. SEM het getoon dat die fosfaat-PU bedekkings geen mikrogaatjies (Eng. pinholes) gehad het nie, terwyl die nie-fosfaat PU bedekkings wel mikrogaatjies (Eng. pinholes) gehad het. DMA analises het getoon dat die fosfaatbevattende PUs hoër Tg-waardes gehad het as die nie-fosfaatbevattende PUs, en dat die inkorporasie van die fosfaat monomeer die stabiliteit en die meng-misbaarheid tussen die harde- en sagte segmente van die PU bevorder.

Die geeksfolieerde PU wat 1% nano-klei bevat het baie beter in terme van MVTR geprester as die PU wat mikro-vulstowwe bevat. Dit het ook gemaak dat die PU-bedekte papier nie aan mekaar vasgesteek het nie, met minimum verandering aan die MVTR.

ACKNOWLEDGEMENTS

I would like to express my gratitude to:

Prof. R. D. Sanderson, my promoter, for giving me this opportunity.

The NRF for financial assistance.

PRP-Resins, for their assistance and use of their laboratory facilities.

Dr. M. Hurndall, for her advice and assistance.

Dr. M. Bredenkamp, for his help with NMR-analysis.

Lusane Wahlberg, for work done on nylon fiber coatings.

The DMA, TGA, GPC, NMR and SEM operators at US.

The TEM and SEM operators at UCT.

Family and friends, for their support.

The financial assistance of the National Research Foundation (NRF) towards this research is hereby acknowledged. Opinions expressed and conclusions arrived at, are those of the author and are not necessarily to be attributed to the NRF.

TABLE OF CONTENTS

1	INTRODUCTION.....	1
1.1	INTRODUCTION.....	1
1.2	PAPERBOARD.....	1
1.3	URETHANES.....	2
1.4	OBJECTIVES.....	3
1.5	REFERENCES.....	3
2	PAPERBOARD.....	4
2.1	TERMINOLOGY.....	4
2.2	GRADES OF PAPERBOARD.....	5
2.2.1	<i>Kraft paperboard.....</i>	<i>5</i>
2.2.2	<i>Recycled paperboard.....</i>	<i>5</i>
2.3	WASTE PAPER RECYCLING.....	5
2.3.1	<i>Waste paper recycling process.....</i>	<i>5</i>
2.3.2	<i>Wet strength additives.....</i>	<i>8</i>
2.3.3	<i>Dry strength additives.....</i>	<i>9</i>
2.4	COATING PROCESS.....	10
2.4.1	<i>Typical polymers used in paper coatings.....</i>	<i>11</i>
2.5	REFERENCES.....	13
3	POLYURETHANES.....	15
3.1	INTRODUCTION.....	15
3.2	POLYURETHANE DISPERSIONS.....	16
3.3	TYPES OF POLYURETHANE DISPERSIONS.....	17
3.3.1	<i>Non-ionic polyurethane dispersions.....</i>	<i>17</i>
3.3.2	<i>Cationic polyurethane dispersions.....</i>	<i>17</i>
3.3.3	<i>Anionic polyurethane dispersions.....</i>	<i>18</i>
3.3.4	<i>Amphiphilic polyurethane dispersions.....</i>	<i>18</i>
3.4	REACTIONS OF ISOCYANATES.....	19
3.4.1	<i>Primary reactions of isocyanates.....</i>	<i>20</i>
3.4.2	<i>Secondary reactions of isocyanates.....</i>	<i>20</i>
3.4.3	<i>Self-addition reactions.....</i>	<i>21</i>
3.4.3.1	<i>Dimerization.....</i>	<i>21</i>
3.4.3.2	<i>Trimerization.....</i>	<i>21</i>
3.4.3.3	<i>Polycarbodiimides.....</i>	<i>22</i>
3.5	HEALTH ASPECTS OF ISOCYANATES.....	22

3.6	REFERENCES	23
4	EXPERIMENTAL	27
4.1	INTRODUCTION	27
4.2	SYNTHESIS OF POLYOLS	28
4.2.1	<i>Raw materials</i>	28
4.2.2	<i>Experimental setup</i>	29
4.2.3	<i>Preparation of polyol</i>	29
4.2.4	<i>Polyol formulation</i>	29
4.3	CALCULATIONS	31
4.3.1	<i>Acid-value determination</i>	31
4.3.2	<i>Hydroxyl-value determination</i>	32
4.3.3	<i>NCO-value determination</i>	33
4.4	SYNTHESIS OF POLYURETHANES	34
4.4.1	<i>Raw materials</i>	34
4.4.2	<i>Experimental procedure</i>	35
4.4.2.1	Synthesis of the urethane polymer	35
4.4.2.2	Neutralization of the pendant carboxylic acid groups	36
4.4.2.3	Dispersion of PU-ionomer into water.....	36
4.4.3	<i>Polyurethane reaction scheme</i>	37
4.5	POLYURETHANE-WAX COMPOSITES	38
4.6	PU-FILLER COMPOSITES	39
4.6.1	<i>Introduction</i>	39
4.6.2	<i>Type of fillers</i>	40
4.6.3	<i>Incorporation of fillers into the PU-matrix</i>	40
4.6.4	<i>Formulation</i>	41
4.7	REFERENCES	42
5	ANALYTICAL TECHNIQUES	44
5.1	INTRODUCTION	44
5.2	FOURIER TRANSFORM INFRARED (FTIR) SPECTROSCOPY	44
5.3	NUCLEAR MAGNETIC RESONANCE (NMR) SPECTROSCOPY	45
5.4	GEL PERMEATION CHROMATOGRAPHY (GPC)	45
5.5	PARTICLE SIZE ANALYSIS	45
5.6	TRANSMISSION ELECTRON MICROSCOPY (TEM).....	45
5.7	SCANNING ELECTRON MICROSCOPY (SEM)	46
5.8	VISCOSITY	46

5.9	MOISTURE VAPOR TRANSMISSION RATE (MVTR)	46
5.10	BLOCKING TEST	47
5.11	DYNAMIC MECHANICAL ANALYSIS (DMA).....	47
5.12	STATIC CONTACT ANGLE (SCA) DETERMINATION	48
5.13	THERMOGRAVIMETRIC ANALYSIS (TGA)	49
5.14	DIFFERENTIAL SCANNING CALORIMETRY (DSC)	49
5.15	REFERENCES	49
6	CHARACTERIZATION OF POLYURETHANE DISPERSIONS	51
6.1	INTRODUCTION	51
6.2	SELF-ASSEMBLY MECHANISM OF THE POLYURETHANE-WAX COMPOSITES	52
6.3	EFFECT OF COATING THICKNESS ON DISPERSION AND COATING PROPERTIES	53
6.4	EFFECT OF EMULSION VISCOSITY ON DISPERSION AND COATING PROPERTIES.....	54
6.5	EFFECT OF IONIC CONTENT ON DISPERSION AND COATING PROPERTIES	56
6.5.1	<i>Effect of DMPA on dispersion and coating properties.....</i>	<i>57</i>
6.5.2	<i>Effect of PBTCA on dispersion and coating properties</i>	<i>58</i>
6.5.3	<i>Effect of neutralizing base on dispersion and coating properties</i>	<i>58</i>
6.5.3.1	Degree of neutralization	59
6.6	POST MODIFICATION USING TEA	64
6.7	COMBINED EFFECT OF VISCOSITY AND IONIC CONTENT ON THE SELF-ASSEMBLY MECHANISM	65
6.8	MOISTURE VAPOUR TRANSMISSION RATE (MVTR) AND BLOCKING.....	66
6.8.1	<i>Effect of soft segment content.....</i>	<i>66</i>
6.8.2	<i>Effect of PBTCA, CHDCA and wax content on MVTR and blocking.....</i>	<i>67</i>
6.8.2.1	Effect of PBTCA.....	67
6.8.2.2	Effect of CHDCA.....	67
6.8.2.3	Effect of Wax C78.....	68
6.8.2.4	Blocking effect	68
6.9	SCANNING ELECTRON MICROSCOPY	69
6.9.1	<i>SEM images of uncoated paperboard surface.....</i>	<i>69</i>
6.9.2	<i>Effect of phosphorous on the polyurethane surface</i>	<i>70</i>
6.9.3	<i>Effect of CHDCA on the polyurethane surface</i>	<i>72</i>
6.10	REFERENCES	72
7	MECHANICAL, THERMAL AND SPECTROSCOPIC CHARACTERIZATION.....	73
7.1	INTRODUCTION	73
7.2	DYNAMIC MECHANICAL ANALYSIS	74

7.2.1	<i>Effect of hard segment content</i>	75
7.2.2	<i>Effect of PBTCA</i>	75
7.2.3	<i>Effect of DMPA</i>	76
7.2.4	<i>Effect of CHDCA</i>	76
7.2.5	<i>Effect of wax content</i>	77
7.3	THERMOGRAVIMETRIC ANALYSIS (TGA)	78
7.3.1	<i>Effect of hard segment content</i>	78
7.3.2	<i>Effect of PBTCA content</i>	79
7.3.3	<i>Effect of CHDCA content</i>	79
7.3.4	<i>Effect of wax content</i>	80
7.4	DIFFERENTIAL SCANNING CALORIMETRY (DSC)	80
7.5	GPC ANALYSIS	81
7.5.1	<i>GPC analysis of the polyesters</i>	81
7.5.1.1	<i>Effect of PBTCA content on the molecular weight of the polyester</i>	81
7.5.1.2	<i>Effect of CHDCA content on the molecular weight of the polyester</i>	83
7.5.2	<i>GPC analysis of the polyurethanes</i>	87
7.6	FOURIER TRANSFORM INFRARED SPECTROSCOPY	88
7.6.1	<i>Monitoring of NCO content</i>	88
7.6.2	<i>Characterization of the polyurethane</i>	89
7.7	NMR ANALYSIS	92
7.7.1	<i>¹H-NMR analysis</i>	92
7.7.2	<i>¹³C-NMR analysis</i>	98
7.7.3	<i>³¹P-NMR analysis</i>	105
7.8	REFERENCES	107
8	POLYURETHANE-FILLER COMPOSITES FOR PAPERBOARD APPLICATION	108
8.1	INTRODUCTION	108
8.2	MICRO-FILLER INCORPORATION.....	109
8.2.1	<i>SEM and TEM analysis of PU-filler microcomposites</i>	110
8.2.2	<i>DMA analysis of PU-Serina clay microcomposites</i>	112
8.3	NANO-FILLER INCORPORATION	113
8.3.1	<i>Nano-filler incorporation using Method 1</i>	115
8.3.1.1	<i>Nano-filler incorporation outside the PU emulsion particle</i>	115
8.3.1.2	<i>Nano-filler incorporation inside the PU emulsion particle</i>	115
8.3.1.3	<i>TGA analysis of PU-filler nanocomposites</i>	117
8.3.1.4	<i>DSC analysis of PU-clay nanocomposites</i>	117
8.3.1.5	<i>SEM and TEM analysis of nano-filler/PU composites</i>	118

8.3.2	<i>Nano-filler incorporation using Methods 2a and 2b</i>	119
8.3.3	<i>Nano-filler incorporation using Method 3</i>	128
8.3.4	<i>MVTR and DMA results of the PU-clay nanocomposites</i>	133
8.4	CONCLUSIONS.....	137
8.5	REFERENCES	138
9	CONCLUSIONS.....	140
9.1	CONCLUSIONS.....	140
APPENDICES	143
	APPENDIX 1: PRP POLYURETHANE PROPERTIES	143
	APPENDIX 2: WAX PROPERTIES	144
	APPENDIX 3: POLYURETHANE-WAX COMPOSITES.....	149
	APPENDIX 4: MVTR TEST METHOD.....	151
	APPENDIX 5: BLOCKING TEST METHOD.....	152
	APPENDIX 6: COATING WEIGHT DETERMINATION.....	154
	APPENDIX 7: PARTICLE SIZE ANALYSIS.....	155
	APPENDIX 8: RECYCLABILITY EVALUATION.....	166
	APPENDIX 9: NMR SPECTRA OF POLYESTER AND POLYURETHANE	171

LIST OF TABLES

1	INTRODUCTION	1
2	PAPERBOARD	4
	TABLE 2.1: PAPERBOARD TERMINOLOGY	4
	TABLE 2.2: PROPERTIES OF PAPERBOARD WITH FUNCTIONAL COATINGS	10
3	POLYURETHANES	15
4	EXPERIMENTAL	27
	TABLE 4.1: MONOMERS USED TO PREPARE THE POLYOLS	28
	TABLE 4.2: POLYOL FORMULATIONS.....	30
	TABLE 4.3: RAW MATERIALS USED TO PREPARE PUS	34
	TABLE 4.4: FILLERS USED FOR INCORPORATION INTO PU-MATRIX	40
5	ANALYTICAL TECHNIQUES	44
	TABLE 5.1: TYPICAL PROPERTIES OBTAINED FROM DMA ANALYSIS	47
6	CHARACTERIZATION OF POLYURETHANE DISPERSIONS	51
	TABLE 6.1: TABULATED MVTR AND BLOCKING DATA OF PU COATINGS	67
7	MECHANICAL, THERMAL AND SPECTROSCOPIC CHARACTERIZATION	73
	TABLE 7.1: TG'S OF PU WITH AND WITHOUT WAX C78 INCORPORATION.....	74
	TABLE 7.2: MOLECULAR WEIGHT AND MOLECULAR WEIGHT DISTRIBUTION DATA FOR SYNTHESIZED POLYESTER GLYCOLS.....	86
	TABLE 7.3A: ¹ H-NMR ANALYSIS OF SYNTHESIZED POLYESTER	95
	TABLE 7.3B: ¹ H-NMR ANALYSIS OF SYNTHESIZED POLYURETHANE.....	96
	TABLE 7.3C: ¹ H-NMR ANALYSIS OF NMP SOLVENT AND TEA NEUTRALIZING BASE IN POLYURETHANE SYNTHESIS	97
	TABLE 7.4A: ¹³ C-NMR ANALYSIS OF SYNTHESIZED POLYESTER	102
	TABLE 7.4B: ¹³ C-NMR ANALYSIS OF SYNTHESIZED POLYURETHANE.....	103
	TABLE 7.4C: ¹³ C-NMR ANALYSIS OF SOLVENTS AND NEUTRALIZING BASE IN SYNTHESIZED POLYURETHANE.....	104
8	POLYURETHANE-FILLER COMPOSITES FOR PAPERBOARD APPLICATION	108
	TABLE 8.1: EFFECTS OF MICRO-FILLER ON MVTR AND BLOCKING OF PU COATED PAPERBOARD.	109
	TABLE 8.2: METHODS FOR PREPARING THE POLYURETHANE/NANO-COMPOSITES	113
	TABLE 8.3: THE TERTIARY AMINES OF THE CLOISITE MODIFIED NANO-CLAYS	114
	TABLE 8.4: EFFECT OF NANO-FILLER INCORPORATED OUTSIDE PU DISPERSION PARTICLES.....	115

TABLE 8.5: EFFECT OF NANO-FILLER INCORPORATION INSIDE PU DISPERSION PARTICLES	116
TABLE 8.6: MVTR RESULTS OF PU-CLAY NANOCOMPOSITES PREPARED VIA METHODS 1 TO 3	133
9 CONCLUSIONS.....	140
APPENDICES	143
TABLE A.1.1: CHEMICAL COMPOSITION OF PRP URETHANE	143
TABLE A.1.2: CHEMICAL COMPOSITION OF POLYOL IN PRP URETHANE	143
TABLE A.2.1: PROPERTIES OF WAX C78.....	145
TABLE A.8.1: RECYCLABILITY TEST RESULTS	170

LIST OF FIGURES

1 INTRODUCTION.....	1
2 PAPERBOARD	4
FIGURE 2.1: WASTE PAPER RECYCLING PROCESS.....	5
3 POLYURETHANES	15
FIGURE 3.1: TDI ISOMERS	19
FIGURE 3.2: DIMERIZATION OF AN AROMATIC ISOCYANATE	21
FIGURE 3.3: TRIMERIZATION OF BOTH ALIPHATIC AND AROMATIC ISOCYANATES.....	21
FIGURE 3.4: CONDENSATION OF ISOCYANATES TO FORM CARBODIIMIDES AND SUBSEQUENT URETHONE-IMINES	22
4 EXPERIMENTAL	27
FIGURE 4.1: PU SYNTHESIS SCHEME	37
5 ANALYTICAL TECHNIQUES	44
FIGURE 5.1: SCA IMAGE OF DE-IONIZED WATER DROPLET ON COATED PAPERBOARD SURFACE.....	48
FIGURE 5.2: 50-MM LONG EMOSKOP LENS SET USED FOR SCA MEASUREMENTS	48
6 CHARACTERIZATION OF POLYURETHANE DISPERSIONS	51
FIGURE 6.1: SELF-ASSEMBLY MECHANISM DURING THE COATING PROCESS	52
FIGURE 6.2: EFFECT OF IONIC CONTENT ON THE MOBILITY OF THE NON-POLAR CHAINS OF THE PU EMULSION	53
FIGURE 6.3: EFFECT OF COATING THICKNESS ON MVTR.....	53
FIGURE 6.4: EFFECT OF COATING THICKNESS ON SCA	54

FIGURE 6.5: EFFECT OF VISCOSITY ON SCA OF COATED PAPERBOARD	55
(PU CONTAINS 5.1% DMPA)	55
FIGURE 6.6: EFFECT OF VISCOSITY ON MVTR OF COATED PAPERBOARD.....	55
(PU CONTAINS 5.1% DMPA)	55
FIGURE 6.7: THE EFFECT OF IONIC CONTENT ON THE POLYURETHANE DISPERSION PARTICLES	56
FIGURE 6.8: EFFECT OF IONIC CONTENT ON SCA OF COATED PAPERBOARD AT OPTIMUM VISCOSITY OF 250 MPA.S.....	57
FIGURE 6.9: EFFECT OF PH ON THE PARTICLE SIZE DISTRIBUTION OF THE PU DISPERSION MEASURED BY LIGHT SCATTERING.....	59
FIGURE 6.10: VISUAL EFFECT OF PH ON THE PARTICLE SIZE DISTRIBUTION OF THE PU DISPERSION, MEASURED BY LIGHT SCATTERING.....	60
FIGURE 6.11: VISUAL EFFECT OF PH ON THE PARTICLE SIZE DISTRIBUTION OF THE PU DISPERSION, MEASURED BY TEM	61
FIGURE 6.12: EFFECT OF EXCESS TEA NEUTRALIZING BASE	62
FIGURE 6.13: EFFECT OF PH ON SCA OF THE PU DISPERSIONS.....	63
FIGURE 6.14: SCHEMATIC ILLUSTRATION OF THE EFFECT OF TEA ON THE EMULSION VISCOSITY AND PARTICLE SIZE (TRANSPARENCY) OF THE PU DISPERSIONS.....	64
FIGURE 6.15: EFFECT OF VISCOSITY ON SCA OF PU COATED PAPERBOARD CONTAINING	65
4.6 TO 6.0% DMPA	65
FIGURE 6.16: EFFECT OF SOFT SEGMENT CONTENT ON MVTR.....	66
FIGURE 6.17: EFFECT OF WAXC78 ON THE MVTR OF THE PU COATINGS	68
FIGURE 6.18: SEM IMAGES OF THE BLANK PAPERBOARD SURFACE	69
FIGURE 6.19: SEM IMAGES SHOWING THE EFFECT OF NON-PHOSPHATED PU COATED PAPERBOARD	70
FIGURE 6.20: SEM IMAGES SHOWING THE EFFECT OF PHOSPHATED PU COATED PAPERBOARD	71
7 MECHANICAL, THERMAL AND SPECTROSCOPIC CHARACTERIZATION.....	73
FIGURE 7.1: EFFECT OF HARD SEGMENT CONTENT ON TG OF THE POLYURETHANE	75
FIGURE 7.2: EFFECT OF PBTCA CONTENT ON TG OF THE POLYURETHANE.....	75
FIGURE 7.3: EFFECT OF DMPA CONTENT ON TG OF THE POLYURETHANE	76
FIGURE 7.4: EFFECT OF CHDCA CONTENT ON TG OF THE POLYURETHANE.....	76
FIGURE 7.5: EFFECT OF CHDCA CONTENT ON VISCOSITY OF THE POLYESTER	77
FIGURE 7.6: EFFECT OF WAXC78 ON THE PU THAT IS NOT FULLY COMPATIBLE	77
FIGURE 7.7: EFFECT OF HARD SEGMENT CONTENT ON THERMAL STABILITY OF THE POLYURETHANE	78
FIGURE 7.8: EFFECT OF PBTCA CONTENT ON THERMAL STABILITY OF THE POLYURETHANE	79
FIGURE 7.9: EFFECT OF CHDCA CONTENT ON THERMAL STABILITY OF THE POLYURETHANE	79

FIGURE 7.10: EFFECT OF WAX CONTENT ON THERMAL STABILITY OF THE POLYURETHANE	80
FIGURE 7.11: SECOND HEATING PROFILE OF THE PU-WAX C78 COMPOSITES	80
FIGURE 7.12A: EFFECT OF PBTCA CONTENT ON THE MOLECULAR WEIGHT OF THE POLYESTER (NORMALIZED TO HIGHEST PEAK)	82
FIGURE 7.12B: EFFECT OF PBTCA CONTENT ON THE MOLECULAR WEIGHT OF THE POLYESTER (NORMALIZED TO 1 ST PEAK).....	82
FIGURE 7.13A: EFFECT OF CHDCA CONTENT ON THE MOLECULAR WEIGHT OF THE POLYESTER (NORMALIZED TO HIGHEST PEAK) CONTAINING 6% PBTCA	83
FIGURE 7.13B: EFFECT OF CHDCA CONTENT ON THE MOLECULAR WEIGHT OF THE POLYESTER (NORMALIZED TO 1 ST PEAK) CONTAINING 6% PBTCA.....	83
FIGURE 7.14A: EFFECT OF CHDCA CONTENT ON THE MOLECULAR WEIGHT OF THE POLYESTER (NORMALIZED TO HIGHEST PEAK) CONTAINING 8% PBTCA	84
FIGURE 7.14B: EFFECT OF CHDCA CONTENT ON THE MOLECULAR WEIGHT OF THE POLYESTER (NORMALIZED TO 1 ST PEAK) CONTAINING 8% PBTCA.....	84
FIGURE 7.15A: EFFECT OF CHDCA CONTENT ON THE MOLECULAR WEIGHT OF THE POLYESTER (NORMALIZED TO HIGHEST PEAK) CONTAINING 10% PBTCA	85
FIGURE 7.15B: EFFECT OF CHDCA CONTENT ON THE MOLECULAR WEIGHT OF THE POLYESTER (NORMALIZED TO 1 ST PEAK) CONTAINING 10% PBTCA.....	85
FIGURE 7.16A: MWD OF PU FROM POLYESTER (NORMALIZED TO HIGHEST PEAK).....	87
FIGURE 7.16B: MWD OF PU FROM POLYESTER (NORMALIZED TO 1 ST PEAK).....	87
FIGURE 7.17: MONITORING THE NCO-CONTENT BY FTIR DURING PU SYNTHESIS (AT 4 SCANS, 4.0 CM ⁻¹)	88
FIGURE 7.18: FTIR SPECTRA OF NON-PHOSPHATED AND PHOSPHATED POLYESTERS.....	89
FIGURE 7.19: FTIR-SPECTRA OF NON-PHOSPHATED AND PHOSPHATED POLYURETHANES.....	90
FIGURE 7.20A: ¹ H-NMR SPECTRA OF POLYESTER CONTAINING ALL FOUR MONOMERS	92
FIGURE 7.20B: ¹ H-NMR SPECTRA OF POLYURETHANE	93
FIGURE 7.21: ¹³ C-NMR SPECTRA OF POLYESTER AND PU BETWEEN 10 TO 80 PPM	98
FIGURE 7.22: ¹³ C-NMR SPECTRA OF POLYESTER AND PU BETWEEN 110 TO 180 PPM	100
FIGURE 7.23: ¹³ C-NMR SPECTRUM OF PU, FOCUSING ON THE TDI LINKAGE.....	101
FIGURE 7.24: ³¹ P-NMR SPECTRA OF PBTCA-CONTAINING POLYESTER AND POLYURETHANE	106
8 POLYURETHANE-FILLER COMPOSITES FOR PAPERBOARD APPLICATION	108
FIGURE 8.1: SCHEMATIC ILLUSTRATION OF THE THREE MAIN TYPES OF POLYMER NANOCOMPOSITES	108
FIGURE 8.2: EFFECT OF MICRO-FILLER CONTENT ON MVTR OF PU COATED PAPERBOARD.....	110
FIGURE 8.3: SEM AND TEM IMAGES OF PU-TALC COATED PAPERBOARD.....	111
FIGURE 8.4: DMA ANALYSIS OF PU-SERINA CLAY MICROCOMPOSITE FILMS	112

FIGURE 8.5: EFFECT OF NANO-FILLER ON MVTR OF PU COATED PAPERBOARD	116
FIGURE 8.6: EFFECT OF NANO-FILLER CONTENT ON THERMAL STABILITY OF PU	117
FIGURE 8.7: EFFECT OF NANO-FILLER CONTENT ON DSC ANALYSIS OF PU	117
FIGURE 8.8: SEM AND TEM IMAGES OF PU-NC 93A COMPOSITE COATED PAPERBOARD	118
FIGURE 8.9: TEM ANALYSIS OF A POLYESTER-CLAY NANOCOMPOSITE CONTAINING 1.5% NC 30B, PREPARED USING <i>METHOD 2A</i> , DURING <i>STAGE 1</i>	120
FIGURE 8.10: TEM ANALYSIS OF A POLYESTER-CLAY NANOCOMPOSITE PRECURSOR CONTAINING 1.5% NC 30B AND NMP-SOLVENT, PREPARED USING <i>METHODS 2A AND 2B</i> , DURING <i>STAGE 2</i>	121
FIGURE 8.11: TEM ANALYSIS OF A PU-CLAY NANOCOMPOSITE EMULSION CONTAINING 1.0% NC 30B, PREPARED USING <i>METHODS 2A AND 2B</i>	122
FIGURE 8.12: TEM IMAGES OF PU-NC 30B COMPOSITE FILMS, PREPARED USING <i>METHODS 2A AND 2B</i>	123
FIGURE 8.13: SEM IMAGES OF PAPERBOARD COATED WITH PU-NC 30B AND 0% WAXC78 COMPOSITE FILMS, PREPARED USING <i>METHOD 2A</i>	124
FIGURE 8.14: SEM IMAGES OF PAPERBOARD COATED WITH PU-NC 30B AND 15% WAXC78 COMPOSITE FILMS, PREPARED USING <i>METHOD 2A</i>	125
FIGURE 8.15: SEM IMAGES OF PAPERBOARD COATED WITH PU-NC 30B AND 0% WAXC78 COMPOSITE FILMS, PREPARED USING <i>METHOD 2B</i>	126
FIGURE 8.16: SEM IMAGES OF PAPERBOARD COATED WITH PU-NC 30B AND 15% WAXC78 COMPOSITE FILMS, PREPARED USING <i>METHOD 2B</i>	127
FIGURE 8.17: TEM IMAGES OF PU-NC 30B COMPOSITE DISPERSIONS, PREPARED USING <i>METHOD 3</i>	128
FIGURE 8.18: TEM IMAGES OF PU-NC 30B COMPOSITE FILMS, CONTAINING 0% WAXC78, PREPARED USING <i>METHOD 3</i>	129
FIGURE 8.19: TEM IMAGES OF PU-NC 30B COMPOSITE FILMS, CONTAINING 15% WAXC78, PREPARED USING <i>METHOD 3</i>	130
FIGURE 8.20: SEM IMAGES OF PU-NC 30B COATED PAPERBOARD, CONTAINING 0% WAXC78, PREPARED USING <i>METHOD 3</i>	131
FIGURE 8.21: SEM IMAGES OF PU-NC 30B COATED PAPERBOARD, CONTAINING 15% WAXC78, PREPARED USING <i>METHOD 3</i>	132
FIGURE 8.22: DMA ANALYSIS OF PU-NC 93A NANOCOMPOSITE FILMS WHICH WERE PREPARED USING <i>METHOD 1</i>	134
FIGURE 8.23: DMA ANALYSIS OF PU-NC 30B NANOCOMPOSITE FILMS, PREPARED USING <i>METHOD 2A</i>	135
FIGURE 8.24: DMA ANALYSIS OF PU-NC 30B NANOCOMPOSITE FILMS, PREPARED USING <i>METHOD 2B</i>	135

FIGURE 8.25: DMA ANALYSIS OF PU-NC 30B NANOCOMPOSITE FILMS, PREPARED USING <i>METHOD 3</i>	136
.....	
APPENDICES	143
.....	
FIGURE A.2.1: DMA SPECTRUM OF WAX A15/31	144
FIGURE A.2.2: DMA SPECTRUM OF WAX C78	144
FIGURE A.2.3: UNCOATED NYLON FIBER AT 5000X AND 10000X MAGNIFICATION	146
FIGURE A.2.4: PU-COATED NYLON FIBER AT 5000X AND 10000X MAGNIFICATION	147
FIGURE A.2.5: NYLON FIBER COATED WITH MIXTURE CONTAINING PU & 15% WAX C78 AT 5000X AND 10000X MAGNIFICATION	148
FIGURE A.3.1: SCREENING OF PRP-WAX COMPOSITES CONTAINING 23 RESPECTIVE SCHUMANN SASOL WAXES IN TERMS OF MVTR	149
FIGURE A.3.2: DETERMINATION OF OPTIMUM WAX CONCENTRATION IN PRP-WAX COMPOSITES	150
FIGURE A.7.1: PARTICLE SIZE ANALYSIS OF PU DISPERSION AT PH 6.90 AT 20,3°C	155
FIGURE A.7.2: PARTICLE SIZE ANALYSIS OF PU DISPERSION AT PH 6.98 AT 20,3°C	156
FIGURE A.7.3: PARTICLE SIZE ANALYSIS OF PU DISPERSION AT PH 7.14 AT 20,3°C	157
FIGURE A.7.4: PARTICLE SIZE ANALYSIS OF PU DISPERSION AT PH 7.29 AT 20,3°C	158
FIGURE A.7.5: PARTICLE SIZE ANALYSIS OF PU DISPERSION AT PH 7.42 AT 20,3°C	159
FIGURE A.7.6: PARTICLE SIZE ANALYSIS OF PU DISPERSION AT PH 7.60 AT 20,3°C	160
FIGURE A.7.7: PARTICLE SIZE ANALYSIS OF PU DISPERSION AS DETERMINED BY TEM AT PH 6.90	161
FIGURE A.7.8: PARTICLE SIZE ANALYSIS OF PU DISPERSION AS DETERMINED BY TEM AT PH 6.98	162
FIGURE A.7.9: PARTICLE SIZE ANALYSIS OF PU DISPERSION AS DETERMINED BY TEM AT PH 7.14	163
FIGURE A.7.10: PARTICLE SIZE ANALYSIS OF PU DISPERSION AS DETERMINED BY TEM AT PH 7.29	164
FIGURE A.7.11: PARTICLE SIZE ANALYSIS OF PU DISPERSION AS DETERMINED BY TEM AT PH 7.42 AND PH 7.60 RESPECTIVELY	165
FIGURE A.9.1: ¹ H AND ¹³ C-NMR SPECTRA OF POLYESTERS WITH VARIOUS MONOMER COMPOSITIONS	171
FIGURE A.9.2: ¹³ C AND ¹³ C-APT NMR SPECTRA OF POLYESTER SS 0810	172
FIGURE A.9.3: ¹³ C AND ¹³ C-APT NMR SPECTRA OF POLYURETHANE (SYNTHESIZED FROM POLYESTER SS 0810)	173

ABBREVIATIONS

AA	Adipic acid
APT	Attached proton test
CHDCA	1,4-Cyclohexane dicarboxylic acid
DMA	Dynamic mechanical analysis
DMPA	Dimethylolpropionic acid
DSC	Differential scanning calorimetry
EG	Ethelene glycol
ELSD	Evaporative light scattering detector
E/VA	Ethylene-vinyl acetate copolymer
FSA	Formamidine sulphitic acid
FTIR	Fourier transform infrared
GPC	Gel permeation chromatography
HDI	1,6-Hexamethylene diisocyanate
HCl	Hydrochloric acid
HEMA	Hydroxyethylene methacrylate
HPA	3-Hydroxypivalic acid
HSC	Hard segment content
KOH	Potassium hydroxide
MDI	4,4-Diphenylmethane diisocyanate
MF	Melamine formaldehyde
MMA	Methyl methacrylate
MVTR	Moisture vapour transmission rate
MW	Molecular weight
MWD	Molecular weight distribution
NaCl	Sodium chloride
NMR	Nuclear magnetic resonance
NPG	Neopentyl glycol
PAMAM-EPI	Polyamide-polyamine-epichlorohydrin
PAS	Photo-acoustic cell
PBTCA	2-Phosphonobutane-1,2,4-tricarboxylic acid
PE	Polyethylene
PEI	Polyethyleneimine
PP	Polypropylene
PU	Polyurethane
PVA	Polyvinyl acrylate

PVAc	Polyvinyl acetate
PVDC	Polyvinylidene chloride
PVOH or PVAI	Polyvinyl alcohol
RH	Relative humidity
SCA	Static contact angle
SEM	Scanning electron microscopy
SSC	Soft segment content
TDI	Toluene diisocyanate
TEA	Triethylamine
TEM	Transmission electron microscopy
Tg	Glass transition temperature
TGA	Thermogravimetric analysis
UF	Urea formaldehyde

1 INTRODUCTION

1.1 Introduction

The development of environmentally friendly coatings from conventional solvent-borne systems has been going on for more than 25 years [1]. Solvent-borne systems are being replaced by the development of high solid coatings, powder coatings, and water-borne coatings. The latter are preferred due to their compatibility with conventional coating systems.

Water-borne coatings are produced by emulsion polymerization which includes acrylics, polyester and polyurethane dispersions. Water-borne polyurethane systems combine low volatility content properties with the good film properties of solvent-borne systems, along with the inherent favourable properties of the urethanes.

1.2 Paperboard

Various homo- and copolymers are currently used as coatings for paperboard (see Section 2.4.1). Amongst the desired coating properties, end-use performance and fiber recyclability are very important, which also include:

- Blocking resistance
- Low moisture vapour transmission rate (MVTR)
- Easy processability and coatability
- Environmentally friendly
- Recyclability of coated paperboard
- Non-toxicity for food application
- Low cost

Currently, polyvinylidene chloride (PVDC) coatings exhibit the lowest MVTR-values when tested under tropical conditions, i.e. 38°C and 90% RH [2]. The disadvantages associated with the use of this type of coating include the actual coating process, which requires two coats and very careful drying conditions, and also its poor recyclability [3]. Hydrochloric acid (HCl) is released upon burning the PVDC coating, which is environmentally unfriendly, and it is not recommended for usage in cold temperatures due to the polymer's brittleness at these cold conditions.

Hot-melts, such as polyethylene (PE), are used for cold food packaging. Their major disadvantage is that the coating makes the paperboard non-recyclable.

To increase coating performance and fiber recyclability, two methodologies have been used, which include: (1) the modification of current wax-based coatings, to increase performance and fiber recyclability; and (2) the development of new aqueous-based coating formulations to eliminate wax-based coatings altogether. Other coatings currently being used do not comply with all of the above requirements.

1.3 Urethanes

In industry, many different polymers are used to coat paper surfaces in order to obtain a wide variety of properties, including decorative, barrier or functional properties.

Amongst these polymers, polyurethanes (PUs) are the least used for paper coating applications to date. This is mainly due to their high cost, especially that of the isocyanate component. In the past, up-scaling a polyurethane production produced many problems, especially the high reactivity of the isocyanate group towards impurities such as water, etc. Today, however, the side reactions have been largely reduced, from being a problem to now being under control. Other than the high cost, PUs have almost no other disadvantages.

The advantages of PUs however often outweigh their disadvantages. The main advantage is that the polyurethane can be tailor-made to enhance certain desired properties for a specific application. The desired PU properties required in the paperboard application include: minimum MVTR values for PU coating to function as a barrier coating against water vapour transmission, particle size control, good to excellent film formation properties, wax compatibility, minimum blockage of the coated paperboard (to each other), thermal and chemical stability and recyclability of the coated paperboard. Other advantages of PUs include their characteristic inherent properties such as thermal, chemical and abrasion resistance.

1.4 Objectives

The main objective of this study was therefore to study polyurethanes as a possible barrier coating for dry food packaging that meets all the requirements mentioned in Section 1.2. As polyurethanes can be tailor-made to specific specifications, their application as a coating material for paperboard in the packaging industry can be extremely versatile.

The specific objectives of this study are the following:

- I. Synthesizing a hydrophobic polyester-based polyol with a molecular mass of 900 to 1500 g/mol, which will be used further for polyurethane syntheses.
- II. Synthesizing a polyurethane with ionic groups for self-dispersibility in water to form a stable aqueous polyurethane dispersion.
- III. Investigating the effect of the hard segment content of PU on the coating properties.
- IV. Investigating the effect of 1,4-cyclohexane dicarboxylic acid (CHDCA) containing monomer on the coating properties.
- V. Investigating the effect of self-assembly of the PU on the coating properties, in regards to ionic content and emulsion viscosity.
- VI. Investigating the effect of various nano-fillers and micro-fillers on the coating properties.
- VII. Investigating the effect of wax incorporation into the PU coating matrix on the coating properties.
- VIII. Fully characterizing the polyurethane using TGA, DSC, DMA, FTIR, NMR, SCA, MVTR, TEM and SEM.

1.5 References

1. D. Dieterich, W. Keberle, H. Witt, *Angew. Chem. Int. Ed.* **9 (1)**, 40, 1970.
2. G. A. Gordon, D. J. Hine and J. H. Young (Editors), *Paper and Board in Packaging*, Pergamon Press, New York, 1963.
3. R. R. A. Higham, *A Handbook of Paperboard and Board*, **Vol. 1**, Business Books Limited, London, 1970.

2 PAPERBOARD

2.1 Terminology

Paper is generally termed board (or paperboard) when it weighs more than 220 g/m² and when its thickness exceeds 0.30 mm (0.12 in), while the United Kingdom uses a lower limit of 0.25 mm (0.010 in) [1,2,3]. The terminologies [1-6] used for board or paperboard depend mainly on its various end-usages, several of which are tabulated in Table 2.1 below.

Table 2.1: Paperboard terminology

Terminology	Description
Container board	This is used for corrugated and solid fiberboard boxes.
Boxboard	This term applies to folding cartons, which can be further divided into: <ul style="list-style-type: none">• Special food board• Folding boxboard• Setup (rigid) boxboard
Strawboard	This consist of straw semichemical pulp, which is mainly used for book covers, rigid boxes, picture mountings, etc.
Wood pulpboard	This consists of groundwood pulp, which is used for containerboard, shoe board, and making traveling cases.
Leatherpulp board	This contains at least 50% leather, which is used for boots, shoes and cases.
Resin board	The board is stocked (impregnated) with a thermoplastic resin, which is used for forming and insulation purposes.
Printer's board	Examples include art board, ivory board and bristol board.

2.2 Grades of paperboard

Paperboard grades include Kraft and recycled paperboard, which can be applied to both the packaging and building industries.

2.2.1 Kraft paperboard

Kraft paperboard is used in the packaging industry. It includes *bleached* and *unbleached* paperboard [7]. About half of the bleached paperboard is coated, and then used in folding milk cartons, index cards, cups, and plates [8].

Unbleached paperboard is used in linerboard and as corrugated medium for the production of corrugated boxes, of which recycled fiber is being increasingly used.

2.2.2 Recycled paperboard

Recycled paperboard is made from waste papers and other inexpensive pulps, of which 90 to 98% is recycled paper and the rest virgin stock. About 80% of all waste paper comes from corrugated boxes, newspapers and office papers [9,10]. Grades of recycled paperboard include gypsum (calcium sulphate) liner, core (tube) stock, and clay-coated folding boxboard, which is used in roofing felt, fiberboard, shoe and cereal boxes, etc. These grades have a grayish cast because the furnish, which is the combination of all the materials used to make paper, is not de-inked.

2.3 Waste paper recycling

Here emphasis is put on the recycling process and additives/agents for wet and dry strength.

2.3.1 Waste paper recycling process

The main processes in the waste paper recycling process [1-6,8-13] are summarized in Figure 2.1 below.

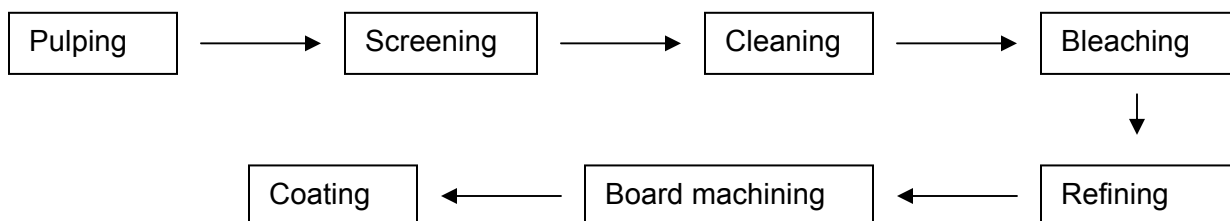


Figure 2.1: Waste paper recycling process

The pulping process takes place in a pulper [11], which acts as a large blender that disperses the paper pulp into an aqueous slurry. Inside the pulper is a chain or ragger that collects light waste such as wires, plastic sheeting, stringy materials, wet strength paper, tapes and other material. The accumulated waste material forms a rag rope, which is then pulled out slowly over a long period of time, and cut into manageable sizes. Heavy contaminants like nuts, bolts, rock and pipe-fittings are removed as junk via the junk remover.

Thereafter, de-inking occurs in the pulper, typically at 40-70°C and at pH 9-11, depending on the quality and end-use of the pulp. De-inking can be accomplished by either two processes, which are wash de-inking or flotation de-inking. In wash de-inking the ink/print particles are detached from the fiber surface, forming a suspension in the water phase, with an average particle diameter of about 1 to 10 µm. The suspended ink/print particles are then washed out during dewatering. In flotation de-inking, the pulped wastepaper is fed into cells, in which air is injected with the stock, and whereby the ink/print particles adhere to the air bubbles, rise to the surface, and are then removed. Here the ink/print particles require mainly a hydrophobic surface and a size of about 10 to 50 µm in diameter in order to adhere to the air bubbles. The pulp is mixed with water, and then goes to pressure screens.

At the pressure screens, the pulp is forced through small holes or slots to remove dirt, sand and other large particles from the pulp. The pressure screens consist of at least one multistage coarse screening system, for the removal of relatively large debris, followed by at least one multistage fine screening system, for the removal of relatively fine debris. Coarse screens have perforations in the range of 12 to 20 mm, followed by another coarse screen with perforations in the range of 1.2 to 2.0 mm. Fine screens have perforations in the range of 0.25 to 0.40 mm, followed by another coarse screen with perforations in the range of 0.15 to 0.25 mm. Screening is used in sequence with cleaning processes, to check the quality and consistency of the stock before and after each cleaning stage.

The cleaning process involves the removal of contaminants from the stock. There are usually at least two centrifugal cleaning stages, but frequently three or four are used. Each stage is designed to remove different types and sizes of contaminants. This

involves firstly the removal of heavy particles (contaminants with a high specific gravity) from the stock via a first set of centrifugal cleaners [8,10]. Here medium-sized contaminants with a high specific gravity such as paper clips, glass and grit, are removed by high-density, high-consistency cleaners, followed by the removal of small contaminants with a high specific gravity such as fine grit, sand, coating flakes and adhesives, by high-density, low-consistency cleaners. Afterwards, lightweight (lighter-than-water) contaminants such as tacky material, pitch, plastics, waxes and other polymers are removed via another set of low-density, low-consistency centrifugal cleaners.

Bleaching agents are added for increased product whiteness during the bleaching process. Bleaching agents are sometimes added to the pulper to help with ink removal, but they are more efficient when added after the pulp is cleaned and screened. Bleaching agents include oxidative or reducing agents. Of the oxidative bleaching chemicals that are available, hydrogen peroxide is the most commonly used for wastepaper, whereas hydrosulphite is the most commonly used reductive bleaching agent for wastepaper. Sodium hydrosulphite has a positive effect on color destruction and is therefore often used in combination with hydrogen peroxide [14]. New bleaching agents under development include oxidative bleaching agents such as oxygen [14,15] and ozone [17,18], and reducing bleaching agents such as formamidine sulphitic acid (FSA) [19].

When quality levels achieved by cleaning and screening are inadequate for a particular product, additional techniques like fractionation and dispersion are used. Fractionation or classification is a process that divides a mixture of fibers into two or more classes, usually according to their length. Fiber length affects the degree of interfiber bonding, which influences tear strength and also burst and tensile strengths. Generally, tear resistance is increased with increased fiber length [3]. Dispersion or kneading is primarily used to increase optical characteristics by disguising the presence of contaminants. Dispersion also enhances burst and tensile properties. After the stock has reached satisfactory quality levels, it is passed on to be refined.

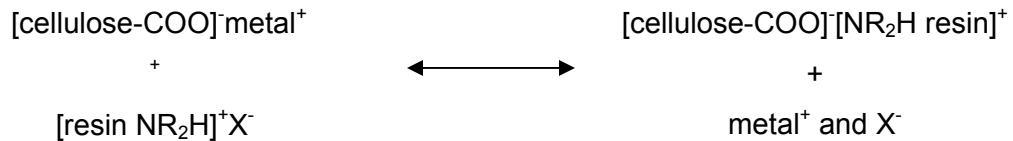
The refining process involves making wet fibers ready for the board machine to obtain maximum fiber entanglements, which significantly increases the sheet strength.

The board machining process takes place where the sheet is built layer by layer, then pressed and rolled until the desired board thickness is reached. From here the sheets pass through drying tunnels, after which they pass through two or three sets of heavy calendering rollers for smoothing and flattening. The first calender stack after drying is called the wet stack, and the second set is called the dry stack. Water, starch solutions, etc., are normally applied to the paperboard on the wet stack to improve smoothness and to impart properties such as water resistance, oil resistance, scuff resistance, flame proofing, etc.

2.3.2 Wet strength additives

A paper possesses wet strength when a considerable part of its strength remains after being saturated with water. Water breaks the interfiber hydrogen bonds in the paper, resulting in a decrease in wet strength. Thus the wet strength of paper can be improved if the interfiber hydrogen bonds are protected or reinforced; protected by inhibiting swelling and water sorption within and around the fibers; reinforced by forming primarily hydrogen or covalent bonds between the fibers.

The mechanism of the wet strength additive can be illustrated by means of an ion exchange between cellulose and the cationic resins:



Wet strength additives are natural (e.g. gums and starches) and synthetic (e.g. N-containing) chemicals [20-23]. Commonly used cationic resins include urea formaldehyde (UF), melamine formaldehyde (MF), polyethyleneimine (PEI), and polyamide-polyamine-epichlorohydrin (PAMAM-EPI) [4,11,23]. UF is the traditional wet strength resin, but has been largely replaced by MF due to the health aspects of formaldehyde emission.

Cationic PEI is retained on cellulose by carboxyl groups, which bind acid dyestuffs and also retain fillers like TiO₂ and CaCO₃ effectively. PEI has, however, been replaced by a more effective cationic PAMAM-EPI.

Advantages of the use of wet strength additives include:

- they bond additives and other compounds to the fiber
- they increase burst or tensile strength
- they keep surface fibers together to prevent linting, which causes defective printing.
- they can decrease drying times, thereby increasing production

2.3.3 Dry strength additives

Dry strength of a paper sheet is an inherent structural property which is due primarily to the development of interfiber bonds, such as hydrogen bonds, covalent bonds and mechanical entanglements during consolidation and drying of the fiber network. The additives commonly used [20-23] to impart dry strength include:

- starch derivatives
- mannogalactans (gums), which include locust bean gum, guar gum and tara gum
- cellulose derivatives
- synthetic dry strength agents which consist primarily of polyacrylamides

The predominant group of dry strength additives is the starch derivatives. Starch is used as a dry-strength agent, drainage aid, retention aid, coating binder and adhesive in corrugated board, etc. Starch is reacted with amine containing materials such as $\text{RCH}_2\text{OCH}_2\text{CH}(\text{OH})\text{CH}_2\text{-N}(\text{CH}_3)_3^+$ to introduce cationic groups. Anionic and ampholytic (cationic and anionic) starches are also available. Potato starch contains about 0.1% phosphorous, and imparts a slight negative charge due to the phosphate groups.

Polyacrylamide is used for heavy paper or paperboard to increase its dry strength, by hydrogen bonding. It must be added after the final refining stage, when alum is well distributed. Pure polyacrylamide is not an effective bonding agent due to poor retention under wet-end conditions. It needs carboxyl groups (COOH) from acrylic acid (about 10%), and aluminum dimer $[\text{Al}(\text{OH})^{+2}]$ to accomplish effective retention. For dry strength, the molecular weight of the polyacrylamide is controlled to about 250,000 – 500,000.

Guar gum improves some strength properties such as bursting, tensile and internal strength, while also decreasing linting and improving sheet formation.

Cellulose derivatives include carboxymethyl cellulose (CMC), methyl cellulose and hydroxyl cellulose, of which CMC is primarily used.

In conclusion, although the overall surface charge of the paperboard is anionic, these wet strength additives cover the paperboard's surface with long chains containing amine groups, which can also be very good for the adhesion of a polyurethane coating.

2.4 Coating process

There are two types of coatings: printable clay-type coatings and functional coatings. Surface coatings are normally applied to paperboard to impart specific characteristics [12,13].

Printable clay-type coatings are used on paperboard to improve surface receptivity to ink, mask original surface characteristics, reduce abrasion and fiber fluffing (picking) during printing, upgrade the texture of the paperboard, and to increase the attractiveness and sales value of the paperboard.

Functional coatings are normally applied to the opposite side of the printable pigmented coatings to impart *barrier-type* properties and/or *physical (material)-type* properties, as shown in Table 2.2. Functional coatings can also be applied to both sides.

Table 2.2: Properties of paperboard with functional coatings

Barrier-type properties	Physical (material)-type properties
Grease resistance	Slip or anti-slip
Water resistance	Abrasion or non-abrasion
Water vapour resistance	Release or block resistance
Gas permeation resistance	Heat sealability
	High gloss, clarity, etc.

2.4.1 Typical polymers used in paper coatings

The most common resins used in paperboard coatings [2,11,12,23-26] include:

- Styrene and butadiene
- Starch
- Casein
- Polyvinyl acrylate
- Polyvinyl alcohol (PVOH or PVAI)
- Polyvinylidene chloride (PVDC)
- Polyvinyl acetate (PVAc)
- Polyethylene (PE) and polypropylene (PP)

These resins have usually lack some of the characteristic properties needed to make the ideal coating for a specific application. They are usually modified via copolymerisation to enhance certain properties and characteristics of the coatings to better suit its end-use.

PVOH provides strong durable coatings with good optical properties, and the films are completely resistant to almost all organic solvents, oils and greases. When used with starch and casein, some properties are improved, such as better ink holdout, increased gloss, better water resistance and increased flexibility [12,24,25].

Starch is predominantly used to lower the coating cost. Starch can be modified or crosslinked to increase water resistance properties [12].

Casein forms a tough film, and when treated with formaldehyde it increases water resistance. Casein is used in high quality coatings for offset printing, where desired surface properties include toughness, water resistance and high gloss [12,23].

Acrylic coatings are commonly used on paperboard for food packaging due to their low residual odor. Typical properties include high gloss and good ink holdout, which increase print quality. They also have excellent heat, light and chemical resistance, but they are relatively expensive coatings [2,24,26,27].

PVAc provides good heat-sealability, grease and moisture resistance [12]. Copolymers of vinyl acetate and vinyl chloride are used for improved grease resistance coatings [24].

Polybutadiene and *styrene-butadiene* latexes are mainly used to increase coating strength, and also as pigment binders. The latex contributes smoothness, gloss, wet-rub

resistance, flexibility and gloss ink holdout. Butadiene-styrene copolymers are also used for water vapour resistant heat-sealable coatings [2,12,24,26,28].

PVDC emulsions provide coating systems with high solids content, minimum viscosity and excellent barrier properties. Vinylidene chloride is normally copolymerized with vinyl chloride or vinyl acrylate, resulting in excellent barrier properties such as moisture vapour, gas and grease resistance. It is mainly used in dry food packaging as a moisture vapour resistance coating. PVDC, however, requires two coats, that are often pre-coated with a PVC coating [11]. Process conditions include careful after-drying. The fusion temperature is also very important. Other copolymers include acrylates, such as butadiene sulfone-acrylate, methylacrylate, butyl methacrylate and methacrylonitrile-methyl methacrylate [2,12].

Medium density PE is normally used on frozen food cartons. It has good strength, shock resistance and water vapor resistance, but poor grease resistance [2,11]. PE is also used in aseptic packaging for liquids and semi-liquids products [29].

Paraffin wax is one of the oldest moisture protective coatings [11]. Advantages include low cost and easy application, while disadvantages include brittleness (flaking of coated board) and adhesive difficulty.

Microcrystalline wax is a good laminating material that gives high barrier properties. By adding rubber-type polymers, the adhesive properties are also increased. This makes microcrystalline wax suitable for laminating chipboard to a variety of lining papers at high speed [11].

Hot melts cover a blend of thermoplastic resins and wax-extended copolymers, such as ethylene-vinyl acetate (E/VA) and ethylene-ethyl acrylate copolymer/wax systems. They are used to coat fiberboard containers and folding cartons, for protective cartons and wet foods, such as fruit, vegetables, fish, poultry, etc. [11,12].

Other paperboard coatings include the use of polyesters in water-based coatings [26,30].

2.5 References

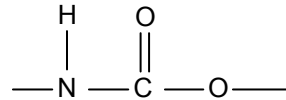
1. J. N. Stephenson (Editor-in-Chief), *Manufacture and Testing of Paper and Board*, **Vol. 3**, McGraw-Hill Book Company Inc., New York, 1953.
2. G. A. Gordon, D. J. Hine and J. H. Young (Editors), *Paper and Board in Packaging*, Pergamon Press, New York, 1963.
3. J. L. Bowyer, R. Shmulsky, J. G. Haygreen, *Forest Products and Wood Science*, Fourth Ed., Iowa state press, Iowa, 2003
4. R. G. Macdonald (Editor) and J. N. Franklin (Tech. Editor), *Papermaking and Paperboard making*, Second Edition **Vol. III**, McGraw-Hill Book Company Inc., New York, 1970.
5. J. N. Stephenson (Editor), *The Manufacture of Pulp and Paper*, **Vol. 4**, McGraw-Hill Book Company Inc., New York, 1928.
6. R. W. McKinney, *Technology of Paper Recycling*, Chapman and Hall, London, 1995.
7. N. DeKing, *Pulp and Paper*, **77**(11), 7, Nov. 2003.
8. N. DeKing, *Pulp and Paper*, **77**(10), 7, Oct. 2003.
9. G. H. Ireland, *Paperboard on the Multi-Vat Cylinder Machine*, Chemical Publishing Company Inc., New York, 1968.
10. C. J. Biermann (Editor), *Essentials of Pulping and Papermaking*, Academic Press Inc., San Diego, California, 1993.
11. R. R. A. Higham, *A Handbook of Paperboard and Board*, **Vol. 1**, Business Books Limited, London, 1970.
12. M. Kouris, M. J. Kocurek, *Pulp and paper manufacture*, 3rd Ed., **Vol. 8**, Joint Textbook Committee of the Paper Industry (TAPPI), Atlanta, USA, 1990.
13. D. T. Harper, *Paper Coatings*, Chemical Technology Review No.79, Noyes Data Corporation, New Jersey, USA, 1976.
14. M. Hache, T. Joachimides, *Tappi Journal*, **75**(7), 187, 1992.
15. S. A. Heimbürger, T. Y. Meng, *Pulp and Paper*, **66**(2), 117, 1992.
16. R. Naddeo, V. Magnotta, T. Kulikowski, V. Ayala, G. Jezerc, *Pulp and Paper*, **66**(11), 71, 1992.
17. J. Kogan, M. Muguet, *Prog. Paper Recycling*, **37**, November, 1992.
18. P. Forsberg, J. M. Genco, W. Ballantyne, S. T. DiNovo, *Prog. Paper Recycling*, **53**, November, 1993.
19. W. H. Matzke, H. H. Selder, *Tappi Pulping Conference*, Book 1, 203, 1988.

20. D. Eklund, T. Lindstrom, Paper Chemistry, DT Paper Science Publications, Grankulla, Finland, 1991.
21. J. C. Roberts (Editor), Paper Chemistry, Chapman and Hall, New York, 1991.
22. C. O. Au, I. Thorn (Editors), Applications of Wet-end Paper Chemistry, Chapman and Hall, London, 1995.
23. R. Strauss, Protein Binders in Paper and Paperboard Coating, Badger Printing Division, Appleton, Wisconsin, 1975.
24. M. Kouris (Technical Editor), Paper Coating Additives, Mack Printing Company, Easton (USA), 1963.
25. A. R. Sinclair, Synthetic Binders in Paper Coatings, Badger Printing Division, Appleton, Wisconsin, 1975.
26. M. Vaha-Nissi, J. Lahti, A. Savolainen, K. Rissa, T. Lepisto, *Appita Journal*, **54**(2), 106, 2001.
27. W. Lau, S. L. Egolf, J. H. E. Promislow, A New Class of Hydrophobic Latex Binders, *Proc. PITA Coating for Performance in Print and Packaging Conf.*, Edinburgh, Scotland, 1999.
28. www.paperloop.com, Feb. 2005. (F. Kotoye, Paperloop Magazines)
29. www.packaging-online.com, Feb. 2005. (P. Fretty, Paperboard Packaging)
30. K. Salsman, Waterborne Polyester Resins in repulpable Paper Coatings, *Paperage*, July 1998.

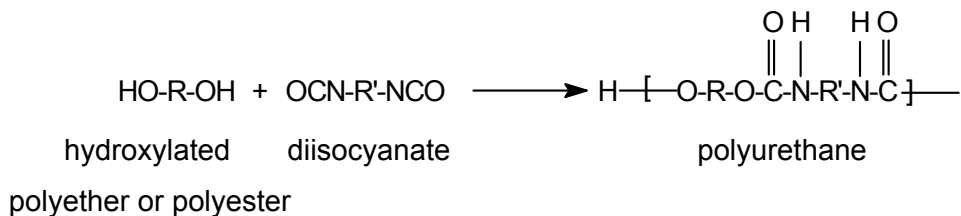
3 POLYURETHANES

3.1 Introduction

Polyurethanes (PUs) is the collective name for an extensive group of polymers with various compositions and correspondingly varied property profiles, which are characterized by the following chain linkage:



Most polyurethanes are prepared by the polyaddition reaction of a diisocyanate and a polyol, which does not eliminate any by-product [1].



By altering the R and R' groups, properties such as molecular weight, degree of crosslinking, effective intermolecular forces, chain stiffness and crystallinity, can be changed. This makes PUs one of the most versatile polymers. PUs can be used for making fibers, flexible and rigid foams, soft and hard elastomers, rigid and flexible moldings, coatings, sealants, adhesives, and thermoplastic and thermosetting plastics.

Fully reacted PUs are non-toxic, and regularly used for their biocompatibility to blood, tissue, enzymes and other biological fluids and processes [2-5]. Non-toxicity and biocompatibility are necessary properties for the use and bio-compatibilisation of foreign materials in human bodies [6-10], such in artificial hearts, limbs, hip joint replacements, vascular catheters, arteries, membranes and nano-capsules in drug delivery systems.

PUs have recently been investigated for their use as an anti-bacterial surface coating onto numerous types of medical devices, by using a biodegradable PU to release antibiotic drugs in response to inflammatory related cells [11,12].

The complete characterization of a PU is necessary to fully understand the relationship between the chemical structure and morphology, and its chemical structure and physical properties. The physical and mechanical properties are linked to the morphology and chemical structure of the PU. The physical and mechanical properties of PUs depend on factors such as:

- Soft and hard segment composition
- Polymer chain lengths and the sequence of length distribution of both soft and hard segments
- Degree of branching and crosslinking
- Molecular weight

Morphology factors, especially phase compatibility, are very important factors in PUs, as PUs tends to phase separate as a result of increasing differences between the hard and soft segments. These differences include crystallinity, polarity, flexibility, and hard to soft segment ratio. This means that if the one segment, such as the hard segment is too hard, crystalline, polar or too rigid compared to the soft segment, then the micro-phase will increase in incompatibility. These incompatibilities between hard and soft segment can be decreased by the incorporation of a compatibilising agent, which is normally incorporated into the soft segment. This may be necessary for specific applications.

3.2 Polyurethane dispersions

In the 1970s, increasing environmental legislation was imposed to limit volatile organic solvent emissions into the atmosphere. This led to the development of aqueous polyurethane dispersions. The synthesis and characterization of PU dispersions are well described in the literature [13-27]. PU dispersions have received considerable attention due to their usefulness in coatings [28].

Ionic groups are frequently introduced into PU dispersions by monomers or chain extenders containing tertiary amine groups, and pendent sulfonic or carboxylic acid groups. These acid groups are subsequently neutralized to produce ionomers, which can then be dispersed into water.

Ionic polyurethane dispersions can be produced in a wide particle-size range, between the limiting cases of true high molecular mass solutions or viscous gels and coarse suspensions. The preferred particle size for stable dispersions is 30 to 800 nm, and for suspensions 10-100 μm . The film-forming capacity, even of hard products and at low temperatures, is outstanding because the ionically modified particle surfaces are swollen by hydration.

Ionic polyurethane dispersions are superior to conventional surface-active agents for emulsifying nonionic, nonhydrophilized polyurethanes, especially when their structure is adapted to the substrate to be dispersed. High and low molecular mass urethane ionomers are also good substrates or emulsifiers for emulsion polymerization.

3.3 Types of polyurethane dispersions

The first isocyanate-based dispersion was developed by Schlack in 1943, but water-dispersible PU was only introduced in the late 1960s [29]. There are various types of PU dispersions, which include non-ionic, cationic, anionic and amphiphilic polyurethane dispersions.

3.3.1 Non-ionic polyurethane dispersions

Non-ionic PU dispersions include PU dispersions with a hydrophilic monomer, such as polyether, derived from ethylene and propylene oxide. Advantages offered by these polyethers include mechanical and storage stabilities, while disadvantages include their susceptibility to water damage due to their inherent hydrophilicity [30].

3.3.2 Cationic polyurethane dispersions

Cationic polyurethane dispersions are very simple to produce and their salt-forming component can be widely varied. These dispersions are prepared by incorporating monomers containing tertiary amine groups such as n-methyl diethanolamine into the PU backbone. The tertiary amine may be quaternized by an alkylating agent, aryl halides, or with an acid. Synthesis mechanisms and properties of cationic PU dispersions are discussed in the literature [31-44]. Cationic polyurethane dispersions are especially suitable for the adherent coating of anionic substrates such as glass and leather.

3.3.3 Anionic polyurethane dispersions

Anionic PU dispersions are the most important of all the PU dispersions. They are mainly prepared by introducing ionic groups during addition polymerization or by post-polymer modification techniques. Ionic groups, including sulfonic, carboxylate and phosphoric acid groups, bring about significant changes in the properties of PU [13,28,35-47], transforming PUs that are generally waterproof in nature to water-wetting or even water-soluble ones.

A versatile and effective way of controlling the ionic content on the polymer backbone is by the introduction of ionic groups, using ionic diols such as dimethylol propionic acid (DMPA). Here the two primary hydroxyl groups react with the isocyanate, while the tertiary carboxylic acid is very unreactive due to steric hindrance. These pendent carboxylic acid groups are neutralized by means of a suitable base to generate the ionic centers.

3.3.4 Amphiphilic polyurethane dispersions

Amphiphilic PU dispersions are mainly prepared by introducing both anionic and cationic groups into the polymer backbone: usually pendent acid (eg. dimethylol propanoic acid) and tertiary nitrogen (eg. *N*-methyl diethanolamine) containing groups. These PU dispersions are dependent on pH, type of neutralizing agent, and also on the mol ratio between the cationic and anionic groups. These dispersions are usually unstable at neutral pH, but form mini-emulsions near neutral pH, and stable dispersions at high and low pH. At high pH, the PU behaves more like an anionic dispersion, whereas at low pH it behaves more like a cationic dispersion, with a variety of practical applications [48-50].

Amphiphilic characteristics can also be introduced into the PU by the formation of zwitterionomers, whereby the tertiary nitrogen in the PU chain is quaternized using 1,3-propane sultone [49-55]. These zwitterionomers can also be formed via post-polymer modification, whereby PUs that do not contain tertiary amino groups are converted by the initial exchange of urethane protons using NaOH or NaH, followed by the reaction of sultones or lactones [56-59].

3.4 Reactions of isocyanates

The most commonly used aromatic isocyanates are toluene diisocyanate (TDI) and 4,4-diphenylmethane diisocyanate (MDI), and some modifications of these products.

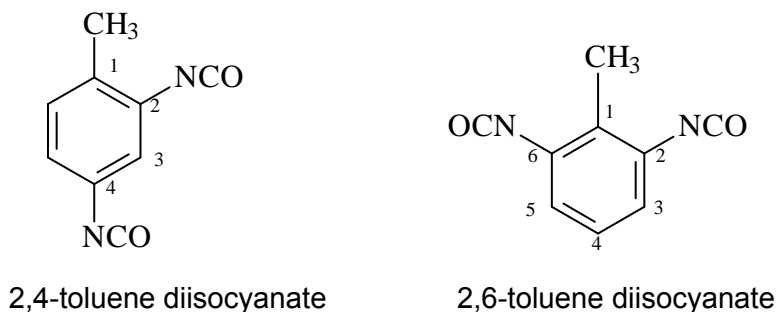
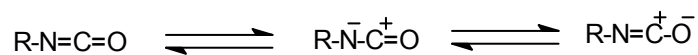
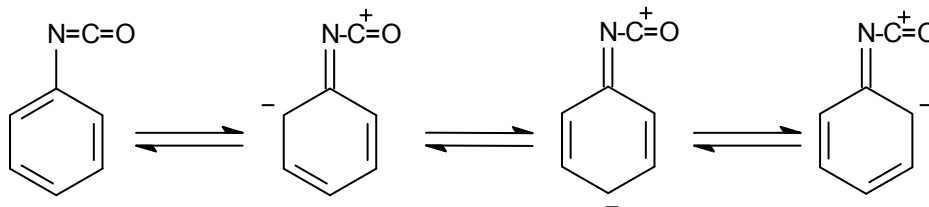


Figure 3.1: TDI isomers

The highly unsaturated isocyanate (-N=C=O) group is very reactive with a wide range of compounds, including itself. It can react with almost any compound that contains an active hydrogen. The expected resonance structure is as follows:



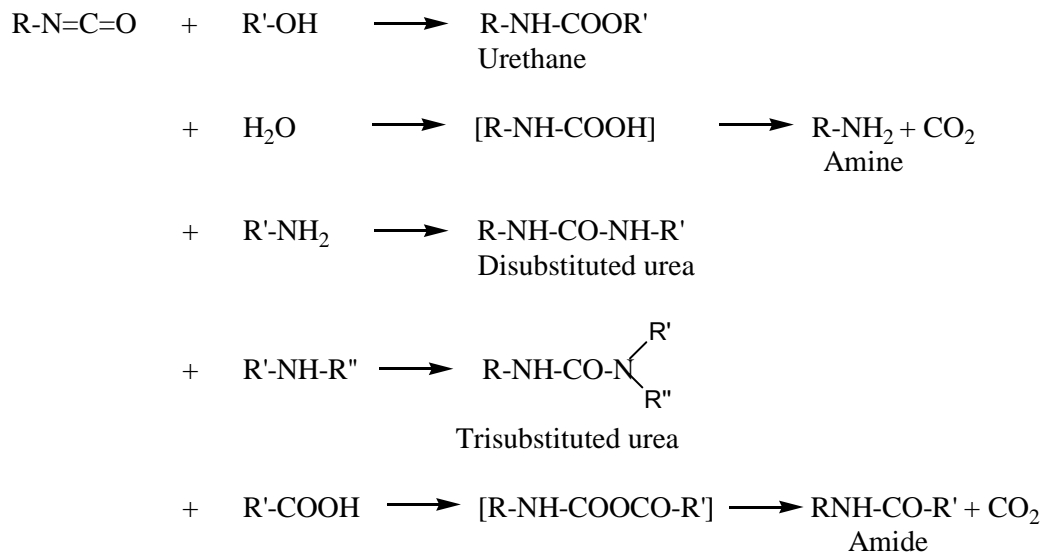
Aromatic isocyanates are more reactive than aliphatic isocyanates. This is due to the delocalization of the negative charge into the aromatic ring, thereby increasing the electrophilic character of the carbonyl ion, as seen in the following scheme.



In addition, electronegative substituents on the aromatic ring increase the reactivity of the NCO-groups, whereas electropositive substituents decrease the reactivity. Steric hinderance on either the isocyanate or the reactive hydrogen compound will retard the reaction.

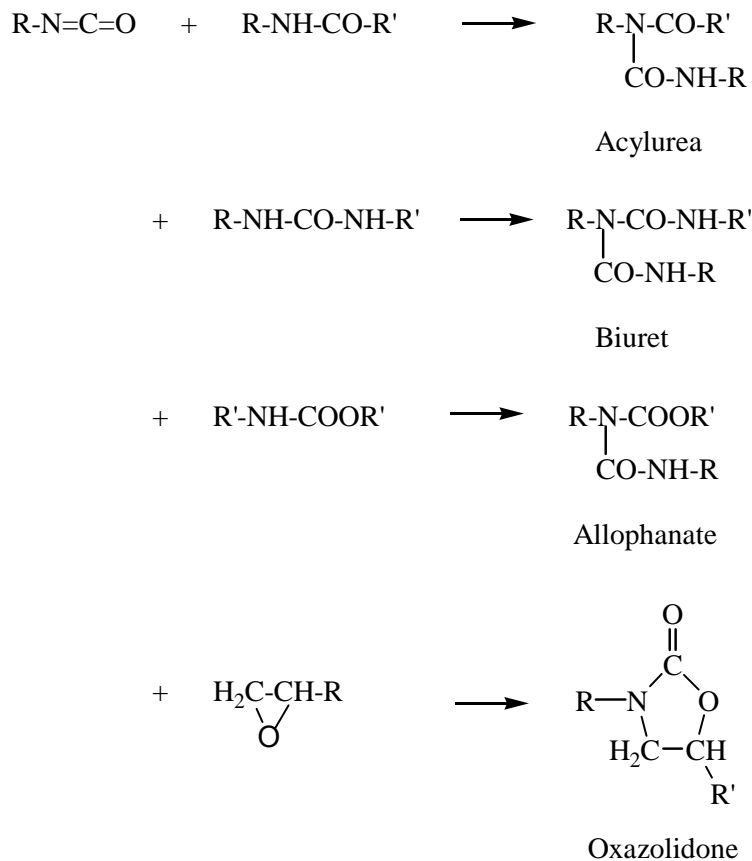
3.4.1 Primary reactions of isocyanates

The primary reactions of isocyanates include:



3.4.2 Secondary reactions of isocyanates

Secondary reactions of isocyanates include:



3.4.3 Self-addition reactions

The isocyanate group (-N=C=O) is a highly unsaturated one and readily undergoes dimerisation and trimerisation to form uretidiones and isocyanurates respectively.

3.4.3.1 Dimerization

The rate of dimerization of aromatic isocyanates is dependent on the electronic or steric influences of ring substituents. Dimerization, as shown in Figure 3.2, is an equilibrium reaction that is greatly retarded by ortho-substituents. Dissociation of these dimers occurs at elevated temperatures, which are used for blocked polyurethane coatings [28].

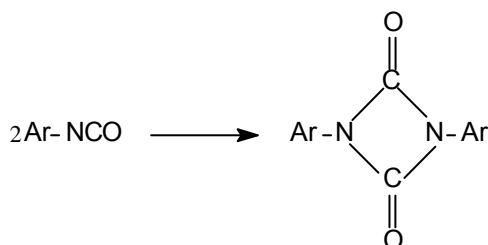


Figure 3.2: Dimerization of an aromatic isocyanate

3.4.3.2 Trimerization

Both aliphatic and aromatic isocyanates can form trimers. Trimerization is however not an equilibrium reaction, which can be stable up to 200°C. The rate of trimerization is also greatly reduced by ortho-substituents on aromatic isocyanates.

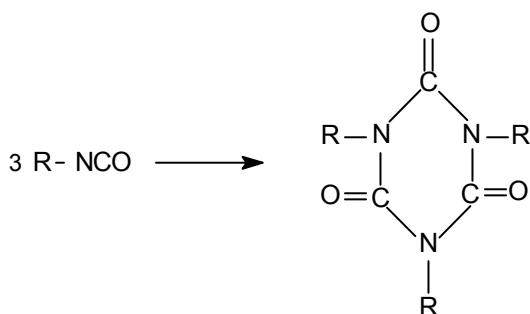


Figure 3.3: Trimerization of both aliphatic and aromatic isocyanates

3.4.3.3 Polycarbodiimides

Isocyanates can also react with itself via a condensation reaction to form carbodiimides with the characteristic -N=C=N- bond, by releasing CO_2 as byproduct. This reaction takes place at very high temperatures, which can however be reduced to room temperature with the help of catalysts, such as phospholene oxide [60]. Carbodiimides can react further with isocyanates to form subsequent urethane-imines [61], as shown in Figure 3.4, and they can also react with water to form ureas.

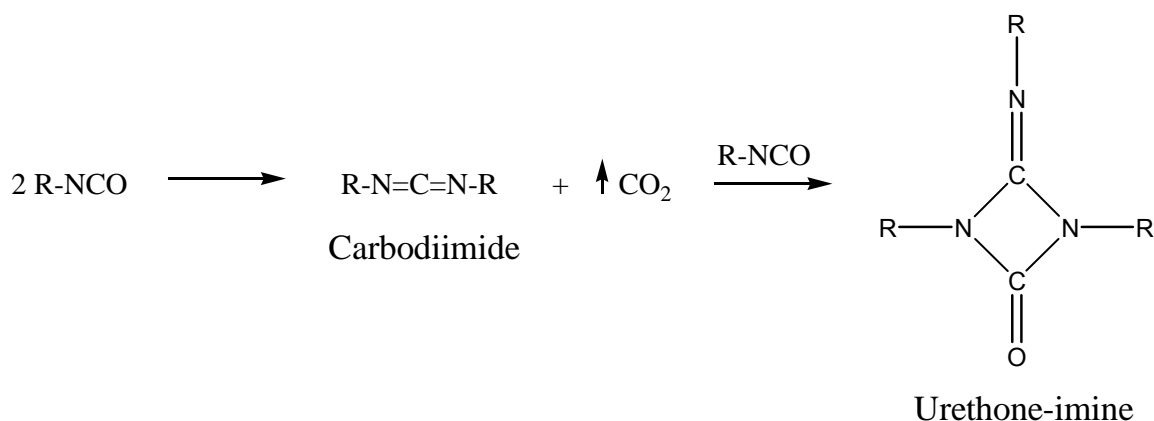


Figure 3.4: Condensation of isocyanates to form carbodiimides and subsequent urethane-imines

3.5 Health aspects of isocyanates

Isocyanates have an inherent toxicity; harmful effects follow the inhalation of free isocyanate groups in vapour, mists and particles, or eye and skin contact with liquid or vapour isocyanate. Of all the isocyanates, HDI (hexamethylene di-isocyanate) and TDI are amongst the cheapest isocyanates with the highest vapour pressures, making them the most dangerous. In view of HDI's extreme hazardous nature, its usage is very limited, and is replaced by safer derivatives. TDI is the most widely used of all the isocyanates, which includes its use in flexible polyurethane foams, surface coatings, cast elastomers, sealants and adhesives.

In relatively high concentrations, isocyanates have a strong irritant effect on the respiratory tract in most people, as discussed in various articles [62-65]. Some people may develop bronchial sensitivity to isocyanates. These people, when later exposed to even very low concentrations of isocyanates, which may even be below the exposure

standard, may react by developing asthma-like symptoms, such as chest tightness, cough, wheeze and shortness of breath. Such attacks may occur up to several hours after cessation of exposure (for example, during the night) but, if a person is particularly sensitive, the attack may occur earlier.

Asthmatic people are more prone to sensitisation and other adverse reactions. People with a history of hay fever, atopic conditions, asthma, recurrent acute bronchitis, interstitial pulmonary fibrosis, pulmonary tuberculosis, occupational chest disease and impaired lung function should be advised against risking exposure to isocyanates. A significant proportion of people who become sensitised to isocyanate do so in the first two months of exposure.

3.6 References

1. O. Bayer, *Angew. Chem.*, **A59**, 257, 1947.
2. N. Morimoto, Y. Iwasaki, N. Nakabayashi, K. Ishihara, *Biomaterials*, **23**, 4881, 2002.
3. N. Sheikh, *Nuclear Instr. and Methods in Phy. Research B*, **208**, 215, 2003.
4. Y. H. Kim, D. K. Han, K. D. Park, S. H. Kim, *Biomaterials*, **24**, 2213, 2003.
5. L. Poussard, F. Burel, J.-P. Couvercelle, Y. Merhi, M. Tabrizian, C. Bunel, *Biomaterials*, **25**, 3473, 2004.
6. Y. J. Li, R. Bahulekhar, T. M Chen, Y. F. Wang, M. Kodama, T. Nakaya, *Macromol. Chem. Phys.*, **197**, 2827, 1996.
7. I. Khan, N. Smith, E. Jones, D. S. Finch, R. E. Cameron, *Biomaterials*, Part I, Accepted 24 Feb. 2004
8. Y. Yuan, F. Ai, X. Zang, W. Zhuang, J. Shen, S. Lin, *Colloids and Surfaces B: Biointerfaces*, **35**, 1, 2004.
9. D. A. Wang, J. Ji, C. Y. Gao, G. H. Yu, L. X. Feng, *Biomaterials*, **22**, 1549, 2001.
10. K. Bouchemal, S. Briancon, E. Perrier, H. Fessi, I. Bonnet, N. Zydowicz, *International J. of Pharm*, **269**, 89, 2004.
11. G. L. Y. Woo, M. W. Mittelman, J. P. Santerre, *Biomaterials*, **21**, 1235, 2000.
12. R. N. S. Sodhi, V. P. Sahi, M. W. Mittelman, *J. Electron Spec. and Rel. Phenomena*, **121**, 249, 2001.

13. H. A. Al-Salah, K. C. Frisch, H. X. Xiao, and J. A. McLean, Jr., *J Polym. Sci. Polym. Chem.*, **25**, 2127, 1987.
14. T. Y. T. Chui, A. S. Coote, C. Butler, M. H. George, and J. A. Barrie, *Polym. Comm.*, **29**, 40, 1988.
15. T. Y. T. Chui, P. K. H. Lam, M. H. George, and J. A. Barrie, *Polym. Comm.*, **29**, 317, 1988.
16. P. K. H. Lam, M. H. George, and J. A. Barrie, *Polym. Comm.*, **30**, 2320, 1989.
17. P. K. H. Lam, M. H. George, and J. A. Barrie, *Polym. Comm.*, **32**, 80, 1991.
18. Y. Chen and Y. L. Chen, *J. Appl. Polym. Sci.*, **46**, 435, 1992.
19. J. Ding, G. Xue, C. Yang, and R. Chen, *J. Appl. Polym. Sci.*, **45**, 1087, 1992.
20. D. K. Kakati, R. Gosain, and M. H. George, *Polymer*, **35**, 398, 1994.
21. M. Xu and C. Yang, *J. Appl. Polym. Physics*, **33**, 745, 1995.
22. K. Lee and B. Kim, *Polymer*, **37**(11), 2251, 1996.
23. M. Yen and S. Kuo, *J. Appl. Polym. Sci.*, **61**, 1639, 1996.
24. J. J. Lee, R. M. Shieh, H. H. Chang, and D. Y. Chao, *J. Appl. Polym. Sci.*, **60**, 2265, 1996.
25. Z. Wang, D. Gao, J. Yang, and Y. Chen, *J. Appl. Polym. Sci.*, **73**, 2869, 1999.
26. M. S. Sanchez-Adsuar, E. Papon, J-J. Villenave, *J. Appl. Polym. Sci.*, **76**, 1596, 1999.
27. H. C. Jung, S. J. Kang, W. N. Kim, Y. B. Lee, K. H. Choe, S. H. Hong, S. B. Kim, *J. Appl. Polym. Sci.*, **78**, 624, 2000.
28. K. Mequanint, PhD Dissertation, University of Stellenbosch, 2001.
29. D. Dieterich, W. Keberle, H. Witt, *Angew. Chem. Int. Ed.* **9** (1), 40, 1970.
30. G. Oertel, Polyurethane Hand Book, Hanser Publisher, New York, 26, 1985.
31. S. L. Hsu, H. X. Xiao, H. H. Szmant, and K. C. Frisch, *J. Appl. Polym. Sci.*, **29**, 2467, 1984.
32. H. A. Al-Salah, H. X. Xiao, J. A. McLean, and K. C. Frisch, *J. Polym. Sci., Polym. Chem.*, **26**, 1609, 1988.
33. S. Chen and W. Chan, *J. Polym. Sci., Polym. Physics*, **28**, 1499, 1990.
34. J. Lee and B. Kim, *J. Polym. Sci. Polym. Chem.*, **32**, 1983, 1994.
35. S. L. Hsu, H. X. Xiao, H. H. Szmant, and K. C. Frisch, *J. Appl. Polym. Sci.*, **29**, 2467, 1984.
36. S. A. Chen and W. C. Chan, *Makromol. Chem.*, **189**, 1523, 1988.
37. B. K. Kim and T. K. Kim, *J. Appl. Polym. Sci.*, **43**, 393, 1991.

38. C. Yang, T. G. Grasel, J. L. Bell, R. A. Register, and S. L. Cooper, *J. Polym. Sci., Polym Physics*, **29**, 581, 1991.
39. S. A. Chen and J. S. Hsu, *Makromol. Chem.*, **193**, 423, 1992.
40. S. Ramesh and G. Radhakrishnan, *Polymer*, **35**(14), 3107, 1994.
41. S. Ramesh and G. Radhakrishnan, *J. Polym. Mat.*, **12**(1), 71, 1995.
42. S. Ramesh and G. Radhakrishnan, *J. Polym. Sci. Polym. Chem.*, **34**, 1713, 1996.
43. C. Lee, J. Kim, K. Suh, *J. Appl. Polym. Sci.*, **78**, 1853, 2000.
44. C. L. Wang, D. Y. Chao, *J. Appl. Polym. Sci.*, **78**, 1932, 2000.
45. R. Adhikari, P. A. Gunatillake, S. J. McCarthy, G. F. Meijs, *J. Appl. Polym. Sci.*, **78**, 1071, 2000.
46. M. Lin, W. Tsen, Y. Shu, F. Chuang, *J. Appl. Polym. Sci.*, **79**, 881, 2001.
47. K. K. S. Hwang, C. Z. Yang, S. L. Cooper, *Polym. Eng. Sci.*, **21**(15), 1027, 1981.
48. M. A. Cohen Stuart, G. J. Fleer, J. Lyklema, W. Norde, J. Scheutjens, *Adv. Colloid Interface Sci.*, **34**, 477, 1991.
49. S. Forster, M. Schmidt, *Adv. Polym. Sci.*, **120**, 51, 1995.
50. E. A. Bekturov, S. E. Kudaibergenov, S. R. Rafikov, *Macromol. Chem. Phys. C*, **30** (2), 233, 1990.
51. J. A. Miller, K. K. S. Hwang, C. Z. Yang, S. L. Cooper, *J. Elast. Plast.*, **15**, 174, 1983.
52. J. A. Miller, K. K. S. Hwang, C. Z. Yang, S. L. Cooper, *J. Macromol. Sci. Phys. Ed.*, **B22**(2), 321, 1983.
53. C. Z. Yang, K. K. S. Hwang, S. L. Cooper, *Makromol. Chem.*, **184**, 651, 1983.
54. T. A. Speckhard, K. K. S. Hwang, C. Z. Yang, W. R. Laupan, S. L. Cooper, *J. Macromol. Sci. Phys. Ed.*, **B23**(4), 175, 1984.
55. D. Dietrich, *Prog. Org. Coat.*, **9**, 281, 1981.
56. D. C. Lee, R. A. Register, C. Z. Yang, S. L. Cooper, *Macromolecules*, **24**, 2576, 1991.
57. S. A. Visser, S. L. Cooper, *Macromolecules*, **24**, 2576, 1991.
58. S. A. Visser, S. L. Cooper, *Polymer*, **33**(5), 920, 1992.
59. H. Park, D. Kim, K. Hwang, B. Yoon, J. Wu, J. Park, H. Hahm, W. Im, *J. Appl. Polym. Sci.*, **80**, 2327, 2001.
60. T. Campbell, V. Foldi, *Macromol. Synth.*, **3**, 609, 1968.

61. K. Wagner, K. Findeisen, W. Schafer, W. Dietrich, *Angew. Chem.*, **93**, 855, 1981.
62. N. Lamba, K. Woodhouse, S. Cooper, *Polyurethanes in Biomedical Applications*, CRS press 1998.
63. D. I. Bernstein, A. Cartier, J. Cote, J. L. Malo, L. P. Boutlet, M. Wanner, J. Milot, *Am. J. Respir. Crit. Care Med.*, **166**, 445, 2002.
64. E. C. Mapp, A. A. Fryer, N. De Marzo, N. D. Marzo, V. Pozzato, M. Padoan, P. Boschetto, *J. Allergy Clin. Immunol.*, **109**, 867, 2002.
65. E. L. J. Van Rensen, P. S. Hiemstra, K. F. Rabe, P. J. Sterk, *Am. J. Respir. Crit. Care Med.*, **165**, 1275, 2002.

4 EXPERIMENTAL

4.1 Introduction

Segmented polyurethanes are block copolymers with alternating soft and hard blocks that generally separate into two phases or domains due to their structural differences. Hard domains play the role of physical crosslinks and act as high modulus fillers, while the soft segments provide extensibility [1-2]. The ratio of soft to hard blocks or segments has a significant effect on the physical properties and appearance of a polyurethane. Polyurethanes with a 70wt% soft segment content (SSC) are generally soft thermoplastic rubbers whereas PUs with 50wt% SSC are generally hard rubbers [3]. This difference is due to the PUs with a 70wt% SSC having globular hard domains dispersed in the soft segment matrix, whereas co-continuous phases and even lamellar morphology have been postulated for PUs with a 50wt% SSC. In this study, polyurethane dispersions were prepared with a 70wt% SSC to ultimately form a thin thermoplastic coating for paperboard.


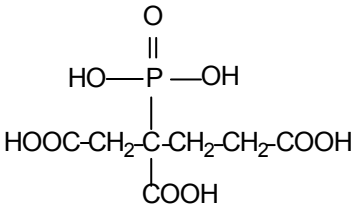
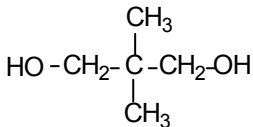
The segmented PU emulsions were prepared by firstly synthesizing a linear polyester-based polyol as a precursor, and then using this to synthesize the PU emulsion. The polyester-based polyols were synthesized from a selection of four monomers, namely adipic acid (AA), neopentyl glycol (NPG), 1,4-cyclohexane dicarboxylic acid (CHDCA) and 2-phosphonobutane 1,2,4-tricarboxylic acid (PBTCA). The polyester was based on AA and NPG as the primary monomers, while CHDCA and PBTCA formed the secondary monomers. A maximum of 15% CHDCA and 10% PBTCA was used in the polyol synthesis. The purpose of using the CHDCA monomer was to increase the hydrophobicity of the polyol, while the PBTCA was added to further enhance the desired properties, especially in terms of barrier properties. The phosphorous-containing monomer (PBTCA) was incorporated into the soft segment polyol [4,5], while hydroxyl terminated phosphorous-containing monomer can also be reacted as a chain extender during urethane formation as shown by T. Chang *et al.* [6]. The phosphorous monomer (PBTCA) selected contained reactive acid groups, which would thus be incorporated into the polyol.

4.2 Synthesis of polyols

4.2.1 Raw materials

The raw materials used for the synthesis of the polyols are tabulated in Table 4.1.

Table 4.1: Monomers used to prepare the polyols

Raw materials for polyol synthesis	Form	Source
1,4-Cyclohexane dicarboxylic acid (CHDCA) 	White Powder	Eastman Chemicals
Adipic acid (AA) $\text{HOOC}-(\text{CH}_2)_4-\text{COOH}$	White Powder	ICI
2-Phosphonobutane-1,2,4- tricarboxylic acid (PBTCA) 	50% clear watery solution	Bayer
Neopentyl glycol (NPG) 	White Flakes	Perstop Polyols

All the monomers were used as supplied. The phosphate-containing monomer (PBTCA), supplied in a 50% water solution, could also be added as a solid by first removing the water under vacuum at about 100°C, resulting in a solid, hygroscopic, glassy material.

4.2.2 Experimental setup

The following equipment was used to synthesize the polyols:

- Four-neck 1-liter glass reactor
- Thermocouple
- Mechanical stirrer
- N₂ gas
- Teflon seals and gaskets
- Heating mantle
- Temperature control unit
- Reflux condenser

4.2.3 Preparation of polyol

The reactor was charged with NPG, which was then melted at about 120 to 140°C. This was followed by the addition of the acids CHDCA, AA, and then PBTCA, under slow agitation. The reactor was sealed and the temperature was increased in the following increments to 230°C: 120°C for 60 min, 135 to 140°C for 60 min, 155 to 160°C for 40 min, and 180 to 185°C for 20 min. Once the reaction temperature reached 230°C, the agitation speed was increased and xylene was added until refluxing commenced. The reaction mixture was stirred under reflux for about 2 to 3 hours, until the desired acid value was obtained. The progress of the reaction was monitored by measuring the acid value obtained by acid-base titrations (see Section 4.3.1). As the reaction neared its end-point, the agitation speed was increased to increase the interaction between the reactants. The polyester was cooled to 80°C, dried and degassed under vacuum for 48 hours, and then stored. Before use in urethane synthesis, the polyester was further dried in a vacuum oven at 80°C for 12 to 24 h to remove any traces of moisture.

Water obtained as a by-product from the polyester condensation reaction was used to check any glycol loss during the reaction. If glycol was lost, it was replaced.

4.2.4 Polyol formulation

The following polyols were prepared, as shown below in Table 4.2, of which the acid and hydroxyl values were measured in mg KOH/g (see Section 4.3.2), viscosity was

measured in mPa.s using the Gardner-Holtz test method, and molecular mass was measured in g/mol using GPC (see Section 7.5).

Table 4.2: Polyol formulations

Monomers	SS 0000 (Mass %)	SS 0600 (Mass %)	SS 0605 (Mass %)	SS 0610 (Mass %)	SS 0615 (Mass %)
NPG	53.00	51.90	51.60	51.30	51.00
AA	47.00	42.10	37.40	32.70	28.00
PBTCA	0.00	6.00	6.00	6.00	6.00
CHDCA	0.00	0.00	5.00	10.00	15.00
Analytical values					
COOH-value (mg KOH/g)	2.8	3.8	3.9	3.8	4.0
OH-value (mg KOH/g)	244	243	245	240	247
Ave. Molecular mass (Mn)	980.2	1090	1081	979	1089
Polydispersity (Mn/Mw)	2.096	2.139	2.172	2.092	2.197
Viscosity (mPa.s) @ 25°C, in 20% NMP	380	500	507	590	931
Monomers					
Monomers	SS 0800 (Mass %)	SS 0805 (Mass %)	SS 0810 (Mass %)	SS 0815 (Mass %)	
NPG	51.60	51.30	51.00	50.70	
AA	40.40	35.70	31.00	26.30	
PBTCA	8.00	8.00	8.00	8.00	
CHDCA	0.00	5.00	10.00	15.00	
Analytical values					
COOH-value (mg KOH/g)	3.9	3.8	3.7	4.0	
OH-value (mg KOH/g)	244	243	241	248	
Ave. Molecular mass (Mn)	1192	1165	1168	1208	
Polydispersity (Mn/Mw)	2.501	2.352	2.505	2.627	
Viscosity (mPa.s) @ 25°C, in 20% NMP	694	630	885	1642	
Monomers					
Monomers	SS 1000 (Mass %)	SS 1005 (Mass %)	SS 1010 (Mass %)	SS 1015 (Mass %)	
NPG	51.20	50.90	50.60	50.30	
AA	38.80	34.10	29.40	24.70	
PBTCA	10.00	10.00	10.00	10.00	
CHDCA	0.00	5.00	10.00	15.00	
Analytical values					
COOH-value (mg KOH/g)	3.9	4.0	3.8	4.0	
OH-value (mg KOH/g)	243	245	244	250	
Ave. Molecular mass (Mn)	1471	1300	1308	1390	
Polydispersity (Mn/Mw)	3.531	2.864	2.702	3.410	
Viscosity (mPa.s) @ 25°C, in 20% NMP	1290	1070	1666	2270	

4.3 Calculations

The calculations necessary to monitor the synthesis of both the polyesters and urethanes are explained below. They include acid- and hydroxyl-value determinations for the polyesters, and also NCO-value determinations for the urethanes.

4.3.1 Acid-value determination

The unreacted carboxylic acid content was visually determined by acid-base titration, using 0.5*N* potassium hydroxide (KOH) and phenolphthalein as indicator.

The procedure [7] involved weighing a small mass of the polyol (about 2 g) into a conical flask and adding 25 ml of a neutral ethylene acetate solution. The mixture was then heated and vigorously stirred until the sample dissolved, after which it was titrated with 0.5*N* KOH, using phenolphthalein as an indicator.

The acid number (in mg KOH per g polyol) was calculated by the following formula:

$$\text{Acid number} = (56.1 VN) / Wt \quad (4.1)$$

Where:

V : The volume (in ml) of KOH consumed in the titration

N : Normality of the KOH titrant

Wt : Weight (in grams) of the polymer sample.

4.3.2 Hydroxyl-value determination

The hydroxyl value of polymers is generally determined by acetylation of the polymer sample with acetic anhydride in a pyridine solution [7]. The excess anhydride is decomposed by water, and the resulting acetic acid formed in both the hydrolysis and the acetylation process is titrated with a standard alkali solution using phenolphthalein as indicator.

The acetylating procedure involved weighing a small mass of the polyol (about 2 g) into a conical flask and adding 20 ml of a 1:3 mixture of acetic anhydride and pyridine, in the presence of ethyl acetate, and reacting for 2 hours at 105°C. This was followed by hydrolysis with hot water.

Thereafter, the flask was connected to a reflux condenser and the contents heated to 105°C for about 1 to 2 hours to complete dissolution of the material, while occasionally shaking the flask. On completion of the reaction, the content was homogenized with 25 ml of n-butanol. The acid formed was then titrated with 0.5*N* KOH, using phenolphthalein as indicator.

The hydroxyl number (in mg KOH per g polymer) was calculated by the following formula:

$$\text{Hydroxyl number} = [56.1 (V_1 - V_2) N] / \text{Wt} + \text{Acid value} \quad (4.2)$$

Where:

V_1, V_2 : The volume (in ml) of 0.5*N* KOH used for titration of the sample and the blank, respectively

N : Normality of the KOH titrant

Wt : Weight (in g) of the polymer sample.

4.3.3 NCO-value determination

Isocyanate groups can be quantitatively determined by either volumetric or spectroscopic techniques. The volumetric determination involves treating the sample with excess amine, followed by a back-titration of the excess amine with hydrochloric acid solution [6]. The volumetric procedure involves weighing about 0.5 g of the pre-polymer and 25 ml of toluene into a conical flask, and allowing the mixture to dissolve completely. The solution is then treated with 25 ml of 0.1*N* *n*-butylamine in toluene, and shaken for 15 minutes. This is followed by the addition of 100 ml of isopropyl alcohol and 4 to 6 drops of 0.1% bromophenol blue indicator solution, followed by the titration with 0.1*N* HCl.

The isocyanate group content (%) is calculated by the following formula:

$$\% \text{ [NCO]} = [4.202 (V_1 - V_2) N] / Wt \quad (4.3)$$

Where:

V_1, V_2 : The volume (in ml) of the HCl consumed in the titration of the blank and the sample, respectively

N : Normality of the KOH titrant

Wt : Weight (in g) of the polymer sample.

The NCO group can also be determined by Fourier transform infrared spectroscopy. This is done by measuring the relationship between the intensity of the band at 2270 cm^{-1} (characteristic of the isocyanate group, see Section 6.5) and that of the band at 2950 cm^{-1} (CH stretching vibrations, assumed as internal reference). This method is rapid and simple, but a calibration curve has first to be prepared. The infrared spectrum obtained is however useful in showing the presence of NCO groups at 2270 cm^{-1} .

4.4 Synthesis of polyurethanes

4.4.1 Raw materials

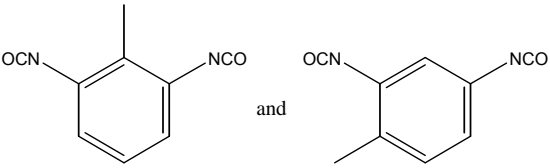
The raw materials used for the synthesis of the PUs are summarized in Table 4.3 below. It is very important to eliminate all traces of moisture when making the polyurethane.

Thus the reactants were dried as follows prior to use:

- NMP was dried over a 3Å molecular sieve
- Polyol was dried and degassed overnight at 80°C in a vacuum oven

The other reactants were all used as received.

Table 4.3: Raw materials used to prepare PUs

Raw materials	Form	Source
Dimethylolpropionic acid (DMPA) $\begin{array}{c} \text{CH}_3 \\ \\ \text{HO-CH}_2\text{-C-CH}_2\text{-OH} \\ \\ \text{COOH} \end{array}$	White powder	Perstop Polyols
Toluene diisocyanate (TDI)  2,6-TDI (20%) 2,4-TDI (80%)	Liquid at room temperature	Bayer
Polyester macro-diol HO-----OH	Viscous polymer	Experimentally synthesized
Triethylamine (TEA) $(\text{CH}_3\text{-CH}_2)_3 \text{N}$	Clear liquid	BASF

4.4.2 Experimental procedure

Polyurethanes can be polymerized by either a one-shot or pre-polymer process. The one-shot process entails addition of all the monomers in one step, whereas in the pre-polymer process the monomers are added in intervals. The pre-polymer process has more advantages than the one-shot process, as more control over the reaction is possible, resulting in a smaller molecular mass distribution and better polymer morphology.

The PU was synthesized using the pre-polymer process; it involved:

- Synthesis of the urethane polymer
- Neutralization of the pendant carboxylic acid groups
- Dispersion of the PU-ionomer into water

4.4.2.1 Synthesis of the urethane polymer

The first step in the synthesis of the urethane polymer is the synthesis of the hard segment. The reactor was charged with TDI and DMPA, and then placed in a waterbath, after which N₂-gas and slow agitation were applied. An exothermic reaction resulted as the NMP was added to the reaction mixture at room temperature. After 20 minutes, ethylene glycol (EG) chain extender was added to the reaction through a dropping funnel, which also resulted in an exothermic reaction. The reaction mixture was kept at a maximum temperature of 55 to 65°C.

The second step involved the addition of the soft segment. At this stage the waterbath was removed and replaced with a heating mantle. The polyester was softened and degassed at 80°C for 6 to 12 hours before use. It was then pre-mixed with NMP to reduce its viscosity, then added to the reaction mixture, which was at about 50°C. The reaction was kept at 60 to 65°C for 90 minutes, and then the temperature was increased to between 70 to 80°C for 30 minutes.

4.4.2.2 Neutralization of the pendant carboxylic acid groups

The third step involved the neutralization of the pendant acid groups of the DMPA. The calculated amount of the neutralizing agent (triethylamine) was added dropwise to the fully reacted polyurethane solution at 55 to 60°C and the mixture stirred for about 15-30 minutes to yield the anionomer. The amount of the neutralizing agent needed was calculated using Equation 4.4:

$$\text{Mass of neutralizing agent} = \frac{m \times (\text{A.V}) \times (\text{E.A})}{5.61 \times 1000} \quad (4.4)$$

Where:

- m: Mass of the solid polymer
- A.V: Acid value of the solid polymer
- E.A: Equivalent weight of the neutralizing agent

4.4.2.3 Dispersion of PU-ionomer into water

The fourth step involved the emulsification/dispersion of the PU-ionomer into water. The reaction mixture was cooled to about 50 to 55°C, then the water was added under high shear over 15 to 30 minutes. The use of warm water was preferred, as it was then easier to disperse the PU-ionomer.

The emulsification or dispersion mechanism can be explained using conductivity [8-10] or viscosity measurements [4,5,11-14], which can be described as follows:

- (i) As water is added to the organic PU ionomer solution, its viscosity first decreases to a minimum owing to a reduction of the ionic association.
- (ii) The viscosity then increases owing to a swelling of the hydrophilic segments on increased aggregation of the hydrophobic chain segments, at which point phase separation starts.
- (iii) Addition of more water produces turbidity, an indication that the formation of a dispersed phase has begun, subsequently leading to a drop in viscosity due to the completion of aggregation of hydrophobic segments in a continuous interpenetrating water plasticizing hydrophilic zone.

(iv) Finally, the viscosity levels off as the ionic groups are situated on the particle surface, so stabilizing its structure and with the hydrophobic segments incorporated within the particle.

4.4.3 Polyurethane reaction scheme

A schematic representation of the PU synthesis is shown in Figure 4.1 below.

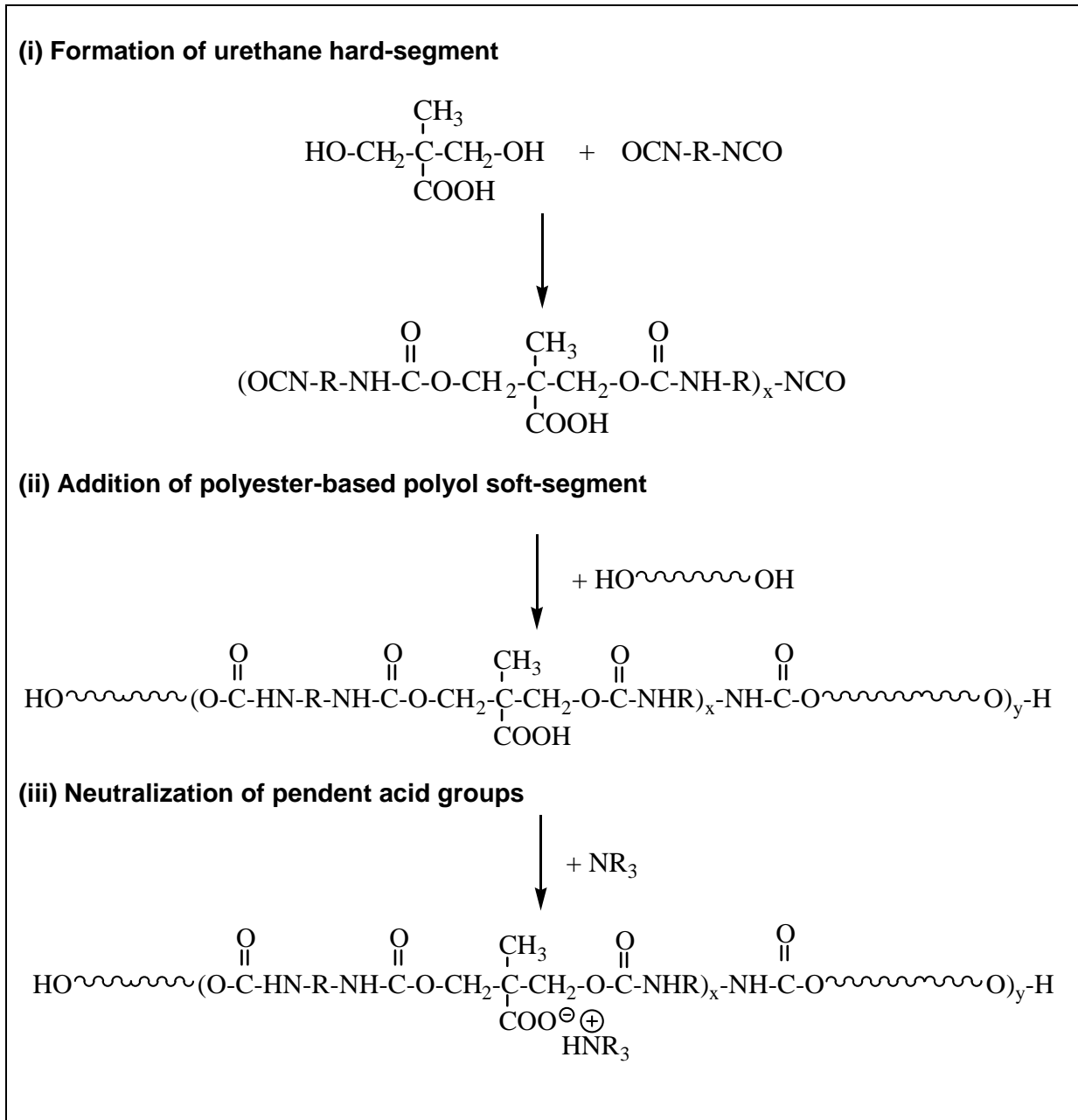


Figure 4.1: PU synthesis scheme

4.5 Polyurethane-wax composites

Urethanes have an advantage in that they are recyclable polymers; hence a very good candidate material for recyclable paper. However, PUs are not fully hydrophobic and do pass moisture vapour (this is measured in terms of MVTR, meaning moisture vapour transmission rate; and the technique is presented in Appendix 4).

Waxes are generally added to emulsion-based paper coatings to enhance certain properties such as MVTR and blocking. Wax coatings on their own cause problems during the paperboard recycling process, in which they render the paperboard un-recyclable. Thus, to eliminate recycling problems, the wax content should be kept under 20% of the total coating mixture.

A series of waxes obtained from Schumann-Sasol were screened as a two-component composite with a PRP urethane (see Appendix 3). Optimum MVTR results were obtained when the PRP-wax composites contained 15% wax C78. Composite performances were evaluated in terms of MVTRs, measured under tropical conditions: 38°C and 90% relative humidity (RH) over a period of 24 hours.

The characteristic properties of wax C78 are listed in Appendix 2. The SEM images show the flaky structure of the polyurethane matrix in which 15% wax C78 is incorporated. These flaky, hydrophobic wax particles are very important for imparting anti-blocking properties into the coating mixture.

4.6 PU-filler composites

4.6.1 Introduction

The effect of filler incorporation into the PU matrix was investigated by using both nano and micro-fillers. Nano-composites are a new class of materials showing better thermal, mechanical and barrier properties than micro-composites, due to their much better interfacial interaction between the nano-particle and the polymer matrix, compared to that of micro-particles and the polymer matrix. Nano-composites based on clay and layered silicates have been widely investigated [15-17]. The most commonly used layered silicates are montmorillonite, saponite and hectorite [18]. Natural montmorillonite has a layered structure made up of disc-shaped silicate layers of approximately 100 nm in diameter and 1 nm in thickness [19]. Natural montmorillonite is hydrophilic, but it can take on a hydrophobic character via ion-exchange reactions with various organic cations, such as alkylammonium cations [20-23].

The shape and morphology of the nano-filler is an important factor, one which can markedly improve properties of nanocomposites such as mechanical, thermal, optical, barrier and permeability [24-30]. Anisotropic nano-particles can be incorporated into polyamide films to increase gas permeability, which is important for food packaging. For barrier coatings, thin platelet fillers are added to polymers to increase resistance to oil and grease. Nano-platelets can be obtained from smectic montmorillonite [31]. In this study, composite coating mixtures were prepared from hydrophobically modified montmorillonite clays and the synthesized polyurethane matrix.

Micro-composites were experimentally prepared by incorporating micro-fillers such as kaolin clay, barium sulphate and talc into the synthesized polyurethane matrix, while nano-composites were prepared from two hydrophobically modified montmorillonite clays.

4.6.2 Type of fillers

The type of fillers used for incorporation into the PU-matrix are summarized in Table 4.4.

Table 4.4: Fillers used for incorporation into PU-matrix

Raw materials	Particle size range	Form	Source	Additional information
NC 15A	Nano	White Powder	Southern Clay Products	See also Table 8.3
NC 93A	Nano	White Powder	Southern Clay Products	See also Table 8.3
NC 30B	Nano	White Powder	Southern Clay Products	See also Table 8.3
	Kaolin Clay	Micro	White Powder	Serina
	BaSO ₄	Micro	White Powder	ICIESSE S.p.A Milan - Italy
	Talc	Micro	White Powder	Micronised Products

4.6.3 Incorporation of fillers into the PU-matrix

Fillers were incorporated into the PU matrix via the following methods:

- Dry or wet filler addition into PU matrix
- Filler added directly into PU matrix either before or after PU emulsification
- Nano-fillers were first dispersed into polyester, and then added to PU synthesis
- Nano-fillers were added to isocyanate during polyurethane synthesis

The wetting of fillers before addition helps to exfoliate (break-up) filler agglomerates, as in the case of the nano-clays. This was done at room temperature, using acetone, MEK or NMP as wetting agents. Also, the hydrophobic fillers blended more easily with the PU matrix when wetted first, especially if added after PU emulsification.

The idea of adding fillers before PU emulsification was to determine whether the filler particles could be encapsulated within the PU emulsion particle. The advantage of this would be the formation of a stable polymer-filler emulsion system without the use of surfactants, soaps and stabilising agents, which could lead to destabilisation of the PU emulsion particles and even pinhole formation during the coating process [32]. However, since the PU particle size was in the nano-range, only nano-particle fillers such as the nano-clays could be encapsulated.

Nano-fillers were also dispersed into the polyester, and then added to the PU synthesis. This was done to investigate its efficiency on the exfoliation process of the nano-clays into the polyurethane matrix.

Lastly, nano-filler was added to the reactive isocyanate group during polyurethane synthesis to investigate its efficiency on the exfoliation process of the nano-clay. For this purpose, nano-clay N30B was used; it contained an amine ion-exchanged group with two OH-groups (see Table 8.3).

4.6.4 Formulation

PU filler mixtures were prepared both with and without wax C78 inclusion. The 15% wax was calculated as a weight% with respect to the TSC of the PU-wax mixture, whereas the % filler, as shown below in equation 4.5, was calculated as a weight% with respect to the TSC of the whole mixture.

$$\text{Filler}_{\text{Dry mass}} = \frac{[\% \text{ Filler} / 100] \times [\text{PU}_{\text{Dry mass}} + \text{Wax}_{\text{Dry mass}}]}{1 - [\% \text{ Filler} / 100]} \quad \dots\dots\dots (4.5)$$

4.7 References

1. Z. S. Petrovic, J. Ferguson, *Prog. Polym. Sci.*, **16**, 695, 1991.
2. G. Oertel (Ed.), *Polyurethane Handbook*, 2nd Ed., London, Elsevier, 1991.
3. Z. S. Petrovic, I. Javni, *J. Polym. Sci. B Polym. Phys.*, **27**, 545, 1989.
4. K. Mequanint, *Polyurethane Dispersions: Synthesis, characterization and application for primers in coil coating*, MSc Dissertation, University of Stellenbosch, 1997.
5. K. Mequanint, *Self-assembling metal coatings from phosphated and silicone-modified polyurethane dispersions*, PhD Dissertation, University of Stellenbosch, 2001.
6. T. Chang, W. Shen, Y. Chui, H. So, *Polym. Degrad. Stab.*, **49**, 353, 1995.
7. J. Urbanski, E. Horwood, *Handbook of analysis of synthetic polymers and plastics*, Halsted Press, Chichester, New York, 1977.
8. J. L. Salager, *Encyclopedia of Emulsion Technology*, P. Becker Ed., **Vol. 3**, Dekker, New York, 1998.
9. B. W. Brooks, H. N. Richmond, *Colloids Surf.*, **58**, 131, 1991.
10. M. Zerfa, S. Sajjadi, B. W. Brooks, *Colloids Surf. A Physiochem. Eng. Asp.*, **155** (2), 323, 1999.
11. D. Dieterich, W. Kerberle, H. Wtt, *Angew Chem. Int. Ed.*, **9**, 40, 1970.
12. O. Lorenz, H. Hick, *Angew Makromol. Chem.*, **72**, 115, 1978.
13. C. H. Yang, S. M. Lin, T. C. Wen, *Pol. Eng. Sci.*, **35** (8), 722, 1995.
14. L. M. Saw, B. W. Brooks, K. J. Carpenter, D. V. Keight, *J. Colloid Interface Sci.*, **257**, 163, 2003.
15. B. K. G. Theng, *The Chemistry of Clay-Organic Reactions*, Wiley, New York, 1974.
16. M. Ogawa, K. Kuroda, *Bull. Chem. Soc. Jpn*, **70**, 2593, 1997.
17. W. J. Choi, S. H. Kim, Y. J. Kim, S. C. Kim, *Polymer*, **45**, 6045, 2004.
18. M. Alexandre, P. Dubois, *Materials Sci. and Eng.*, **28**, 1, 2000.
19. L. Zhu, X. Ren, S. Yu, *Environ. Sci. Technology*, **32**, 3374, 1998.
20. S. A. Boyd, S. Shaobai, J. F. Lee, M. M. Mortland, *Clay Miner.*, **36**, 125, 1988.
21. J. F. Lee, M. M. Mortland, C. T. Chiou, D. E. Kile, S. A. Boyd, *Clay Miner.*, **38**, 113, 1990.
22. J. F. Lee, C. K. Lee, L. C. Juang, *J. Colloid Interface Sci.*, **217**, 172, 1999.
23. N. M. Soule, S. E. Burns, *J. Geotech. Geoenviron. Eng.*, **127**, 363, 2001.

24. Y. Kojima, A. Usuki, M. Kawasumi, A. Okada, Y. Fukushima, T. Kurauchi, O. Kamigaito, *J. Mater. Res.*, **8**, 1185, 1993.
25. P. B. Messersmith, E. P. Giannelis, *J. Polym. Sci. A. Polym. Chem.*, **33**(7), 1047, 1995.
26. E. P. Giannelis, *Adv. Mater.*, **8**, 29, 1996.
27. C. Zilg, R. Thomann, R. Mulhaupt, J. Finter, *Adv. Mater.*, **11**(1), 49, 1999.
28. P. C. LeBaron, Z. Wang, T. J. Pinnaviai, *Appl. Clay Sci.*, **15**, 11, 1999.
29. M. Alexandre, P. Dubois, *Mater. Sci. Eng.*, **28**, 1, 2000.
30. K. J. Yao, M. Song, D. J. Hourston, D. Z. Luo, *Polymer*, **43**(3), 1017, 2002.
31. S. B. Hendricks, *J. Geol.*, **50**, 276, 1942.
32. J. C. Padget, *J. Coat. Technol.*, **66** (839), 84, 1994.

5 ANALYTICAL TECHNIQUES

5.1 Introduction

The following analytical techniques were used to characterize the polymers during and after polyurethane synthesis:

- Fourier Transform Infrared spectroscopy (FTIR)
- Nuclear Magnetic Resonance spectroscopy (NMR)
- Gel Permeation Chromatography (GPC)
- Particle Size Analysis
- Transmission Electron Microscopy (TEM)
- Scanning Electron Microscopy (SEM)
- Viscosity
- Moisture Vapor Transmission Rate (MVTR)
- Blocking Test
- Dynamic Mechanical Analysis (DMA)
- Thermogravimetric Analysis (TGA)
- Differential Scanning Calorimetry (DSC)
- Static Contact Angle analysis (SCA)

5.2 Fourier transform infrared (FTIR) spectroscopy

The emergence and disappearance of functional groups during PU synthesis [1-3] was followed and characterized by FTIR analysis. The NCO content during PU synthesis was determined by extracting a polymer sample from the reactor vessel and dissolving it in MEK solvent. The sample was then run against a MEK background between sodium chloride (NaCl) discs on a Perkin Elmer 1650 instrument at 4 scans. This was a fast way to check if any NCO groups were still present before the addition of water. Other infrared analyses were performed on a Perkin Elmer Paragon 1000 FTIR instrument at 128 scans, using a photo-acoustic cell (PAS), so eliminating sample preparation.

5.3 Nuclear magnetic resonance (NMR) spectroscopy

NMR analyses were done using a Varian VXR 300MHz Spectrometer and a Varian ^{Unity} Inova 600MHz NMR Spectrometer, with chloroform-*d* as the primary solvent. The other deuterated solvent used was water-*d*. The PBTCA was received as a 50% water mixture, to which 10% water-*d* was added for NMR analysis. This was done to minimize H-interaction between PBTCA-monomers, and to check its purity. NMR analysis includes ¹H, ¹³C-APT (APT = Attached Proton Test), ¹³C and ³¹P spectra.

5.4 Gel permeation chromatography (GPC)

GPC analyses were done on a Waters instrument using a PL mixed E 3 μm column that could detect molecular masses up to 30 000, in conjunction with an evaporative light scattering detector (ELSD), eliminating solvent peaks. The samples to be analyzed were dissolved in THF at room temperature, of which 100 μl was injected at a flow rate of 1 ml/min, at a column temperature of 30°C. The molecular masses of the samples were correlated to polystyrene standards.

5.5 Particle size analysis

A Zetasizer 1000HSa light scattering instrument from Malvern Instruments was used for particle size analysis of the polyurethane dispersions. The instrument was calibrated using a nano-standard of 220 nm particle size, before urethane samples were run.

5.6 Transmission electron microscopy (TEM)

Analyses were done at the Electron Microscopy Unit at UCT, Cape Town; a LEO 912 instrument at 120 kV and Analysis Software from SIS (Soft Imaging Software) were used.

PU samples were first embedded in an epoxy-based Spurr's resin, and then dried at 80°C for 24 hours. TEM samples were prepared by microtoming the dried embedded samples into 100 nm slices using a Reichert Ultracut S instrument, which were then picked up on 200 to 300 mesh copper grids.

Electron microscopy was also used for particle size analysis, whereby the PU dispersion was first reduced to a viscosity of 25 to 50 mPa.s, and then stained with a 2% solution of methylamine tungstate of neutral pH.

5.7 Scanning electron microscopy (SEM)

Scanning electron microscopy (SEM) [4-6] was used to evaluate surface characteristics of the paperboard-coated PU films. Emphasis was put on surface defects such as pinholes and weak fiber coverage. A SEM instrument model ABT-60 from Topcon, using *Analysis Image Capturing* software from *Soft Imaging System*, was used. The images were obtained at 7kV at a working distance of 10 mm, using secondary electron imaging.

Sample preparation included cutting the dry coated-paperboard into small blocks of about 1 cm², then coating them with a thin micro-layer (± 1 to 2 molecular layers) of 24 carat gold. Gold plating was done to increase the sample's electron transferring ability, so as to obtain clearer images.

5.8 Viscosity

The viscosities of the polyesters were determined by the Garden-Holts test method at 25°C and 80% solids content using NMP as solvent, and then converted to mPa.s via conversion charts.

The viscosities of the polyurethane dispersions were determined at ambient temperature using a Brookfield viscometer, model LVT.

5.9 Moisture vapor transmission rate (MVTR)

A Heraeus Vötsch humidity cabinet, Type VTRK 300, was used to determine the moisture vapor transmission rate of coated paper. The method employed was based on the method described in detail in Appendix 4. The experiments were performed under tropical conditions, i.e. at 38°C and 90% relative humidity.

Sample preparation:

Emulsion coating mixtures were applied to Mondi cartonboard by means of a threaded coating bar, equipped with end-fittings to prevent it from rolling during the coating

process. The coating was applied to the paperboard at an average coating speed of 0.067 m/s, after which it was dried in an oven at between 110 to 130°C for 30 to 90 seconds. Discs were pressed out of the coated paperboard, from which the MVTR, degree of blocking and average coating weight were determined, as described in Appendices 3, 4 and 5 respectively.

5.10 Blocking test

The blocking test is critical to determine whether a pallet of coated paperboard sheets will stick to each other or not as a result of the applied coating. The test involves putting a 28 kg weight on a stack of coated paperboard discs, and applying ± 0.5 bar pressure over a 24 hour period at ambient temperature ($\pm 22^\circ\text{C}$). After 24 hours, the samples were removed and carefully pulled apart, notifying the amount of sticking (blocking) that occurred. (See Appendix 5 for detailed test method and interpretation of various blocking levels.)

5.11 Dynamic mechanical analysis (DMA)

The mechanical properties of a material, such as the modulus (stiffness) and damping (energy dissipation), are measured by dynamic mechanical analysis [7-10] as a function of temperature and frequency under oscillatory stress. Typical materials that are analyzed by DMA analysis include coatings, adhesives, elastomers, composites, ceramics, metals, and viscous thermoset liquids. Typical properties obtained from the DMA technique, are listed in Table 5.1 below:

Table 5.1: Typical properties obtained from DMA analysis

Modulus	Rate of cure
Glass transition temperature (T _g)	Degree of cure
Gelation	Impact resistance correlations
Viscosity	Sound absorption correlations
Damping characteristics	Polymer morphology

The DMA samples were prepared by first drying the PU emulsions in Teflon holders overnight at 50°C, followed by ± 6 hours at 120°C. The dried films were analyzed on a Perkin Elmer DMA 7e instrument, coupled to a thermal analyzer controller model TCA 7/DX, using a 1-mm probe and N₂ carrier gas set at a pressure just below 200 kPa.

5.12 Static contact angle (SCA) determination

SCA analysis was done by placing a 1 µl droplet of de-ionized water onto the coated paperboard surface, then taking a picture (see Figure 5.1) using an Emoskop magnifying lens (see Figure 5.2), and a Fujifilm digital camera at full zoom, model FinePix 4700zoom. The 50-mm long Emoskop lens consists of a 5x magnifier middle piece, and a 10x magnifier bottom piece, as shown in Figure 5.2b. The top and middle pieces were used, which combine to give an adjustable 2.5x telescope.

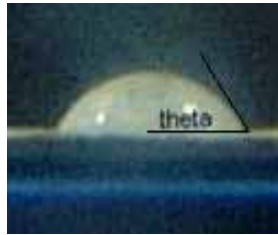


Figure 5.1: SCA image of de-ionized water droplet on coated paperboard surface



Figure 5.2: 50-mm long Emoskop lens set used for SCA measurements

This process was repeated 8 to 10 times per sample. The static contact angle between the droplet and coated paperboard surface was calculated by measuring the height and the length of the droplet, as shown below in equation 5.1. The formula used was:

$$\begin{aligned} \text{Tan } (\Theta/2) &= 2h/\ell \\ \Theta &= 2 \times \tan^{-1}(2h/\ell) \end{aligned} \quad \dots\dots\dots (5.1)$$

Where, h = height of droplet
 ℓ = length of droplet
 Θ (theta) = static contact angle in degrees

5.13 Thermogravimetric analysis (TGA)

Thermogravimetric analysis (TGA) [8,9,11,12] measures the percentage weight change of a material as a function of time or temperature in a controlled atmospheric environment. The measurements are primarily used for determining material compositions and to predict their thermal stability up to 1000°C. The dried PU films were analyzed on a TGA-7 instrument from Perkin Elmer.

5.14 Differential scanning calorimetry (DSC)

Differential scanning calorimetry [8,9,13,14] measures heat flow associated with transitions in materials as a function of time and temperature. It is used to characterize polymers and organic materials. The dried PU films were analyzed on a Pyris 1 instrument from Perkin Elmer. Typical glass transition temperatures and wax melting temperatures were obtained from DSC analyses.

5.15 References

1. B. Elvers, S. Hawkins, W. Russey, *Ulmann's Encyclopedia of Industrial Chemistry*, **Vol. B5** (page 429-469), VCH Publishers, New York, 1993.
2. D. J. David and H. B. Staley, *Analytical Chemistry of the Polyurethanes*, **Vol. XVI**, Part III, Wiley-Interscience, 1969.
3. K. D. Berlin, G. M. Blackburn, J. S. Cohen, D. E. C. Corbridge and D. M. Hellwege, *Topics in Phosphorus Chemistry*, **Vol. 6**, Wiley-Interscience, New York, 1969.
4. B. Elvers, S. Hawkins, W. Russey, *Ulmann's Encyclopedia of Industrial Chemistry*, **Vol. B6** (page 263-278), VCH Publishers, New York, 1993.
5. J. I. Goldstein, D. E. Newbury, P. Echlin, D. C. Joy, A. D. Romig, Jr., C. E. Lyman, C. Fiori, E. Lifshin, *Scanning Electron Microscopy and X-Ray Microanalysis*, Plenum Press, New York, 1992.
6. P. J. Goofhew, J. Humphreys, R. Beanland, *Electron Microscopy and Analysis*, 3rd Edition, Taylor and Francis, London, 2001.
7. B. Elvers, S. Hawkins, W. Russey, *Ulmann's Encyclopedia of Industrial Chemistry*, **Vol. B6** (pages 9-10), VCH Publishers, New York, 1993.
8. R.T. Bailey, A. M. North, R. A. Pethrick, *Molecular motion in high polymers*, Oxford University Press Inc., New York, 1981.

9. J. W. S. Hearle, *Polymers and their properties*, Ellis Herwood Ltd., Chichester, 1982.
10. A. Klingsberg, R. Piccininni, *Encyclopedia of Polymer Science and Engineering*, **Supplement Vol.** (pages 715-723), Wiley-Interscience, New York, 1986.
11. B. Elvers, S. Hawkins, W. Russey, *Ulmann's Encyclopedia of Industrial Chemistry*, **Vol. B6** (pages 1-8), VCH Publishers, New York, 1993.
12. A. Klingsberg, R. Piccininni, *Encyclopedia of Polymer Science and Engineering*, **Supplement Vol.** (pages 692-701), Wiley-Interscience, New York, 1986.
13. B. Elvers, S. Hawkins, W. Russey, *Ulmann's Encyclopedia of Industrial Chemistry*, **Vol. B6** (pages 4-8), VCH Publishers, New York, 1993.
14. A. Klingsberg, R. Piccininni, *Encyclopedia of Polymer Science and Engineering*, **Supplement Vol.** (pages 702-711), Wiley-Interscience, New York, 1986.
15. S. Wu, *Polymer Interface and Adhesion*, Dekker, New York, p. 257, 1982
16. R. E. Johnson, Jr., and R. H. Dettre, *Surface Colloid Sci.*, **2**, 85, 1969.
17. W. Adamson, *Physical Chemistry of Surfaces*, Wiley-Interscience, New York, 1982.

6 CHARACTERIZATION OF POLYURETHANE DISPERSIONS

6.1 Introduction

The behavior of coatings during application is a critical aspect that must be considered in the development of coating formulations. The most important characteristic that governs a waterborne coating's behavior during application is rheology, of which viscosity is the most commonly used parameter in the paint industry. Studies on viscosity measurements of waterborne polyurethane dispersions are well documented in literature [1-7]. Polyurethane dispersions are usually synthesized in an organic solvent in the absence of water, up to the ionomer stage, due to the isocyanate being water sensitive. Afterwards the polyurethane ionomer is dispersed in water to form the polyurethane dispersion. Dispersion studies usually involve studying phase-inversions via viscosity [3-5,7,8] or conductivity [3,7,9,10] measurements during the dispersion of the polyurethane ionomer.

The self-assembly characteristics of amphiphilic waterborne polyurethanes into particles and the pH dependence of these particles on the dispersion properties have been reported [11-14]. These studies showed that the particles self-assemble into five different structures, and that the different structures are pH dependent.

The present study focuses on the assembly of the soft and hard segments of the PU dispersion particles onto the coated surface, and the resulting properties thereof. The self-assembling polyurethane dispersions prepared for coating applications requires an understanding of the mechanism by which the dispersion is formed and how this affects the properties of the coatings. Phase separation and self-assembly occurs during the coating process. Phase separation is caused due to inherent chemical and physical differences between the hard and soft segments of PUs. In the present study, PUs were synthesized to have a more rigid and polar hard segment than that of the soft segment, thereby promoting phase separation. Self-assembly is caused by the incorporation of PBTCA and wax into the PU matrix to promote the interaction between the hard and soft segments of the PU, thereby improving the overall physical and mechanical properties of the PU coating.

The hard and soft segments of the PU must orient themselves on the paperboard before drying, whereby the hydrophilic hard segment binds to the paperboard, and the hydrophobic soft segment forms the new surface layer. Orientation of the hydrophilic and hydrophobic segments is affected by their mobility in the dispersion phase, of which poor mobility results in poor orientation, and subsequently leads to poor barrier properties. Various techniques were used to characterize the polyurethane anionomers with regard to viscosity, pH, particle size and particle size distribution, surface hydrophobicity, surface morphology and barrier properties.

6.2 Self-assembly mechanism of the polyurethane-wax composites

The self-assembly mechanism involves the polymer needing enough time and space to orient/self-assemble its polar and non-polar segments onto the paperboard during the coating process, as shown below in Figure 6.1; the PBTCA are enriched at the substrate layer [6], and the wax is enriched at the surface layer (The wax enriched surface layer is shown by SEM in Figure A.2.5 in Appendix 2, and SCA in Figure 6.5).



Figure 6.1: Self-assembly mechanism during the coating process

Thus, to achieve optimal or ideal self-assembly, it is important to look at the mobility of the polar and non-polar segments of the PU emulsion particles:

- (i) Molecular mobility of the non-polar segments is influenced by the ionic content around the outer circumference of the emulsion particle. Generally, an increase in ionic content will increase surface charge on the outer emulsion particle, thereby increasing particle size due to an increase in repulsion forces. As the particle size increases, it pulls the non-polar inner chains further apart from each other, resulting in an increase in emulsion transparency and also an increase in mobility of the non-polar inner chains, as shown below in Figure 6.2.

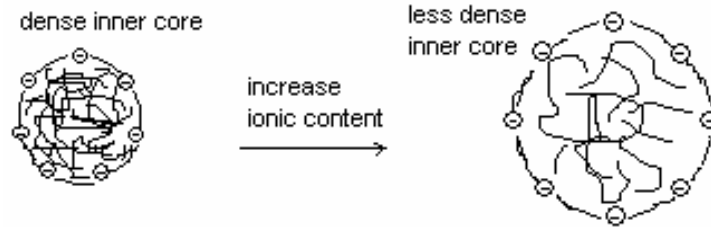


Figure 6.2: Effect of ionic content on the mobility of the non-polar chains of the PU emulsion

(ii) Molecular mobility of the polar segments can easily be followed by measuring the viscosity of the PU emulsion, as described in Section 6.7. Generally, an increase in emulsion viscosity results in an increase in molecular ionic clustering, thereby decreasing the mobility of the polar segments. The viscosity can be reduced by the addition of a solvating agent, such as water, acetone, MEK or NMP.

6.3 Effect of coating thickness on dispersion and coating properties

The paperboard was coated using four different, standard K101 control coater bars of 6, 12, 24 and 50 micron, resulting in different coating thicknesses. Figure 6.3 shows the importance of coating bar height on MVTR during the coating process; the MVTR generally decreases with increasing coating height (with and without wax addition).

An increase in coating thickness also increased the drying time of the PU coating. The average drying temperature was 110 to 130°C, while the drying time varied from 20 to 30 seconds for the 6- to 12-micron coatings, after which the drying time increased from 30 to 60 seconds for the 24-micron coating, and 1 to 4 minutes for the 50-micron coating.

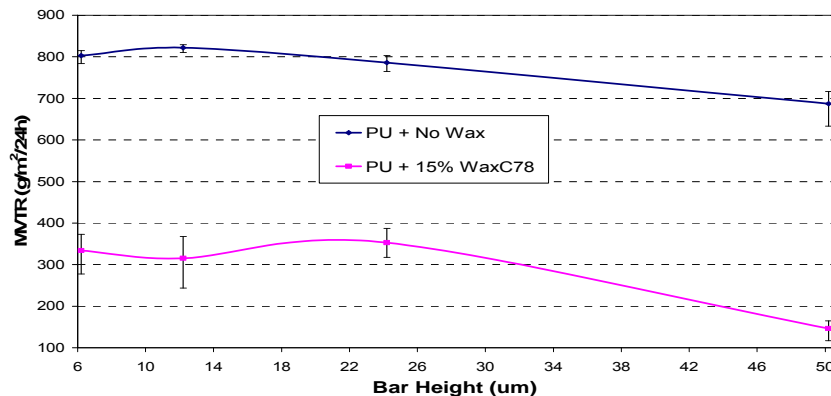


Figure 6.3: Effect of coating thickness on MVTR

However, the degree of blocking generally increases with increasing coating thickness. The surface hydrophobicity can be measured using SCA, as shown in Figure 6.4. In a thin layer, the molecular chains are limited to orientate themselves only in the horizontal plane. This is the case for the 6- and 12-micron bars, except that the 6-micron bar results in the formation of a weaker polymer network due to fewer polymer chains being present.

As the coating bar height increases, the vertical plane also comes into play, which means that the ionic/polar segments can orientate themselves in the vertical plane as well, to form a multi-layered distribution throughout the coating layer, affecting the SCA negatively. This is the case for the 24- and 50-micron bars.

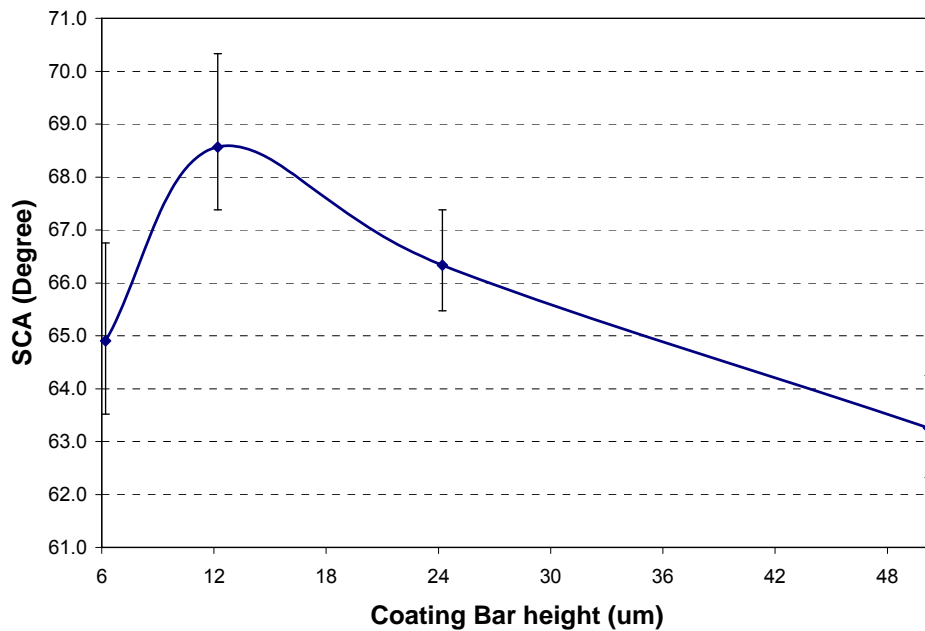


Figure 6.4: Effect of coating thickness on SCA

6.4 Effect of emulsion viscosity on dispersion and coating properties

Emulsion viscosity is an important factor that affects the mobility between the dispersion particles during the coating process. The viscosity of the PU dispersion is affected by the proximity of the dispersion particles relative to each other. If they are too close, then the viscosity is very high due to ionic clustering, resulting in a coating with poor self-assembly and properties. Similarly, if they are too far apart, then the viscosity is very

low, resulting in a coating with poor self-assembly and properties due to a poor polymer network. The effect of viscosity can be easily followed by measuring the SCA, as illustrated in Figure 6.5.

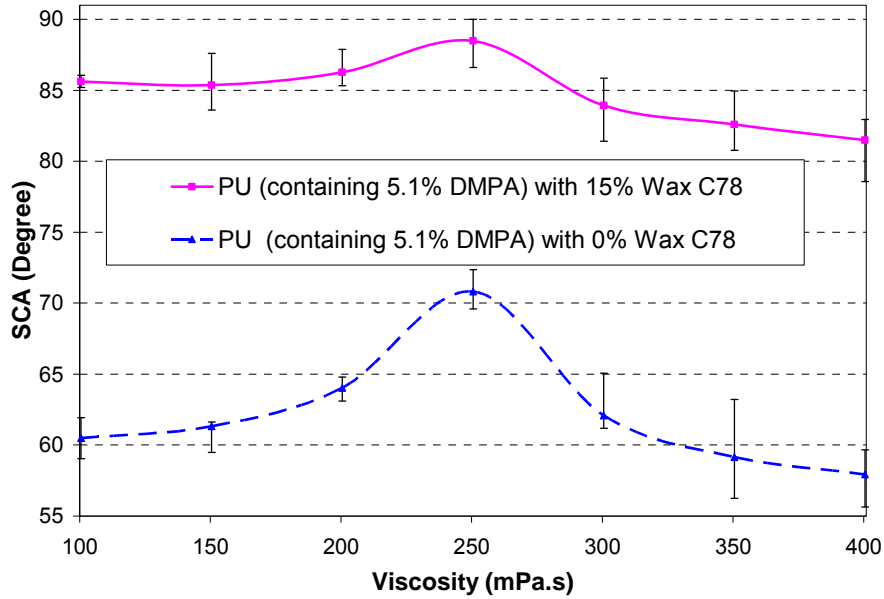


Figure 6.5: Effect of viscosity on SCA of coated paperboard (PU contains 5.1% DMPA)

The effect of emulsion viscosity can also be seen from MVTR results, as shown in Figure 6.6 below.

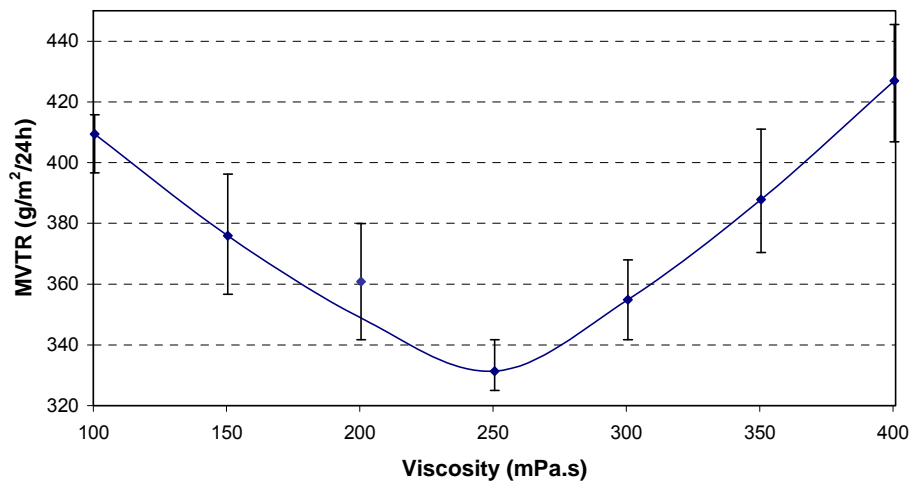


Figure 6.6: Effect of viscosity on MVTR of coated paperboard (PU contains 5.1% DMPA)

6.5 Effect of ionic content on dispersion and coating properties

The ionic content of the PUs is affected by the neutralized % PBTCA and % DMPA, and excess % TEA (neutralizing base). Generally, an increase in ionic content will:

- Increase emulsion stability
- Decrease hydrophobicity
- Decrease solids content at relatively similar PU dispersion viscosities
- Increase dispersion transparency
- Increase mobility of hydrophobic segment

The number of ionic groups is also an important factor, as illustrated below in Figure 6.7. Upon investigating the ionic content, it was found that as the ionic content increased, the white emulsion (A) went to a semi-clear white emulsion (B), then to a semi-clear emulsion/solution intermediate, followed by a clear solution. Also, the dispersion viscosity increased with increased ionic content.

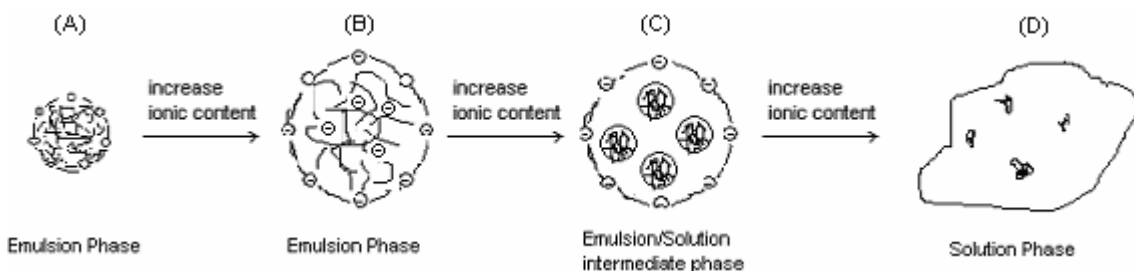


Figure 6.7: The effect of ionic content on the polyurethane dispersion particles

It was generally found that the % PBTCA has a much greater influence on particle size than the % DMPA, and thus also on the mobility of the non-polar polyester segment. This is mainly due to first, the location of the ionic center, as the PBTCA is distributed within the polyester while DMPA is on the edge of the polyester, and second, the excess TEA neutralizing base, which increases the particle circumference.

6.5.1 Effect of DMPA on dispersion and coating properties

DMPA is the primary source of ionic groups after the neutralization of its pendent tertiary acid group. The effect of DMPA content was followed by measuring the SCA of the polyurethane coated paperboard surfaces at constant dispersion viscosity and 100% neutralization, as illustrated in Figure 6.8 below. An increase in SCA is similar to an increase in hydrophobicity of the coated PU surface, which provides direct insight into the self-assembly of the polar and non-polar segments of the polyurethane coating, which can be explained as follows:

The DMPA ionic content starts at 4.6%, due to the PU emulsion being stable above 4.5%. As the % DMPA increases from 4.6% to 5.4%, so too does the mobility of the non-polar segments, giving rise to better assembly of the PU particles onto the paperboard surface during the coating process, which is seen as an increase in SCA values.

SCA has an optimum around 5.4% DMPA, which means that the emulsion particle has obtained maximum self-assembly to form optimum polymer layer. Above 5.4% DMPA, the SCA decreases due to a weaker polymer layer, as in the case of too low emulsion viscosity.

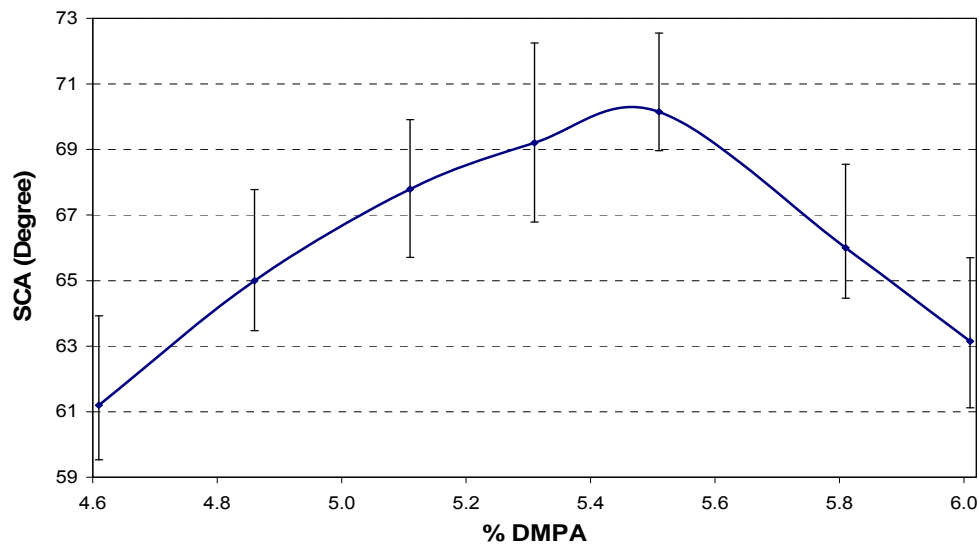


Figure 6.8: Effect of ionic content on SCA of coated paperboard at optimum viscosity of 250 mPa.s

6.5.2 Effect of PBTCA on dispersion and coating properties

PBTCA is the secondary source of ionic groups after the neutralization of its pendent tertiary acid group. Below 10% PBTCA, the acidic phosphoric OH-groups are less reactive in polyester synthesis, but are a source of hydrogen bonding that has a huge effect on the viscosity and dispersibility of the polyurethane. Generally, an increase in % PBTCA increases the ease of dispersibility and emulsion viscosity. Above 15% PBTCA, the phosphoric OH-groups become reactive enough during polyester synthesis, resulting in a crosslinked polyester.

Also, an increase in the % PBTCA increases the compatibility between hard and soft segments of the PU (see DMA results, Section 7.1). This is due to the PBTCA being a polar nucleus in the non-polar polyester soft segment, thereby decreasing the polarity difference between the hard and soft segments, ultimately increasing their compatibility.

6.5.3 Effect of neutralizing base on dispersion and coating properties

The neutralizing base forms an important part in the self-assembly mechanism, and is influenced [6] by:

- Effect of dispersion temperature (kept constant)
- Type of neutralizing base (kept constant)
- Degree of neutralization

The pendent COOH-groups were neutralized by the addition of triethylamine as the neutralizing base to form the PU-ionomer, and then dispersed into water to form the polyurethane dispersion.

6.5.3.1 Degree of neutralization

The degree of neutralization has an effect on the particle size distribution of the polyurethane dispersions. This can be seen in Figures 6.9 and 6.10, which show the particle sizes as determined by light scattering, and by transmission electron microscopy (TEM), as shown in Figure 6.11. See Appendix 7 for detailed light scattering and TEM analysis data.

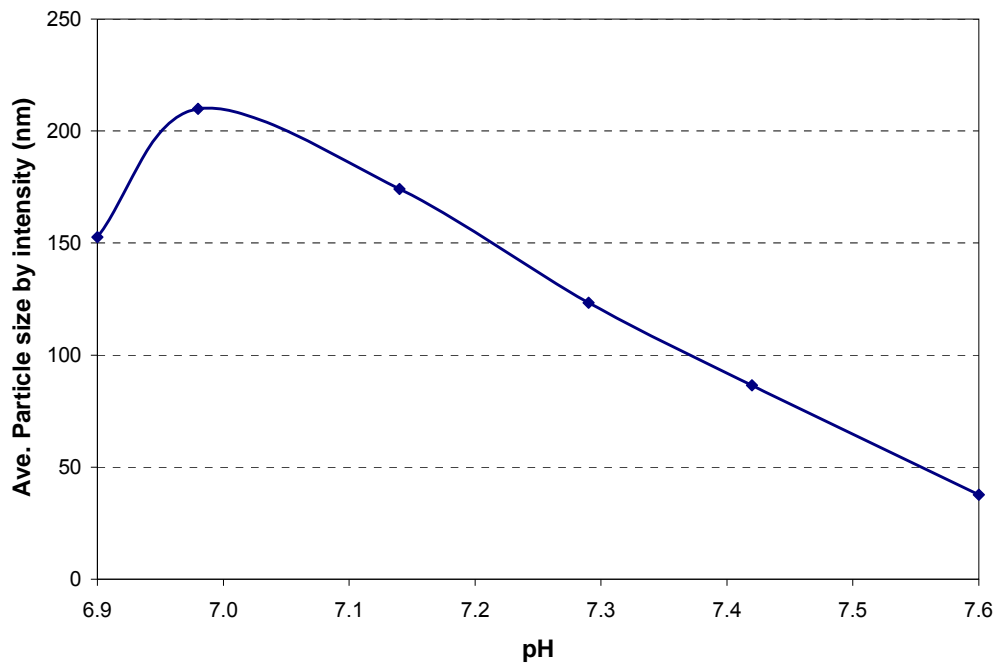


Figure 6.9: Effect of pH on the particle size distribution of the PU dispersion measured by light scattering

The effect of pH on the particle size distribution of the PU dispersion measured by light scattering (shown in Figure 6.9 above), is pictured below in Figure 6.10.

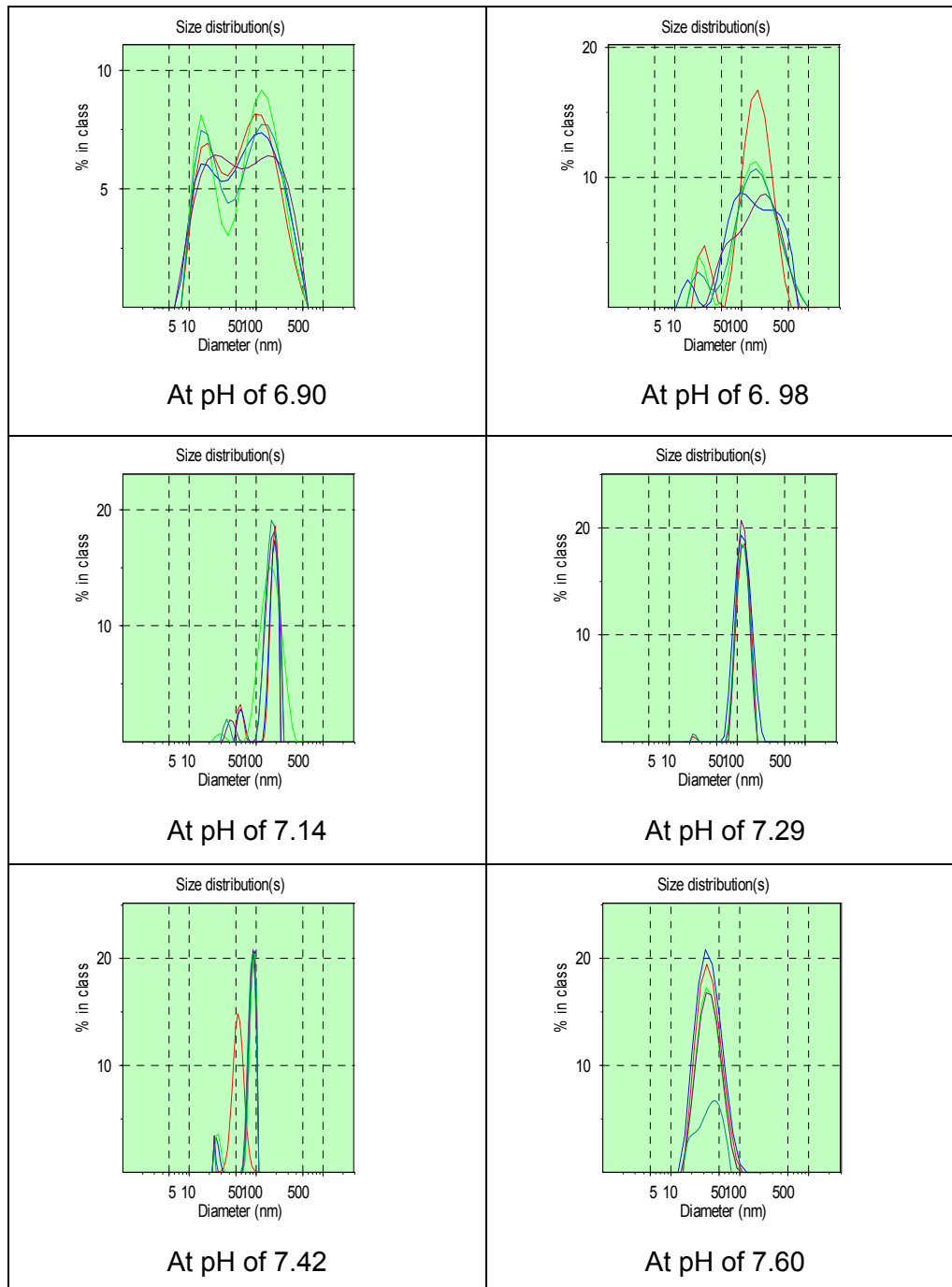


Figure 6.10: Visual effect of pH on the particle size distribution of the PU dispersion, measured by light scattering

The effect of pH on the particle size distribution of the PU dispersion as measured by TEM is pictured below in Figure 6.11.

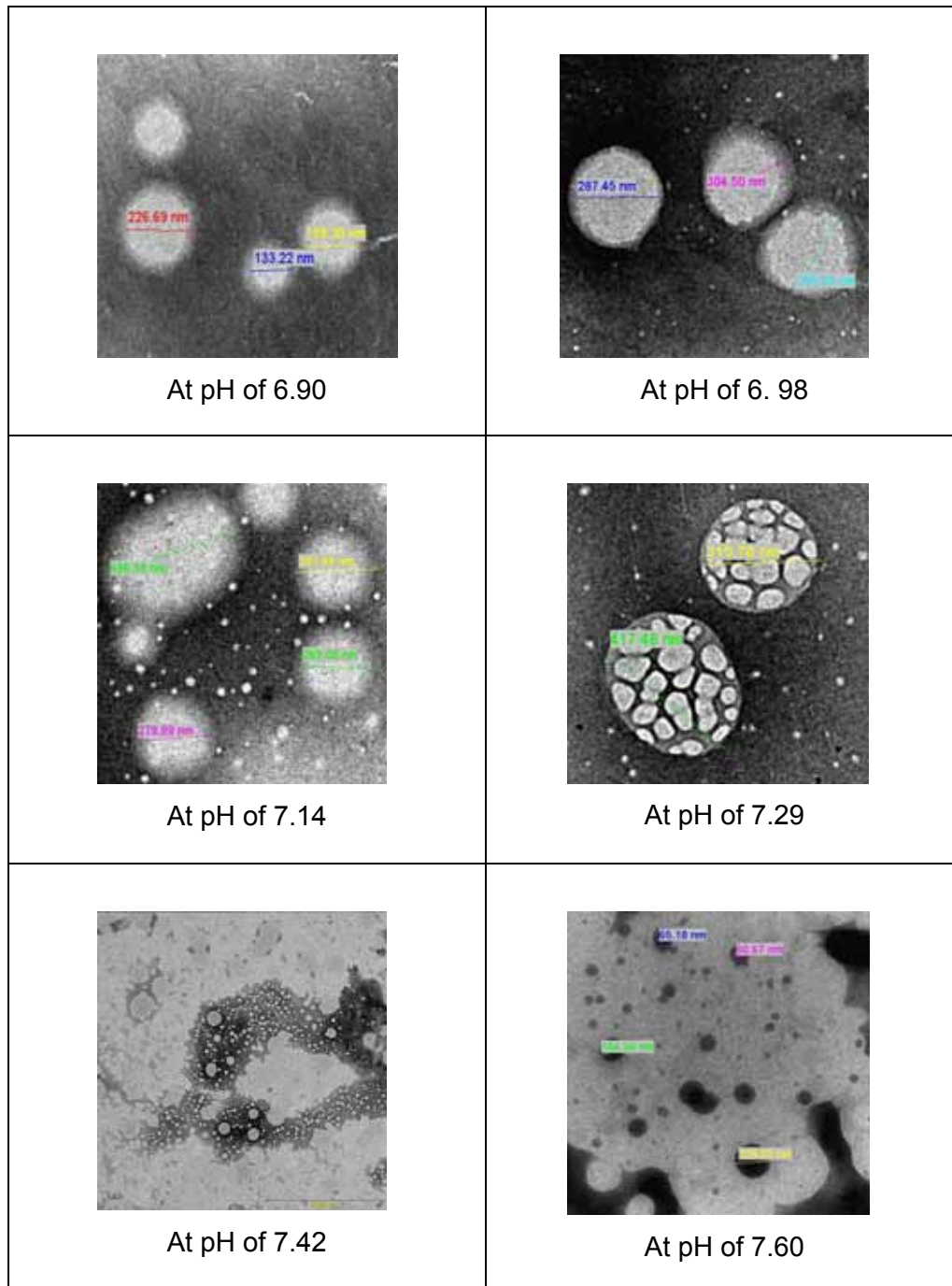


Figure 6.11: Visual effect of pH on the particle size distribution of the PU dispersion, measured by TEM

Figures 6.9 and 6.10 show that the PU dispersion has an average particle size of 152.6 nm at pH 6.90, with 62.6% distributed at 152.6 nm, and 37.4% distributed at 20.8 nm. See also Figures A.7.1 and A.7.7 in Appendix 7.

As the pH is increased from pH 6.90 to 6.98, the average particle size increased from 152.6 to 209.9 nm. Here, the average particle size formed a narrower particle size distribution of 90.3% around 209.9 nm. See also Figures A.7.2 and A.7.8 in Appendix 7.

As the pH is increased from pH 6.98 to 7.14, the average particle size decreased from 209.9 to 174.1 nm. Here, the average particle size also formed a narrower particle size distribution of 95.4% around 174.1 nm. See also Figures A.7.3 and A.7.9 in Appendix 7.

As the pH is increased from pH 7.14 to 7.29, the average particle size decreased from 174.1 to 123.4 nm, with an increasing particle size distribution of 95.4% around 123.4 nm. See also Figures A.7.4 and A.7.10 in Appendix 7.

This phenomenon is confirmed and more clearly understood when looking at the particles via TEM in Figure 6.11 (see also Figures A.7.7 to A.7.11 in Appendix 7), and is explained as follows: At neutral pH, all the pendent acid groups have been neutralized, giving a more uniform particle size distribution. As more neutralizing base is added, the excess TEA interacts with polar groups inside the particle. Partially quaternized triethylamine acts like a phase transfer reagent and can enter particles (as does the uncharged Et_3N). The increase in ionic or hydrophilic concentration within the particle causes the PU particle to increase in size (swelling by water) as shown in Figures 6.12.

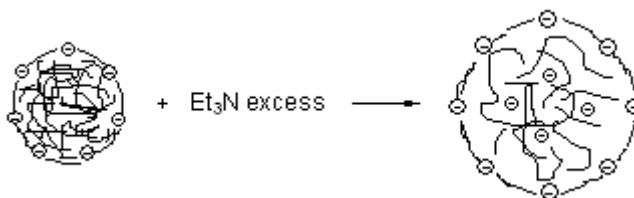


Figure 6.12: Effect of excess TEA neutralizing base

At pH 7.29, which is the optimum shifting from smaller to higher particle size range, the particles enter an emulsion-solution transition phase, as shown in Figures 6.9 to 6.11, and Figure A.7.10 in Appendix 7. Here one sees small particles within the larger

particles. Using optical microscopy and SEM, L. K. Saw *et al.* [15] also found these emulsion-solution transition phase particles, which they related to a high ionic content. They started with a high DMPA content and varied the degree of neutralization from 0 to 100%.

As the pH was increased from pH 7.29 to 7.42, the average particle size decreased from 123.4 to 86.5 nm. Here, the average particle size formed a narrower particle size distribution of 97.5% around 86.5 nm. See also Figures A.7.5 and A.7.11(a and b) in Appendix 7. At this stage, the polyurethane molecules went into solution phase, with small particles and water droplets being visible inside the bigger particles.

As the pH was increased from pH 7.42 to 7.60, the PU went into a complete solution phase, of which the average particle size number decreased from 86.5 to 37.7 nm. Here, the average particle size formed a narrower particle size distribution of 100% around 37.7 nm. See also Figures A.7.6 and A.7.11(c and d) in Appendix 7. Figures 6.11 and A.7.11(c and d) also show an increase in concentration and size of water droplets inside the PU solution.

The effect of pH on the final properties of the PU coating are shown below in Figure 6.13, at a viscosity of 25 to 50 mPa.s. It shows that the optimum self-assembly is obtained in the solution phase, very close to the emulsion/solution inter-phase.

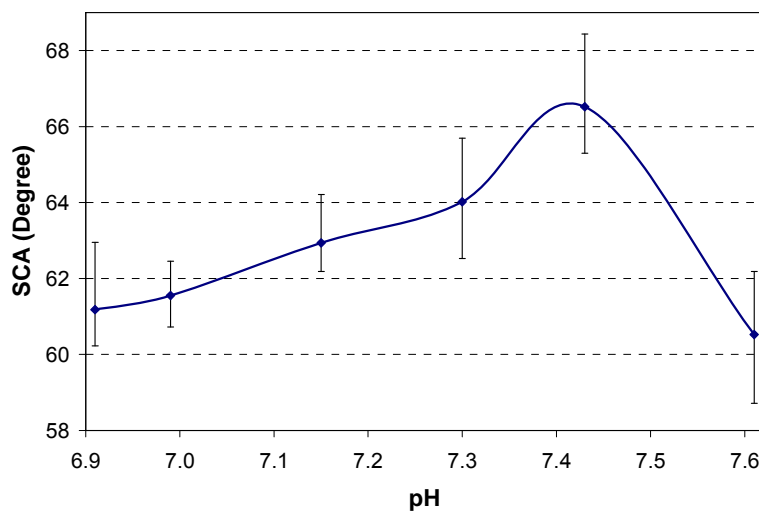


Figure 6.13: Effect of pH on SCA of the PU dispersions

6.6 Post modification using TEA

In general, the synthesized PUs can be labeled as rheology modifiers, of which the emulsion and final PU properties can be adjusted by the addition of extra TEA during or after PU emulsification. Visible properties include emulsion transparency and viscosity, which affect the self-assembly mechanism, thereby affecting the final properties of the PU coatings.

For example, a PU containing a low percentage of pendent COOH-groups (DMPA < 4%) at 100% neutralization will result in a white dispersion at a relative emulsion viscosity of 250 mPa.s and solid content of 37 to 45%.

As more neutralizing base is added to the PU emulsion, the transparency and viscosity increases. Water can be added until a clear emulsion is obtained at a relative emulsion viscosity of 250 mPa.s and solid content of 27 to 35%.

The effect of post modification using TEA is illustrated below in Figure 6.14.

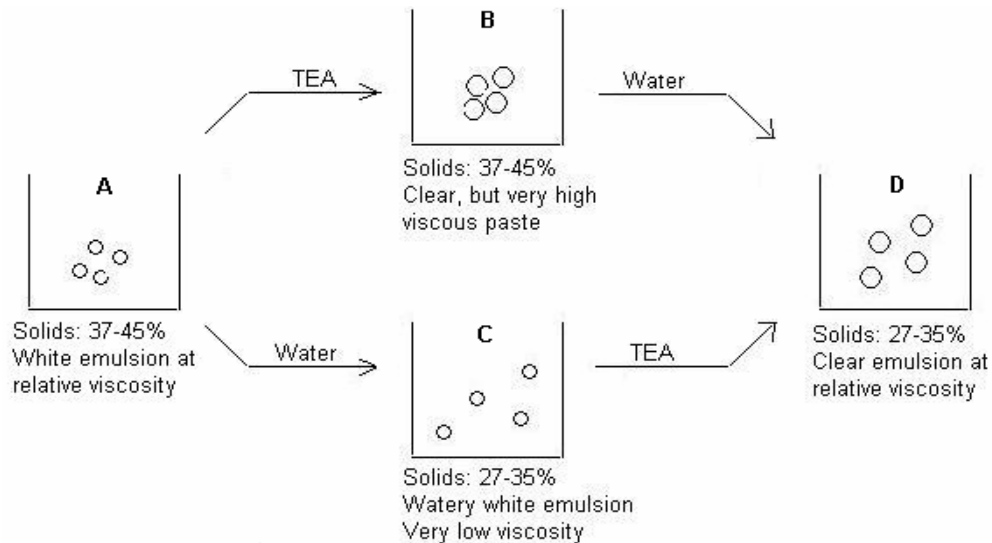


Figure 6.14: Schematic illustration of the effect of TEA on the emulsion viscosity and particle size (transparency) of the PU dispersions

6.7 Combined effect of viscosity and ionic content on the self-assembly mechanism

It was found that a balance between the ionic content and viscosity is needed to give optimum self-assembly during the coating process. This relationship was determined by investigating the static contact angle (SCA) of the coatings at various viscosities and ionic contents, as shown in Figure 6.15 below. An increase in SCA means an increase in hydrophobicity.

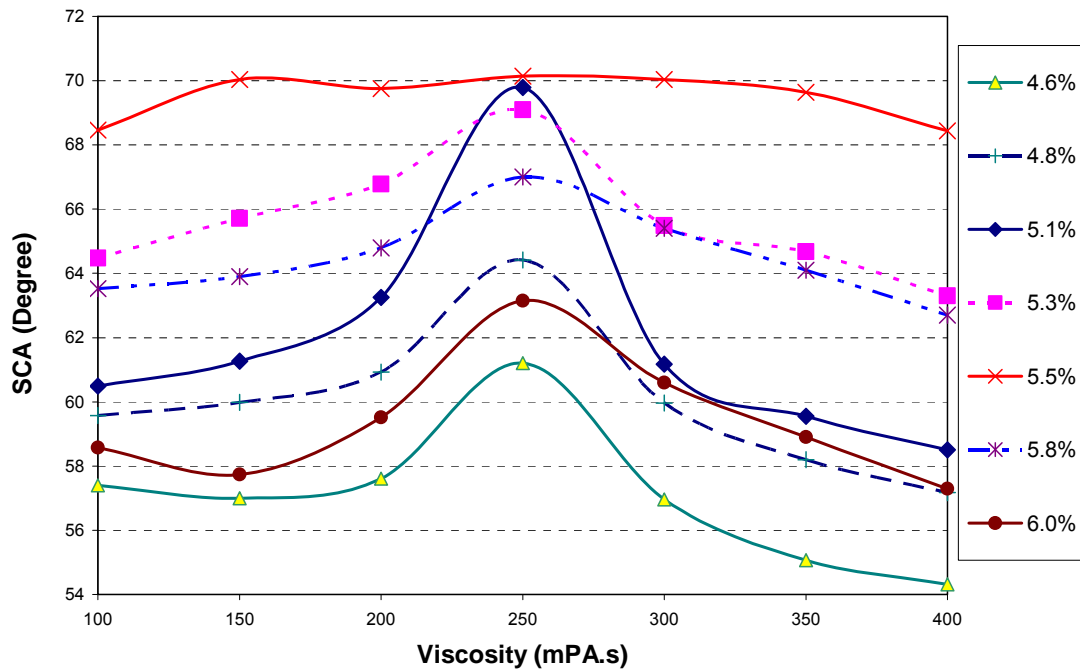


Figure 6.15: Effect of viscosity on SCA of PU coated paperboard containing 4.6 to 6.0% DMPA

Figure 6.15 illustrates that the optimum hydrophobicity of the PU coating was obtained at 250 mPa.s viscosity and 5.5% DMPA. It can also be seen that as the SCA reaches an optimum in terms of ionic content, the viscosity range increases. Figure 6.15 shows the effect of viscosity and ionic content on SCA, which provides insight into the self-assembly mechanism during the coating process.

6.8 Moisture vapour transmission rate (MVTR) and blocking

The composition of the PU formulation has a definite effect on the MVTRs obtained from the different coated paperboard disks.

6.8.1 Effect of soft segment content

Generally, an increase in hard segment content will lead to an increase in T_g , thereby giving rise to better MVTR and blocking results. However, the hard segment content is limited due to the high cost of the isocyanate component.

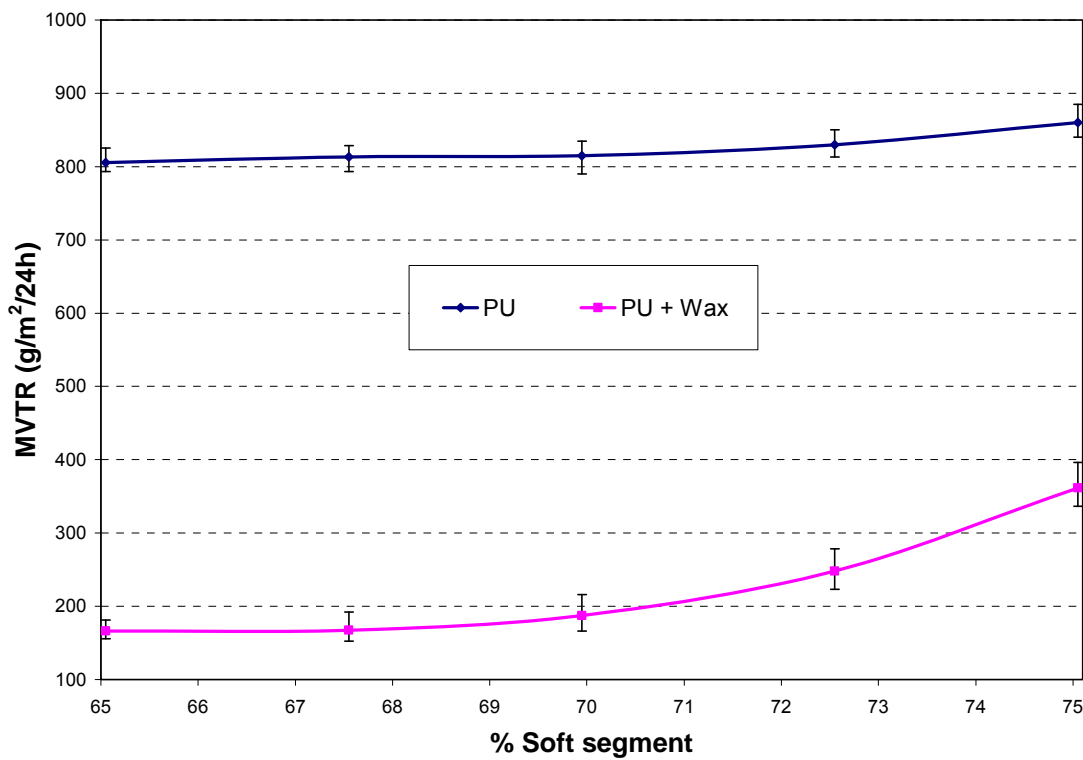


Figure 6.16: Effect of soft segment content on MVTR

In industry, when working with TDI as a thermoplastic coating film, the projected hard segment content should be about 30% (weight %). From the results in Figure 6.16, it was experimentally found that the optimum hard segment content in this case was between 30 to 35% (soft segment content of 65 to 70%).

6.8.2 Effect of PBTCA, CHDCA and wax content on MVTR and blocking

The effects of PBTCA, CHDCA and wax content on the MVTR and blocking results, obtained at 38°C and 90% RH over a 24 h period, are illustrated below in Table 6.1.

Table 6.1: Tabulated MVTR and blocking data of PU coatings

PU coating			No Wax C78 addition		Wax C78 addition	
PU-code	% PBTCA (polyester)	% CHDCA (polyester)	MVTR (g/m ² /24 h)	Degree of blocking	MVTR (g/m ² /24 h)	Degree of blocking
PU-0600	6	0	851	Medium	287	Medium
PU-0605	6	5	867	Medium	267	Medium (-)
PU-0610	6	10	852	Medium	289	Medium (-)
PU-0615	6	15	Too unstable		Too unstable	
PU-0800	8	0	819	Medium	239	Kissing
PU-0805	8	5	820	Medium	219	Kissing
PU-0810	8	10	815	Kissing (+)	187	Kissing (-)
PU-0815	8	15	797	Medium	230	Kissing (-)
PU-1000	10	0	829	Medium (+)	266	Kissing (+)
PU-1005	10	5	786	Kissing (+)	245	Kissing
PU-1010	10	10	780	Kissing (+)	220	Kissing
PU-1015	10	15	776	Medium	221	Kissing

6.8.2.1 Effect of PBTCA

As shown earlier (see Section 6.5.2), the inclusion of PBTCA is an important factor in the PU matrix. It mainly affects the compatibility between the hard and soft segments of the PU, hydrophobicity, T_g, particle size, processing viscosity and emulsion stability. Thus, all of these factors need to be taken into consideration when looking at the MVTR data.

However, the inclusion of 6 to 10% PBTCA-containing polyester into the polyurethane matrix did not result in any significant changes in MVTR, as shown in Table 6.1 and Figure 6.17.

6.8.2.2 Effect of CHDCA

The inclusion of CHDCA into the polyester matrix means that a portion of the flexible AA monomer is substituted with the more rigid and bulky CHDCA monomer. As in the case of PBTCA, its effects also need to be taken into consideration. These effects are generally opposite to those of PBTCA, except in the case of T_g and processing viscosity.

The inclusion of 5 to 15% CHDCA-containing polyester into the polyurethane matrix did not result in any significant changes in MVTR, as shown in Table 6.1 and Figure 6.17.

6.8.2.3 Effect of Wax C78

The PUs were evaluated with a variety of different waxes, as discussed in Section 4.5. results showed that wax C78 gave the best MVTR and lower blocking results. This is probably due to it being semi-crystalline and having a high molecular mass at relatively low acid value. Thus, as expected, the inclusion of wax C78 lowered the MVTR values considerably due to the added surface hydrophobicity and compatibility with the polyurethane, as seen in Figure 6.17.

6.8.2.4 Blocking effect

The blocking effect is an important characteristic in the paperboard industry, as the coated paperboard is stacked in pallets, and if they should stick to each other, the whole pallet will be damaged. See Appendix 5 for the blocking test method used to determine whether coated sheets in a pallet will stick to each other.

Generally, the degree of blocking is decreased by an increase in Tg and wax addition, see Table 6.1, not forgetting the other factors such as optimum self-assembly during the coating process and compatibility. The MVTRs in Table 6.1 are graphically displayed in Figure 6.17 below.

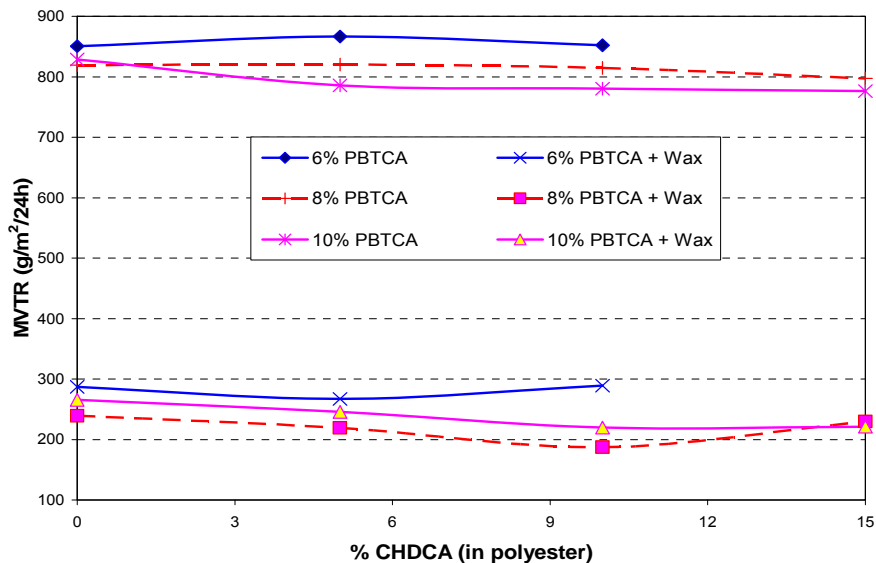


Figure 6.17: Effect of waxC78 on the MVTR of the PU coatings

6.9 Scanning Electron Microscopy

Firstly, it is important to see if the coating method had damaged the coating surface, and also to look at the surface characteristics. This was done by comparing the SEM images obtained to those in the literature. It was concluded that the applied coating method did not damage the coating surface.

6.9.1 SEM images of uncoated paperboard surface

The SEM images displaying the surface characteristics of the uncoated paperboard surface, are shown in Figure 6.18 below.

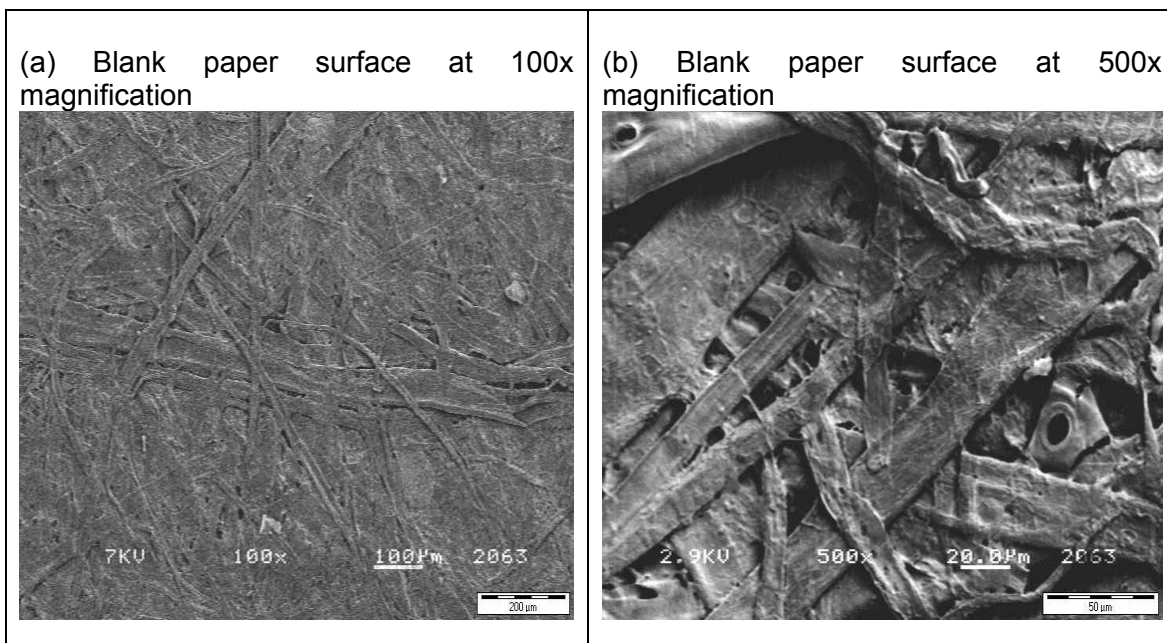


Figure 6.18: SEM images of the blank paperboard surface

The SEM images of the uncoated paperboard in Figure 6.18 above show several holes (pinholes) in between the paper fibers. These pinholes, and the fact that the paperboard has a high affinity for water and water vapour, limits its use as a water vapour barrier.

6.9.2 Effect of phosphorous on the polyurethane surface

The inclusion of phosphate in the PU formulation has a clear effect on the SEM images of the PU films, as shown in Figures 6.19 and 6.20.

The non-phosphated PU paperboard samples in Figure 6.19 show a fair number of pinholes present in the coating, even with the addition of 15% wax C78.

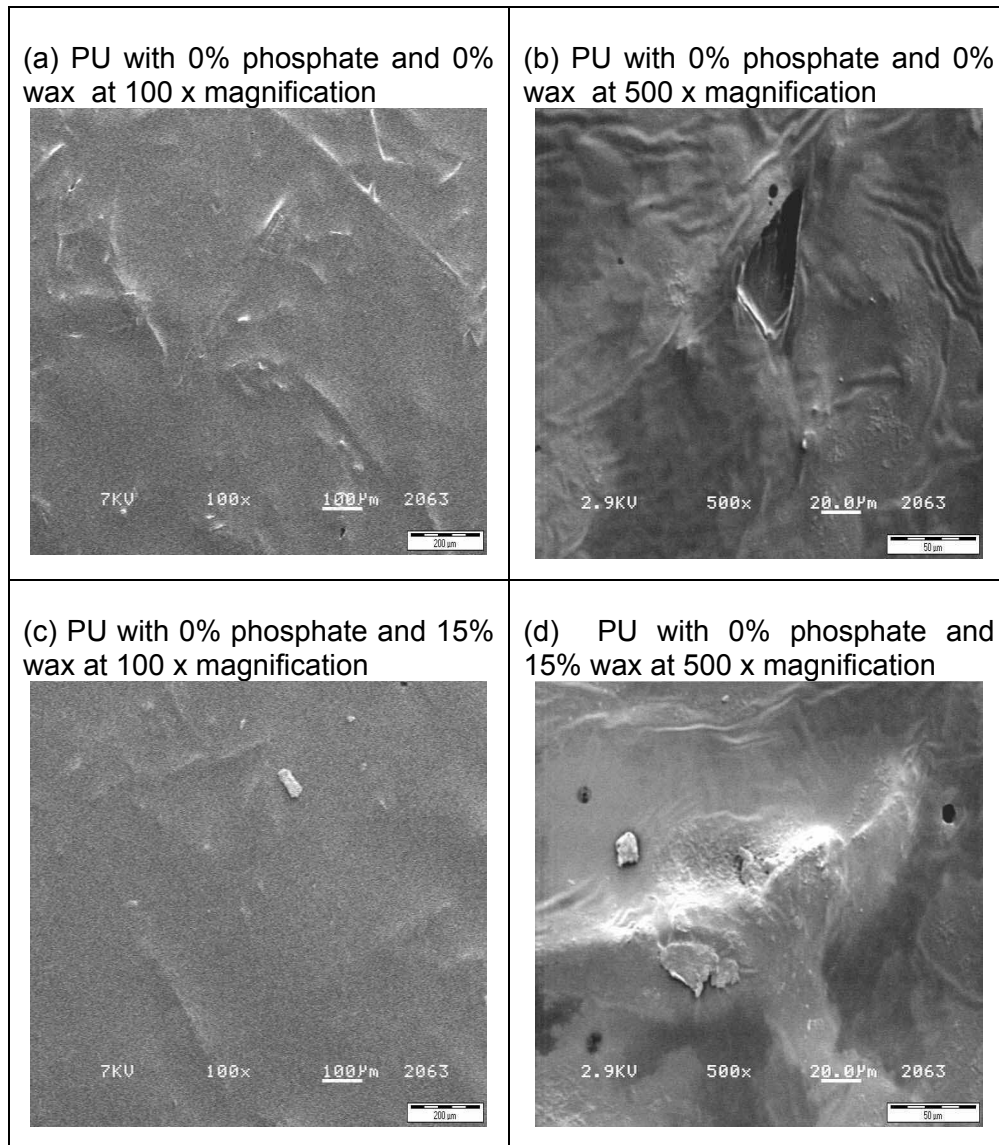


Figure 6.19: SEM images showing the effect of non-phosphated PU coated paperboard

In contrast to the SEM images of the non-phosphated paperboard coatings above, the phosphated PU paperboard samples in Figures 6.20 below, show no pinholes present in the coating, even with the addition of 15% wax C78.

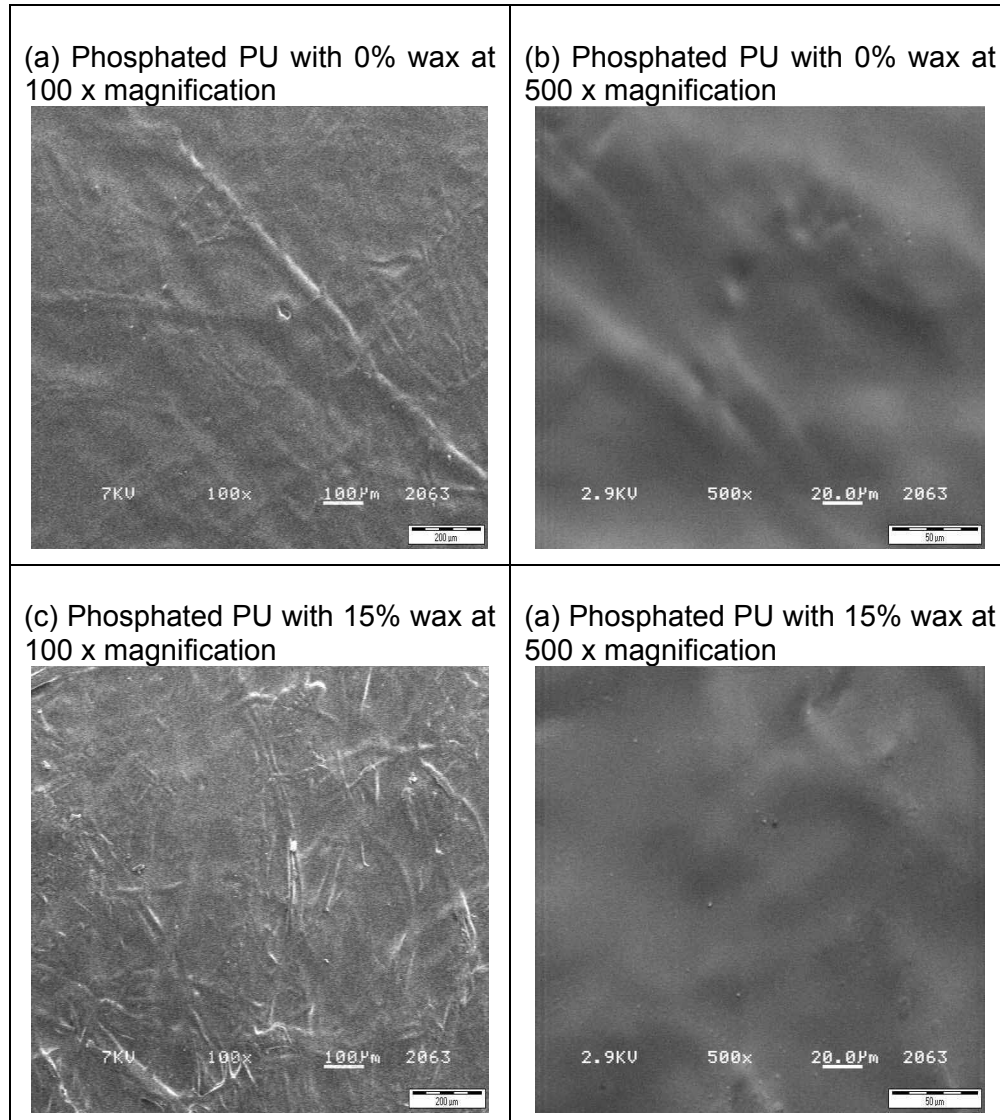


Figure 6.20: SEM images showing the effect of phosphated PU coated paperboard

Also, a much smoother coating surface is obtained by the inclusion of 15% wax C78.

6.9.3 Effect of CHDCA on the polyurethane surface

The CHDCA had an opposite effect to that of PBTCA; the coating tended to destabilize with increasing CHDCA content. But as long as the PU emulsion was stable and the hard and soft segments were fully compatible, then no surface defects such as pinholes were visible.

6.10 References

1. D. Dieterich, W. Keberle, H. Witt, *Angew Chem. Int. Ed.*, **9**, 40, 1970.
2. O. Lorenz, H. Hick, *Angew Makromol. Chem.*, **72**, 115, 1978.
3. S. A. Chen, W. C. Chan, *J. Polym. Sci. B Polym. Phys.*, **28**, 1515, 1990.
4. Y. Chen, Y. L. Chen, *J. Appl. Polym. Sci.*, **46**, 435, 1992.
5. C. H. Yang, S. M. Lin, T. C. Wen, *Polym. Eng. Sci.*, **35** (8), 722, 1995.
6. K. Mequanint, Self-assembling metal coatings from phosphated and silicone-modified polyurethane dispersions, PhD Dissertation, University of Stellenbosch, 2001.
7. L. K. Saw, B. W. Brooks, K. J. Carpenter, D. V. Keight, *J. Colloid Interface Sci.*, **257**, 163, 2003.
8. D. Dietrich, *Prog. Org. Coat.*, **9** (3), 281, 1981.
9. B. W. Brooks, H. N. Richmond, *Colloids Surf.*, **58**, 131, 1991.
10. M. Zerfa, S. Sajjadi, B. W. Brooks, *Colloids Surf., A Physiochem. Eng. Asp.*, **155** (2), 323, 1999.
11. S. A. Chen, W. C. Chen, *J. Polym. Sci. B Polym. Phys.*, **28**, 1499, 1990.
12. S. Nomura, S. L. Cooper, *J. Colloid Interface Sci.*, **205**, 331, 1998.
13. A. J. Dong, G. L. Hou, X. Y. Wang, D. X. Sun, *J. Polym. Sci. B Polym Phys.*, **40** (10), 972, 2002.
14. A. J. Dong, G. L. Hou, D. X. Sun, *J. Colloid Interface Sci.*, **266**, 276, 2003.
15. L. K. Saw, B. W. Brooks, K. J. Carpenter, D. V. Keight, *J. Colloid Interface Sci.*, **257**, 163, 2003.

7 MECHANICAL, THERMAL AND SPECTROSCOPIC CHARACTERIZATION

7.1 Introduction

Thermoplastic polyurethanes (TPUs) are often referred to as multiblock copolymers, consisting of a flexible soft segment and a rigid hard segment. A complete characterization is necessary to fully understand the relationships between the chemical structure and morphology and between the chemical structure and physical properties. The mechanical and physical properties of TPUs are dependent on factors such as; (i) the composition of the soft and hard segments; (ii) the lengths of the soft and hard segments; (iii) the ratio of soft to hard segments; (iv) anomalous linkages; and (v) molecular masses.

The structural differences between the soft and hard blocks results into phase separation. The degree of phase separation affects the properties of the polyurethane. Bulk-phase separation acts like structural flaws in the polymer, but an increase in microphase separation on the molecular level generally leads to an increase in mechanical and physical properties.

Phase separation domains can be decreased by increasing the compatibility between the hard and soft segments. In this study, a hydrophilic ionic group of PBTCA was incorporated into the hydrophobic soft segment. This was done to promote hydrogen bonding between the hard and soft segments of the polyurethane, thereby decreasing phase separation. DMA analysis was used to investigate the microstructure of the polyurethane's hard and soft segments.

7.2 Dynamic mechanical analysis

Dynamic mechanical analysis can be used to obtain insight into the microstructure of the PU [1-6]. By investigating the Tg's of the various PU compositions by DMA analysis, as shown in Table 7.1, it was found that the Tg's were significantly affected by:

- Hard segment content
- PBTCA content
- DMPA content
- CHDCA content
- Wax content

Table 7.1: Tg's of PU with and without wax C78 incorporation

PU coating			No wax C78		15% wax C78	
PU-code	% PBTCA	% CHDCA	Tg (°C) at peak onset	Peak Temp	Tg (°C) at peak onset	Peak Temp
PU-0600	6	0	-23.4	-8.9	-21.1	3.9
PU-0605	6	5	-15.4	1.5	-12.6	12.6
PU-0610	6	10	-8.2	9.4	-3.6	19.4
PU-0615	6	15	Too unstable		Too unstable	
PU-0800	8	0	-17.1	0.5	-11.4	9.0
PU-0805	8	5	-9.6	10.1	0.7	17.4
PU-0810	8	10	8.5	21.4	17.1	25.7
PU-0815	8	15	13.9	28.3	23.0	32.2
PU-1000	10	0	-7.0	11.0	-4.4	19.4
PU-1005	10	5	-1.9	17.4	3.5	22.4
PU-1010	10	10	7.9	25.1	11.4	26.4
PU-1015	10	15	16.9	33.9	18.2	35.1

The Tg's of the PU with and without wax C78 incorporation that are summarized in Table 7.1 show that the Tg generally increased with increased PBTCA and CHDCA content, as well as with 15% wax C78 content.

7.2.1 Effect of hard segment content

Generally, the Tg increased with increasing hard segment content, of which the optimum hard segment content was experimentally found to be between 30 to 35% (weight %), as shown in Figure 7.1 below.

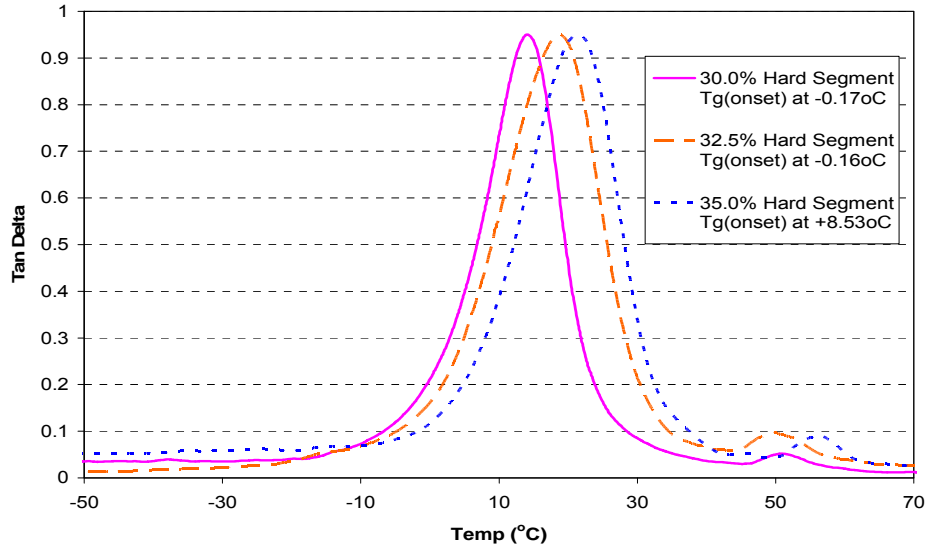


Figure 7.1: Effect of hard segment content on Tg of the polyurethane

7.2.2 Effect of PBTCA

Generally, the Tg increased with increasing PBTCA content, which is due to H-bonding from the hydrophilic (HO)₂-PO group, as shown in Figure 7.2. The PBTCA content is also important for the compatibility between the hard and soft segments of the PU coating.

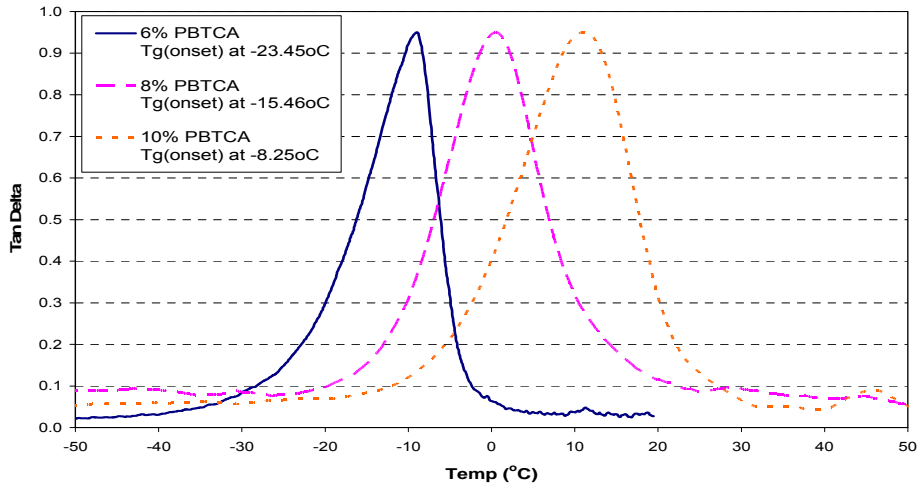


Figure 7.2: Effect of PBTCA content on Tg of the polyurethane

7.2.3 Effect of DMPA

The DMPA content is the primary source of ionic centers for stabilizing the emulsion. As seen from Figure 7.3, the DMPA content did not have a significant affect on the Tg, except when there was a huge difference in polarity (leading to lower compatibility) between the hard and soft segments of the PU, which was the case at 6.0% DMPA.

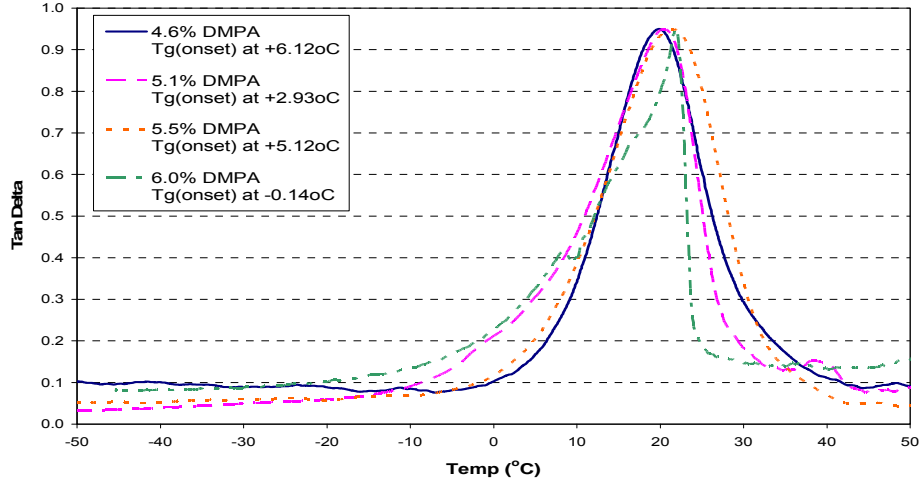


Figure 7.3: Effect of DMPA content on Tg of the polyurethane

7.2.4 Effect of CHDCA

Generally, the Tg increased with increasing CHDCA content, which is due to the chain stiffness it imparts compared to adipic acid, as shown in Figure 7.4. The CHDCA content was kept at a maximum of 15% during PU synthesis to minimize processing difficulties such as huge viscosity increases.

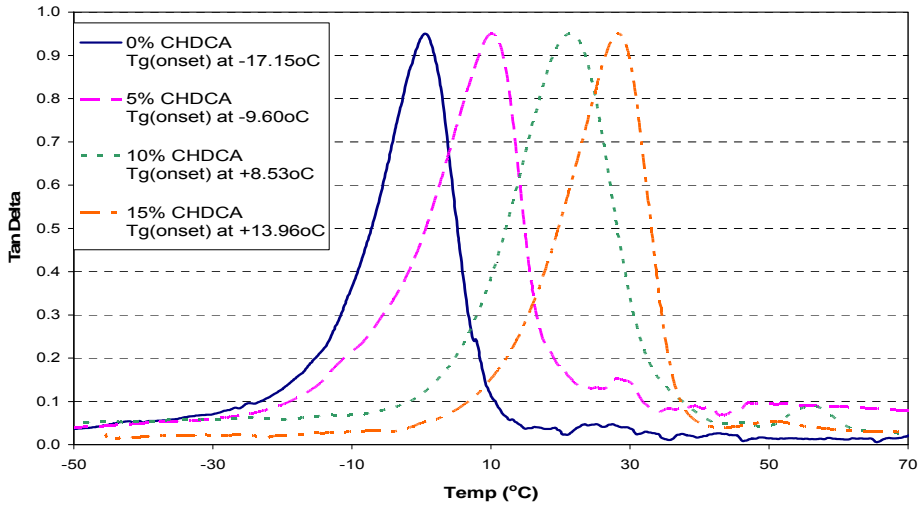


Figure 7.4: Effect of CHDCA content on Tg of the polyurethane

The effect of CHDCA content on the viscosity of the polyester is shown in Figure 7.5. It shows that a CHDCA content of 15% or more imparted huge viscosity increases, which is also the main cause of processing difficulties during polyurethane synthesis.

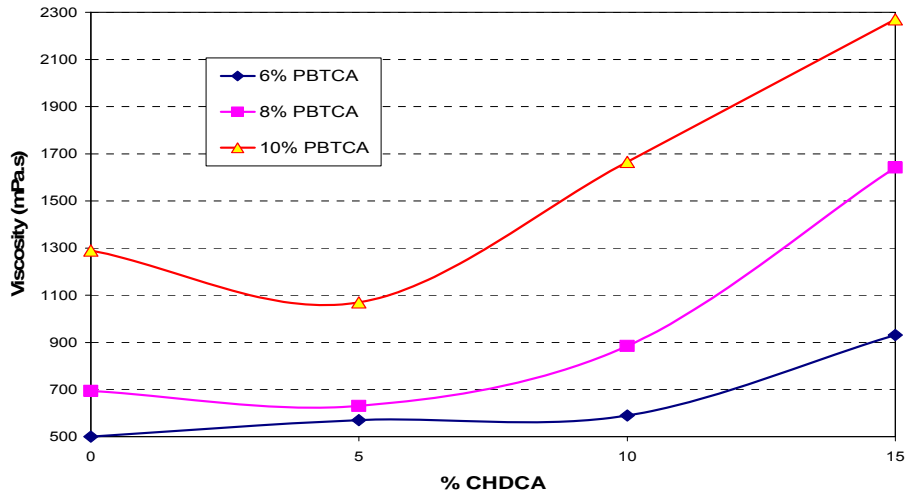


Figure 7.5: Effect of CHDCA content on viscosity of the polyester

7.2.5 Effect of wax content

The inclusion of wax C78 showed no signs of incompatibility if the hard and soft segments of the PU were completely compatible, but if the hard and soft segments were not completely compatible, then the addition of wax increased that incompatibility, as shown in Figure 7.6. Poor compatibility resulted into poor performance, such as high MVTR and increased blocking.

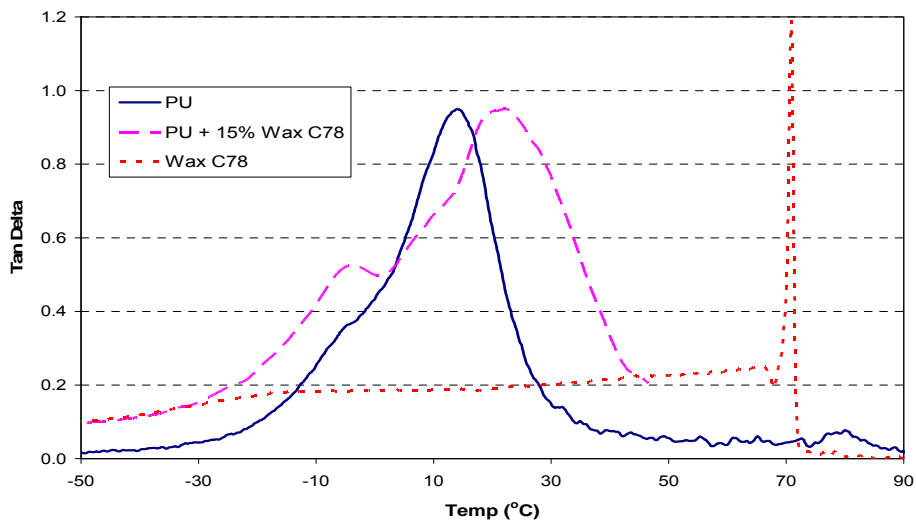


Figure 7.6: Effect of waxC78 on the PU that is not fully compatible

7.3 Thermogravimetric analysis (TGA)

Thermogravimetry is a suitable method widely used to evaluate the thermal properties of polyurethane materials [7,8]. TGA analyses were done on dried PU samples to investigate their thermal stability with regard to the hard segment, PBTCA, CHDCA and the wax content.

7.3.1 Effect of hard segment content

The PU was analyzed for a hard segment content of 30 to 35% (due to it being tacky at room temperature below 30% hard segment content, and brittle above 35%). From the data in Figure 7.7, the PU consisting of 69.9% soft segment gave the best thermal stability. This is due to optimum morphological interactions between the hard and soft segments. Above 70% soft segment, the T_g of the PU was low, rendering it too tacky to be an effective MVTR barrier coating.

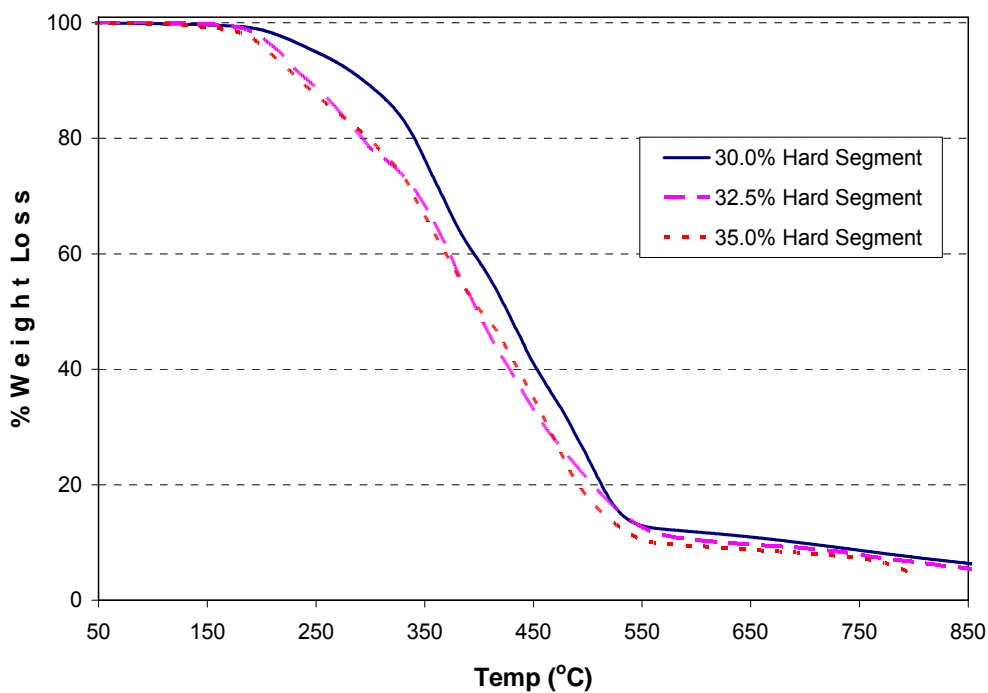


Figure 7.7: Effect of hard segment content on thermal stability of the polyurethane

7.3.2 Effect of PBTCA content

The inclusion of PBTCA increased the chain stiffness due to H-bonding, and only slightly improved the thermal stability of the PU between 450 to 580°C, as shown in Figure 7.8.

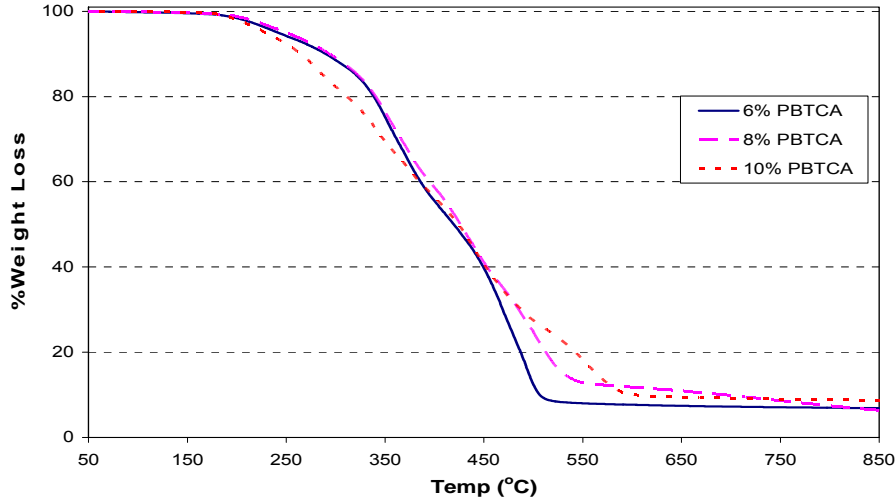


Figure 7.8: Effect of PBTCA content on thermal stability of the polyurethane

7.3.3 Effect of CHDCA content

The inclusion of CHDCA increased the chain stiffness, but did not have a significant effect on the thermal stability of the PU, as shown in Figure 7.9.

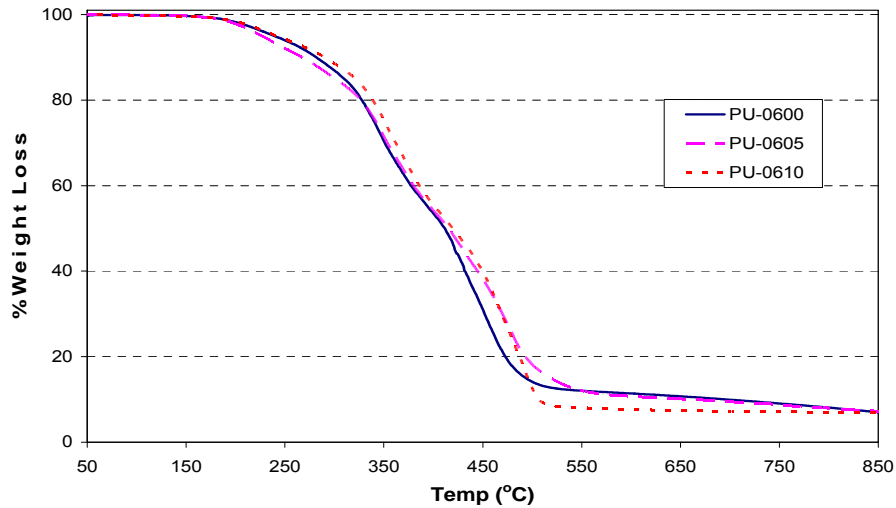


Figure 7.9: Effect of CHDCA content on thermal stability of the polyurethane

7.3.4 Effect of wax content

PU-wax composites with 0, 5, 10, 15, 20, 25, 30 and 40% wax incorporation were prepared. They gave similar results, except for the 0, 15 and 100% wax incorporation, shown in Figure 7.10. The best PU-wax composites was at 15% wax incorporation.

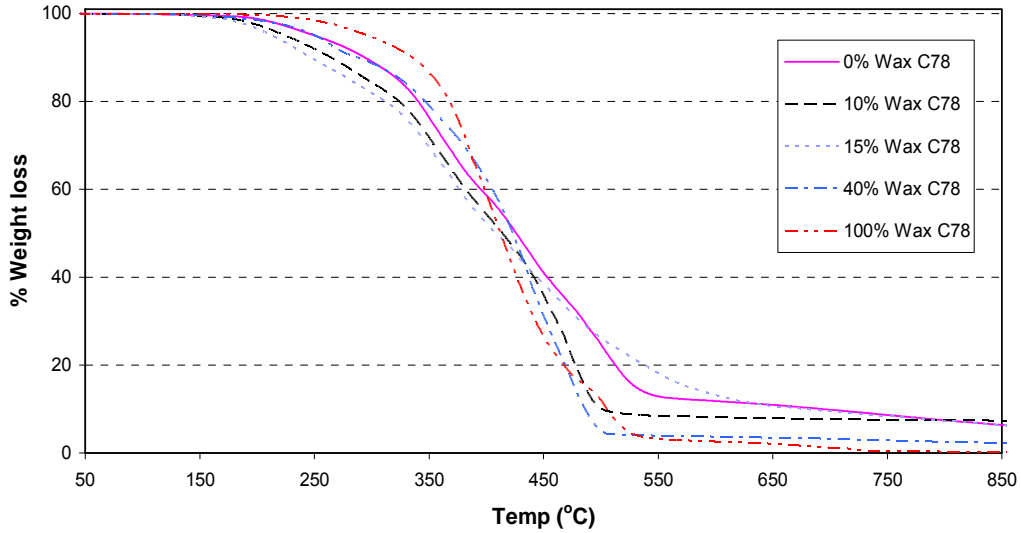


Figure 7.10: Effect of wax content on thermal stability of the polyurethane

7.4 Differential scanning calorimetry (DSC)

During DSC analyses, samples undergo three steps; the first and third are heating steps, and the second is a cooling step. Thus the data shown below are that of the third step.

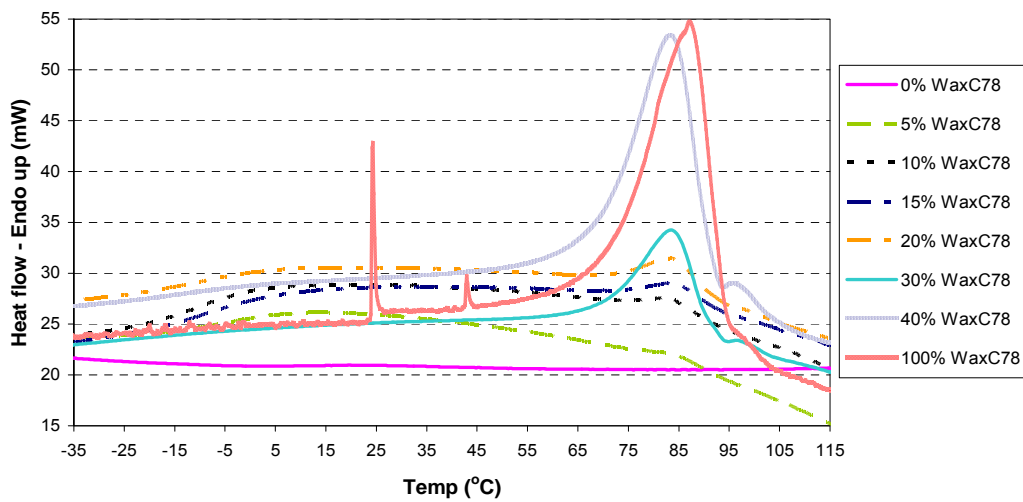


Figure 7.11: Second heating profile of the PU-wax C78 composites

The PUs on their own did not show any melting peaks, as in the case of crystalline waxes. Figure 7.11 shows the incorporation of wax C78 into the PU matrix, reflected by an increase in the melting peak at around 82°C for various wax concentrations.

It can also be seen from Figure 7.11 that wax C78 had three peaks, with maximum peaks at 25, 43 and 85°C. Wax C78 is a combination of two waxes, of which 78% is a Fischer-Tropsch hard wax, while the other 22% is an oxidized polyethylene wax with an acid value of 15 (to help the emulsification process). Thus, the peak at 25°C could be assigned to the lower fraction wax, the 85°C peak to the high fraction wax, and the middle peak at 43°C could be assigned to the interface of the two waxes. When wax C78 was incorporated into the PU matrix the first two peaks disappeared, as they were easily dispersed into the PU, which acts like a compatibiliser. The best compatibility between polyurethane and wax C78 existed to about 15% wax, whereafter the wax began to show a definite phase-separated melting point.

7.5 GPC analysis

GPC analyses were done on both the polyesters and the polyurethanes. The polyesters were synthesized to have similar molecular weight distributions, as were the polyurethanes. Figures 7.12 to 7.16 all show a huge fraction at around a molecular weight (MW) of 320, of which the low MW fractions decrease with increasing MW.

7.5.1 GPC analysis of the polyesters

The effect of the different monomer ratio's during polyester synthesis on the molecular weight was investigated.

7.5.1.1 Effect of PBTCA content on the molecular weight of the polyester

Figure 7.12 shows that when the more flexible AA monomer is partially replaced by the more rigid and heavier PBTCA in the polyester, the number of lower MW fractions decreased and shifted to higher MW fractions.

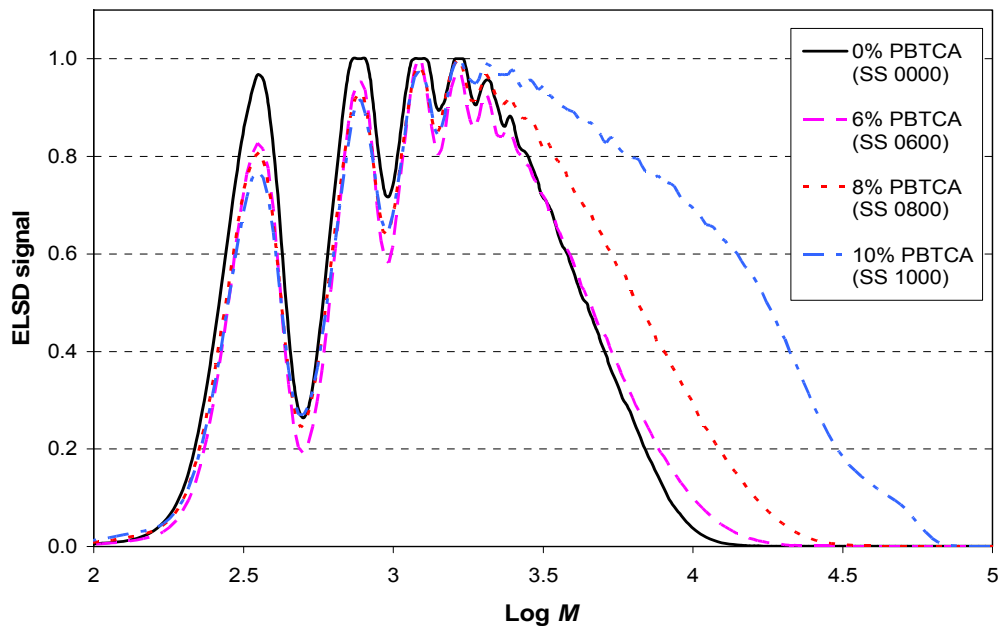


Figure 7.12a: Effect of PBTCA content on the molecular weight of the polyester (normalized to highest peak)

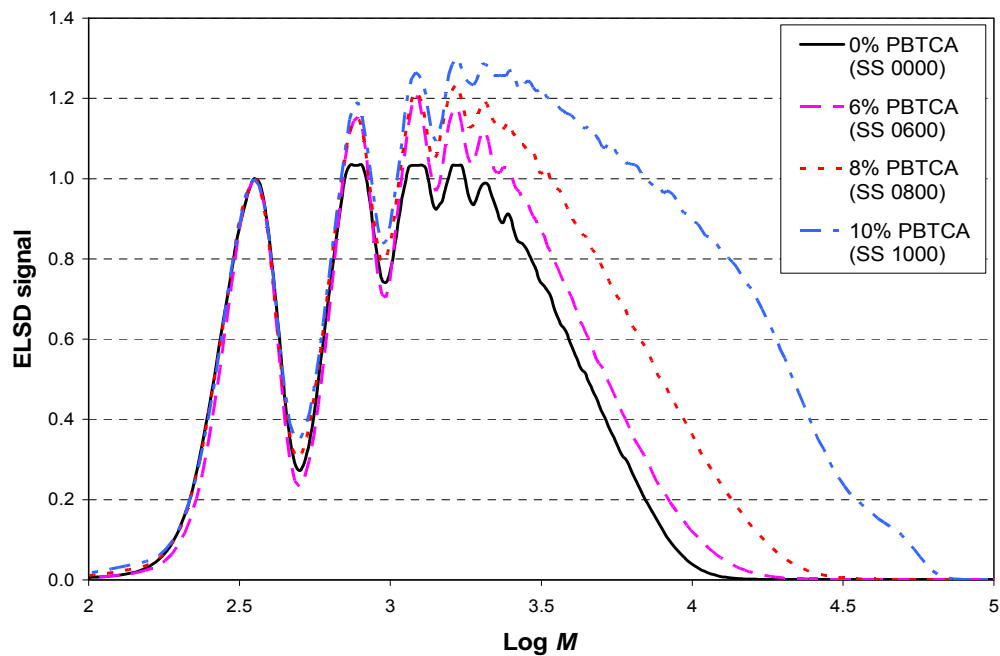


Figure 7.12b: Effect of PBTCA content on the molecular weight of the polyester (normalized to 1st peak)

7.5.1.2 Effect of CHDCA content on the molecular weight of the polyester

The inclusion of CHDCA, as seen in Figures 7.13 to 7.15, showed a similar but lesser trend than in the case with PBTCA. This was due to the more flexible AA monomer being partially replaced by the bulkier more rigid CHDCA monomer. Due to their different reactivities, they react at different temperatures. This could explain the decrease in smaller MW fractions with increasing CHDCA content.

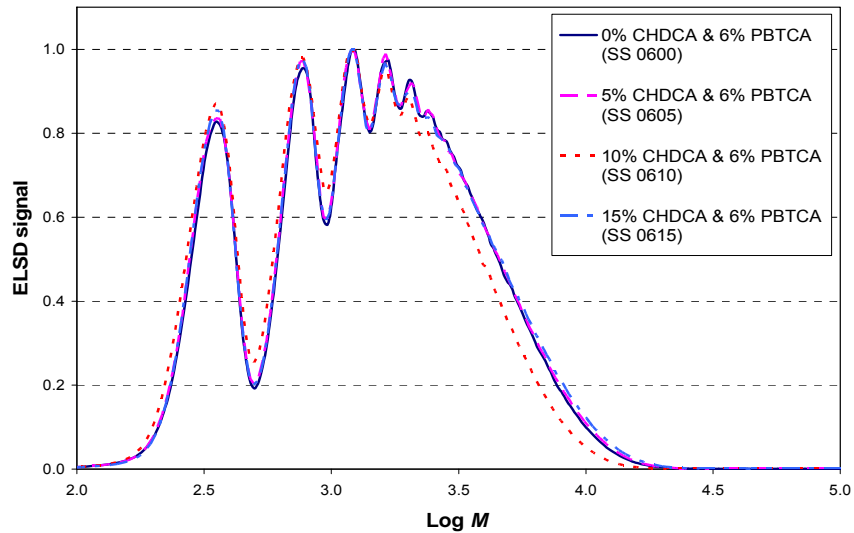


Figure 7.13a: Effect of CHDCA content on the molecular weight of the polyester (normalized to highest peak) containing 6% PBTCA

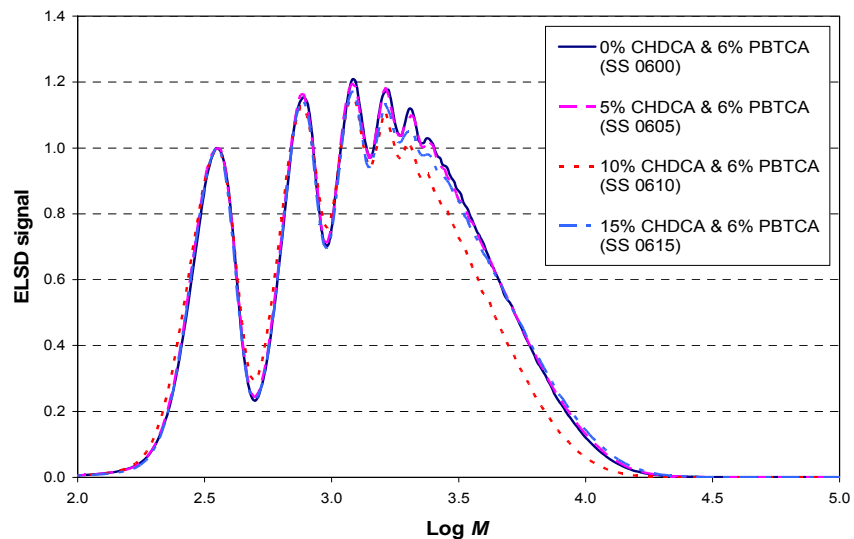


Figure 7.13b: Effect of CHDCA content on the molecular weight of the polyester (normalized to 1st peak) containing 6% PBTCA

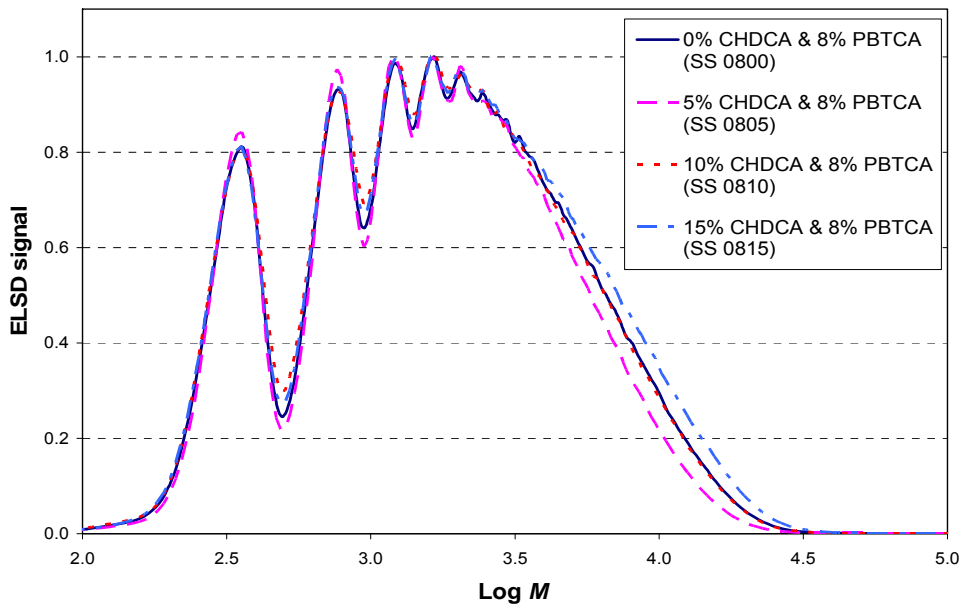


Figure 7.14a: Effect of CHDCA content on the molecular weight of the polyester (normalized to highest peak) containing 8% PBTCA

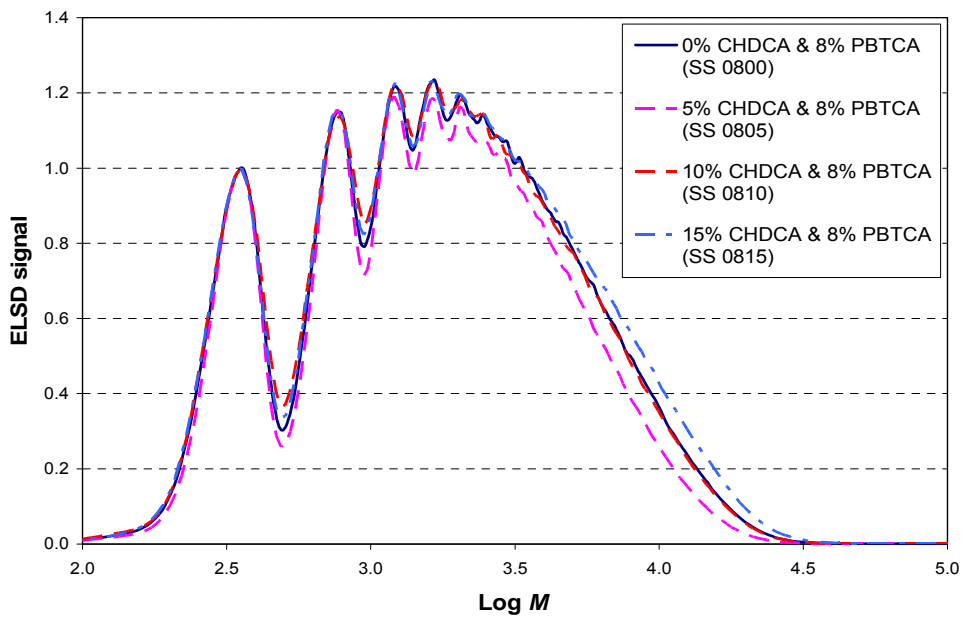


Figure 7.14b: Effect of CHDCA content on the molecular weight of the polyester (normalized to 1st peak) containing 8% PBTCA

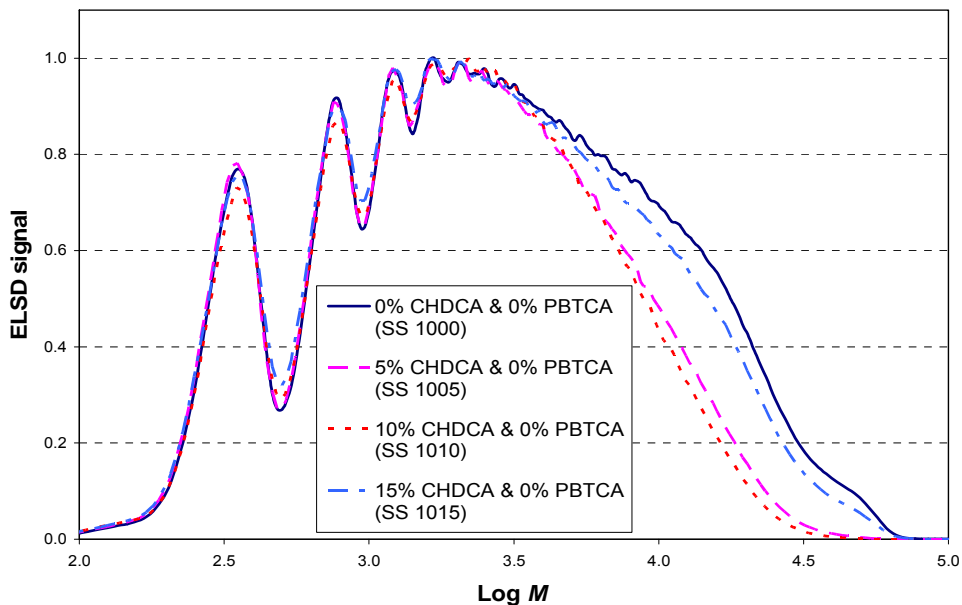


Figure 7.15a: Effect of CHDCA content on the molecular weight of the polyester (normalized to highest peak) containing 10% PBTCA

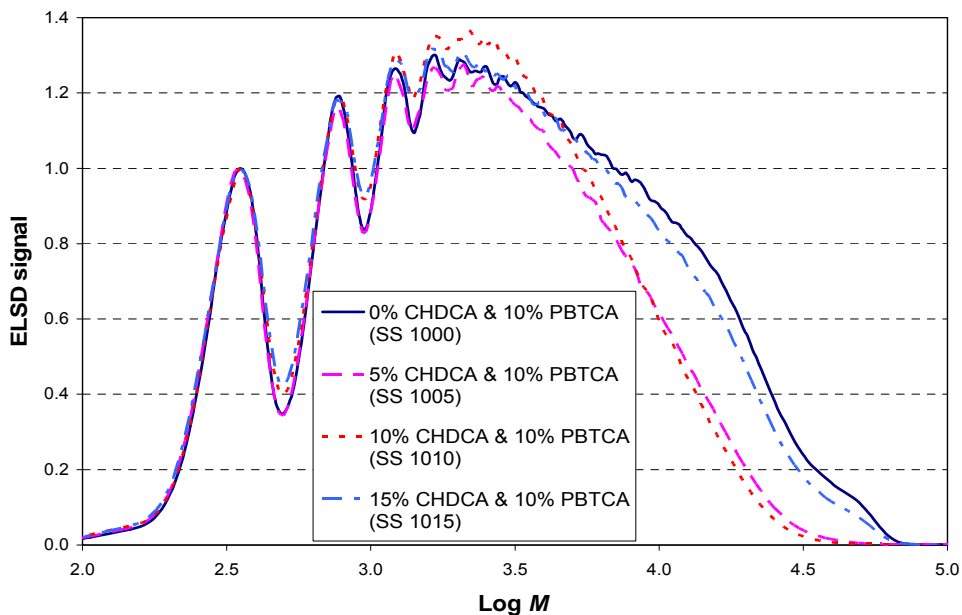


Figure 7.15b: Effect of CHDCA content on the molecular weight of the polyester (normalized to 1st peak) containing 10% PBTCA

The average molecular weight distributions of the synthesized polyesters are presented in Table 7.2 below:

Table 7.2: Molecular weight and molecular weight distribution data for synthesized polyester glycols

Polyester Sample	% PBTCA	% CHDCA	Ave Mn (g/mol)	Ave Mw (g/mol)	Ave Mz (g/mol)	Mn/Mw
SS 0000	0	0	980.2	2054.3	3442.4	2.096
SS 0600	6	0	1090.0	2331.7	4129.8	2.1392
SS 0605	6	5	1081.2	2348.1	4231.7	2.1718
SS 0610	6	10	979.2	2048.0	3557.1	2.092
SS 0615	6	15	1089.1	2392.8	4375.7	2.1970
SS 0800	8	0	1191.9	2980.7	5991.5	2.5008
SS 0805	8	5	1164.9	2739.4	5235.5	2.3516
SS 0810	8	10	1167.8	2924.7	5892.3	2.5045
SS 0815	8	15	1208.3	3174.4	6670.3	2.6272
SS 1000	10	0	1470.6	5192.0	1393.0	3.5305
SS 1005	10	5	1299.7	3721.9	8287.1	2.8637
SS 1010	10	10	1307.5	3532.5	7429.5	2.7017
SS 1015	10	15	1389.5	4738.0	1255.3	3.4099

7.5.2 GPC analysis of the polyurethanes

Figure 7.16 below shows the MWD of a polyurethane prepared from its synthesized polyester, normalized to both the first and highest peaks. It is clear that a very high percentage of the low MW fraction reacted during PU synthesis.

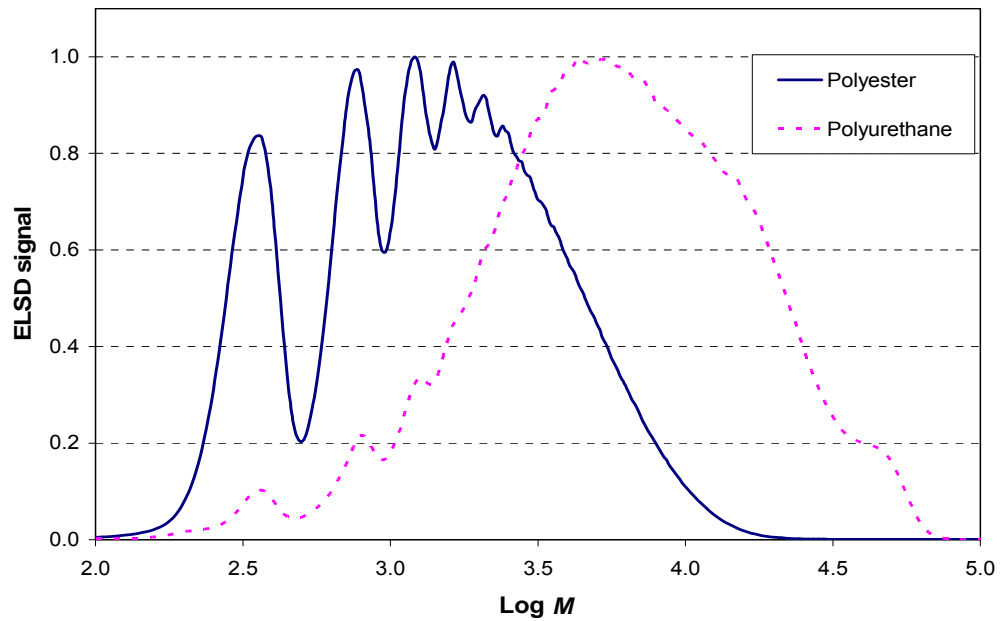


Figure 7.16a: MWD of PU from polyester (normalized to highest peak)

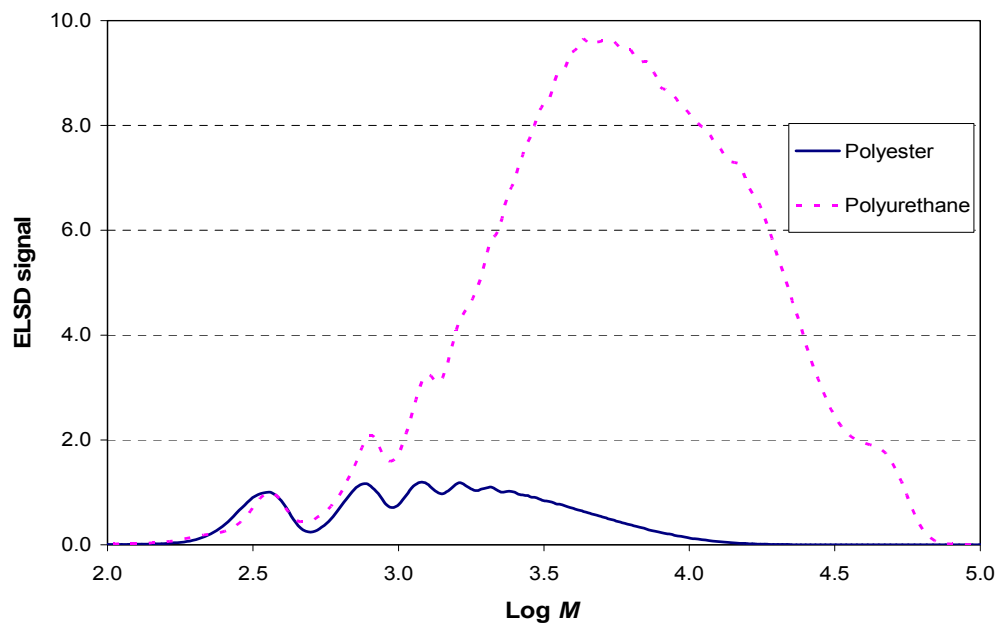


Figure 7.16b: MWD of PU from polyester (normalized to 1st peak)

7.6 Fourier transform infrared spectroscopy

FTIR analysis was used firstly to monitor the isocyanate (NCO-group) consumption during the polyurethane synthesis, and secondly to characterize of the PU itself.

7.6.1 Monitoring of NCO content

The presence of the free NCO-group during the synthesis of the urethane pre-polymer is shown in Figure 7.17a, represented by the NCO-peak at 2260 cm^{-1} .

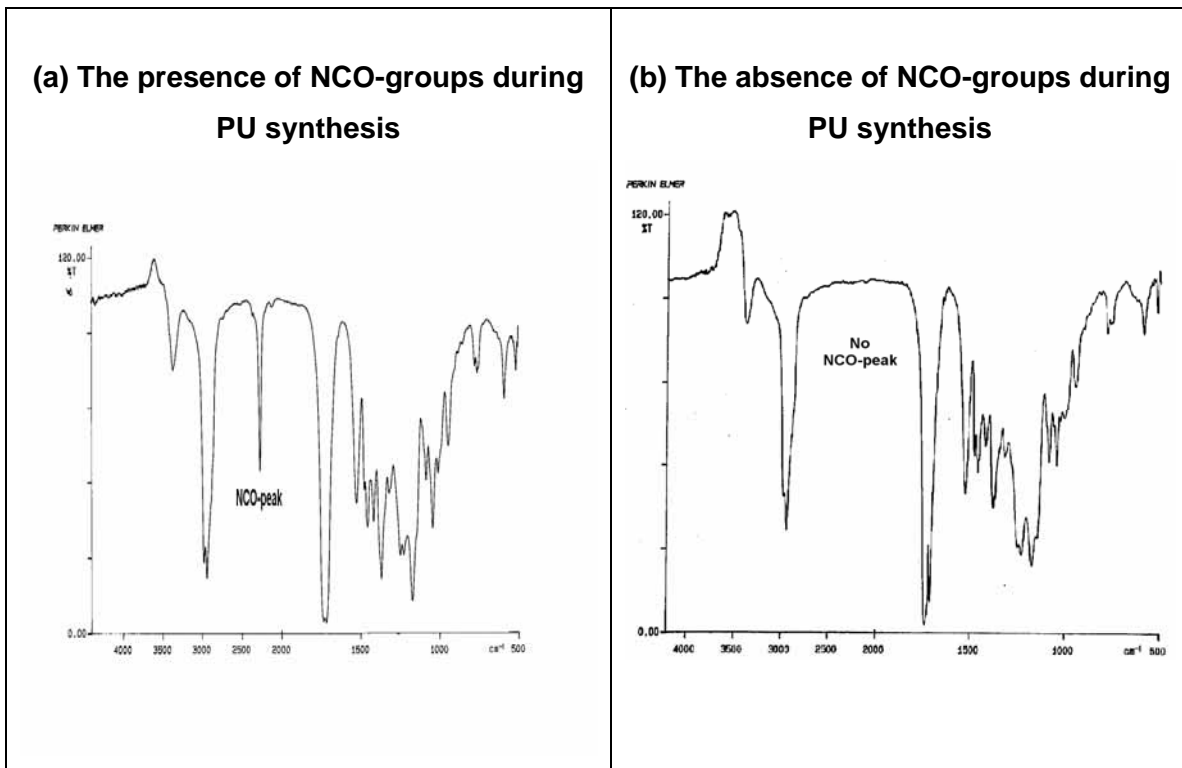


Figure 7.17: Monitoring the NCO-content by FTIR during PU synthesis (at 4 scans, 4.0 cm^{-1})

The absence of the characteristic -NCO peak at 2260 cm^{-1} in Figure 7.17b indicates that all the isocyanate groups were reacted. This is very important, as NCO-groups should not be present during the dispersion stage. If NCO-groups are present during the addition of water, this will result in the formation of a crosslinked structure.

7.6.2 Characterization of the polyurethane

FTIR analyses of the polyester polyols and the dried polyurethane films were done using a photo-acoustic cell (PAS). Figures 7.18 and 7.19 contain the respective FTIR spectra of the polyols and PUs synthesized.

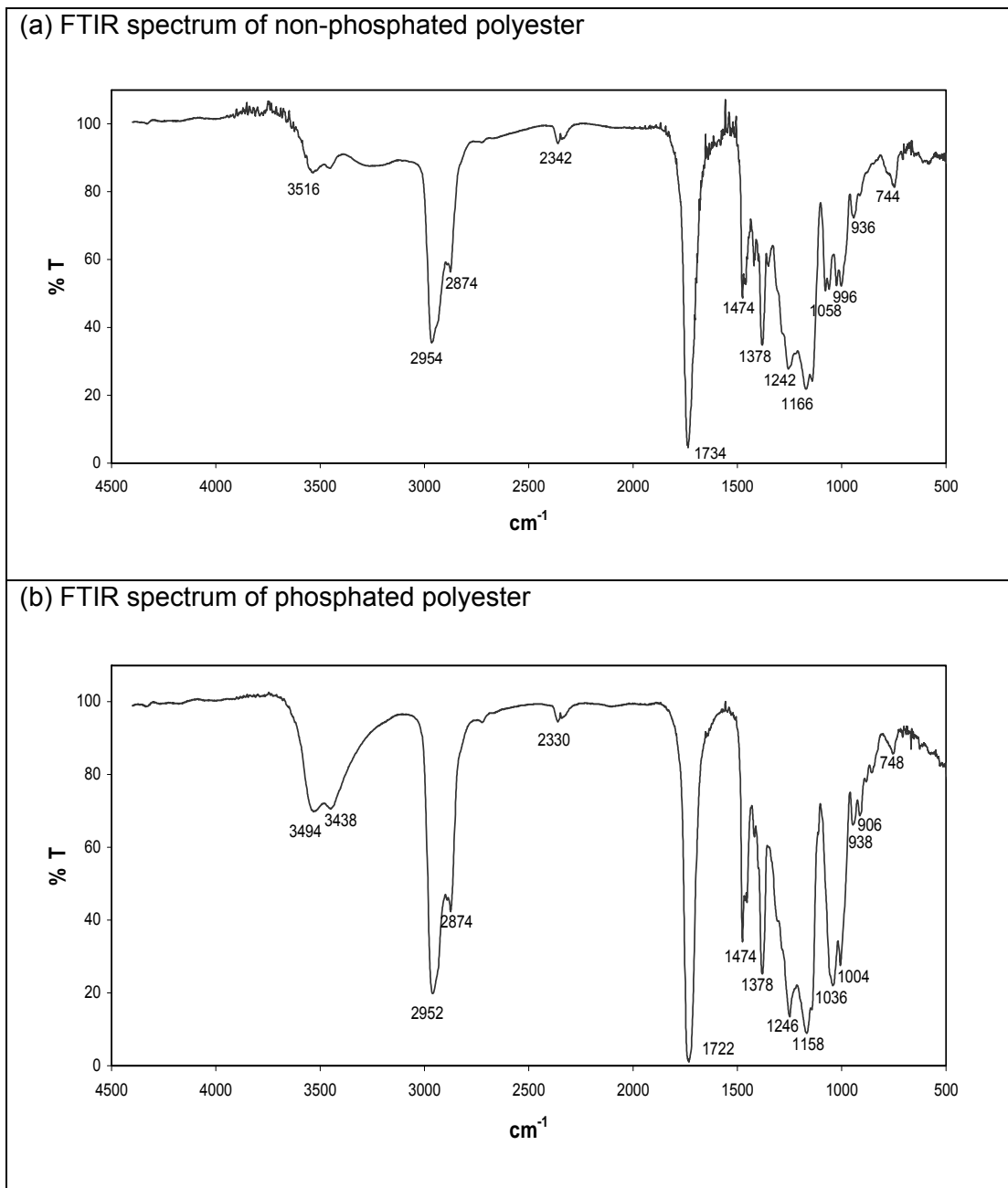


Figure 7.18: FTIR spectra of non-phosphated and phosphated polyesters

The band at 1732 cm^{-1} in all the IR spectra, represents the carbonyl group ($\text{C}=\text{O}$) of the polyester. It is clearly the dominant peak in the IR spectrum of the polyol (Figure 7.18), but it decreases in size in the PU FTIR-spectrum (Figure 7.19). This is due to no additional ester groups being formed during urethane formation [9].

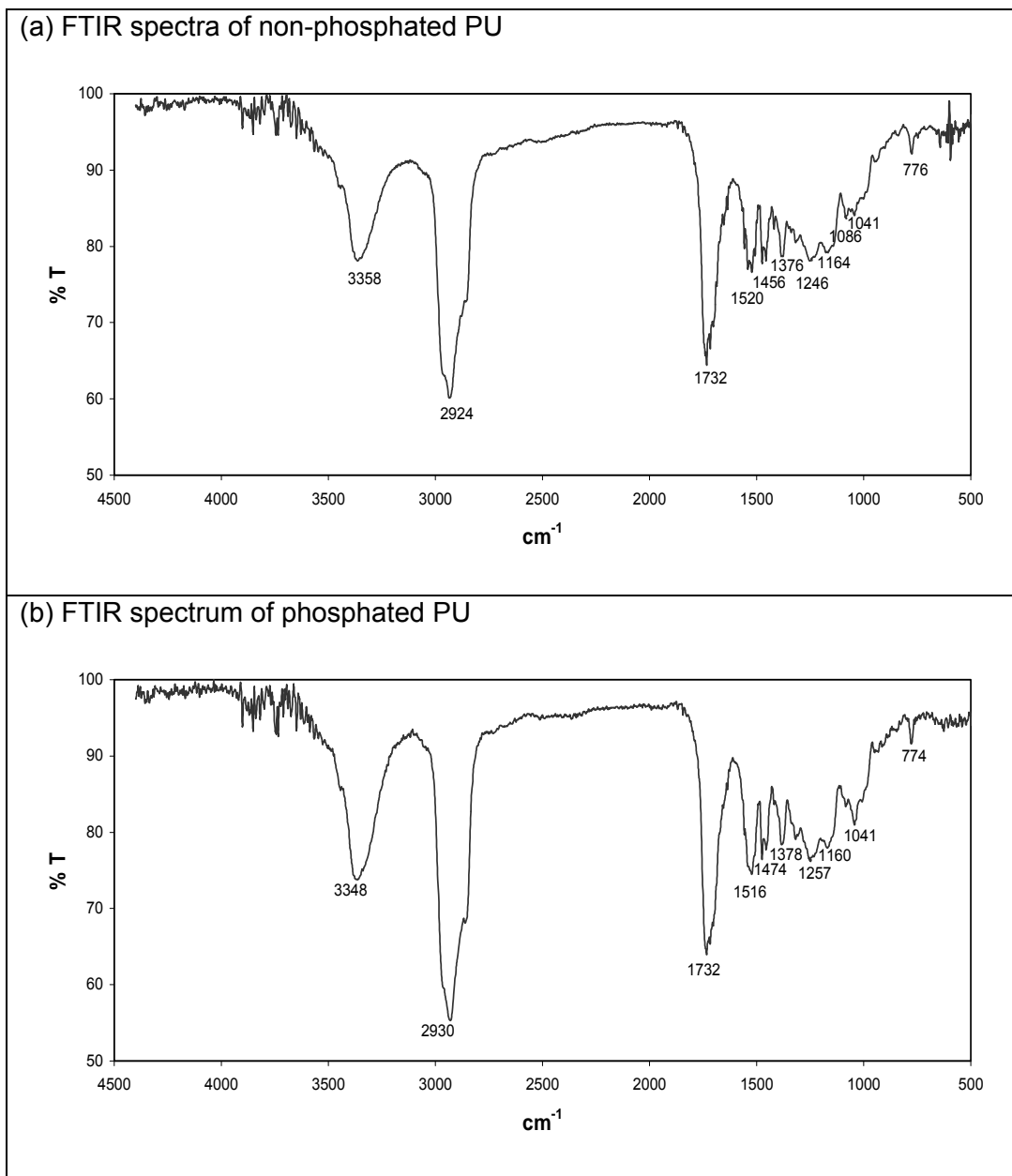


Figure 7.19: FTIR-spectra of non-phosphated and phosphated polyurethanes

The absorption bands between 2800 to 3000 cm^{-1} are due to C-H stretching of the CH_2 and CH_3 groups [10].

In Figure 7.18, the absorption bands of the polyol between 3200 to 3350 cm^{-1} , represent the OH-groups of the polymer. These OH-peaks in Figure 7.19 of the PU FTIR-spectrum are dominated by the NH-stretching band of the urethane group at about 3340 cm^{-1} . The NH deformation vibration [10] is represented by the peak at 1520 to 1530 cm^{-1} in the PU FTIR-spectrum.

The band at 1378 cm^{-1} in the polyol FTIR-spectra of Figure 7.18, represents the C- CH_3 (symmetrical) deformation, while the C-O stretching deformation is represented by the bands between 1140 to 1246 cm^{-1} .

The phosphoryl linkage (P=O) in organic compounds has a broad absorption range at 1080 to 1450 cm^{-1} [11,13]. The effect of strong H-bonding results in large frequency shifts to a lower absorption range. H-bonding resulting from P-OH groups is subjected to shifts of 50 to 80 cm^{-1} . Phosphated compounds containing (HO)-P=O groups have an even stronger H-bonding, which results in larger frequency shifts and increases in intensity. This increase in intensity can be clearly seen by comparing the FTIR-spectra of the two polyols in Figure 7.18, which is in the frequency range of 1004 to 1036 cm^{-1} .

Thomas and Chittenden determined an overall phosphoryl absorption range of 1087 to 1261 cm^{-1} , based on the evaluation of 160 organic compounds containing (HO)-P=O or (HO)₂-P=O groups [12]. Thus the absorption peaks at 1004 and 1036 cm^{-1} in the polyol IR-spectrum of Figure 7.18b, can be assigned to P=O stretching vibrations [11,13].

7.7 NMR analysis

The NMR analyses that were carried out on both the polyester and the polyurethane include ^1H , ^{13}C , ^{13}C -APT and ^{31}P -NMR. These analyses were done to confirm the molecular structure of the polyester and the polyurethane.

To overcome the complexity of interpreting the NMR spectra, the polyester was first synthesized with only two monomers (NPG + AA), this was afterwards increased to three monomers with CHDCA and PBTCA respectively (NPG + AA + CHDCA; and NPG + AA + PBTCA), as shown in Figure A.9.1 in Appendix 9. Here, the CHDCA and PBTCA contents were increased from an average of 10% and 8% respectively, to 20% and 25% respectively. This was done to increase their sensitivity towards NMR analysis. Finally, the monomer content in the polyester was increased to include all four monomers (NPG + AA + CHDCA + PBTCA).

7.7.1 ^1H -NMR analysis

The ^1H -NMR spectrum of the polyester consisting of all four monomers is shown in Figure 7.20a. The ^1H -NMR spectrum of the polyurethane is shown in Figure 7.20b. ^1H -NMR results of the polyester and polyurethane are explained in detail in Table 7.3a and Table 7.3b, respectively. ^1H -NMR data for the solvents and neutralizing base are given in Table 7.3c.

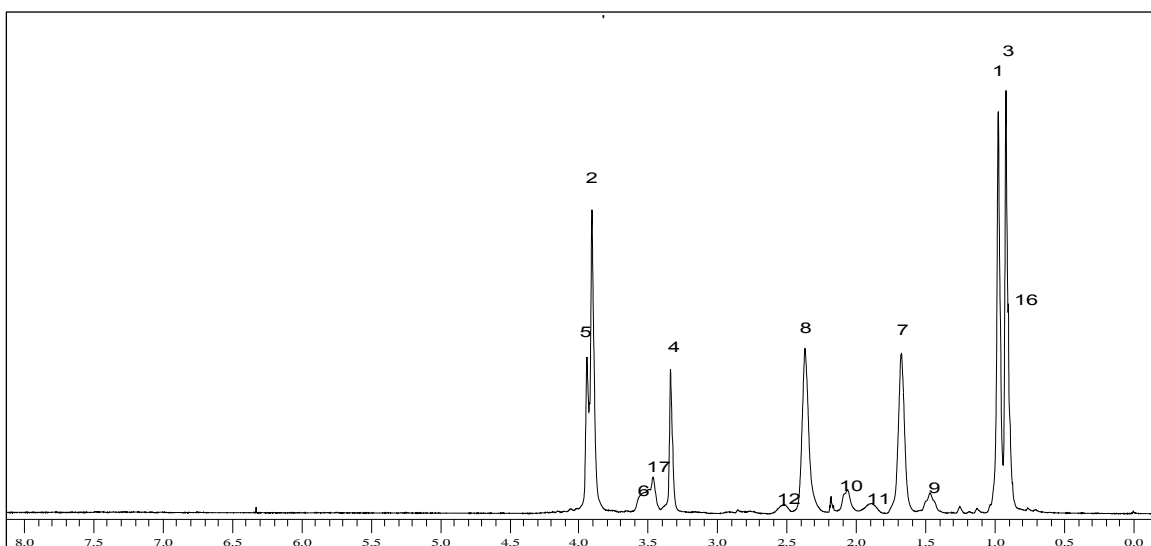


Figure 7.20a: ^1H -NMR spectra of polyester containing all four monomers

The polyester and polyurethane chains are OH-terminated by the NPG molecule, which is located at two different chemical environments; one in the inner chain and the other on the chain end. The polyester has a higher amount of NPG chain-end groups compared to the polyurethane, as the OH-groups are consumed by the isocyanate during polyurethane synthesis. This phenomenon was seen after comparing the difference in CH₃ peak intensities at 0.974 ppm for the inner chain (peak 1) and 0.918 ppm for the outer chain (peak 3) in Figure 7.20a, with those of the polyurethane shown below in Figure 7.20b.

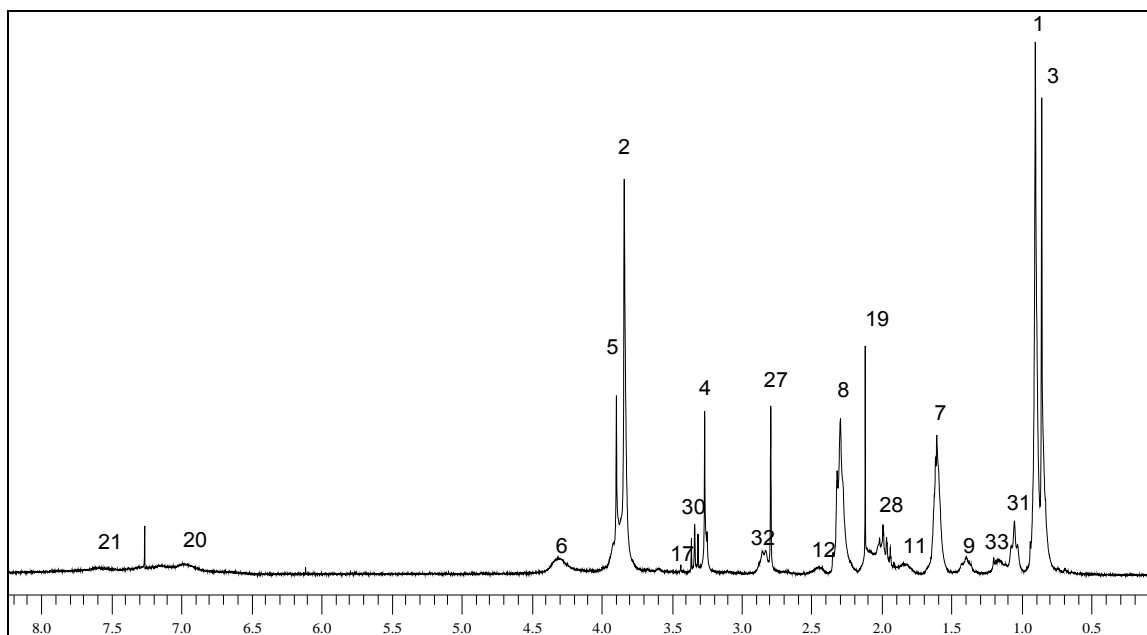


Figure 7.20b: ¹H-NMR spectra of polyurethane

The PBTCA content in Figure 7.20a was very low ($\pm 8\%$ in polyester), and the chemical similarities of its methylene groups to that of AA [14] between 2.32 to 2.37 ppm, made it difficult to separate them for identification from each other. However, these peaks are clearly visible when the PBTCA content was increased to 25%, as shown in Table 7.3a and Figure A.9.1a in Appendix 9.

The *cis/trans* configuration of the CHDCA protons can also be easily identified from spectra in Figure 7.20a and Figure A.9.1a, which showed the *cis/trans* CH₂ protons at 2.060 ppm (peak 10) and 1.446 ppm (peak 9) consecutively, and the *cis/trans* CH protons at 2.518 ppm (peak 12) and 1.888 ppm (peak 11) consecutively. These values were found to be similar to those in literature [15].

Table 7.3a: ¹H-NMR analysis of synthesized polyester

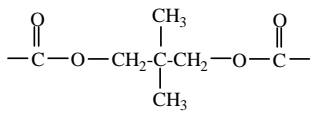
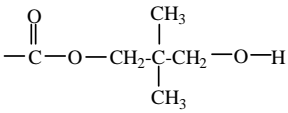
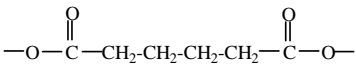

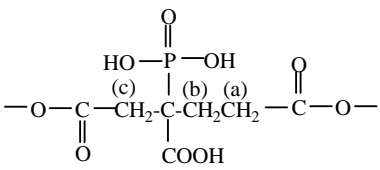
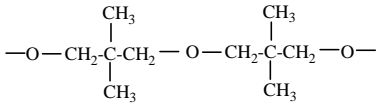
Structure	Group	Chemical Shift (ppm)	Peak no.
	CH ₃ protons of NPG in inner chain CH ₂ protons of NPG in inner chain	0.974 3.903	1 2
	CH ₃ protons of NPG in chain end CH ₂ protons of NPG in chain end adjacent to hydroxyl group CH ₂ protons of NPG in chain end adjacent to ester group OH protons of NPG	0.918 3.903 3.939 3.4-3.6	3 4 5 6
	Internal CH ₂ protons of AA External CH ₂ protons of AA	1.617 2.368	7 8
	CH ₂ protons of CHDCA (<i>trans</i>) CH ₂ protons of CHDCA (<i>cis</i>) CH protons of CHDCA (<i>trans</i>) CH protons of CHDCA (<i>cis</i>)	1.446 2.060 1.888 2.518	9 10 11 12
	<i>Peaks clearer in Figure A.9.1a</i> (a) CH ₂ protons of PBTCA between methylene and carboxyl groups (b) CH ₂ protons of PBTCA between methylene and quaternary carbon (c) CH ₂ protons of PBTCA between quaternary carbon and carboxyl group	2.319 2.276 2.327	13 14 15
	CH ₃ protons of NPG ether group CH ₂ protons of NPG ether group	0.901 3.433	16 17

Table 7.3b: ¹H-NMR analysis of synthesized polyurethane

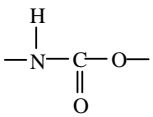
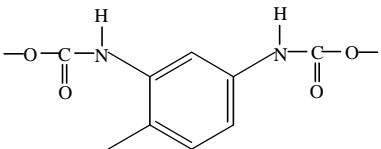
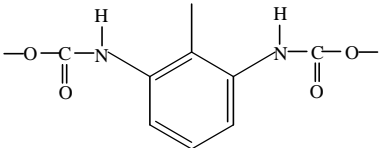
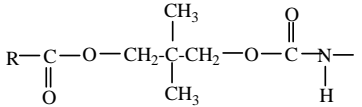
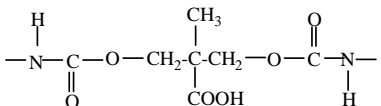
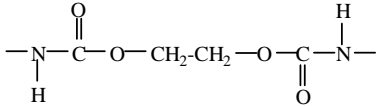
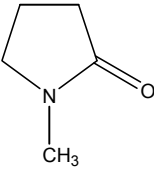
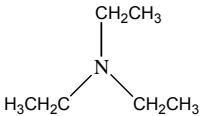
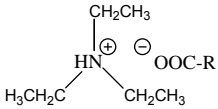
Structure	Group	Chemical Shift (ppm)	Peak no.
	Urethane proton	9.13-9.14	18
	CH ₃ protons of 2,4-TDI CH protons of 2,4-TDI ring	2.117 6.8-7.1	19 20
	CH ₃ protons of 2,6-TDI CH protons of 2,6-TDI ring	2.117 7.4-7.7	19 21
	CH ₃ protons of NPG reacted to TDI CH ₂ protons of NPG reacted to TDI	0.8-1.0 3.8-4.0	22 23
	CH ₃ protons of DMPA CH ₂ protons of DMPA	0.8-1.0 3.8-4.0	24 25
	CH ₂ protons of EG	3.8-4.0	26

Table 7.3c: ¹H-NMR analysis of NMP solvent and TEA neutralizing base in polyurethane synthesis

Structure	Group	Chemical Shift (ppm)	Peak no.
	CH ₃ protons of NMP CH ₂ protons of NMP in the middle of the two CH ₂ groups CH ₂ protons of NMP adjacent to nitrogen CH ₂ protons of NMP adjacent to carboxyl carbon	2.791 1.90 to 2.05 2.25 to 2.36 3.30 to 3.38	27 28 29 30
	CH ₃ protons of TEA CH ₂ protons of TEA	1.00 to 1.05 2.8 to 2.95	31 32
	CH ₃ protons of TEA salt CH ₂ protons of TEA salt	1.15 to 1.25 3.10 to 3.20	33 34

7.7.2 ^{13}C -NMR analysis

The ^{13}C -NMR spectra of the polyester and polyurethane between 10 to 80 ppm are shown in Figure 7.21, and the ^{13}C -NMR spectra of the polyester and polyurethane between 110 to 180 ppm are shown in Figure 7.22.

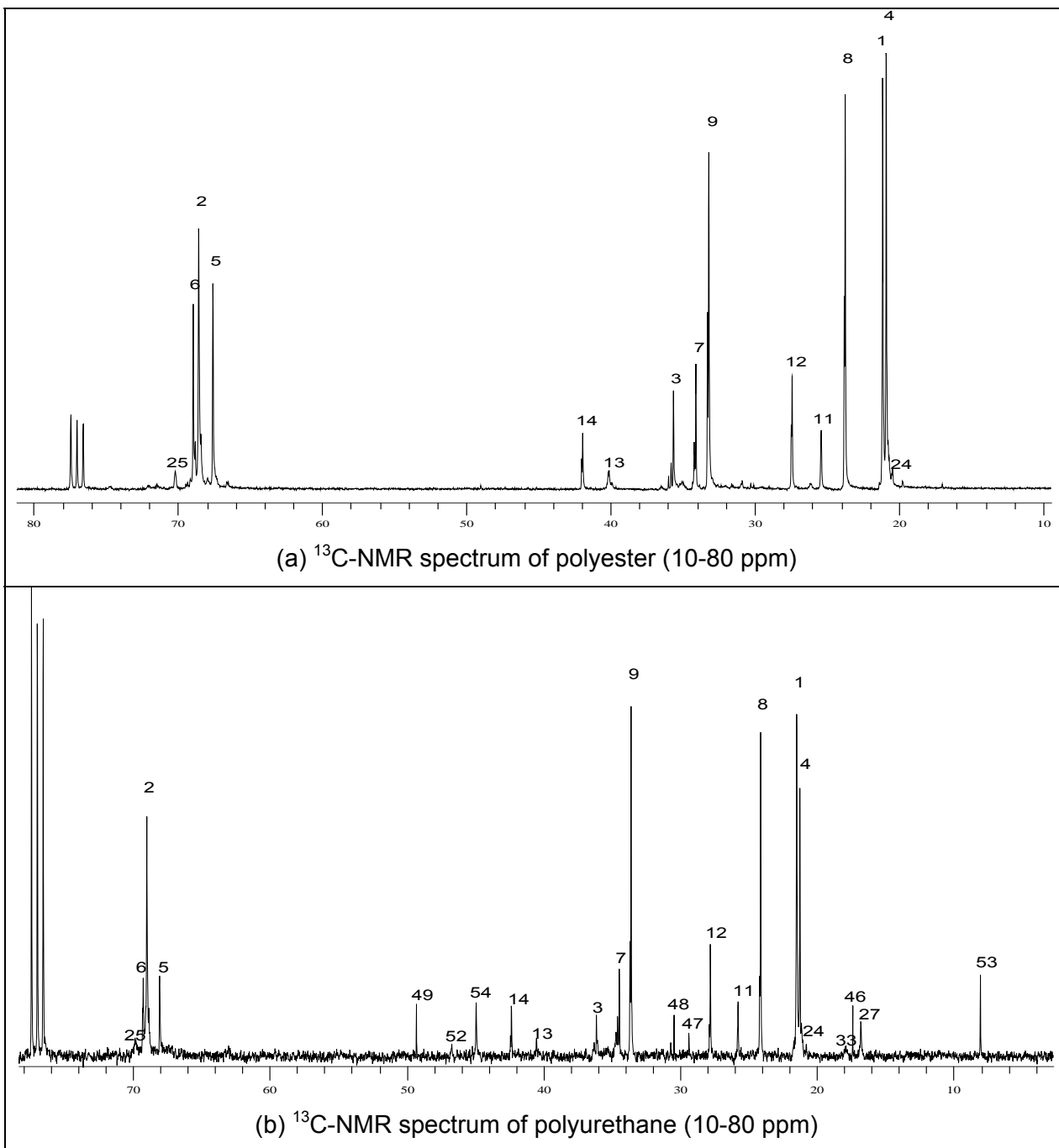


Figure 7.21: ^{13}C -NMR spectra of polyester and PU between 10 to 80 ppm

The polyester and polyurethane chains are both OH terminated. The PU have fewer NPG chain-end groups compared to the polyester, as the NPG chain-end groups is consumed by the isocyanate during polyurethane synthesis. This phenomenon was seen by comparing the difference in CH₃ and CH₂ peak heights in Figures 7.21a and 7.21b. The CH₃ peak height at 21.128 ppm for the inner chain (peak 1) increased compared to that of the outer chain (peak 4) at 20.885 ppm during polyurethane synthesis. Similarly, the CH₂ peak height at 68.566 ppm for the inner chain (peak 2) increased compared to that of the outer chain, which has two peaks due to the difference in chemical environment; one at 67.575 ppm (peaks 5) for the CH₂-OH group and the other at 68.939 ppm (peak 6) for CH₂-COO- group during polyurethane synthesis.

The low PBTCA content (\pm 8% in polyester) in Figures 7.21a and 7.21b make it difficult to separate its three CH₂ peaks from the other peaks in the spectra. However, its peaks are visible when the PBTCA content was increased to 25%, as shown in Table 7.4a and Figure A.9.1b in Appendix 9; the peaks appear at 29.0 to 31.0 ppm for the CH₂ carbon between the methylene and carboxyl carbon (peak 19); 26.0 to 27.0 ppm for the CH₂ carbon between the methylene and quaternary carbon (peak 20); and 31.0 to 32.0 ppm for the CH₂ carbon between the quaternary and carboxyl carbon (peak 21).

The *cis/trans* configuration of the CHDCA group can also be easily identified from the spectra in Figures 7.21a and 7.21b, and also Figure A.9.1a in Appendix 9. It showed the *cis/trans* CH₂ peaks at 27.397 ppm (peak 12) and 25.383 ppm (peak 11) consecutively, and the *cis/trans* CH peaks at 41.932 ppm (peak 14) and 40.097 ppm (peak 13) consecutively. These values were found to be similar to those in literature [15].

The carboxylic acid (-COOH) and ester (-COO-) groups of both the polyester and polyurethane are present between 173 to 180 ppm, as shown in Figure 7.22. The ester peaks have a higher intensity compared to the carboxylic acid groups, which is to be expected due to the polyester being processed to a acid value of below 6.0 gKOH/g.

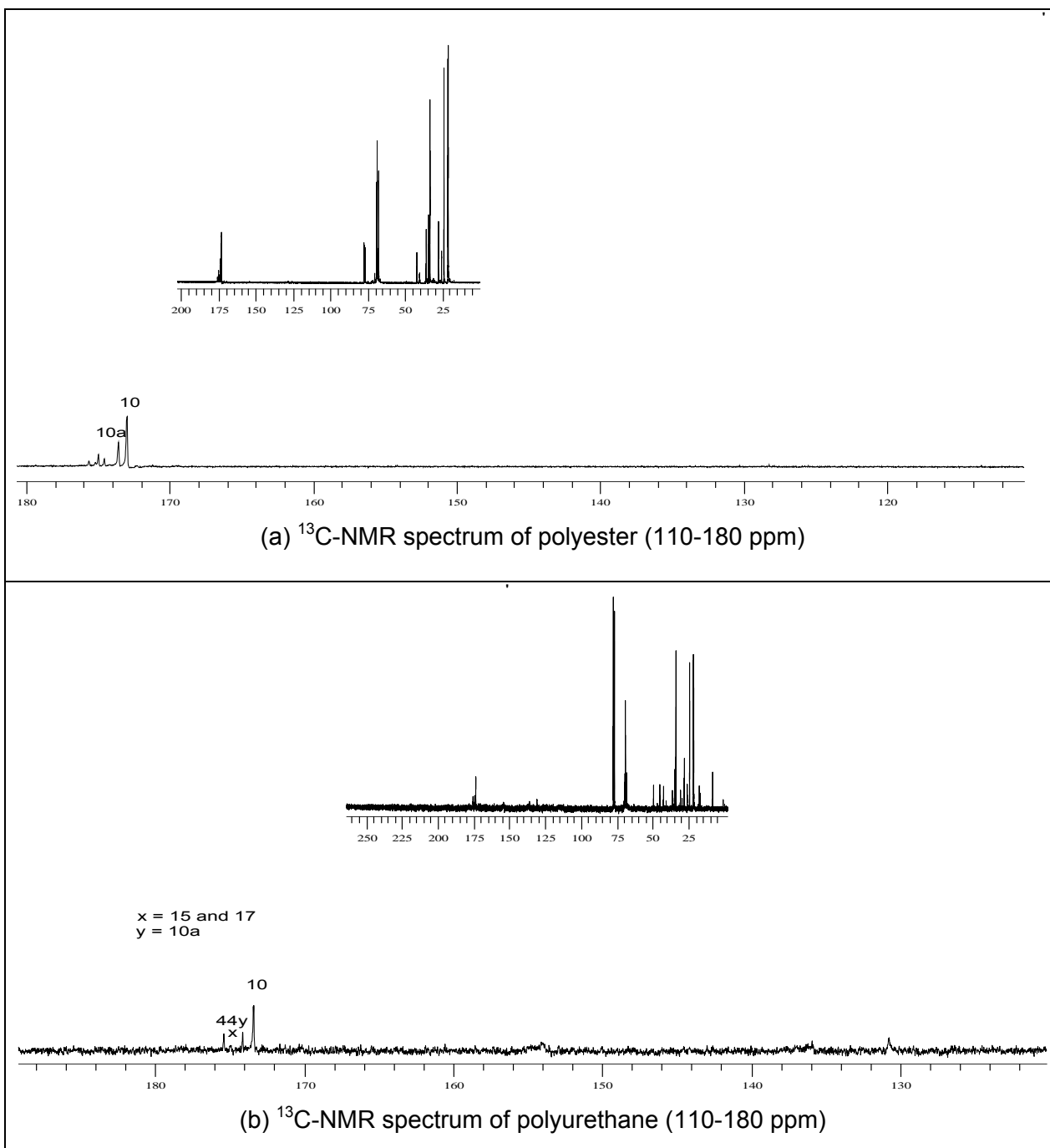


Figure 7.22: ^{13}C -NMR spectra of polyester and PU between 110 to 180 ppm

The ^{13}C -NMR results of both the polyester and polyurethane are tabulated in detail in Table 7.4a and Table 7.4b consecutively, including the ^{13}C -NMR results of the solvents in Table 7.4c.

The ^{13}C -NMR spectrum of both the 2,4- and 2,6-TDI urethane linkages between 110 to 160 ppm is shown in Figure 7.23b, which is explained in detail in Table 7.4b.

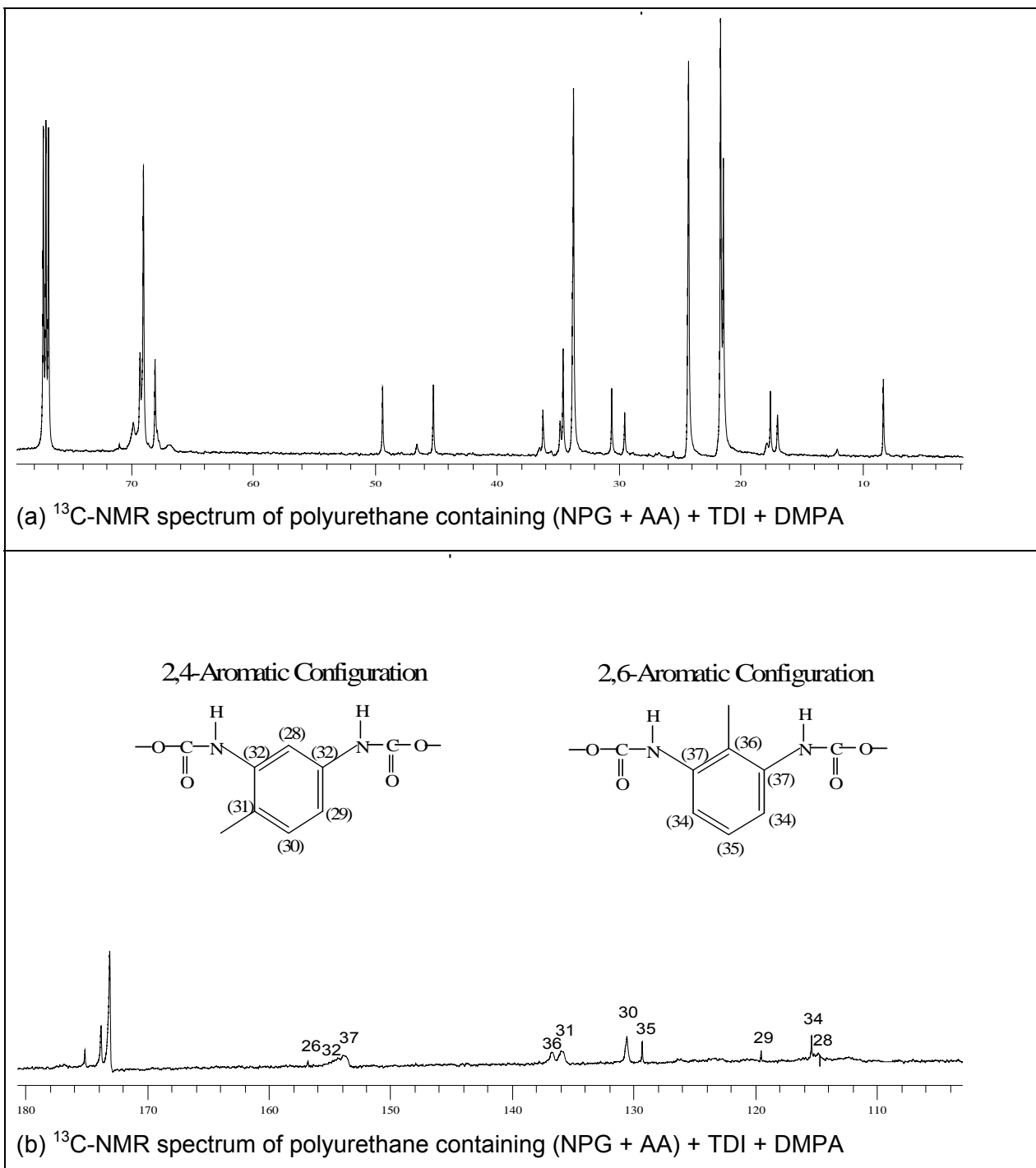
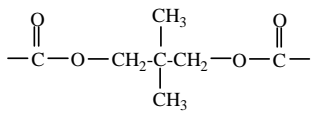
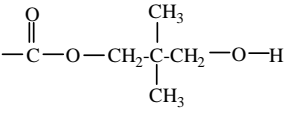
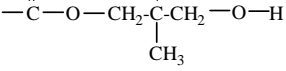
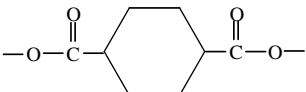
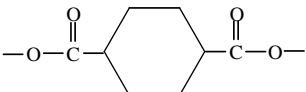
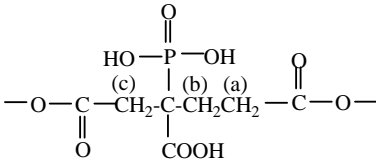


Figure 7.23: ^{13}C -NMR spectrum of PU, focusing on the TDI linkage

Table 7.4a: ¹³C-NMR analysis of synthesized polyester

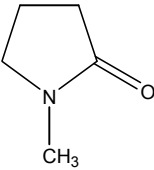
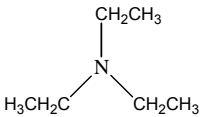
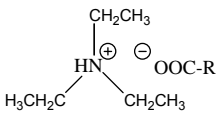
Structure	Group	Chemical Shift (ppm)	Peak no.
	CH ₃ carbon of NPG in inner chain	21.128	1
	CH ₂ carbon of NPG in inner chain	68.566	2
	C carbon of NPG in inner chain	35.361	3
	CH ₃ carbon of NPG in chain end	20.885	4
	CH ₂ carbon of NPG in chain end adjacent to hydroxyl group	67.575	5
	CH ₂ carbon of NPG in chain end adjacent to carboxyl group	68.939	6
	C carbon of NPG in chain end	34.072	7
	Internal CH ₂ carbon of AA	23.747	8
	External CH ₂ carbon of AA	33.179	9
	Carboxylic carbon of AA	173.461	10
	COOH carbon of AA	174.167	10a
	CH ₂ carbon of CHDCA (<i>trans</i>)	25.383	11
	CH ₂ carbon of CHDCA (<i>cis</i>)	27.397	12
	CH carbon of CHDCA (<i>trans</i>)	40.097	13
	CH carbon of CHDCA (<i>cis</i>)	41.932	14
	COO carbon of CHDCA (<i>trans</i>)	175.028	15
	COOH carbon of CHDCA (<i>trans</i>)	175.442	16
	COO carbon of CHDCA (<i>cis</i>)	175.783	17
	COOH carbon of CHDCA (<i>cis</i>)	176.254	18
	<i>Peaks clearer in Figure A.9.1b</i>		
	(a) CH ₂ carbon of PBTCA between methylene and carboxyl groups	29.0-31.0	19
	(b) CH ₂ carbon of PBTCA between methylene and quaternary carbon	26.0-27.0	20
	(c) CH ₂ carbon of PBTCA between carboxyl and quaternary carbon	31.0-32.0	21
	Quaternary carbon of PBTCA	35.0-37.0	22
	Tertiary COOH carbon of PBTCA	178.722	23

	CH ₃ carbon of NPG ether group	20.430	24
	CH ₂ carbon of NPG ether group	70.173	25

Table 7.4b: ¹³C-NMR analysis of synthesized polyurethane

Structure	Group	Chemical Shift (ppm)	Peak no.
	<i>Peak clearer in Figure 7.23b</i> Urethane carbon	156.076	26
	<i>Peaks clearer in Figure 7.23</i> CH ₃ carbon of 2,4-TDI (a ₁) Aromatic carbon of 2,4-TDI (a ₂) Aromatic carbon of 2,4-TDI (b) Aromatic carbon of 2,4-TDI (c) Aromatic carbon of 2,4-TDI (d) Aromatic carbon of 2,4-TDI	16.792 114-115 119.521 130.553 135.553 154-156	27 28 29 30 31 32
	<i>Peaks clearer in Figure 7.23</i> CH ₃ carbon of 2,6-TDI (a) Aromatic carbon of 2,6-TDI (b) Aromatic carbon of 2,6-TDI (c) Aromatic carbon of 2,6-TDI (d) Aromatic carbon of 2,6-TDI	17.864 115.376 129.298 136.709 153-155	33 34 35 36 37
	CH ₃ carbon of NPG reacted to TDI CH ₂ carbon of NPG reacted to TDI C carbon of NPG reacted to TDI	20.0-22.0 68.0-70.0 35.0-37.0	38 39 40
	CH ₃ carbon of DMPA CH ₂ carbon of DMPA Quaternary carbon of DMPA COOH carbon of DMPA	20.0-22.0 68.0-70.0 35.0-37.0	41 42 43 44
	CH ₂ carbon of EG	68.0-70.0	45

Table 7.4c: ^{13}C -NMR analysis of solvents and neutralizing base in synthesized polyurethane

Structure	Group	Chemical Shift (ppm)	Peak no.
	<p>CH₃ carbon of NMP</p> <p>CH₂ carbon of NMP in the middle of the two CH₂ groups</p> <p>CH₂ carbon of NMP adjacent to carboxyl carbon</p> <p>CH₂ carbon of NMP adjacent to nitrogen</p> <p>CO-carbon of NMP</p>	<p>16.792</p> <p>29.362</p> <p>30.434</p> <p>49.272</p> <p>174.86</p>	<p>46</p> <p>47</p> <p>48</p> <p>49</p> <p>50</p>
	<p>CH₃ carbon of TEA</p> <p>CH₂ carbon of TEA</p>	<p>12.424</p> <p>46.690</p>	<p>51</p> <p>52</p>
	<p>CH₃ carbon of TEA salt</p> <p>CH₂ carbon of TEA salt</p>	<p>8.039</p> <p>44.904</p>	<p>53</p> <p>54</p>

7.7.3 ³¹P-NMR analysis

The P-OH and tertiary COOH groups of PBTCA are expected to remain relatively unreacted during polyester and polyurethane synthesis. The tertiary COOH group should stay largely unreacted due to steric hindrance, which leaves the P-OH group more susceptible to further reactions. The P-OH group is of acidic nature, and can thus react with NPG during polyester synthesis, and also with TDI during polyurethane synthesis.

The unreacted P-OH group in the monomeric PBTCA is represented in Figure 7.24a between 20 to 22 ppm. During polyester synthesis, this P-OH peak stayed unreacted and shifted to peaks P1 to P3 between -7 to -2 ppm, as shown in Figures 7.24b. These peaks correlate to those in Figure 7.24c of the polyurethane spectrum, which suggests that the P-OH groups stayed unreacted during polyurethane synthesis.

Figure 7.24d shows a spectrum of a polyester containing 25% PBTCA synthesized until it gelled. A sample that was still flowable above 100°C was taken for NMR analysis. Comparing Figure 7.24d with Figure 7.24b, it is seen that the peaks between -7 to -2 ppm have decreased in intensity, with a simultaneous increase in peak intensity of peak P4 between 22 to 26 ppm, showing that the P-OH had reacted in Figure 7.24d.

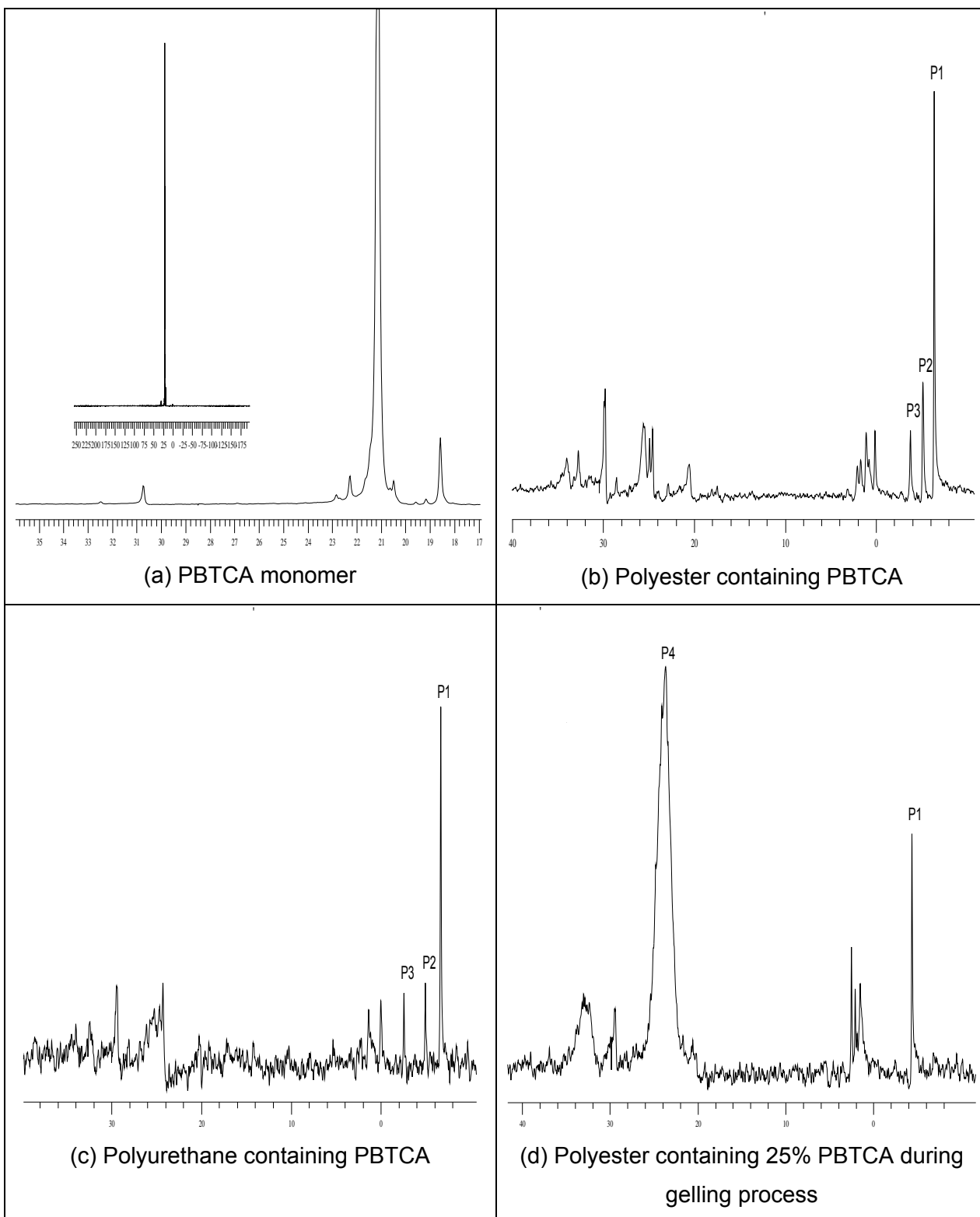


Figure 7.24: ^{31}P -NMR spectra of PB TCA-containing polyester and polyurethane

7.8 References

1. T. Kajiyama and W. J. Macknight, *Trans. Soc. Theol.*, **13**, 527, 1969.
2. K. K. S. Hwang, C. Z. Yang, S. L. Cooper, *Polym. Eng. Sci.*, **21(15)**, 1027, 1981.
3. J. W. S. Hearn, *Polymers and their Properties*, Ellis Horwood Ltd., Chichester, 1982.
4. D. J. Hourston, J. A. McCluskey, *J. Appl. Polym. Sci.*, **30**, 2957, 1984.
5. M. Patel, B. Suthar, *Eur. Polym. J.*, **23**, 399, 1987.
6. R. B. Fox, J. P. Armistead, C. M. Roland, D. J. Moonay, *J. Appl. Polym. Sci.*, **41**, 1281, 1990.
7. T. C. Chang, Y. S. Chiu, H. B. Chen, S. Y. Ho. *Polym. Degrad. Stab.*, **47**, 375, 1995.
8. F. M. B. Coutinho, M. C. Delpech. *Polym. Degrad. Stab.*, **70**, 49, 2000.
9. Gary D. Christian and James E. O'Reilly, *Instrumental Analysis*, Second Edition, Allyn and Bacon Inc., Newton, Massachusetts, 1978.
10. D. J. David and H. B. Staley, *Analytical Chemistry of the Polyurethanes*, **Vol. XVI**, Part III, Wiley-Interscience, 1969.
11. K. D. Berlin, G. M. Blackburn, J. S. Cohen, D. E. C. Corbridge and D. M. Hellwege, *Topics in Phosphorus Chemistry*, **Vol. 6**, Wiley-Interscience, New York, 1969.
12. L. C. Thomas, R. A. Chittenden, *Spectrochim. Acta*, **20**, 467, 1964.
13. G. Socrates, *Infrared Characteristic Group Frequencies, Tables and Charts*, 2nd Edition, John Wiley and Sons, New York, 1994.
14. H. S. Park, D. W. Kim, K. H. Hwang, B. S. Yoon, J. P. Wu, J. W. Park, H. S. Hahm, W. B. Im, *J. Appl. Polym. Sci.*, **80**, 2316, 2001.
15. B. Vanhaecht, M. N. Teerenstra, D. R. Suwier, R. Willem, M. Biesemans, C. E. Koning, *J. Polym. Sci. A Polym. Chem.*, **39**, 833, 2001.
16. J. W. Gooch, H. Dong, F. J. Schork, *J. Appl. Polym. Sci.*, **76**, 105, 2000.
17. M. F. Lin, W. C. Tsen, Y. C. Shu, F. S. Chuang, *J. Appl. Polym. Sci.*, **79**, 881, 2001.
18. C. J. Pouchert, J. Behnke, *The Aldrich Library of ¹³C and ¹H FT NMR Spectra*, Aldrich Chemical Company Inc, Wisconsin, 1993.
19. W. W. Simons, *The Sadtler Guide to Carbon-13 NMR Spectra*, Sadtler Research Laboratories, Philadelphia, 1983.

8 POLYURETHANE-FILLER COMPOSITES FOR PAPERBOARD APPLICATION

8.1 Introduction

Fillers are generally added to coating mixtures to decrease product cost and also to enhance certain properties. For example, carbon black is added to improve conductivity [1-3]; phosphates to improve flame resistance [4-6]; aluminium hydroxide [7], titanium dioxide [8,9], zinc oxide [8], kaolin [9,10] and silica [11-15] to improve mechanical properties.

Recently, nano-fillers have attracted considerable attention in organic-inorganic nanocomposites, since their application has dramatically improved material properties such as heat and radiation resistance, barrier, mechanical and electrical properties in coatings, plastics, adhesives and rubbers [15-19]. These nano-fillers include titanium dioxide, zinc oxide, calcium carbonate, silicone dioxide and montmorillonite-based clays.

The properties of the polymer nanocomposites are however hugely affected by the degree of dispersion of the nano-particles into the polymer matrix, which gives rise to three types of composite materials [20-24], as shown in Figure 8.1: phase separated/unintercalated, intercalated and exfoliated. Phase separated/unintercalated composite materials normally possess poor mechanical and physical properties, whereby its properties increase from intercalated to exfoliated composite materials.

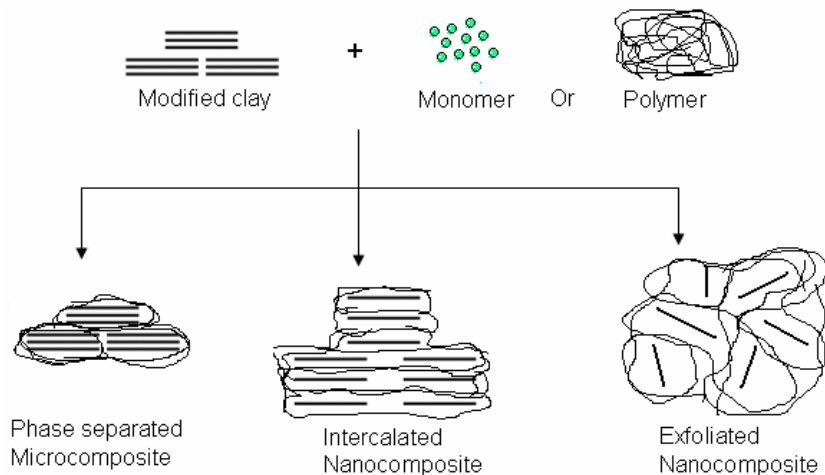


Figure 8.1: Schematic illustration of the three main types of polymer nanocomposites

For paperboard coatings, consideration was given to using flaky fillers to increase the tortuous path-length for moisture to move through the coating (moisture needs to go around the particles), as this should enhance the barrier properties of the coating. For these purposes, both micro- and nano-fillers were investigated.

8.2 Micro-filler incorporation

Micro-fillers are too large to be incorporated inside the PU-dispersion particle, whether added before or after the dispersion stage during PU synthesis, and they precipitate out of the coating mixture after agitation has stopped. The MVTR and blocking results of the micro-fillers that were investigated are shown in Table 8.1.

Table 8.1: Effects of micro-filler on MVTR and blocking of PU coated paperboard

Coating blend	% Micro-filler	No Wax C78 addition		Wax C78 addition	
		MVTR (g/m ² /24h)	Degree of blocking	MVTR (g/m ² /24h)	Degree of blocking
PU	0	815	Medium	187	Kissing
BaSO ₄	5	806	Medium	434	Medium
BaSO ₄	10	805	Medium	436	Kissing
BaSO ₄	15	777	Medium	394	Kissing
BaSO ₄	20	768	Kissing	378	Kissing
BaSO ₄	25	788	Medium	345	Kissing
BaSO ₄	30	826	Kissing	361	Kissing
BaSO ₄	40	834	Medium	446	Kissing
BaSO ₄	50	838	Kissing	503	Kissing
Clay	0	815	Medium	187	Kissing
Clay	5	749	Medium (-)	407	Kissing
Clay	10	799	Medium (-)	342	Kissing
Clay	15	804	Medium (--)	303	Kissing
Clay	20	792	Medium (-)	292	Kissing
Clay	25	763	Medium (-)	319	Kissing
Clay	30	780	Medium (-)	328	Kissing
Clay	40	757	Medium (--)	398	Kissing
Clay	50	805	Kissing	454	Kissing
Talc	0	815	Medium	187	Kissing
Talc	5	823	Medium (-)	339	Kissing
Talc	10	771	Medium (-)	313	Kissing
Talc	15	775	Medium (--)	300	Kissing
Talc	20	766	Medium (-)	279	Kissing
Talc	25	762	Medium (-)	266	Kissing
Talc	30	746	Medium (-)	259	Kissing
Talc	40	766	Medium (--)	287	Kissing
Talc	50	770	Kissing	327	Kissing

The PU-filler microcomposites tabulated in Table 8.1 show that a minimum MVTR is obtained when they contained a micro-filler content of 20 to 30%. The difference in MVTR between the three micro-fillers is due to the differences in their basic filler morphology, such as shape and hydrophobicity. However, the incorporation of wax C78 into the talc-containing PU-filler microcomposite gave the best results, as shown in Table 8.1 and also graphically in Figure 8.2 below. A minimum MVTR was achieved at 30% talc incorporation.

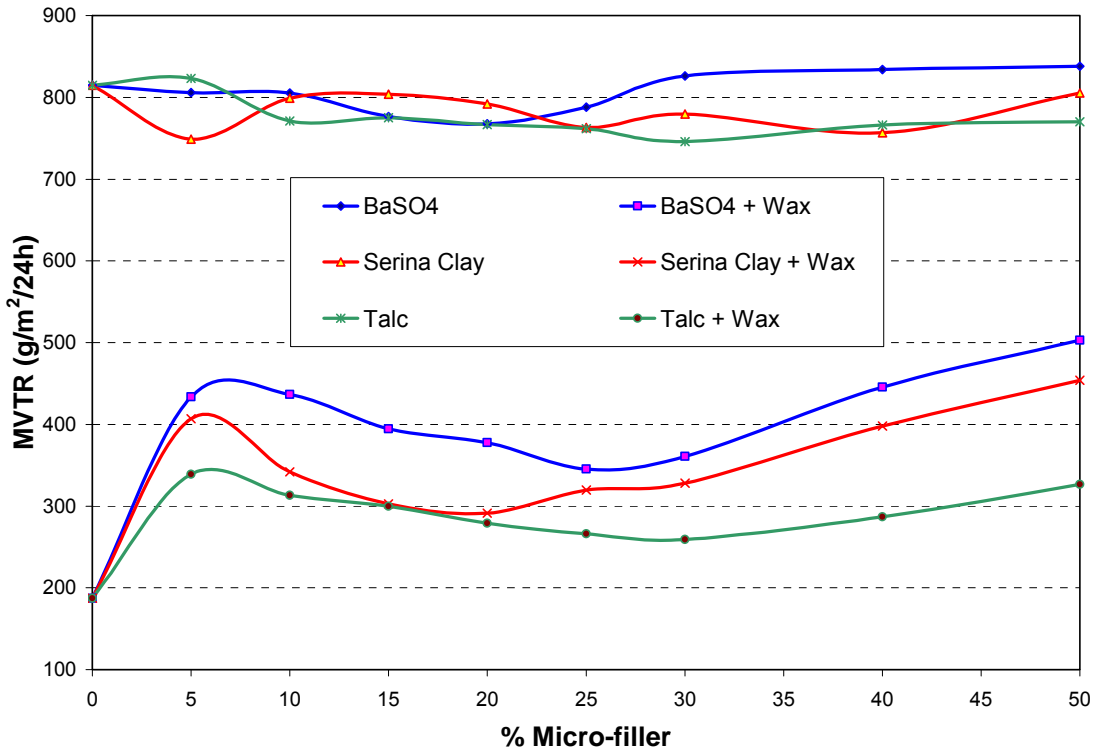


Figure 8.2: Effect of micro-filler content on MVTR of PU coated paperboard

8.2.1 SEM and TEM analysis of PU-filler microcomposites

SEM and TEM analyses were done on the PU-filler microcomposite coatings to determine the optimum filler content. Results are shown in Figure 8.3. It was thought that the filler would form a platelet structure to increase the path length of water vapour moving through the coating layer, thereby resulting in a lower MVTR.

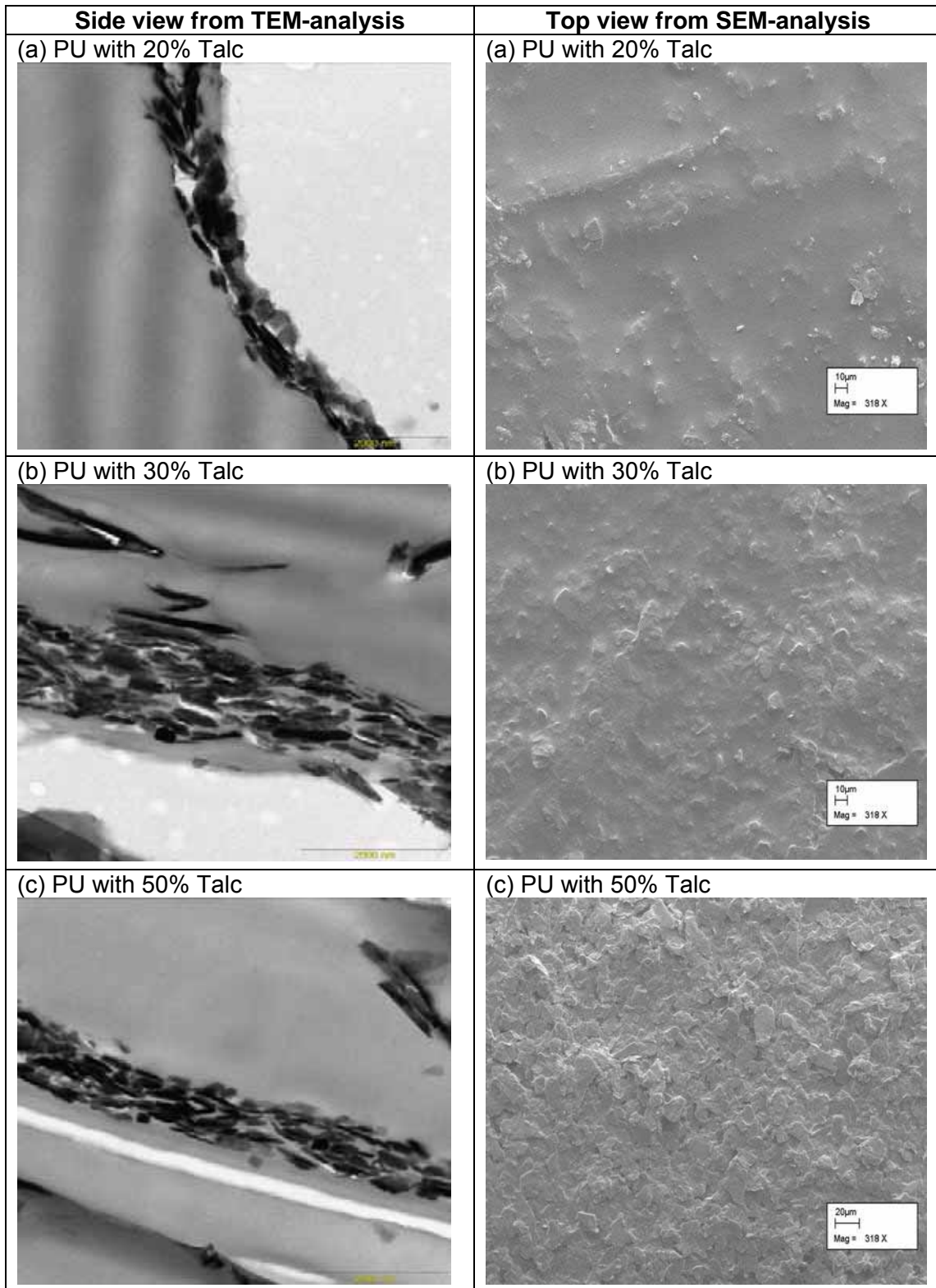


Figure 8.3: SEM and TEM images of PU-Talc coated paperboard

Figure 8.3a shows that a talc content of 20% is too low to form an evenly distributed talc layer within the coating. Here the unevenly distributed talc loses its reinforcing platelet structure, and acts like channels for moisture to move through the coating. This effect can be seen in Table 8.1 by an increase in the MVTR.

Figure 8.3b shows that when the talc content is at 30% or above, the platelets form an evenly distributed talc layer within the coating. At 30% talc content, the talc is mainly evenly distributed, thereby forming a tortuous path, which can be seen by the decrease in MVTR in Table 8.3.

However, above 30% talc content very little PU is covering the talc particle. This results in the formation of more particle-particle interactions, which results in a poor PU-filler composite, as seen in Figure 8.3c, and by the increase in MVTR in Table 8.3.

8.2.2 DMA analysis of PU-Serina clay microcomposites

DMA analyses of the PU-Serina clay microcomposite film series are shown below in Figure 8.4. Incorporation of the micro-filler into the polyurethane matrix exhibited almost no difference in T_g . Also, as expected, the micro-filler did not affect the compatibility between the hard and soft segments of the polyurethane.

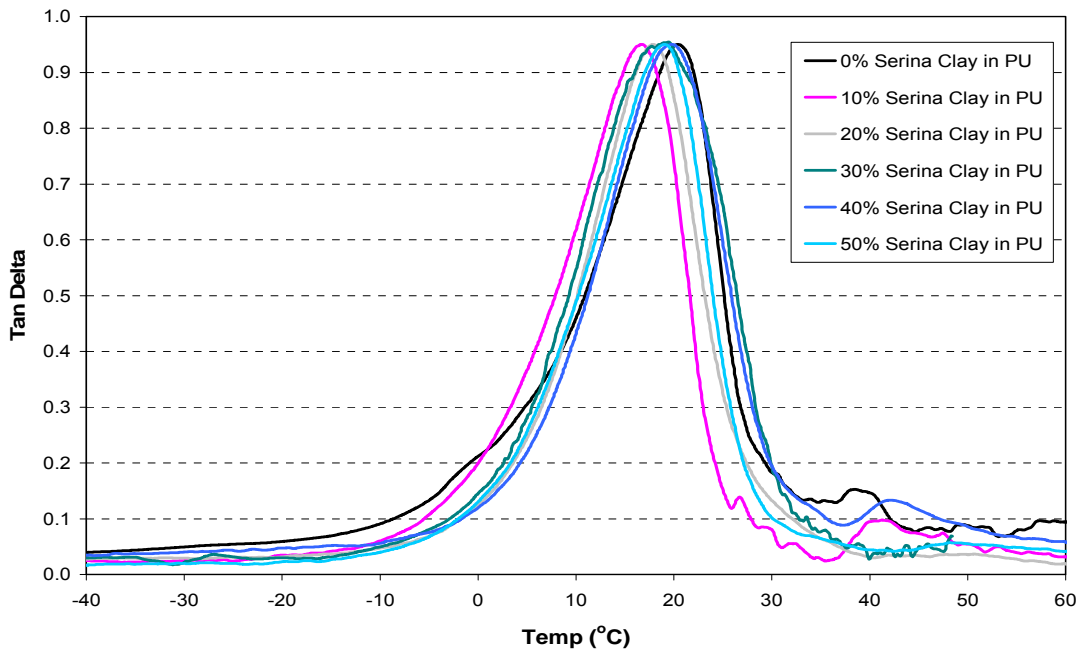


Figure 8.4: DMA analysis of PU-Serina clay microcomposite films

8.3 Nano-filler incorporation

The nano-clay can be incorporated either during the polyester or polyurethane stage. The methods of nano-clay incorporation that were investigated in the above mentioned stages, as are tabulated in Table 8.2.

Table 8.2: Methods for preparing the polyurethane/nano-composites

Method 1 Blending into polyurethane matrix	Method 2a Blending into polyester matrix
<i>Stage 1:</i> Synthesize polyurethane until before neutralization of pendent acid groups	<i>Stage 1:</i> Blend nano-clay and polyester at 80-85°C for 24 h
<i>Stage 2:</i> Pre-mix nano-clay and NMP at room temperature for 15 min	<i>Stage 2:</i> Add 33-35% NMP and blend at 60-65°C for 4 h
<i>Stage 3:</i> Add nano-clay/NMP mixture to un-neutralized polyurethane and blend at 65-70°C for 5 to 10 h, and continue with normal polyurethane synthesis	<i>Stage 3:</i> Add polyester/nano-composite precursor to urethane hard segment during PU synthesis
Method 2b Blending into polyester matrix	Method 3 Blending into reactive isocyanate
<i>Stage 1:</i> Blend nano-clay and polyester at 80-85°C for 30 min	<i>Stage 1:</i> Pre-mix nano-clay and NMP at room temperature for 15 min
<i>Stage 2:</i> Add 33-35% NMP and blend at 60-65°C for 24 h	<i>Stage 2:</i> Add to TDI and blend at room temperature for 15 min
<i>Stage 3:</i> Add polyester/nano-composite precursor to urethane hard segment during PU synthesis	<i>Stage 3:</i> Continue with normal polyurethane synthesis

The nano-clays investigated included NC 30B, NC 93A and NC 15A of the Cloisite nano-clay series (tabulated in Table 8.3), of which NC 93A and NC 15A were used in *Method 1*, while NC 30B was used in *Methods 2 and 3*.

NC 93A and NC 15A were chosen for *Method 1* due to their hydrophobicity and the higher degree of spacing between the nano platelets (as tabulated in Table 8.3).

NC 30B was chosen for *Methods 2 to 3* due to the structure of the tertiary amine (as shown in Table 8.3). Although the spacing between the nano platelets is relatively small compared to some others, the two OH-groups on the quaternary amine should allow for better blending into the polyester matrix, and the OH-groups may also react with the NCO-groups of the TDI monomer as in the case of *Method 3*.

Table 8.3: The tertiary amines of the Cloisite modified nano-clays

Name	Modifier	Anion	Plate distance (XRD)
Cloisite Na ⁺ (unmodified)	Na		11.7Å
Cloisite 30B	$\begin{array}{c} \text{CH}_3 \\ \\ \text{HO-CH}_2\text{-CH}_2\text{-N}^+\text{-CH}_2\text{-CH}_2\text{-OH} \\ \\ \text{T} \end{array}$ <p>Concentration: 90 meq/100g clay</p>	Cl ⁻	18.5Å
Cloisite 93A	$\begin{array}{c} \text{CH}_3 \\ \\ \text{HT-N}^+\text{-HT} \\ \\ \text{H} \end{array}$ <p>Concentration: 90 meq/100g clay</p>	HSO ₄ ⁻	23.6Å
Cloisite 15A	$\begin{array}{c} \text{CH}_3 \\ \\ \text{HT-N}^+\text{-HT} \\ \\ \text{CH}_3 \end{array}$ <p>Concentration: 125 meq/100g clay</p>	Cl ⁻	31.5Å

T = Tallow (±65% C18; ±30% C16; ±5% C14)

HT= Hydrogenated Tallow (±65% C18; ±30% C16; ±5% C14)

Increasing polymer/monomer hydrophobicity from top to bottom

Increasing surface hydrophobicity from top to bottom

8.3.1 Nano-filler incorporation using Method 1

During *Method 1*, the nano-fillers can be incorporated inside or outside the PU dispersion particle. It is incorporated inside before the dispersion stage of the PU, while outside after the dispersion stage. Nano-filler incorporation inside the emulsion particles should form stable dispersions, whereby the use of surfactants is eliminated.

8.3.1.1 Nano-filler incorporation outside the PU emulsion particle

The incorporation of nano-clay outside the PU particle increased the opaqueness and viscosity of the mixture. The emulsion viscosity did not increase too much, as the filler particles positioned themselves between the PU particles, thereby having a small effect on ionic clustering. Also, the nano-clay precipitated out of the mixture after a few minutes. The MVTR results are listed in Table 8.4 and shown in Figure 8.5. No advantage of improved MVTR performance was detected.

Table 8.4: Effect of nano-filler incorporated outside PU dispersion particles

Coating blend	% Nano-filler	No Wax C78 addition		Wax C78 addition	
		MVTR (g/m ² /24h)	Degree of blocking	MVTR (g/m ² /24h)	Degree of blocking
PU	0	815	Medium	187	Kissing
NC 93A	2	843	Kissing	335	Kissing
NC 93A	4	866	Medium	308	Kissing
NC 93A	6	835	Medium	349	Kissing
NC 93A	8	845	Medium	357	Kissing
NC 93A	10	862	Medium	407	Medium
PU	0	815	Medium	187	Kissing
NC 15A	2	816	Medium	389	Kissing
NC 15A	4	782	Medium	378	Kissing
NC 15A	6	790	Kissing	295	Kissing
NC 15A	8	817	Kissing	321	Kissing
NC 15A	10	828	Medium	389	Kissing

8.3.1.2 Nano-filler incorporation inside the PU emulsion particle

To incorporate filler inside the PU dispersion particle, nano-clay was added either before or after neutralization during the PU synthesis. After dispersing the mixture, it formed an unstable opaque dispersion. Upon investigation of the precipitate it was found that the filler was intertwined in-between the PU chains. The pH was increased from 8 to 10, upon which the mixture formed a stable transparent dispersion.

This resulted in a much lower solids content compared to the case where incorporated filler was outside the PU particle. The lower solids content was due to the increase in pH, which also increased the dispersion viscosity due to increasing ionic clustering (see Sections 4.3 and 4.4). The ionic clusters are solvated by the addition of more water, thereby considerably decreasing the solids content. However, it gave much better polymer-filler interaction, as seen from the MVTR results in Table 8.5 and Figure 8.5.

Table 8.5: Effect of Nano-filler incorporation inside PU dispersion particles

Coating blend	% Nano-Filler	No Wax C78 addition		Wax C78 addition	
		MVTR (g/m ² /24h)	Degree of blocking	MVTR (g/m ² /24h)	Degree of blocking
PU	0	815	Medium	189	Kissing
NC 93A	2.5	822	Kissing	229	Kissing
NC 93A	4.3	814	Medium	212	Kissing
NC 93A	8.4	779	Medium	153	Kissing
NC 93A	10	758	Medium	190	Kissing
PU	0	815	Medium	189	Kissing
NC 15A	2.5	802	Medium	230	Kissing
NC 15A	4.3	753	Medium	216	Kissing
NC 15A	8.4	734	Kissing	185	Kissing
NC 15A	10	739	Medium	219	Kissing

The results in Tables 8.4 and 8.5 are combined in Figure 8.5 below.

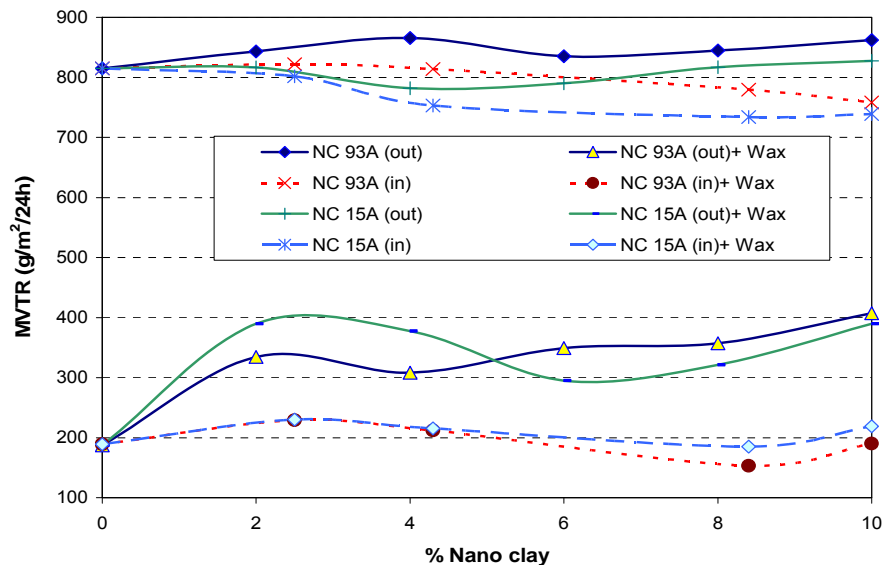


Figure 8.5: Effect of nano-filler on MVTR of PU coated paperboard

8.3.1.3 TGA analysis of PU-filler nanocomposites

Thermal analyses of the nano-filler incorporation showed that it did not improve the thermal stabilities of the PU, as seen in Figure 8.6.

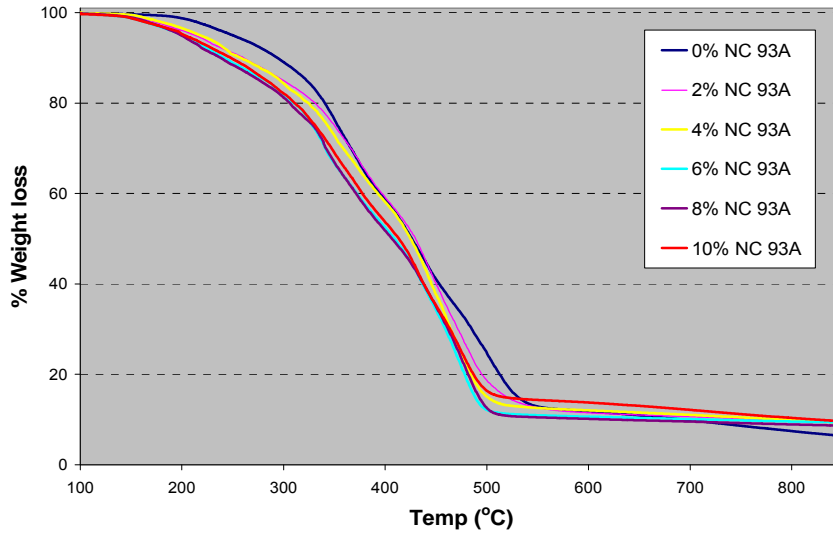


Figure 8.6: Effect of nano-filler content on thermal stability of PU

8.3.1.4 DSC analysis of PU-clay nanocomposites

DSC analyses on the PU-clay nanocomposites showed an increase in a melting peak with increasing filler content during the second heating stage, as seen in Figure 8.7.

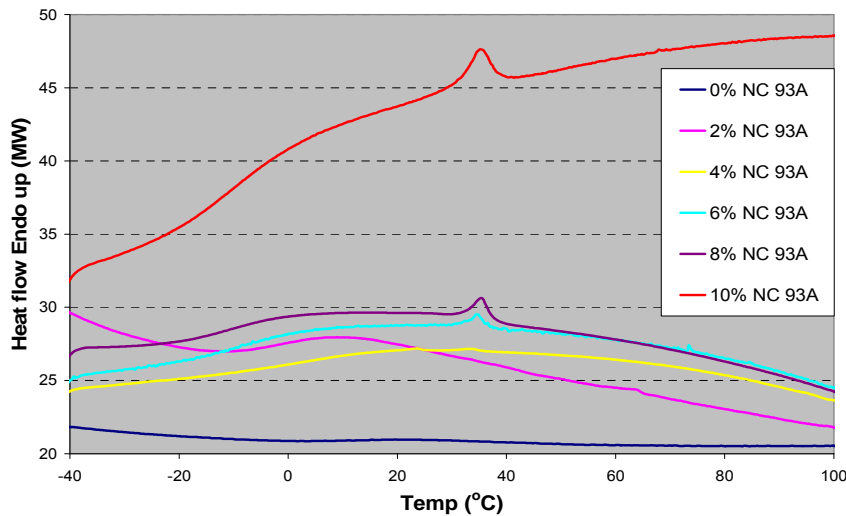


Figure 8.7: Effect of nano-filler content on DSC analysis of PU

8.3.1.5 SEM and TEM analysis of nano-filler/PU composites

SEM was done to investigate the surface morphology of the PU-clay nanocomposites, while TEM was done to investigate the filler distribution in the coating layer.

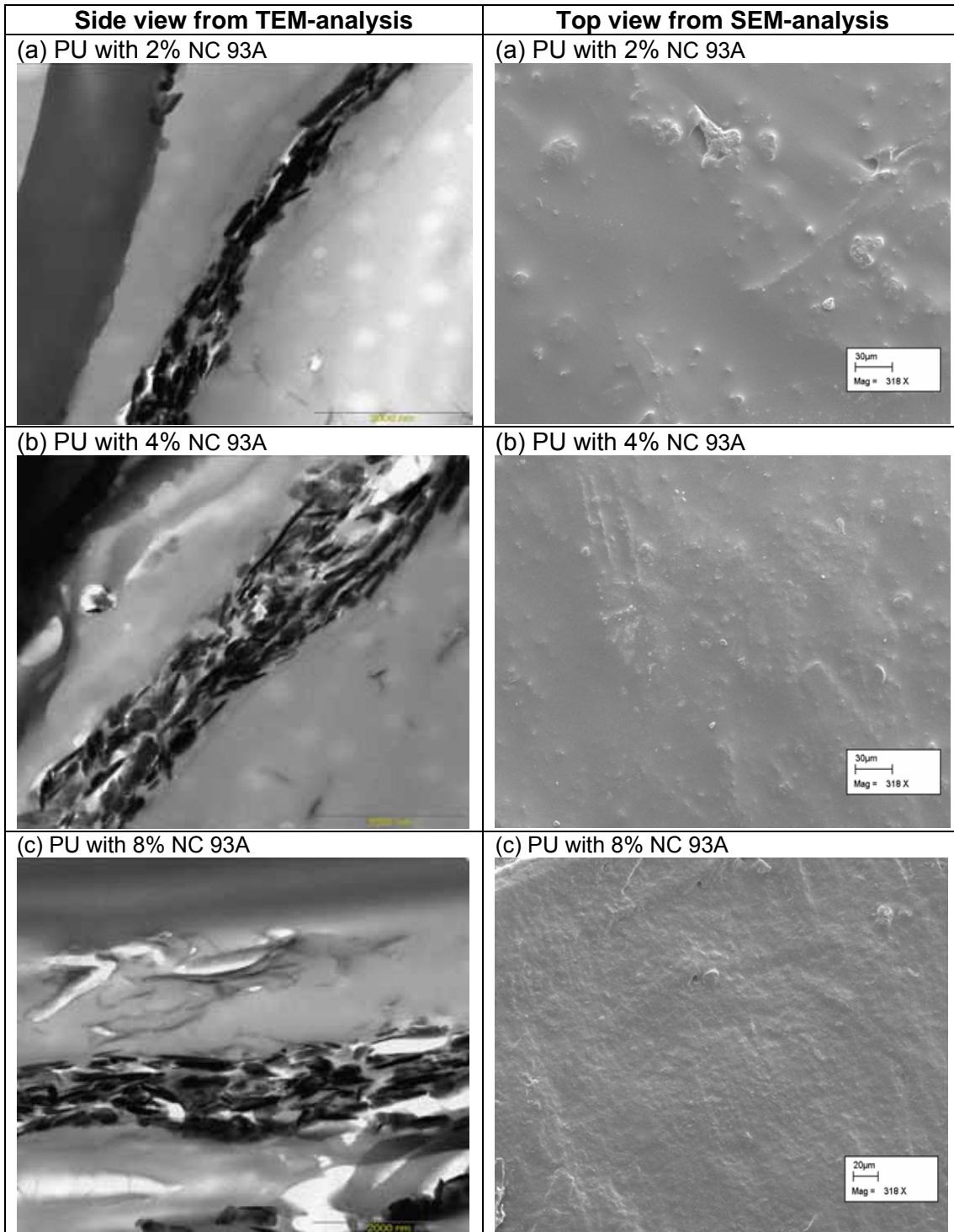


Figure 8.8: SEM and TEM images of PU-NC 93A composite coated paperboard

Analysis of the SEM and TEM images shown in Figure 8.8 illustrates that the nano-filler was un-exfoliated/unintercalated in the PU matrix, whereby the un-exfoliated nano-clay particles acted in the same manner as the micro-filler particles did (refer to Figure 8.3).

Figure 8.8 also shows that the nano-clay was unevenly spread throughout the coating layer at 2% incorporation. This coating showed no platelet structure that would increase the moisture path length. Instead, it acted as a defect in the coating layer; it increased the MVTR, as seen in Table 8.4.

At 4 to 6% nano-filler incorporation, the filler was evenly spread throughout the coating layer. Here the un-exfoliated nano-clay platelet structure was clearly visible, resulting in lower MVTR, as shown in Table 8.4. At 8% nano-filler incorporation the MVTR increased due to a weak polymer-filler network as a result of too much filler, as shown in Table 8.4. Thus, the optimum nano-filler concentration was found to be between 4 to 6% incorporation.

8.3.2 Nano-filler incorporation using Methods 2a and 2b

Nano-filler can be incorporated at the polyester stage either during polyester synthesis, or after polyester synthesis. Due to the instability of the amine group of the modified nano-clay above 200°C, it was decided to incorporate the nano-clay into the polyester matrix after polyester synthesis.

The various stages of filler incorporation into the polyurethane matrix in *Methods 2a* and *2b* were followed by TEM analysis. The dispersion of polyester chains between the nano-clay particles was hampered without the presence of NMP solvent, as seen in Figures 8.9 to 8.12. Figure 8.9 also shows that the polyester contained crystallinity.

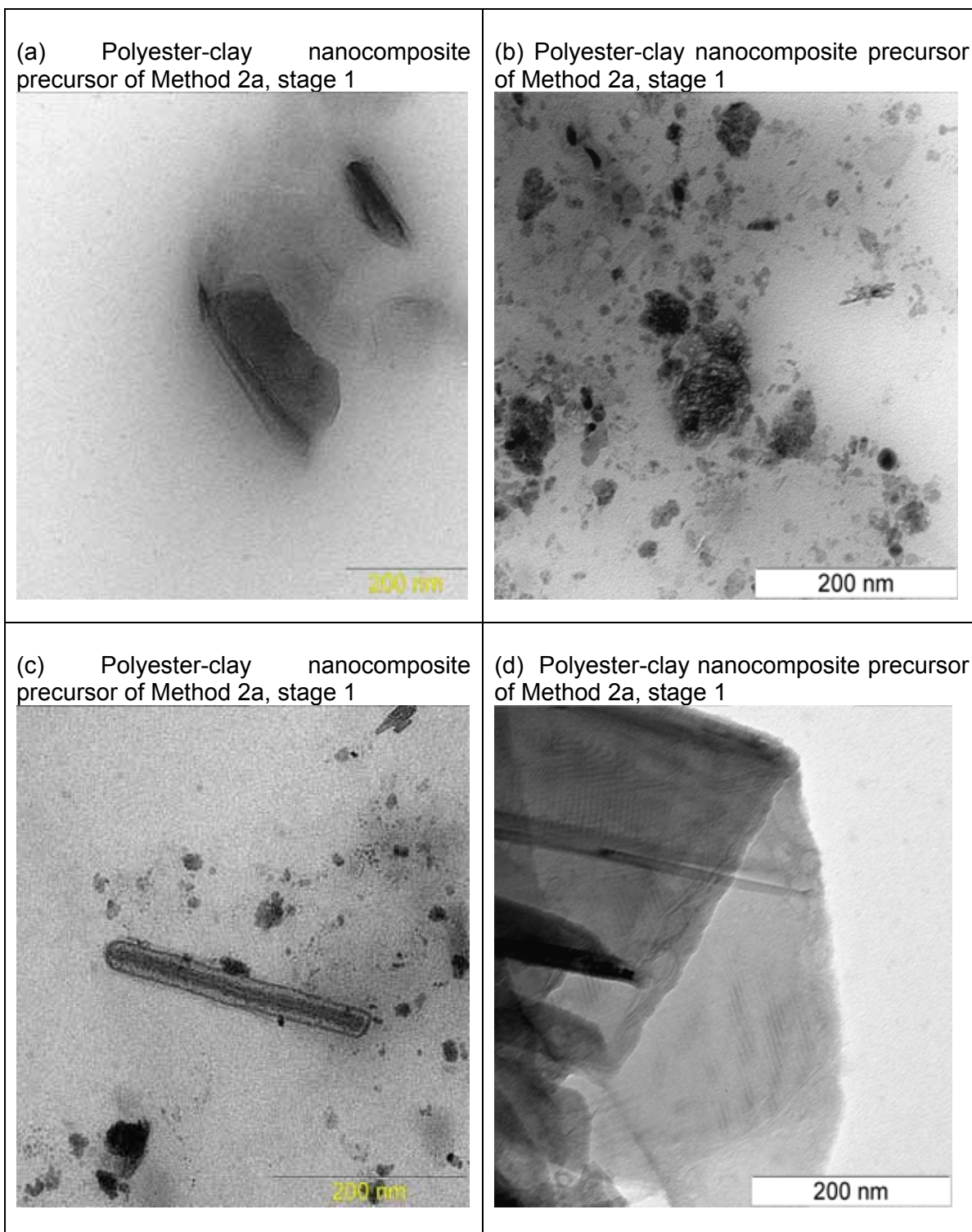


Figure 8.9: TEM analysis of a polyester-clay nanocomposite containing 1.5% NC 30B, prepared using *Method 2a*, during *stage 1*

Figure 8.10 shows the polyester-nano composite at *stage 2* of *Methods 2a and 2b* just before addition to the urethane hard segment. It shows that the clay layers are aggregated in an unintercalated form.

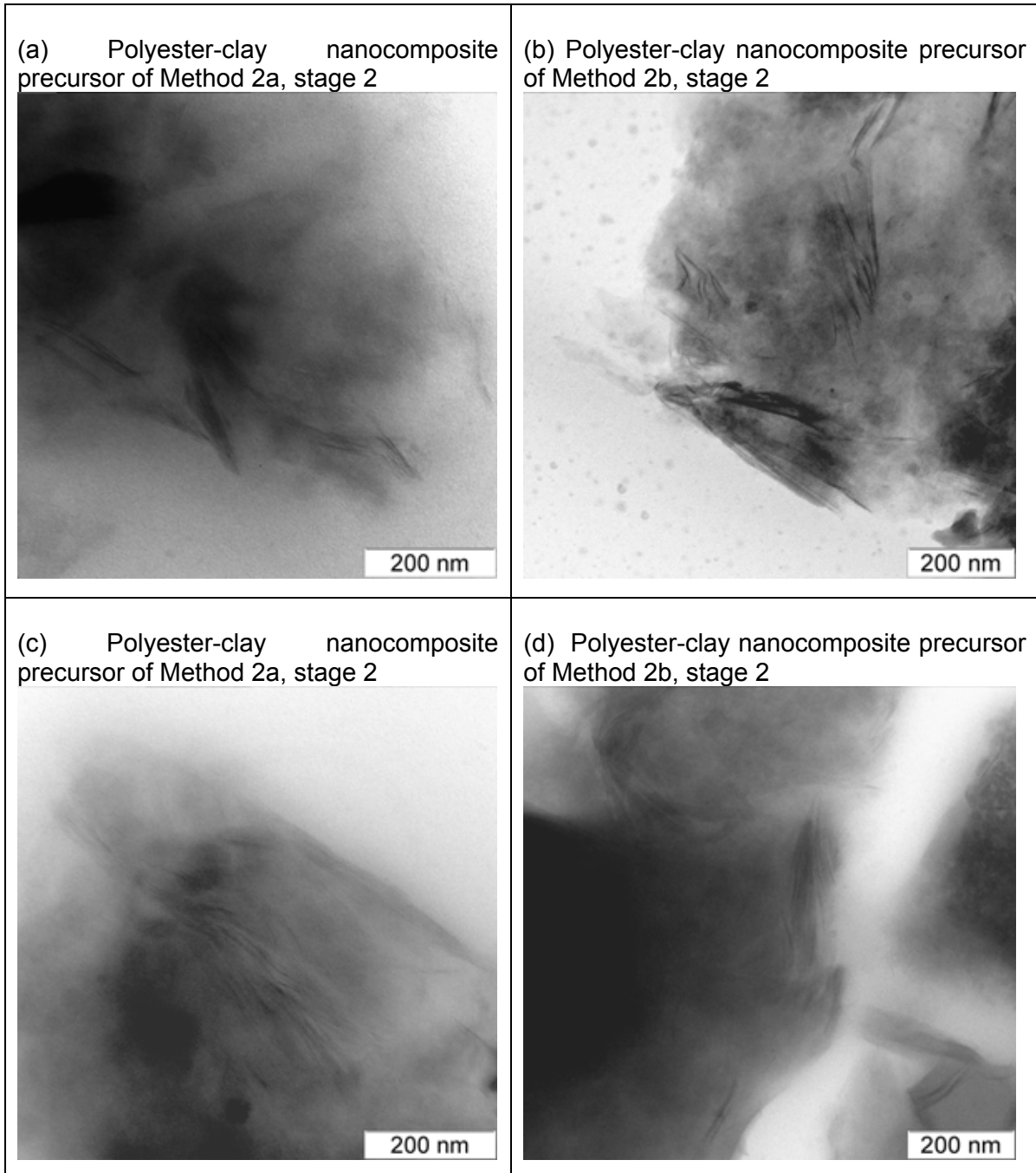


Figure 8.10: TEM analysis of a polyester-clay nanocomposite precursor containing 1.5% NC 30B and NMP-solvent, prepared using *Methods 2a and 2b*, during *stage 2*

Figure 8.11 shows the polyurethane-clay nanocomposite dispersions synthesized via *Method 2*. It shows both unintercalated and intercalated polymer-clay nanocomposite structures from both *Methods 2a and 2b*. However, *Method 2a* contains a much higher percentage of unintercalated structures, compared to *Method 2b* which contains a much higher percentage of intercalated polymer-clay nanocomposite structures.

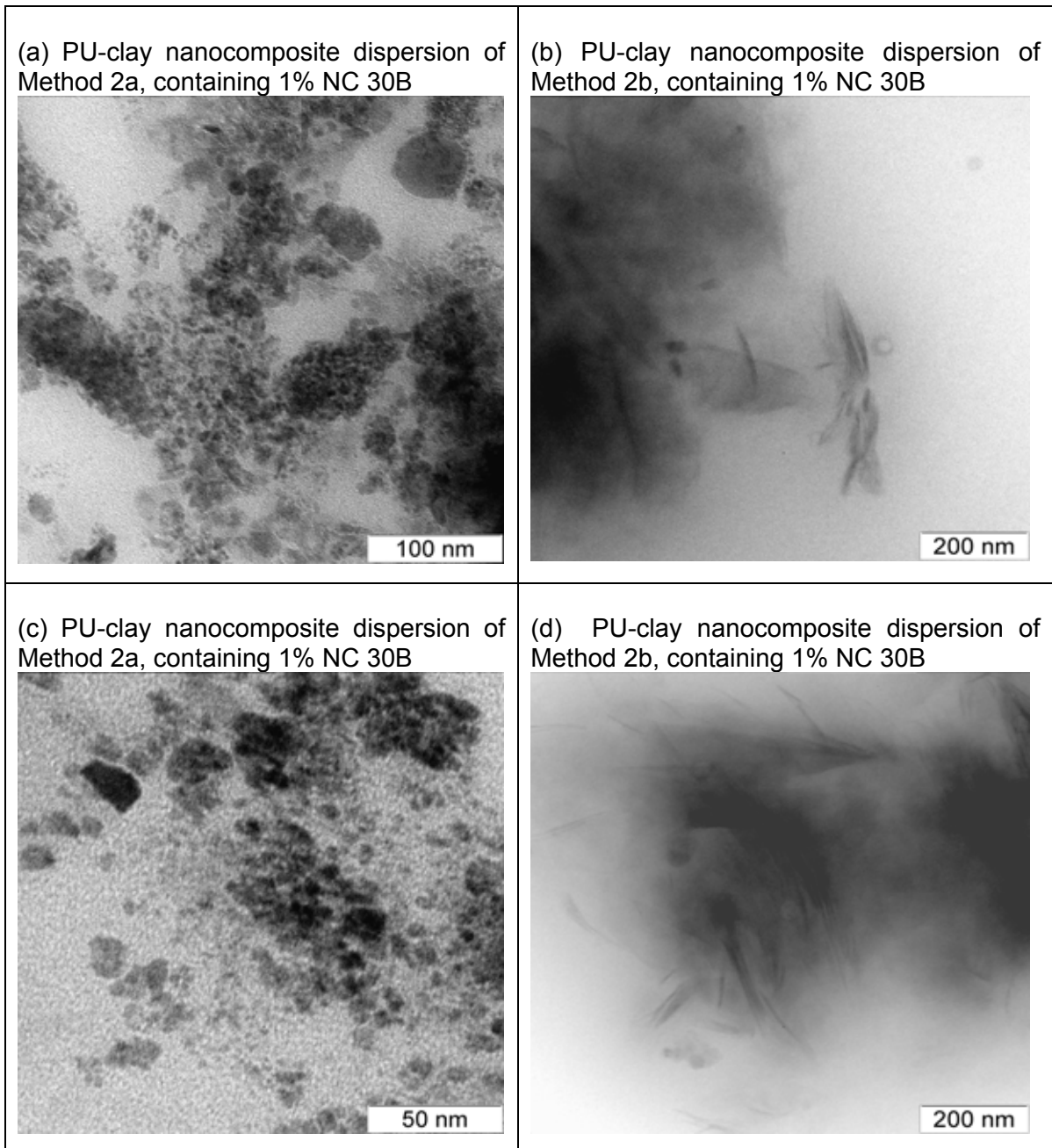


Figure 8.11: TEM analysis of a PU-clay nanocomposite emulsion containing 1.0% NC 30B, prepared using *Methods 2a and 2b*

Figure 8.12 shows the polyurethane-clay nanocomposite films synthesized via *Methods 2a and 2b*. Once again it is clear that *Method 2a* contains a much higher percentage of unintercalated polymer-clay nanocomposite structures, compared to *Method 2b* which contains a much higher percentage of intercalated polymer-clay nanocomposite structures.

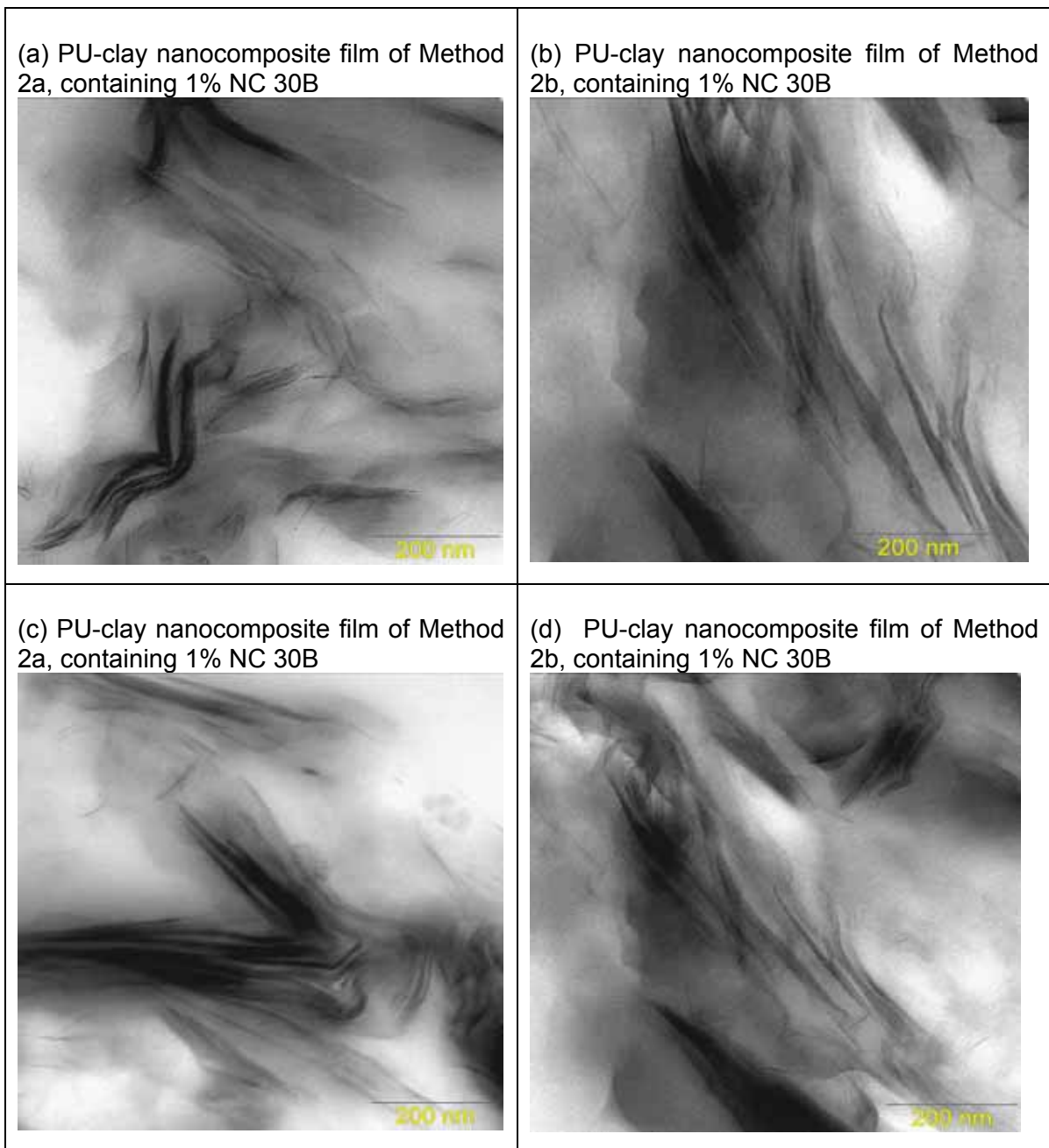


Figure 8.12: TEM images of PU-NC 30B composite films, prepared using *Methods 2a and 2b*

Figures 8.13 and 8.14 shows the SEM images of the polyurethane-clay nanocomposite paperboard coatings synthesized from *Methods 2a*. The unintercalated polymer-clay nanocomposite structures containing 15% wax C78 can be clearly seen in Figure 8.13.

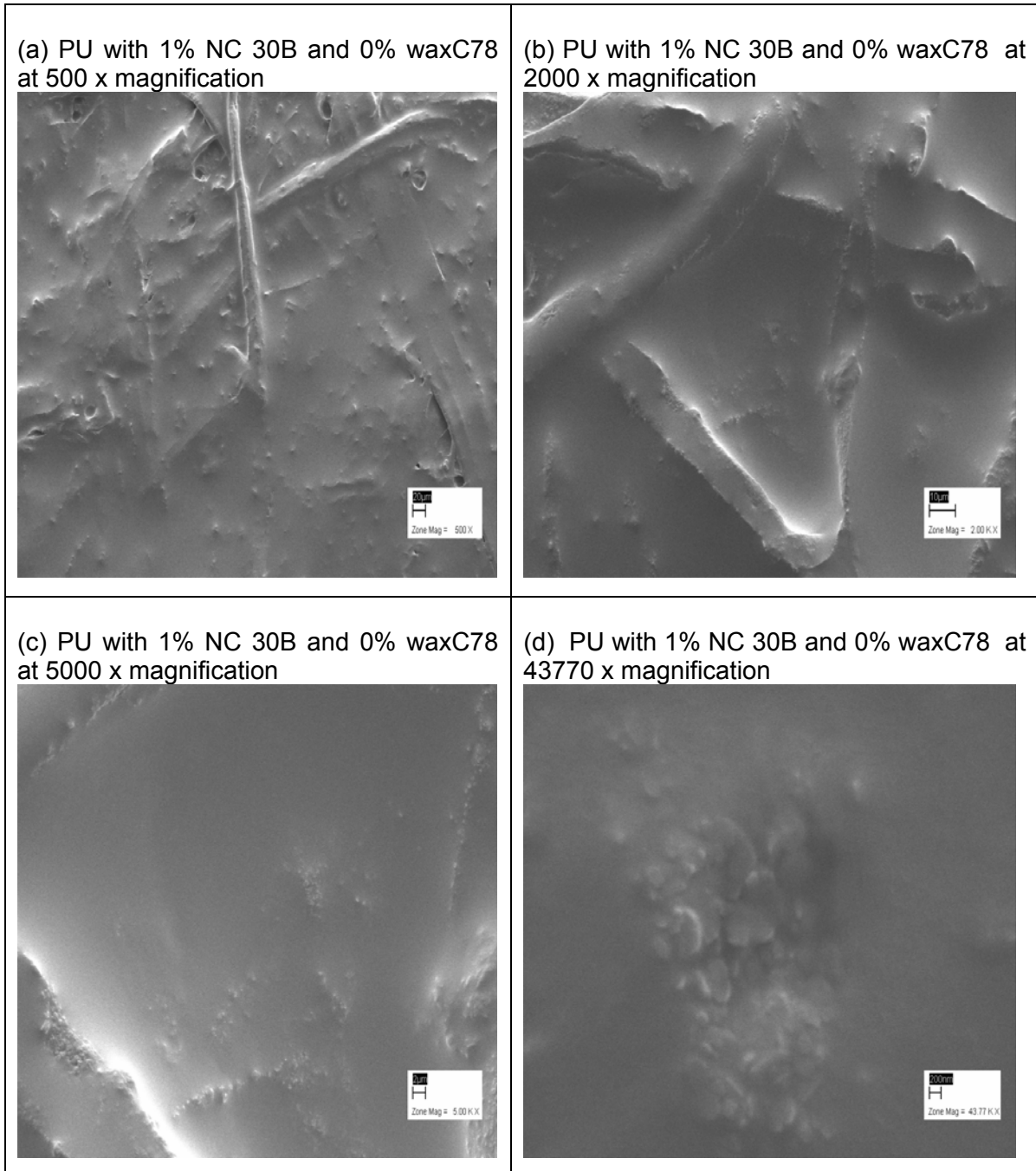


Figure 8.13: SEM images of paperboard coated with PU-NC 30B and 0% waxC78 composite films, prepared using *Method 2a*

Figure 8.14 shows the SEM images of the polyurethane-clay nanocomposite paperboard coatings, synthesized from *Methods 2a*, containing 15% wax C78. Here also, the unintercalated polymer-clay nanocomposite structures can be clearly seen.

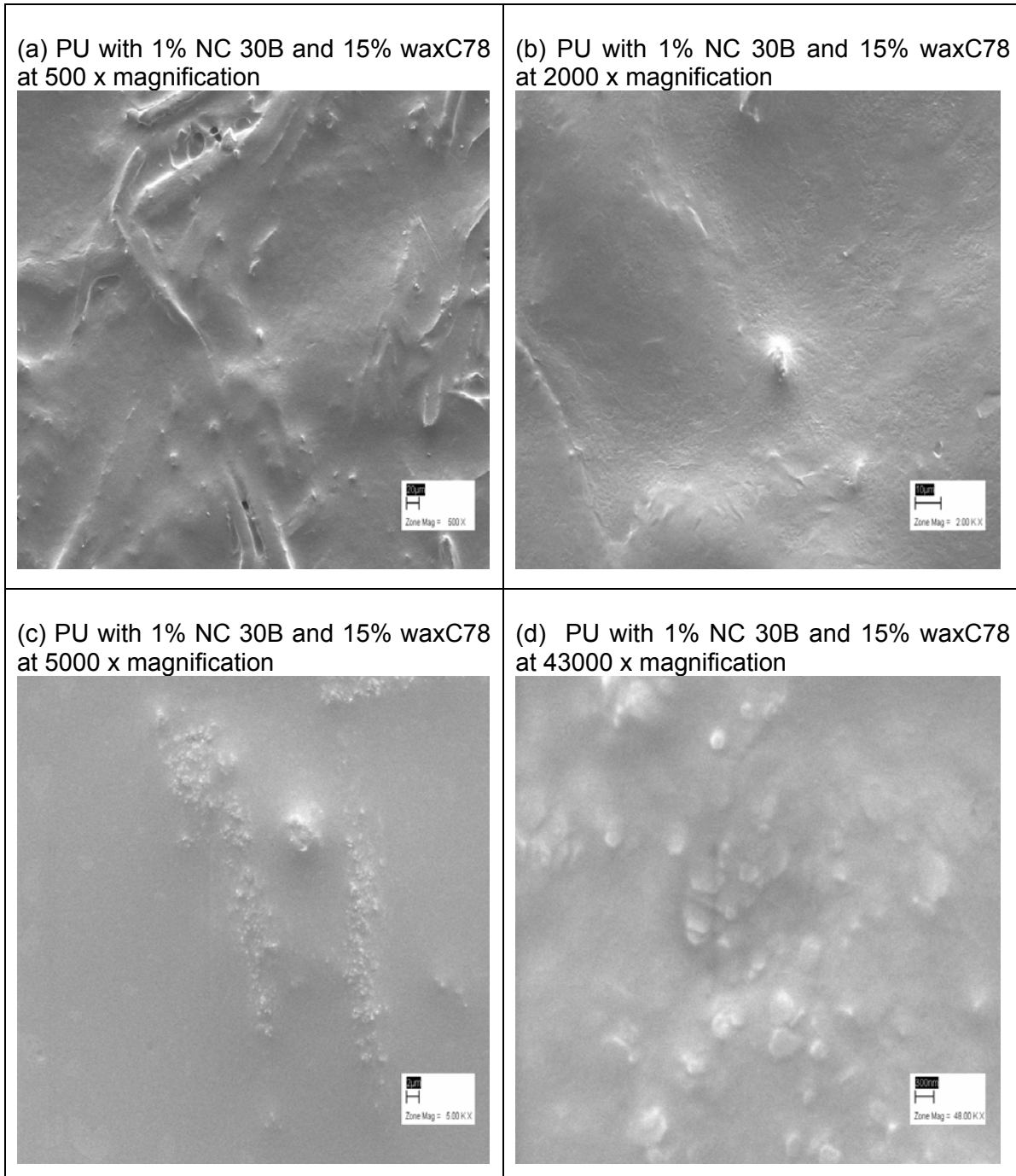


Figure 8.14: SEM images of paperboard coated with PU-NC 30B and 15% waxC78 composite films, prepared using *Method 2a*

Figures 8.15 and 8.16 shows the SEM images of the polyurethane-clay nanocomposite paperboard coatings synthesized from *Methods 2b*. The unintercalated polymer-clay nanocomposite structures containing 0% wax C78 can be clearly seen in Figure 8.15.

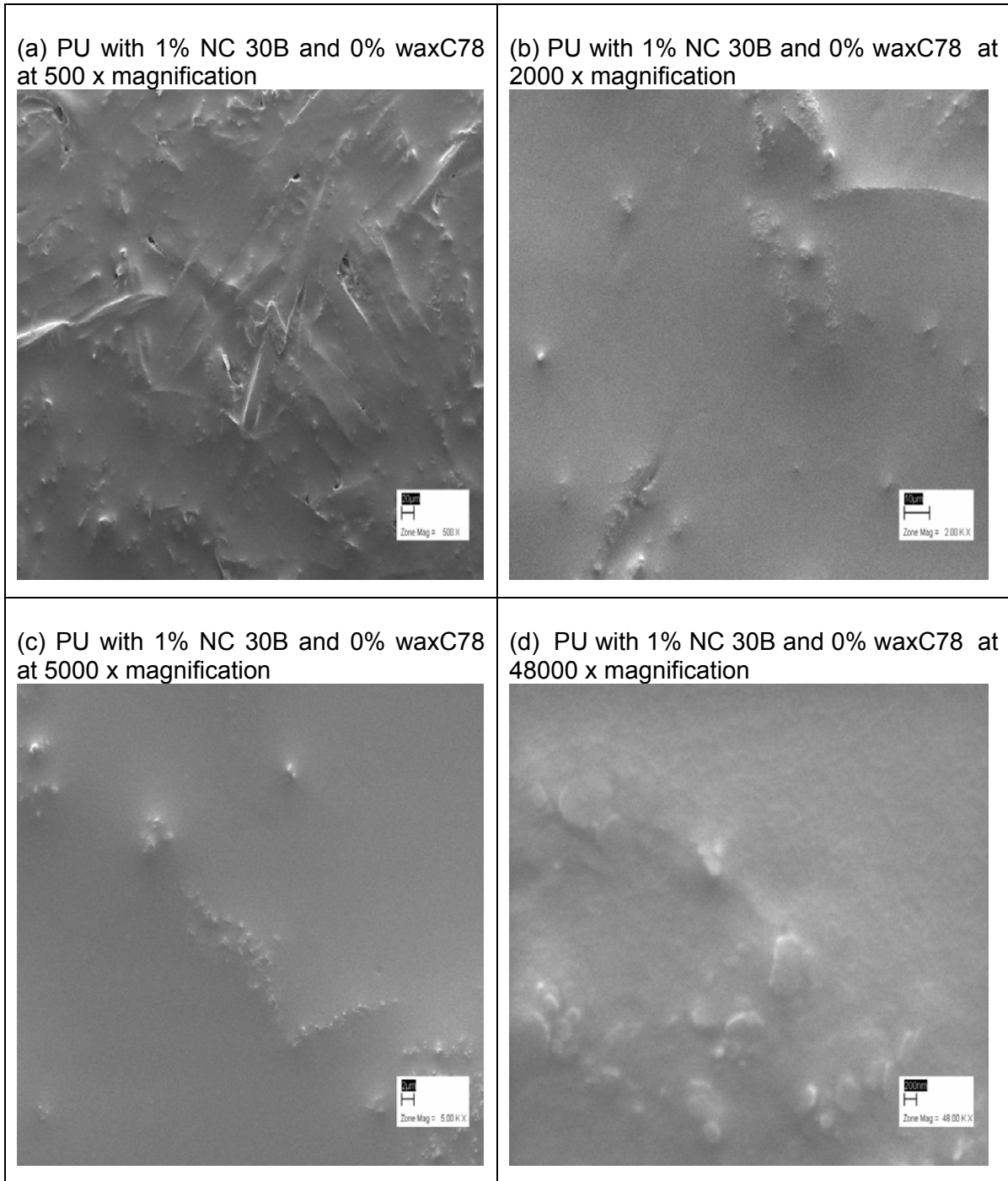


Figure 8.15: SEM images of paperboard coated with PU-NC 30B and 0% waxC78 composite films, prepared using *Method 2b*

Figure 8.16 shows the SEM images of the polyurethane-clay nanocomposite paperboard coatings, synthesized from *Methods 2b*, containing 15% wax C78. Here also, the unintercalated polymer-clay nanocomposite structures can be clearly seen.

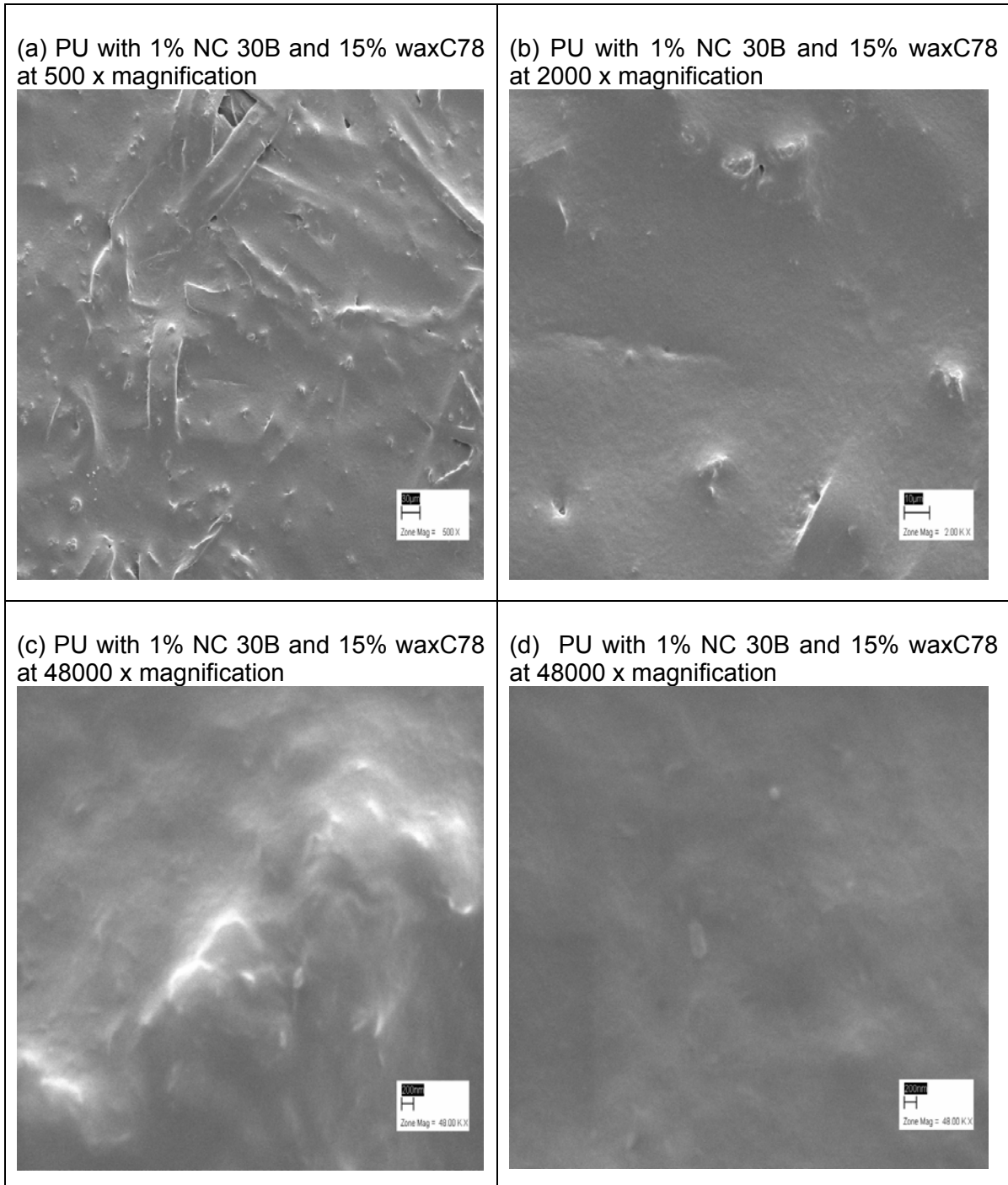


Figure 8.16: SEM images of paperboard coated with PU-NC 30B and 15% waxC78 composite films, prepared using *Method 2b*

8.3.3 Nano-filler incorporation using Method 3

The final step was to exfoliate the nano-clay in the urethane matrix by first wetting the surface of the nano-clay with solvent, and then adding it to the reactive TDI monomer.

Figure 8.17 shows the polyurethane-clay nanocomposite dispersions, synthesized via *Method 3*, containing 1% and 2% nano-filler incorporation. It shows exfoliated polymer-clay nanocomposite structures in both 1% and 2% nano-filler concentrations.

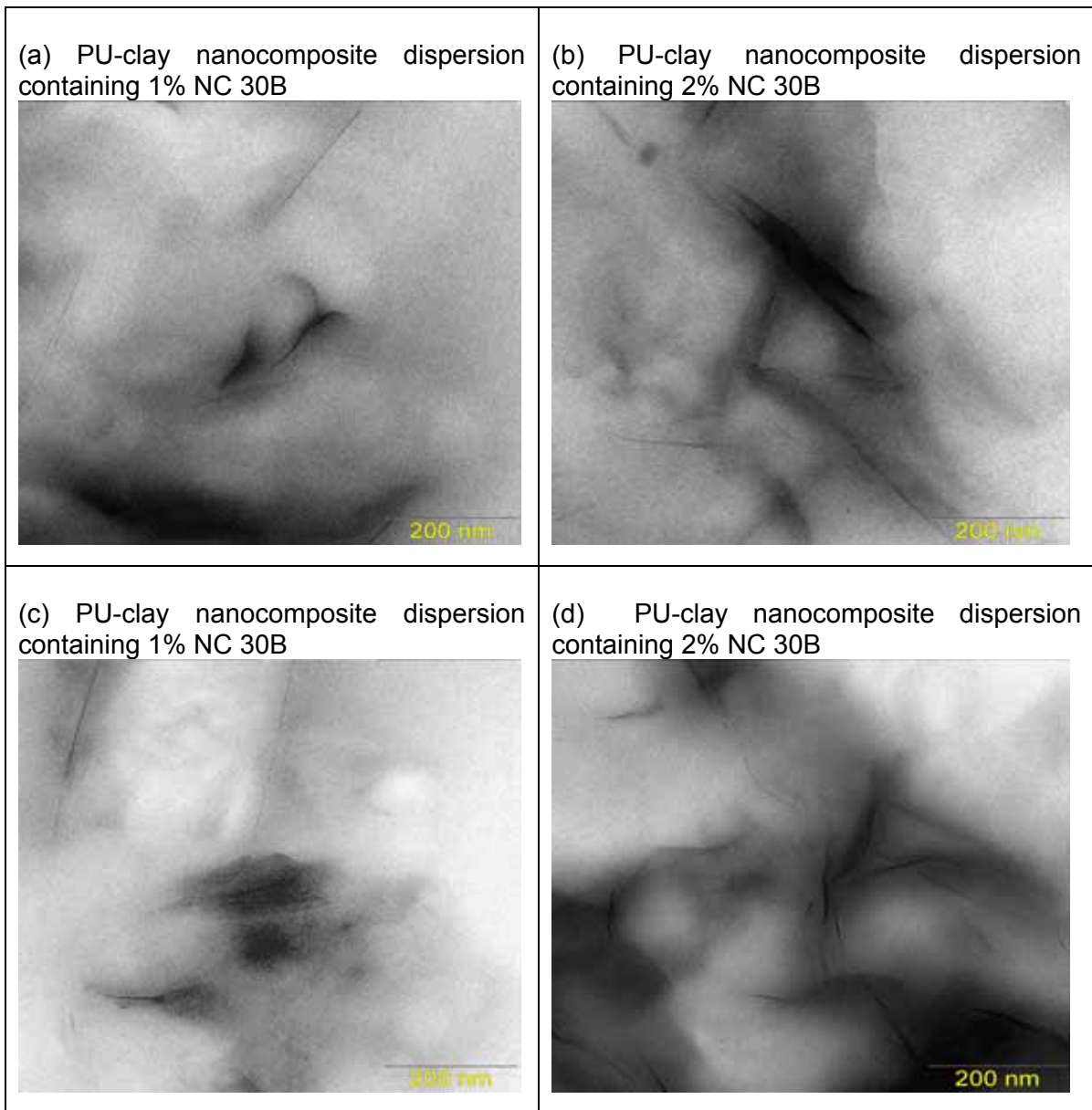


Figure 8.17: TEM images of PU-NC 30B composite dispersions, prepared using *Method 3*

Figure 8.18 and 8.19 shows the polyurethane-clay nanocomposite films synthesized via *Method 3* and containing 1% and 2% nano-filler incorporation. The polyurethane-clay nanocomposite in Figure 8.18 contains no wax. Exfoliation can be clearly seen.

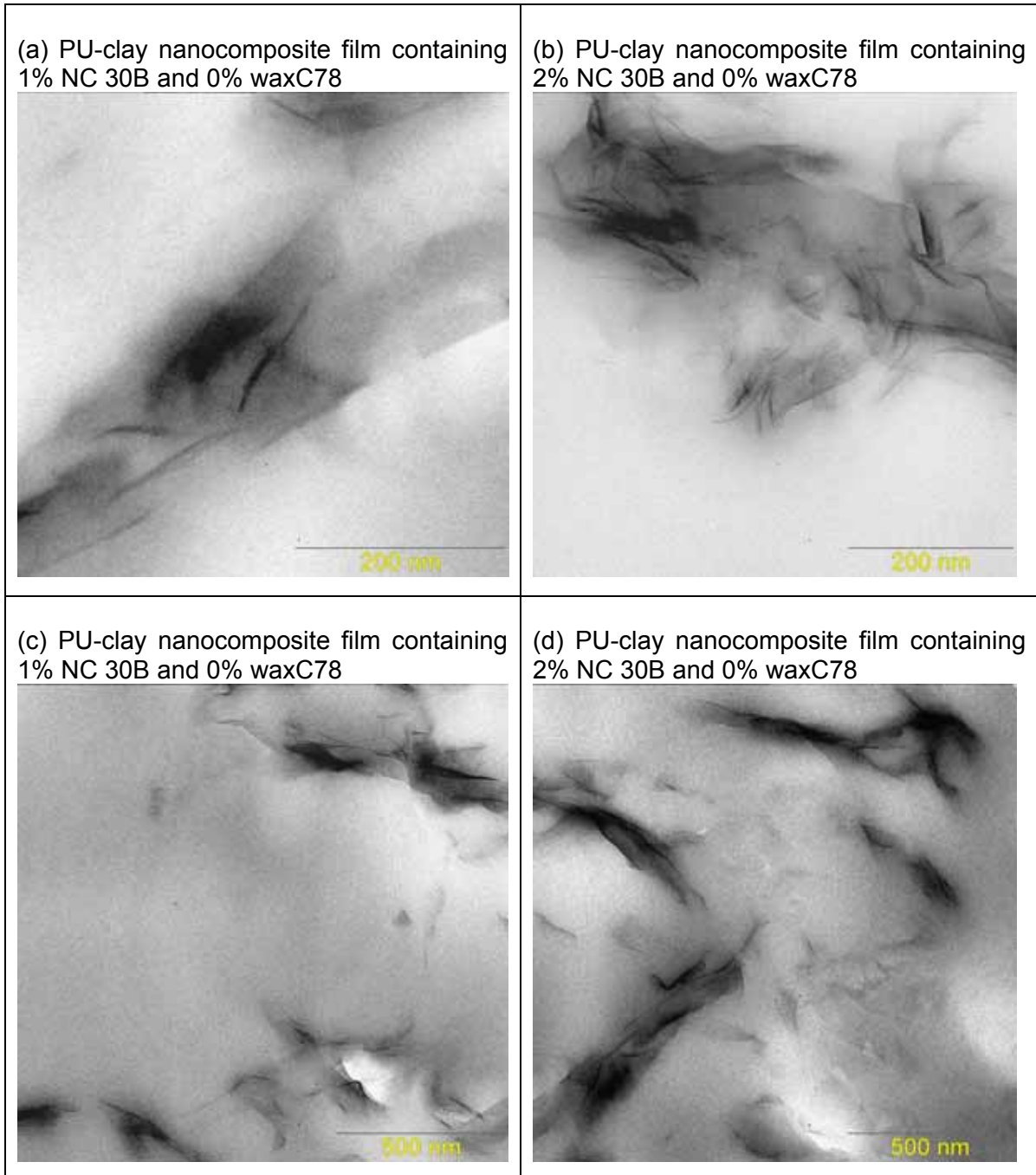


Figure 8.18: TEM images of PU-NC 30B composite films, containing 0% waxC78, prepared using *Method 3*

Figure 8.19 show the polyurethane-clay nanocomposite films synthesized via *Method 3* and containing 1% and 2% nano-filler incorporation. Here, the polyurethane-clay nanocomposite contains 15% wax C78. Exfoliation can be clearly seen.

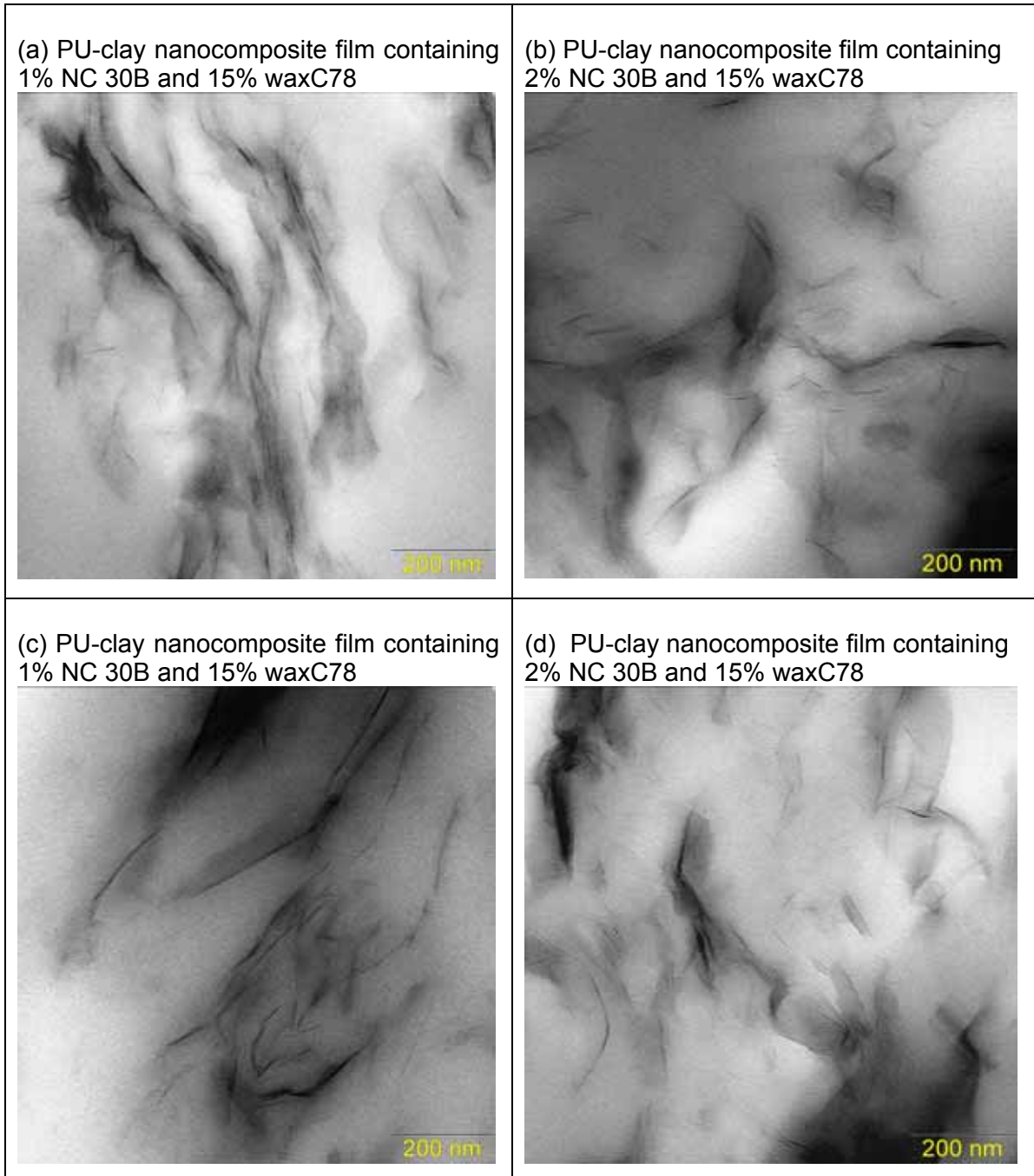


Figure 8.19: TEM images of PU-NC 30B composite films, containing 15% waxC78, prepared using *Method 3*

Figures 8.20 and 8.21 shows the SEM images of the polyurethane-clay nanocomposite coated paperboard coatings synthesized via *Method 3* containing 1% and 2% nano-filler incorporation. These polyurethane-clay nanocomposite in Figure 8.20 contain 0% wax C78, of which a clear coated paperboard surface can be seen from the SEM images.

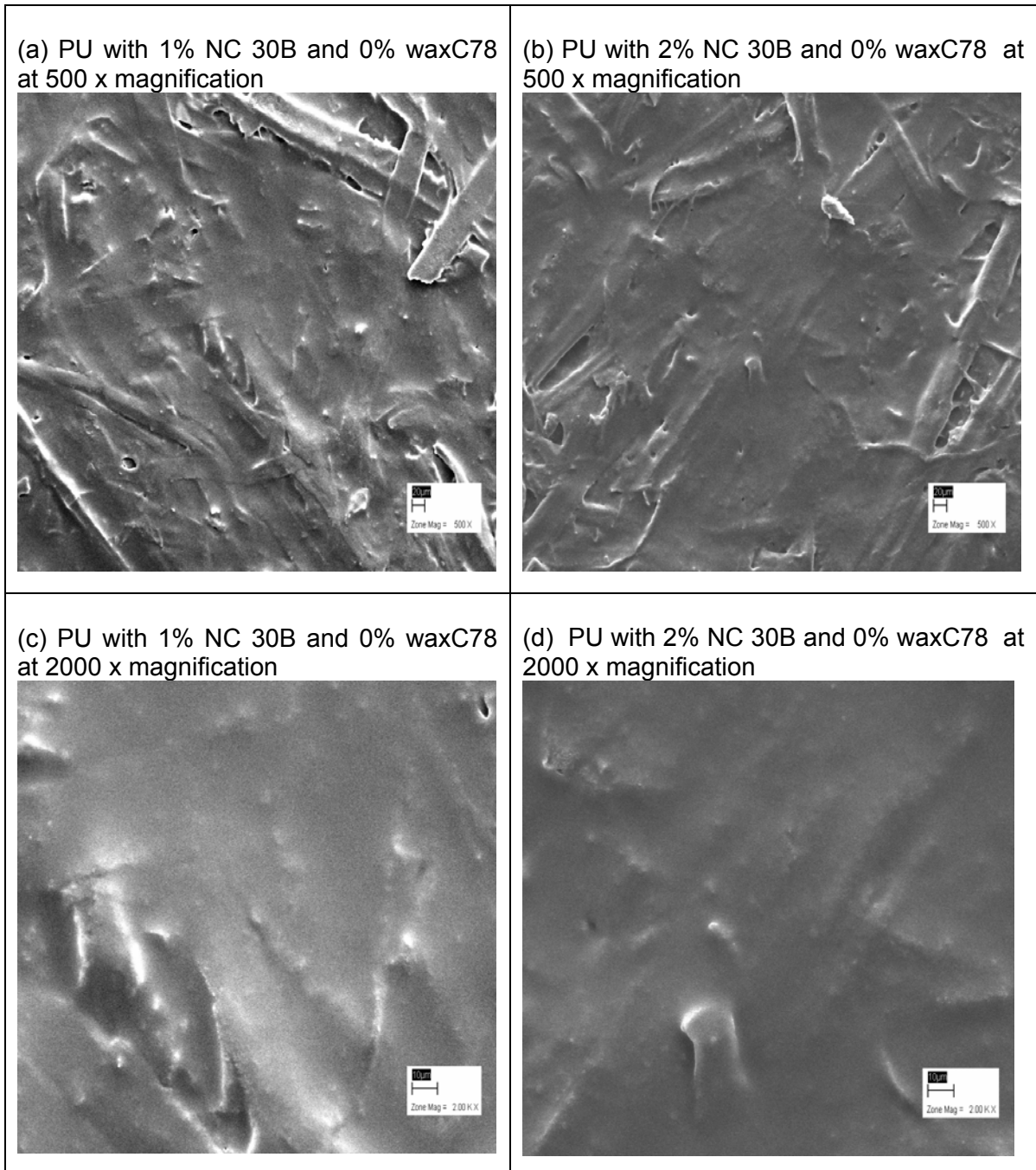


Figure 8.20: SEM images of PU-NC 30B coated paperboard, containing 0% waxC78, prepared using *Method 3*

Figure 8.21 show the SEM images of the polyurethane-clay nanocomposite coated paperboard coatings synthesized via *Method 3* and containing 1% and 2% nano-filler incorporation. These polyurethane-clay nanocomposite in Figure 8.21 contain 15% wax C78, of which a clear coated paperboard surface can be seen from the SEM images.

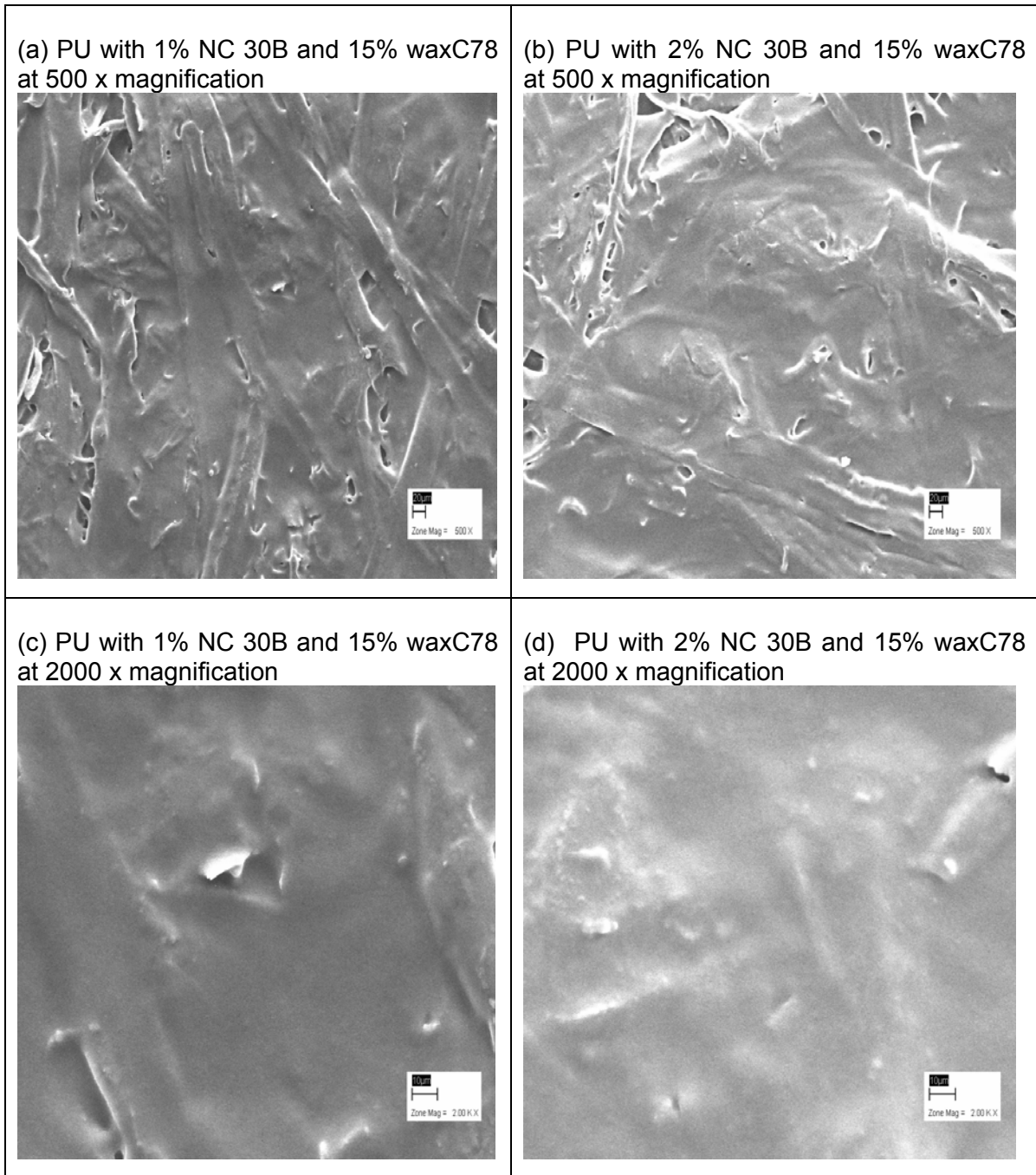


Figure 8.21: SEM images of PU-NC 30B coated paperboard, containing 15% waxC78, prepared using *Method 3*

8.3.4 MVTR and DMA results of the PU-clay nanocomposites

The MVTR results of the PU-clay nanocomposites prepared via *Methods 1 to 3* are tabulated below in Table 8.6.

Table 8.6: MVTR results of PU-clay nanocomposites prepared via Methods 1 to 3

Method	% Nano-filler	No Wax C78 addition		Wax C78 addition	
		MVTR (g/m ² /24h)	Degree of blocking	MVTR (g/m ² /24h)	Degree of blocking
1	0	815	Medium	187	Kissing
	1	817	Medium-Kissing	232	Kissing
2	1	781	Kissing	331	Kissing
2	2	784	Kissing	298	Kissing
3	1	750	None	211	None
3	2	748	None	277	None

By comparing Table 8.5 with Table 8.6, it can be concluded that the methods of preparing the polyurethane-clay nanocomposites have a small effect on the MVTR results of the coated paperboard. However, the incorporation of 15% wax C78 into the polyurethane-clay nanocomposites has a bigger effect on the MVTR results. The preparation method focuses on the degree of exfoliation and dispersion of the nano-clays into the polyurethane matrix, and the compatibility of the nano-clays with regard to the hard and soft segments of the polyurethane, and that of the wax.

Apart from achieving very low MVTR results, the degree of blocking is also a very important factor. Table 8.6 shows that only *Method 3* exhibits 100% anti-blocking properties at 1 and 2% exfoliated nano-clays with and without the addition of 15% wax C78.

In the case of the unintercalated polyurethane-clay nanocomposites synthesized from *Method 1*, the compatibility of the polyurethane's hard and soft segments is not much affected, as seen from the DMA results in Figure 8.22. This results in a paperboard coating with no pinholes, as seen from the SEM images in Figure 8.8. Also, the unintercalated nano-particles act similarly to the dispersed micro-fillers, as seen by comparing the DMA results in Figure 8.4 and Figure 8.22, SEM images in Figures 8.3 and Figure 8.8, and also TEM images in Figure 8.3 with Figure 8.8.

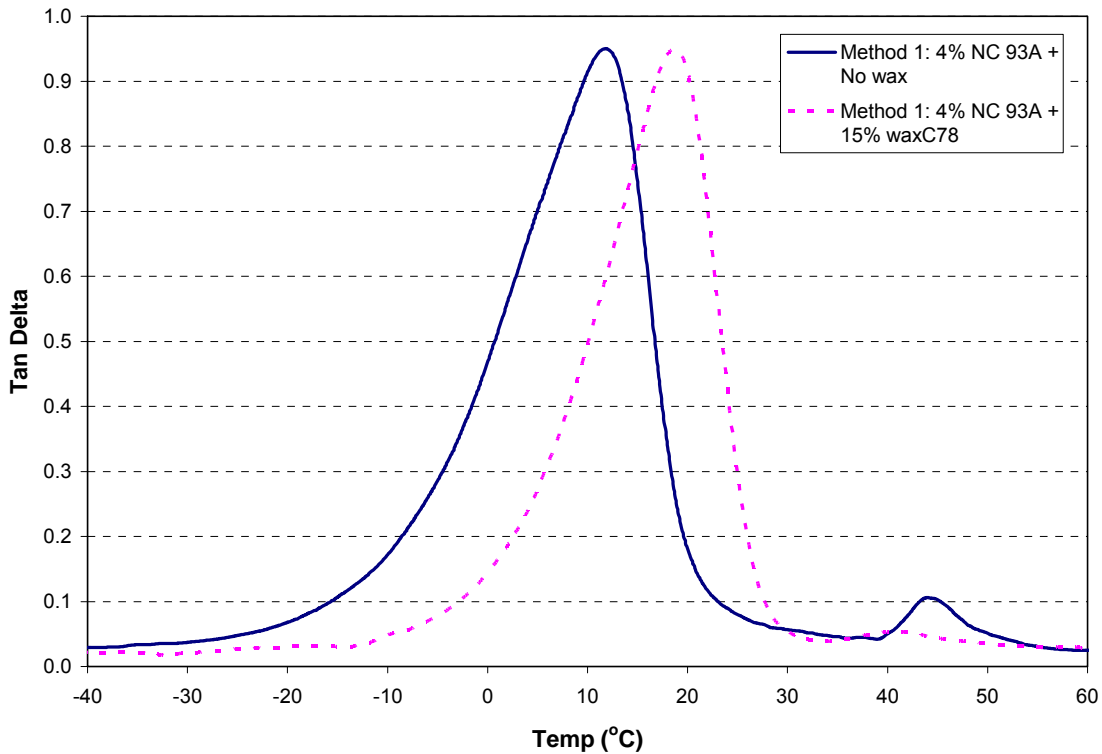


Figure 8.22: DMA analysis of PU-NC 93A nanocomposite films which were prepared using *Method 1*

Method 2a and 2b produced polyurethane-clay nanocomposites containing all three types of composite materials, namely the unintercalated, unintercalated and exfoliated forms. *Method 2a* contained a high degree of unintercalated form, and *Method 2b* a high degree of intercalated form, as evident from comparing the TEM and SEM results in Figures 8.9 to 8.16. Here the compatibility between the hard and soft segments of the polyurethane was affected by the presence of the nano-clay particles, which became significant enough to affect the MVTR results, as seen by the DMA results in Figure 8.23 for *Method 2a*, and Figure 8.24 for *Method 2b* between -15 to -5°C. However, *Method 2b* showed a lower degree of incompatibility than *Method 2a*, which also showed minimal difference in the MVTR results in Table 8.6.

This loss in compatibility may also be deduced from the SEM images in Figures 8.13 to 8.16, by the formation of pinholes in the coated paperboards.

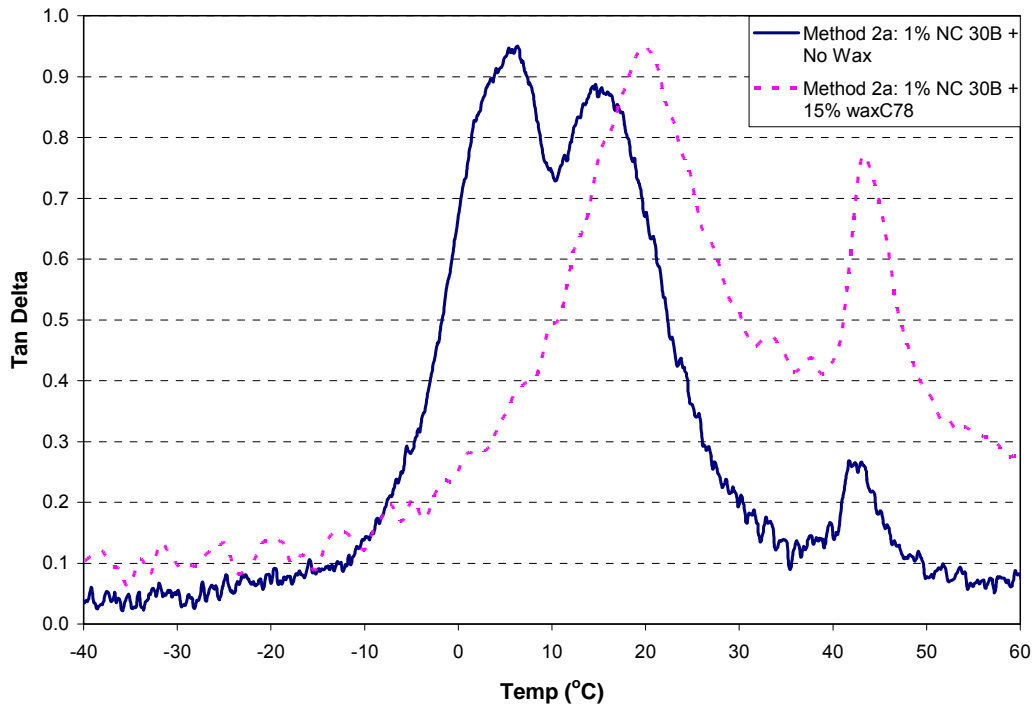


Figure 8.23: DMA analysis of PU-NC 30B nanocomposite films, prepared using *Method 2a*

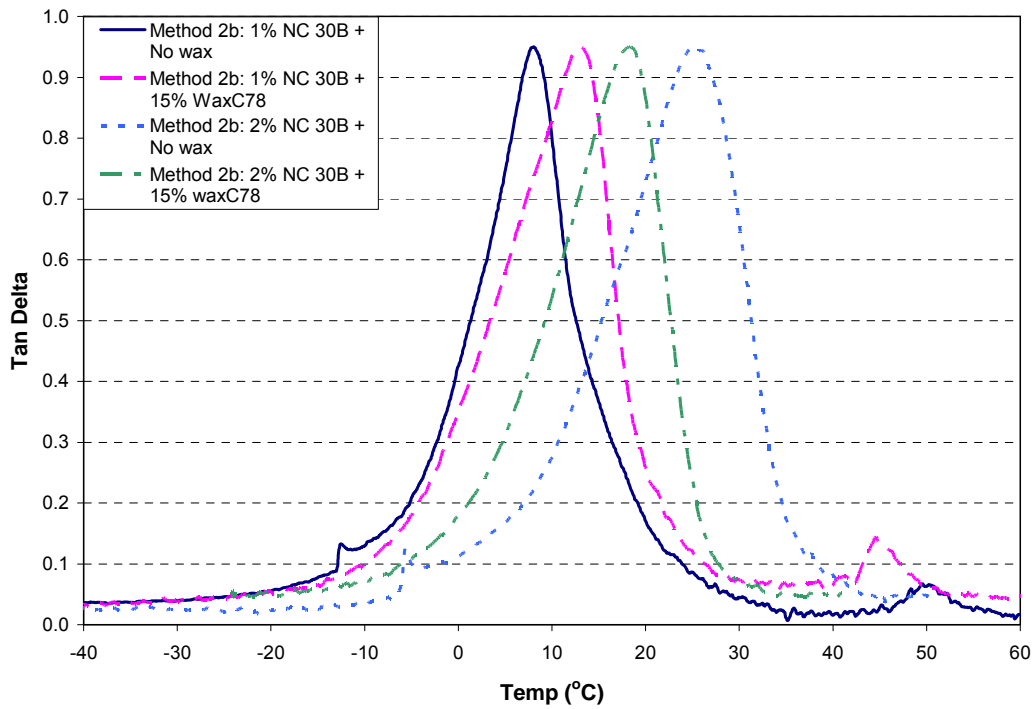


Figure 8.24: DMA analysis of PU-NC 30B nanocomposite films, prepared using *Method 2b*

Method 3 produced polyurethane-clay nanocomposites containing a very high degree of the exfoliated form, seen by comparing the TEM and SEM results in Figures 8.17 to 8.21. The same number of nano particles, when exfoliated, has a bigger effect on the compatibility between the hard and soft segments of the polyurethane, which is the case when comparing Figure 8.25 of *Method 3* to Figures 8.23 and 8.24 of *Methods 2a* and *2b*.

However, an increase from 1% to 2% nano-clay concentration with 15% waxC78 resulted in poorer MVTR results, as seen in Table 8.6. This was mainly due to the disruption of the compatibility between the hard and soft segments of the polyurethane by the exfoliated nano particle, as seen in Figure 8.25, and also due to the differences in hydrophobicity between the nano-clay and wax particles; the nano-clay NC 30B was highly hydrophilic (see Table 8.3) compared to the highly hydrophobic waxC78.

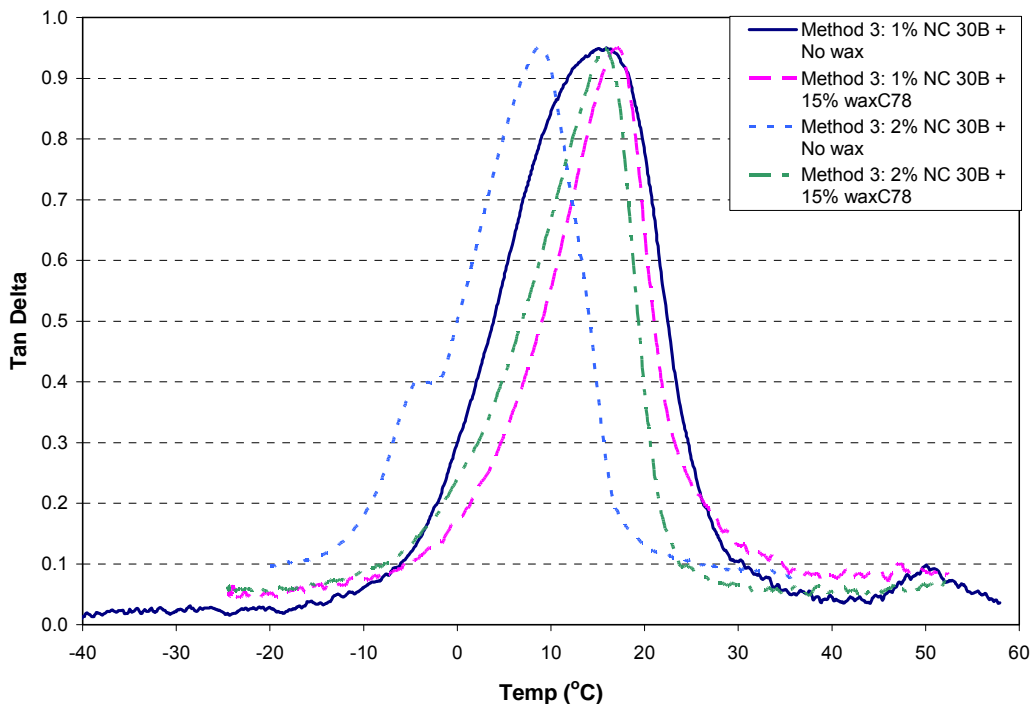


Figure 8.25: DMA analysis of PU-NC 30B nanocomposite films, prepared using *Method 3*

Also, the polyurethane-clay nanocomposites which were prepared using *Method 3* resulted in a coating with no blocking, both with and without wax C78 addition, which is a very important parameter when stacking the paperboard after the coating application.

8.4 Conclusions

In conclusion, the incorporation of nano-clay into the polyurethane matrix affected the mechanical and physical properties of the coating. These properties include reasonably low MVTRs, improved anti-blocking and limited compatibility between the various components in the coating mixture. Analytical methods used were DMA, TEM, SEM, MVTR, and the determination of the degree of blocking.

The major differences between the results were due to the degree of exfoliation of the nano-clay particles into the polyurethane matrix. The degree of nano-clay exfoliation included the un-exfoliated, phase separated/unintercalated, intercalated and exfoliated forms, which was illustrated by *Methods 1, 2a, 2b and 3* consecutively, as shown in Table 8.2.

Analysis of the polyurethane-clay nanocomposites prepared by *Methods 1, 2a, 2b and 3*, showed best results when *Method 3* was applied. *Method 3* produced the best results at a nano-clay loading of 1 weight percent, which was due to full compatibility between the various components in the coating mixture, as seen from the DMA results shown in Figures 8.22 to 8.25. This included: (a) compatibility between the hard and soft segments of the polyurethane itself; (b) miscibility of the exfoliated nano-clay particles in between the hard and soft segments of the polyurethane; (c) compatibility/miscibility of the wax C78 in between the hard and soft segments of the polyurethane and the exfoliated nano-clay particles.

The SEM images of the PU-filler nanocomposites synthesized by *Method 3* as shown in Figures 8.20 and 8.21, are very different from those synthesized via *Method 1* as shown in Figure 8.8, and *Methods 2a and 2b*, shown in Figures 8.13 to 8.16. The difference is that *Method 3* results in coatings with much smoother surfaces compared to the other *Methods*. This signifies that there are no lumps or microparticles, further implying that minimal to no unintercalated and intercalated polymer-clay nanocomposite structures are present.

Also, pinholes are not present in the coatings produced from *Methods 1 and 3*, whereas the coatings from *Methods 2a and 2b* show pinholes, which is a very negative factor in MVTR's.

8.5 References

1. J. Chen, N. Tsubokawa. *J. Macromol. Sci. Pure Appl. Chem. A*, **38**, 383, 2001.
2. J. R. Li, J. R. Xu, M. Q. Zhang, M. Z. Rang. *Macromol. Mater. Eng.*, **288**, 103, 2003.
3. S. G. Chen, J. W. Hu, M. Q. Zang, M. Z. Rang, M. W. Li, *Carbon*, **42**, 645, 2004.
4. S. Banerjee, S. K. Palit, S. Maiti. *J. Polym. Sci. Polym. Chem.*, **32**, 219, 1994.
5. A. R. Horrocks, J. Zhang, M. E. Hall. *Polym. Int.*, **33**, 303, 1994.
6. S. J. Chang, F. C. Chang. *J. Appl. Polym. Sci.*, **72**, 109, 1999.
7. S. K. Dolui. *J. Appl. Polym. Sci.*, **53**, 463, 1994.
8. E. A. Otterstedt, O. E. Otterstedt, J. Ekdahl, J. Backman, *J. Appl. Polym. Sci.*, **34**, 2575, 1987.
9. D. Feldman, M. A. Lacasse. *J. Appl. Polym. Sci.*, **51**, 701, 1994.
10. H. H. Murray, *Applied Clay Science*, **17**, 207, 2000.
11. E. N. Sotnikova, N. S. Pesochinskaya. *Int. Polym. Sci. Technol.*, **14**, 22, 1987.
12. T. G. Marcia-Agullo, J. C. Fernandez-Garcia, N. Pastor-Sempere, A. C. Orgiles-Barcelo, J. M. Martin-Martinez. *J. Adhes.*, **38**, 31, 1992.
13. T. G. Marcia-Agullo, J. C. Fernandez-Garcia, A. Torro-Palau, A. C. Orgiles-Barcelo, J. M. Martin-Martinez. *J. Adhes.*, **50**, 265, 1995.
14. A. M. Torro-Palau, J. C. Fernandez-Garcia, A. C. Orgiles-Barcelo, J. M. Martin-Martinez. *J. Adhes.*, **21**, 1, 2001.
15. S. Zhou, L. Wu, J. Sun, W. Shen. *Progress in Organic Coatings*, **45**, 33, 2002.
16. H. Schmidt, B. Seiferling. *Mater. Res. Soc. Symp. Proc.*, **73**, 739, 1986.
17. H. H. Huang, G. L. Wilkes, J. G. Carlson. *Polymer*, **30**, 2001, 1989.
18. L. M. Liu, Z. N. Qi, X. G. Zhu. *J. Appl. Polym. Sci.*, **71**, 1133, 1999.
19. M. B. Leverkusen, S. G. Leverkusen, T. E. Koln, et al., US Patent 6020419, 2000.
20. M. Alexandre, P. Dubois, *Materials Science and Engineering*, **28**, 1, 2000.
21. M. Biswas, S. S. Ray, *Adv. Polym. Sci.*, **155**, 170, 2001.
22. M. Rosorff, Nano Surface Chemistry. Marcel Dekker Inc., New York-Basel, 653, 2002.
23. S. S. Ray, M. Okamoto, *Prog. Polym. Sci.*, **28**, 1539, 2003.

24. M. Okamoto, Encyclopedia of Nanoscience and Nanotechnology, American Scientific Publishers, California, **8**, 791, 2004.

9 CONCLUSIONS

9.1 Conclusions

- I. Polyester polyols were successfully synthesized by polycondensation to an average molecular mass of 950 to 1500 g/mol, an acid value of 3 to 6 mg/g of KOH and a hydroxyl-value of 150 to 300 mg/g of KOH.
- II. The synthesized polyols were used in the synthesis of segmented polyurethanes. The urethane hard segment consisted of TDI, DMPA, and EG. DMPA was the polyurethane's primary source of ionic centers for dispersion in water. An increase in ionic content decreased the particle size of the polyurethane dispersion, and it also increased the stability of the dispersion.
- III. The PUs showed best MVTR results between 30 to 33% hard segment content. Below this, the PU was too tacky, resulting in bad coating properties. Above this, the PU showed signs of incompatibility between the hard and soft segments, although the coating properties were similar to the PU with the 30 to 33% content.
- IV. Generally, an increase in 1,4-CHDCA content increased the processing and dispersion viscosity, but decreased the ease of dispersability and stability of the PU dispersions. However, the best overall properties were obtained at an optimum CHDCA content of 10%.

Also, an increase in the 1,4-CHDCA content increased the T_g and the hydrophobicity. It also increased the compatibility between hard and soft segments of the PU in terms of hardness (only when the emulsion was stable). This resulted in better barrier properties such as MVTR and anti-blocking.

- V. The self-assembly mechanism was affected by the mobility of the hydrophilic and hydrophobic polyurethane chain segments during the coating process, which is governed by the ionic content and the emulsion viscosity. The mobility of the

hydrophilic segments is affected by the ionic content, and the hydrophobic segments are affected by the emulsion viscosity. Optimum barrier properties were obtained at optimum self-assembly, for which the optimum emulsion viscosity was 250 mPa.s.

The ionic content comprised of the neutralized DMPA and PBTCA, and excess TEA, which should be optimized in order to obtain the optimum barrier properties. DMPA was the primary source of ionic groups for dispersing the PU into water, and for its stability. Generally, a low ionic content produced an unstable emulsion with a high solids content, whereas a high ionic content produced the opposite. In both these extreme cases, the coating resulted in poor barrier properties.

In the case of PBTCA, an increase in % PBTCA generally increased the ease of dispersability, processing and emulsion viscosity, emulsion stability and Tg. Also, by putting the PBTCA into the soft segment, the compatibility between the hard- and soft segments of the PU was increased, resulting in better barrier properties. The PBTCA content should also not be too high (above 15%) as this leads to increased hydrophilicity, and can also cause gelation during polyester synthesis.

The excess TEA reacted with polar groups inside the PU dispersion particle. Partially quaternized triethylamine acted like a phase transfer reagent and entered the PU particles (as did the uncharged Et₃N). The increase in ionic or hydrophilic concentration within the particle caused the PU particle to increase in size (swelling by water). Generally, an increase in excess TEA increases the ease of dispersability, emulsion viscosity and emulsion stability.

- VI. Nano-fillers and micro-fillers were used to investigate their effect on the PU's barrier properties, but both did not significantly improve the barrier properties such as MVTRs. However, the polyurethane-clay nanocomposites gave much better barrier properties when exfoliated into the polyurethane matrix at 1% filler content, and also gave no blocking, with or without wax C78 incorporation. Also, encapsulating the exfoliated nano-filler produced stable nano-composite emulsions without the addition of surfactants.

VII. PU/wax-composites were prepared by adding 15% wax emulsion into the polyurethane emulsion prior to it being coated onto the paperboard. These composites gave better barrier properties when compared to those without any wax. Using this amount of wax in the formulations (15%) avoided problems during the recycling process (see Appendix 7).

APPENDICES

Appendix 1: PRP polyurethane properties

The chemical composition of the PRP urethane is tabulated below in Table A.1.1.

Table A.1.1: Chemical composition of PRP urethane

Raw materials	Mass (wt%)
HMDI	60.40
EG	2.01
DMPA	8.31
NMP	37.75
Polyol	89.72
NMP	34.60
TEA	7.80
DBA	1.76
Water	251.66
Total	494.00

The chemical composition of the polyol used in the PRP urethane is tabulated in Table A.1.2, which was processed to an acid value of between 6 to 8 mgKOH/g.

Table A.1.2: Chemical composition of polyol in PRP urethane

Raw materials	Mass (wt%)
NPG	47.41
AA	22.00
CHDCA	15.46
PBTCA	10.00
Total	100.00

Appendix 2: Wax properties

A.2.1 Properties of wax A15/31

Wax A15/31 is a combination of two waxes that, when dried, form two distinctive layers; one forming a yellowish top layer, and the other a whitish bottom layer. The DMA spectrum of the experimental wax A15/31 is shown in Figure A.2.1.

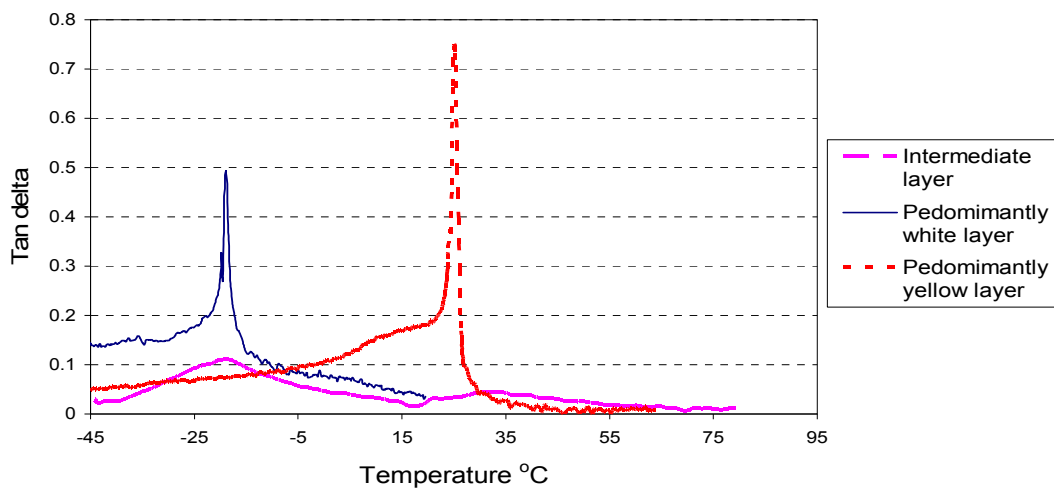


Figure A.2.1: DMA spectrum of wax A15/31

A.2.2 Properties of Wax C78

Wax C78 is also a combination of two waxes that, when dried, form two distinctive layers; one forming a yellowish top layer, and the other a whitish bottom layer. The DMA spectrum of the experimental wax C78 is shown in Figure A.2.2.

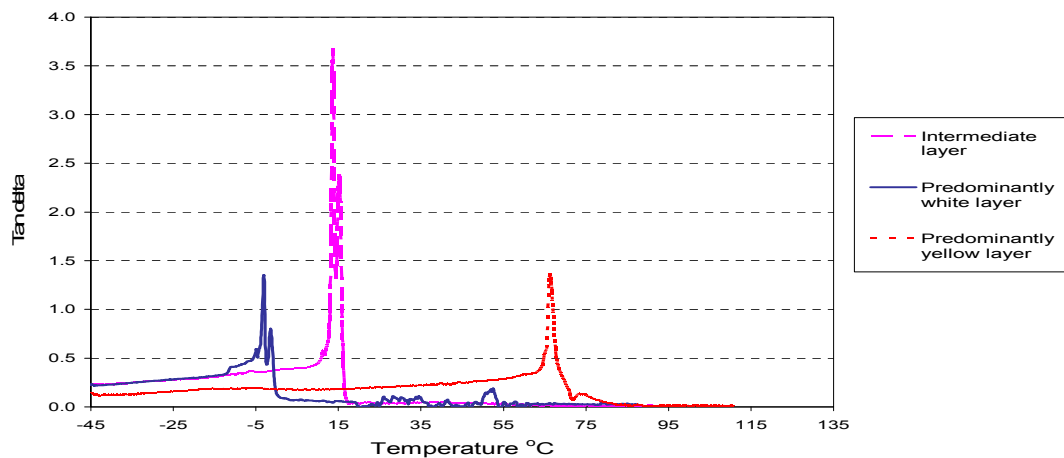


Figure A.2.2: DMA spectrum of wax C78

The properties of wax C78 are tabulated below in Table A.2.1.

Table A.2.1: Properties of wax C78

Properties	Wax C78
Colour	White liquid
Odour	Waxy
Density at 20°C	0.98 g/cm ³
Boiling point (bp)	100°C (water)
Solubility in water (20°C)	Dilutable
Flash point (°C)	Approx. 189 (After evaporation of water)
pH-value, aqueous extract	9.7
Physical state	Liquid
Viscosity @ 30°C (cP)	45
Explosion properties	None

The flakiness of wax C78 can be seen by comparing the SEM images in Figure A.2.3 to Figure A.2.5, in which Figure A.2.3 represents an uncoated nylon fiber, Figure A.2.4 the polyurethane coated nylon fiber, and Figure A.2.5 the nylon fiber coated with the polyurethane-wax composite containing 15% wax C78.

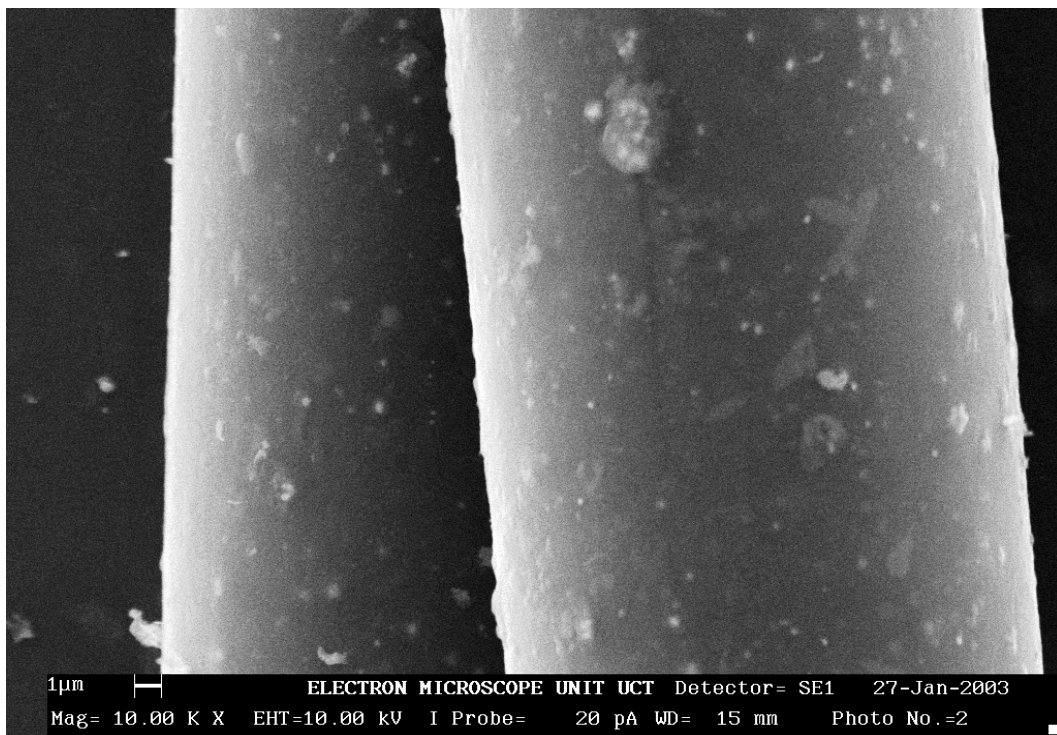
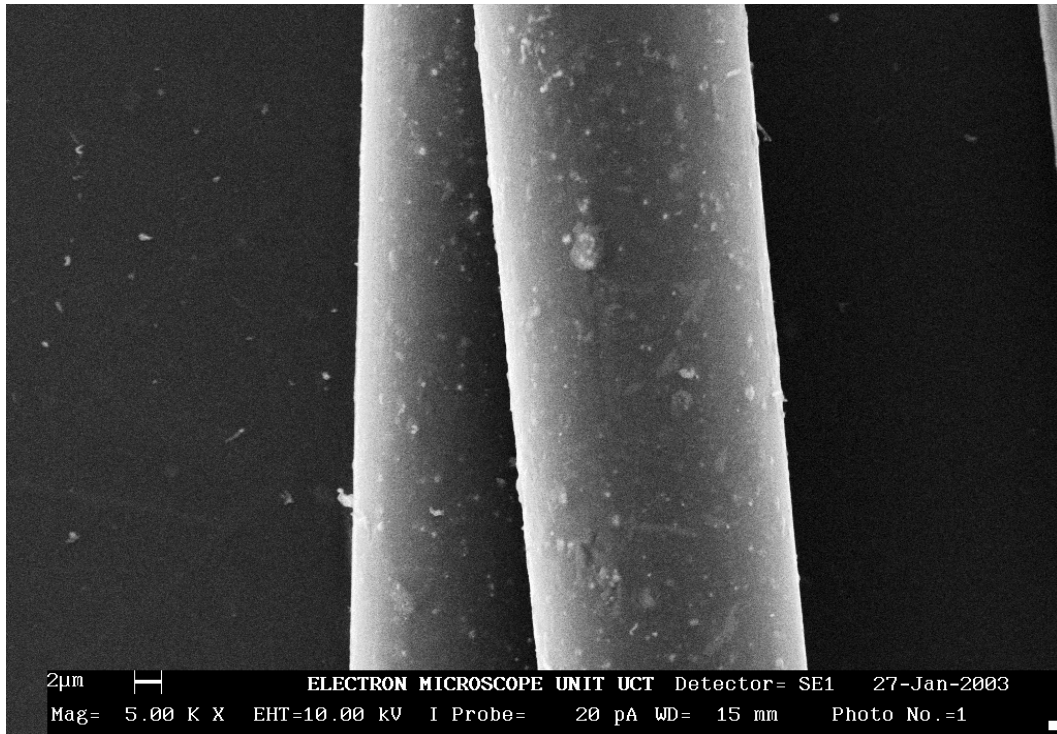


Figure A.2.3: Uncoated nylon fiber at 5000x and 10000x magnification

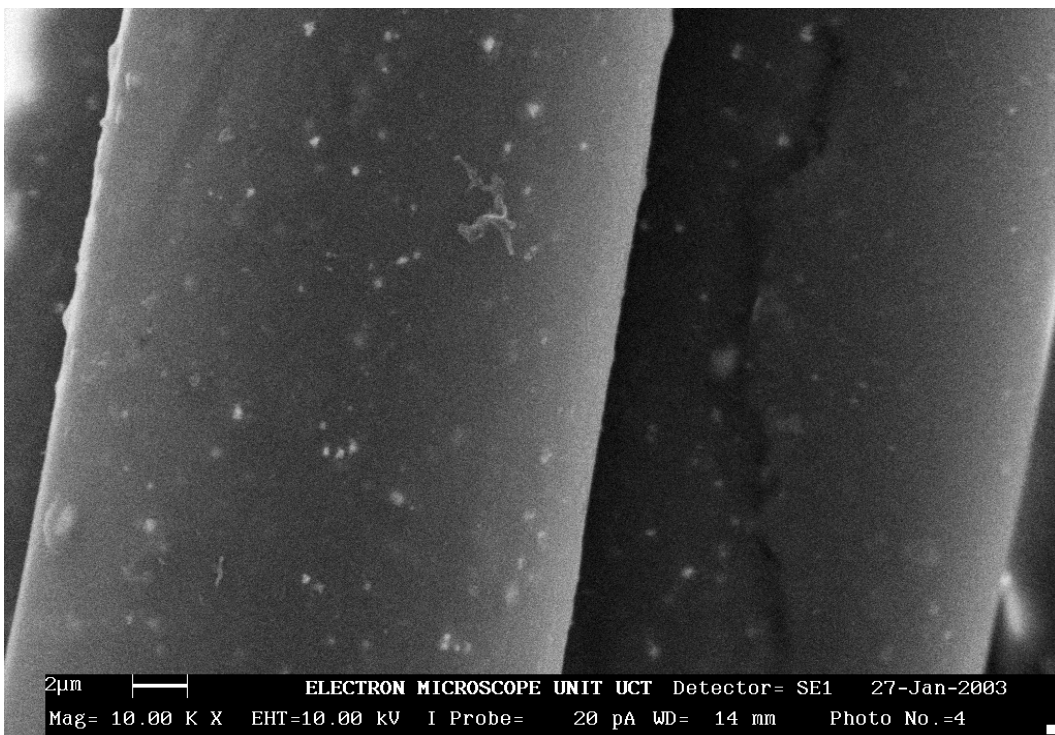
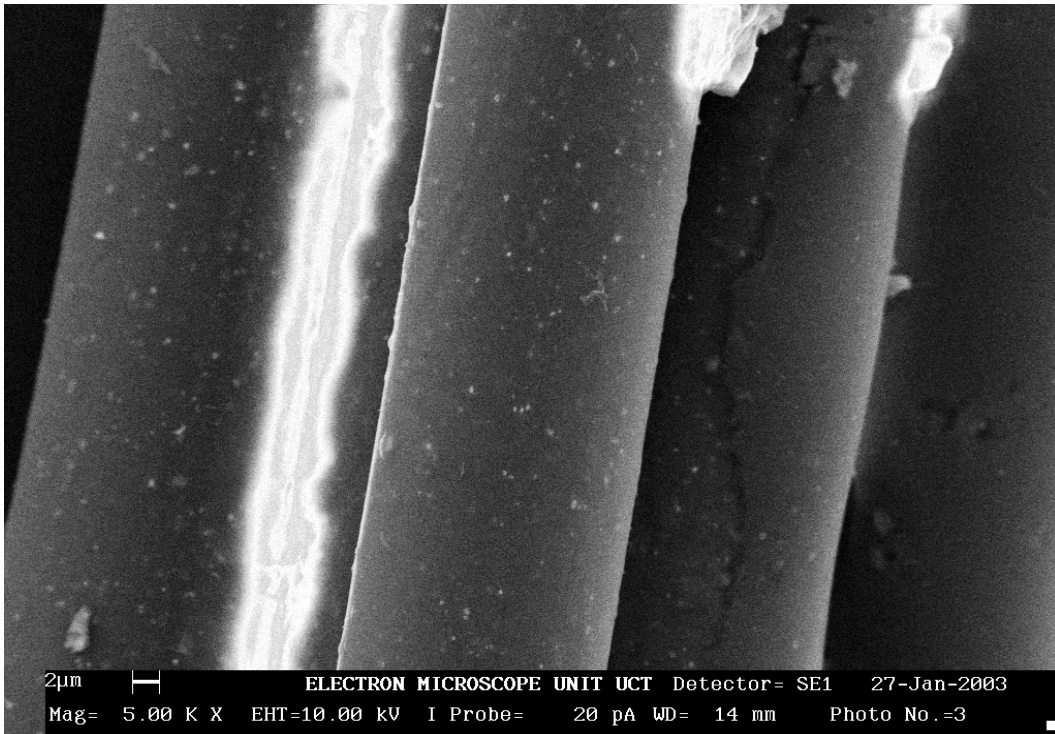


Figure A.2.4: PU-coated nylon fiber at 5000x and 10000x magnification

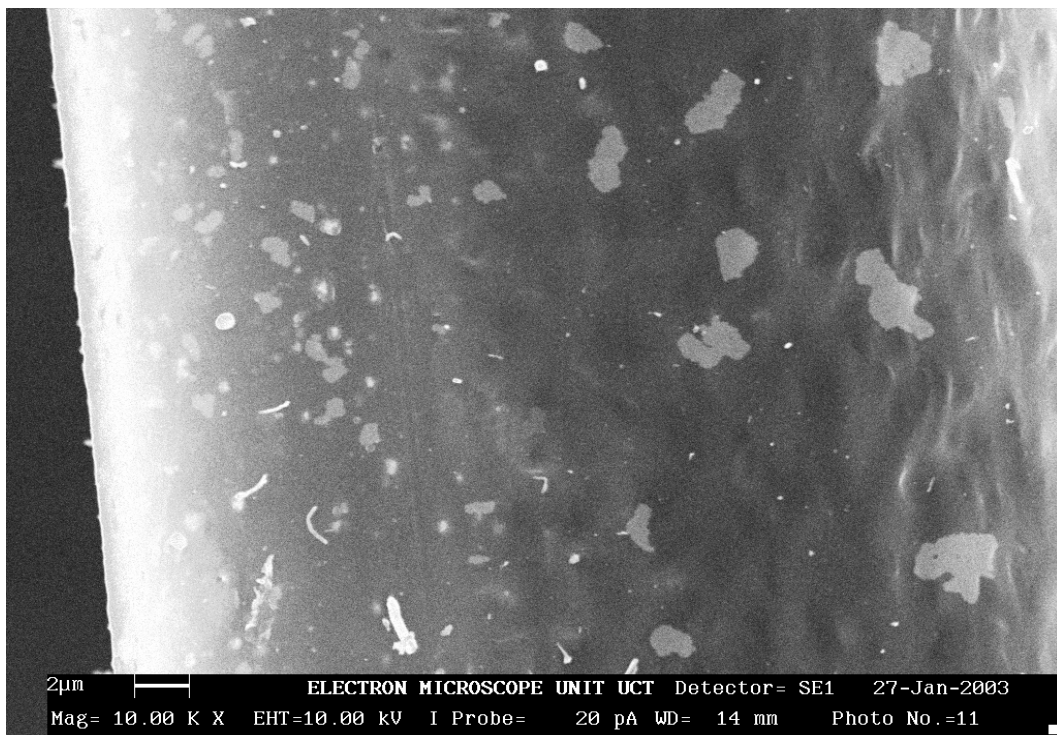
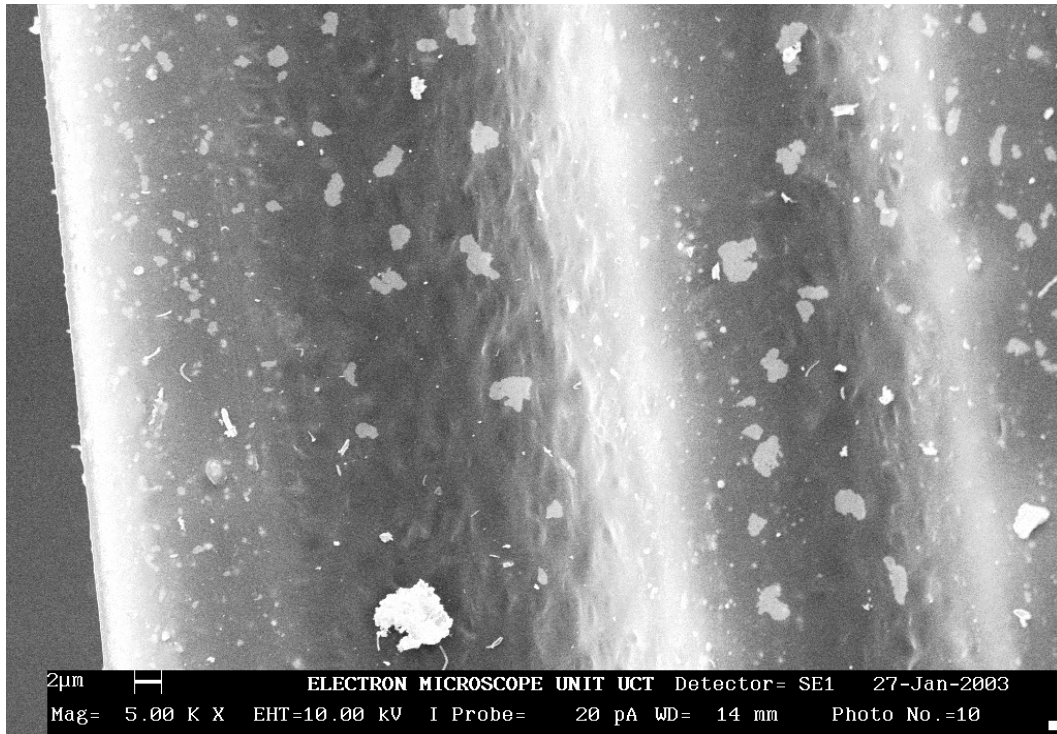


Figure A.2.5: Nylon fiber coated with mixture containing PU & 15% wax C78 at 5000x and 10000x magnification

Appendix 3: Polyurethane-wax composites

A series of waxes obtained from Schumann-Sasol was screened [1] as a two-component composite with a PRP urethane (see Appendix 1 for description of PRP urethane). This was done to determine the best PU-wax composite combination, as shown below in Figure A.3.1.

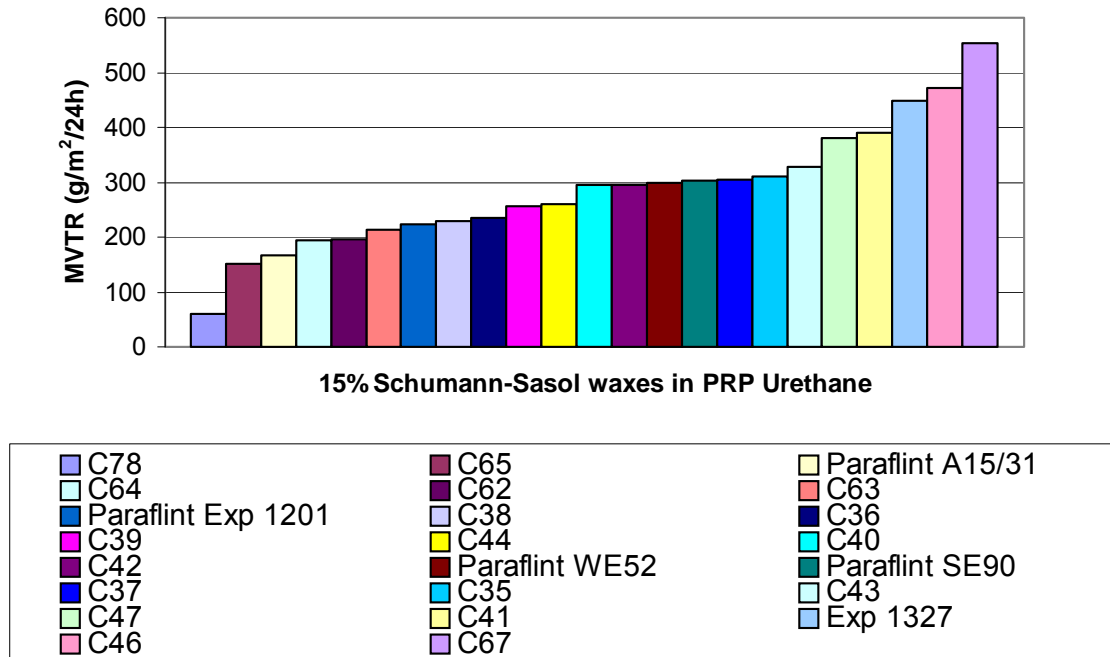


Figure A.3.1: Screening of PRP-wax composites containing 23 respective Schumann Sasol waxes in terms of MVTR

All waxes were tested at a 15% concentration level in a 26.5% total solid content PU dispersion. The composite performance was evaluated in terms of MVTRs, which were measured under tropical conditions; 38°C and 90% relative humidity (RH) over a period of 24 hours.

Two of the best three waxes were chosen to measure the MVTRs of the PRP urethane-wax composites over a range of wax concentrations to determine the optimum wax concentration in the coating mixture. The optimum wax concentration was determined at the lowest MVTR-value. Figure A.3.2 shows the MVTR-results of two PRP urethane-wax composites containing wax C78 and an experimental wax A15/31

respectively (see Appendix 2 for wax properties), of which the optimum wax concentration is at 15% [1].

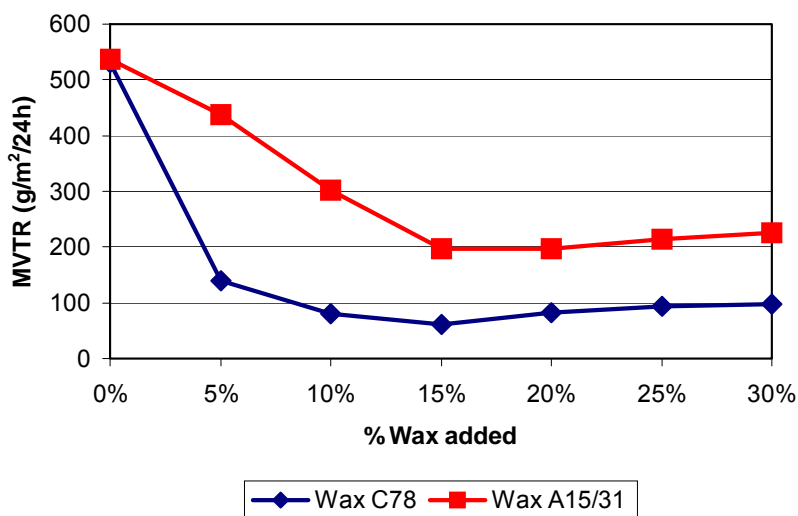


Figure A.3.2: Determination of optimum wax concentration in PRP-wax composites

The results in Figure A.3.1 and Figure A.3.2 indicated that the inclusion of 15% wax C78 into the PRP urethane matrix, produced the best MVTRs. Due to the chemical similarities of PRP urethane and the experimentally synthesized PU, it was thus decided that wax C78 would be used for further investigations.

References

1. Valeska Cloete, Paper-Coating Research Group at the Department of Chemistry and Polymer Science, University of Stellenbosch, part of current PhD studies from 2001.

Appendix 4: MVTR Test Method

This method is based on the MVTR test as developed by Mondi Cartonboard division, South Africa.

Purpose:

A Moisture Vapour Transmission Rate (MVTR) test is done to determine the amount of moisture vapour that will pass through a board in 24 hours under specified conditions of relative humidity and temperature.

Apparatus:

Humidity cabinet set at 38°C and 90% relative humidity.

Moisture resistant vessel of 84-mm diameter, open at the top and equipped with a screw-on open lid with a rubber seal.

A balance, accurate to two decimal places.

Silica gel with a colour indicator.

Test Procedure:

Dry silica gel in an oven for 2 hours at 110°C.

Add 100 g silica gel to the bottom of the vessel.

Cut a round disc sample and fit in the lid of the vessel.

Screw the lid with the sample onto the vessel.

Weigh the vessel on the balance and record the weight (A) to two decimals.

Leave the sample in the humidity cabinet for 24 hours at 38°C and 90% relative humidity.

Re-weigh the vessel after 24 hours and record the weight (B).

Calculate the open area of the vessel in m².

Calculate the MVTR by means of the following equation:

$$MVTR_{24} = \frac{B - A}{Area}$$

MVTR : Moisture Vapour Transmission Rate (g/m²/24h)

A : Weight of jar prior to 24 h exposure (in grams)

B : Weight of jar after 24 h exposure (in grams)

Area : Area of the circle (m²)

Appendix 5: Blocking Test Method

This method is based on the blocking test as developed by V. Cloete [1].

Purpose:

The blocking test is done to determine whether sheets in a pallet will stick to each other if a coating is applied on one or both sides of the sheet.

Apparatus:

A 28 kg weight that applies ± 0.5 bar pressure on a surface of the stacked coated paperboards.

Method:

Obtain two samples of coated sheets and apply pressure to them at a consistent pressure of 50 kPa for 24 hours at $\pm 22^{\circ}\text{C}$.

If only one side is coated then the test can be done either with coating touching coating, or coating touching plain board.

After 24 hours, remove samples from device and carefully pull them apart, noting the amount of sticking (blocking) occurring.

Report:

Report results as follows:

No sticking	: None
Sticking occurs in only certain areas	: Kissing
Sticking occurs over whole area but no fiber tear	: Medium
Sticking occurs over whole area with fiber tear	: Hard

References

1. Valeska Cloete, Paper-Coating Research Group at the Department of Chemistry and Polymer Science, University of Stellenbosch, part of current PhD studies from 2001.

Appendix 6: Coating weight determination

The A5 paperboard is coated halfway (see figure below) with an emulsion coating and dried in an oven between 110 to 130°C for 30 to 90 seconds. Thereafter two circles (with 84 mm diameter) are punched out, representing the uncoated and the coated sections of the paperboard. Both the uncoated and the coated circles are heated to between 110 to 130°C for 60 seconds and then weighed while still hot (W_2 and W_3). See figure below. The dry coating weight is then calculated by means of the following equation:

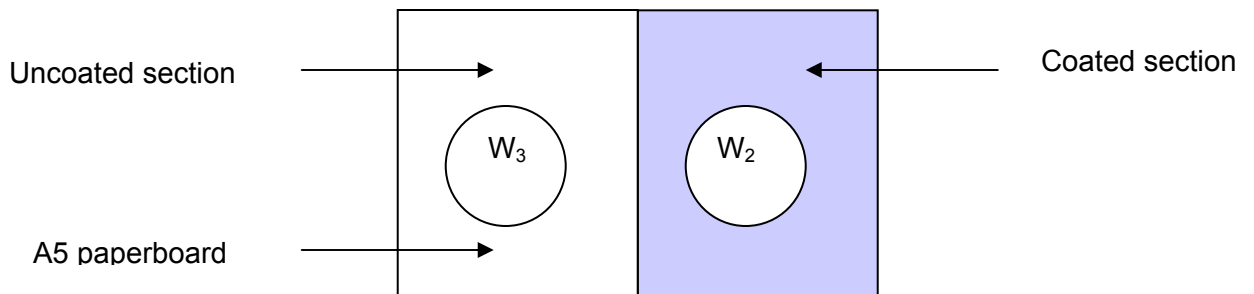
$$\text{Coating} = \frac{(W_2 - W_3)}{\text{Area}}$$

Coating: Dry weight of coating applied (g/m^2)

W_2 : Weight of coated circle (in grams)

W_3 : Weight of uncoated circle (in grams)

Area : Area of circle (m^2)



Appendix 7: Particle size analysis

A.7.1 Particle size analysis by light scattering

The particle size of the polyurethane dispersions were determined by light scattering over a pH range of 6.90 to 7.60. Results are shown in Figures A.7.1 to A.7.6.

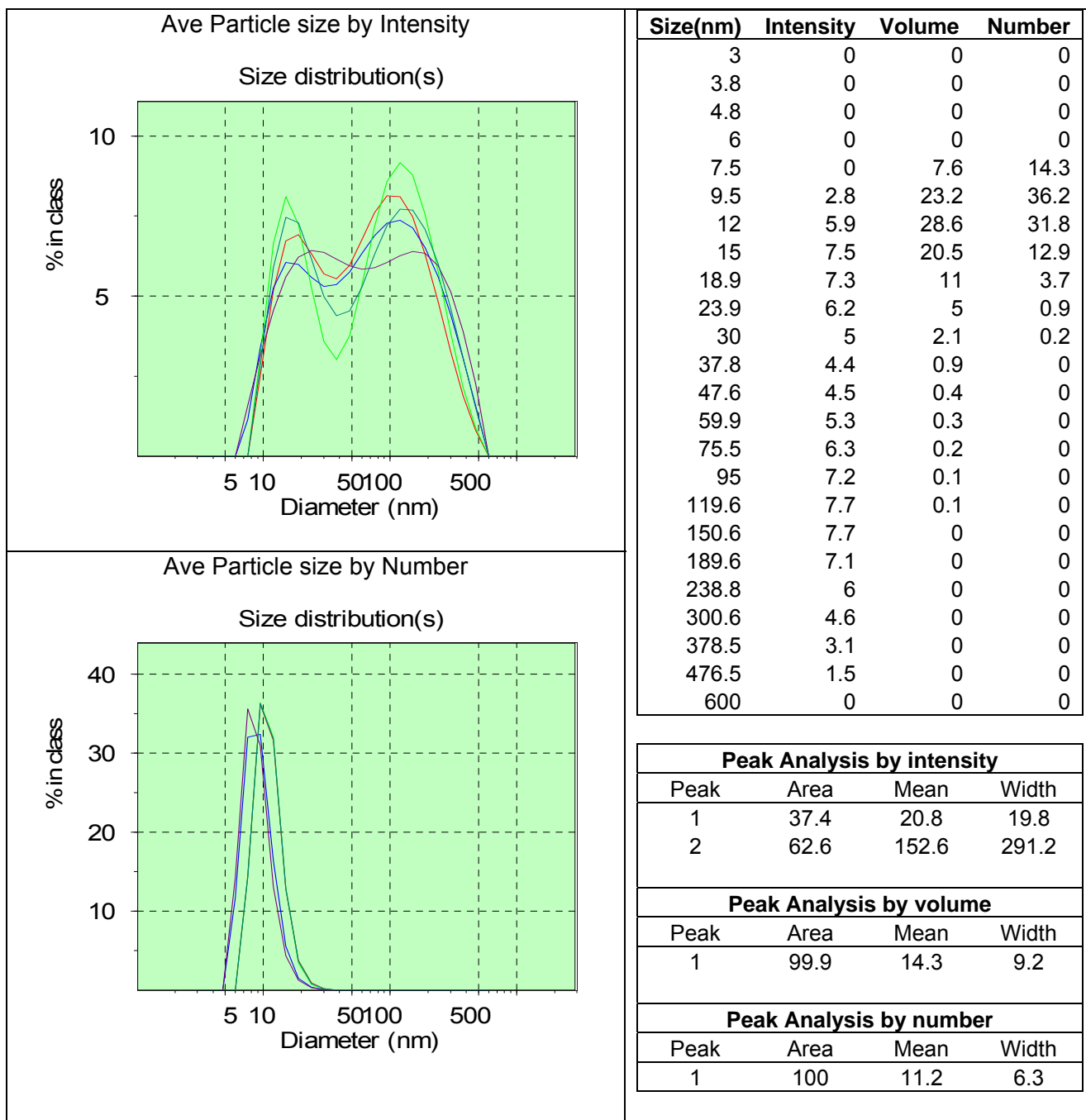


Figure A.7.1: Particle size analysis of PU dispersion at pH 6.90 at 20,3°C

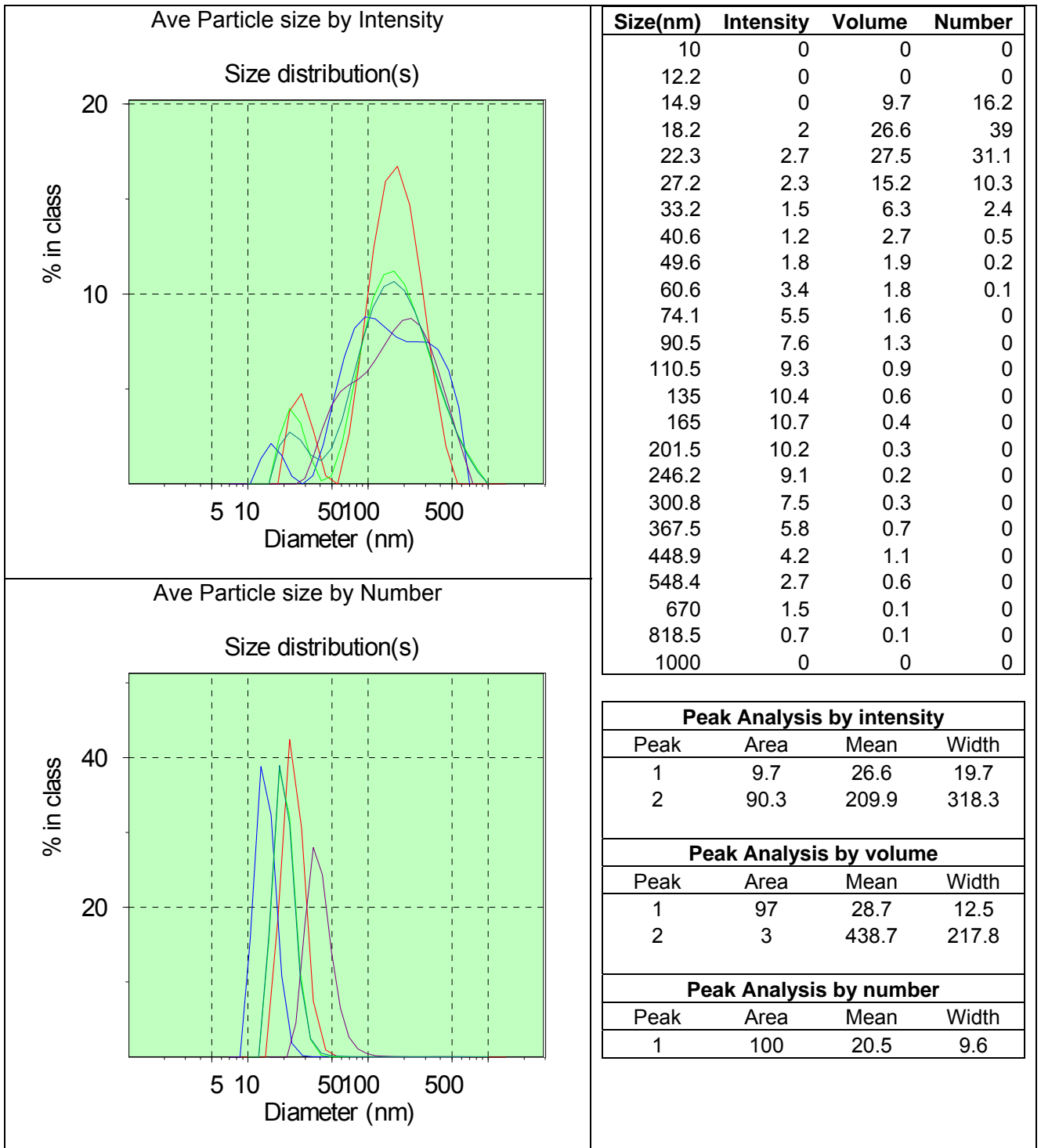


Figure A.7.2: Particle size analysis of PU dispersion at pH 6.98 at 20,3°C

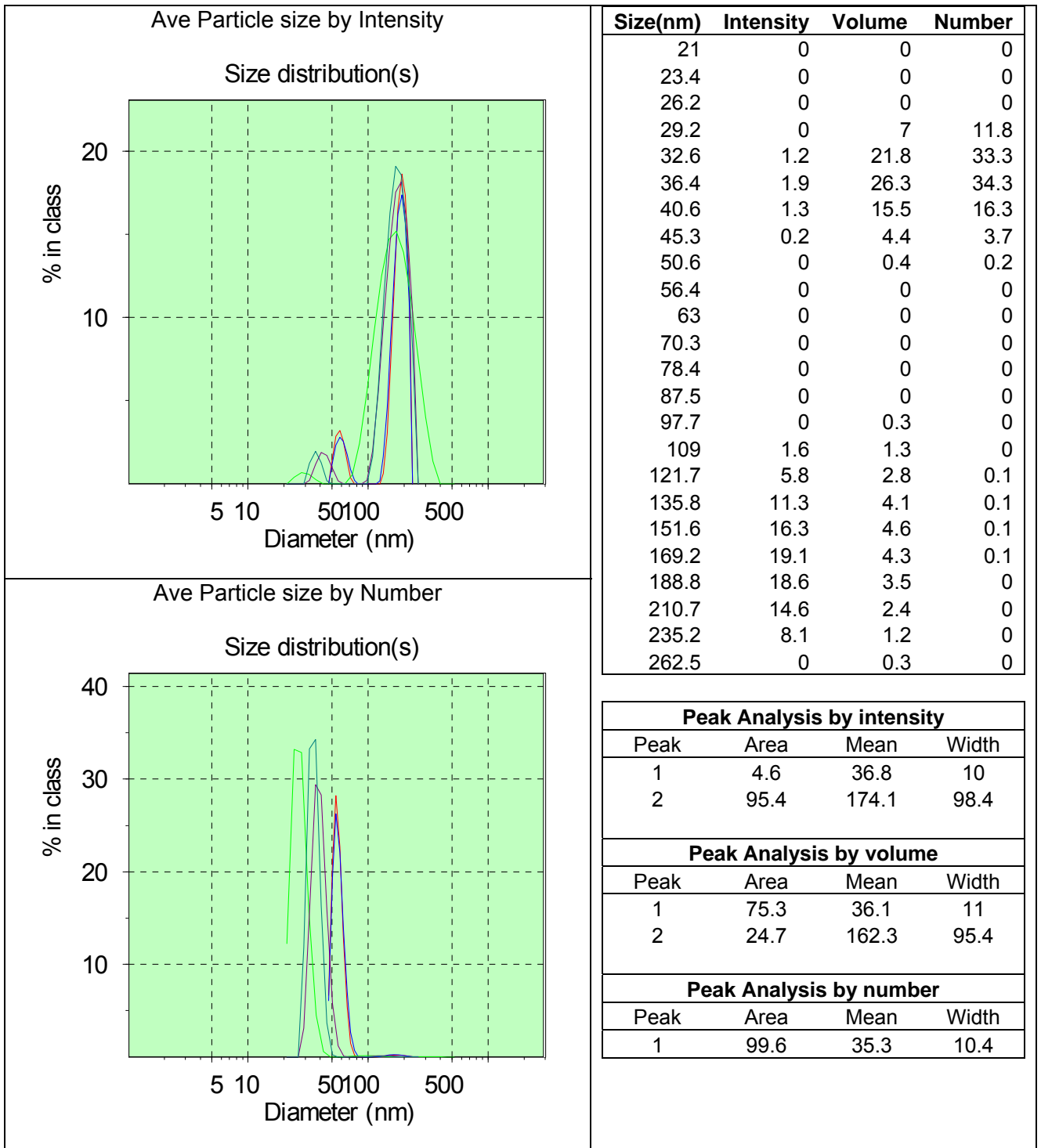


Figure A.7.3: Particle size analysis of PU dispersion at pH 7.14 at 20,3°C

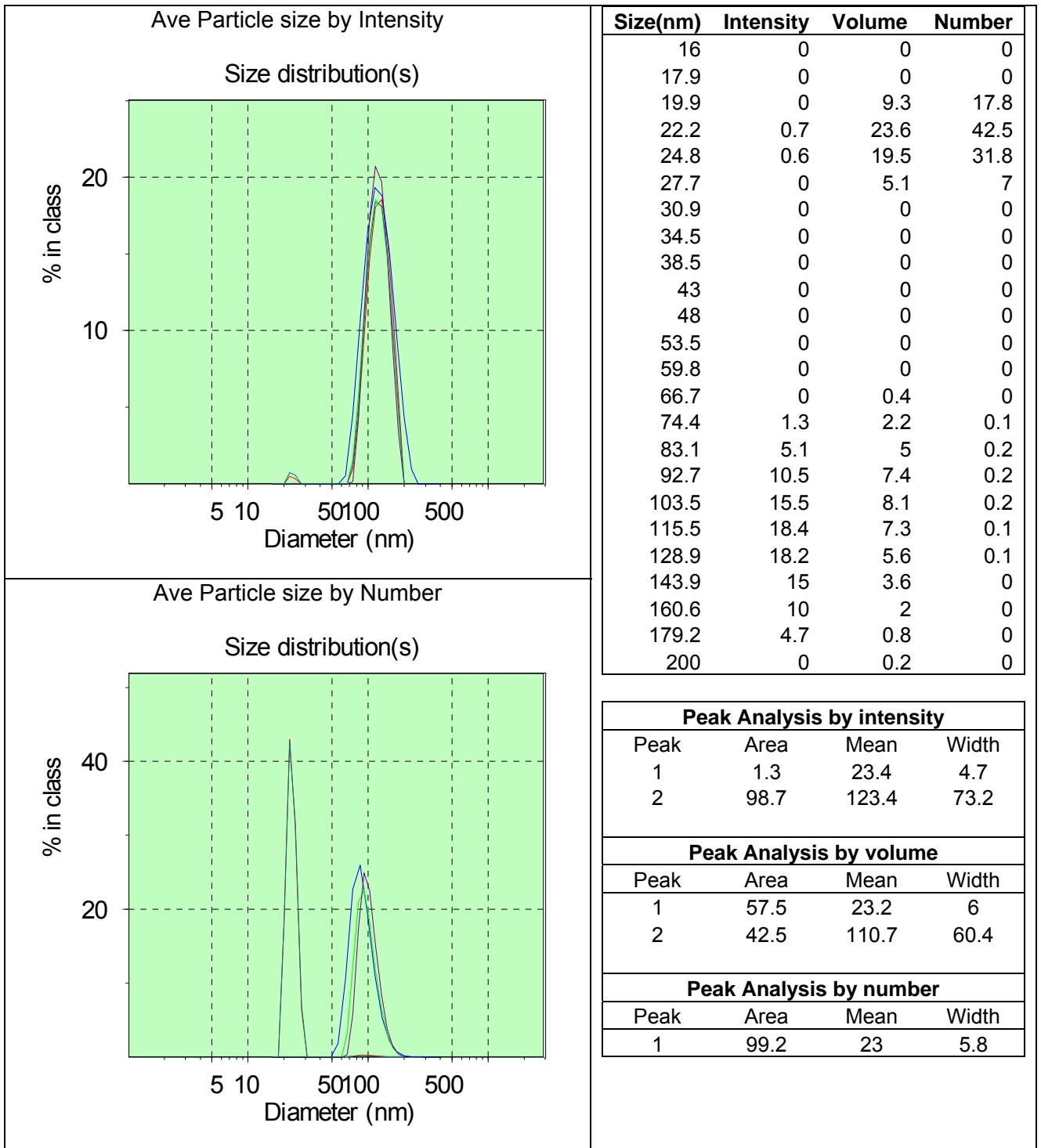


Figure A.7.4: Particle size analysis of PU dispersion at pH 7.29 at 20,3°C

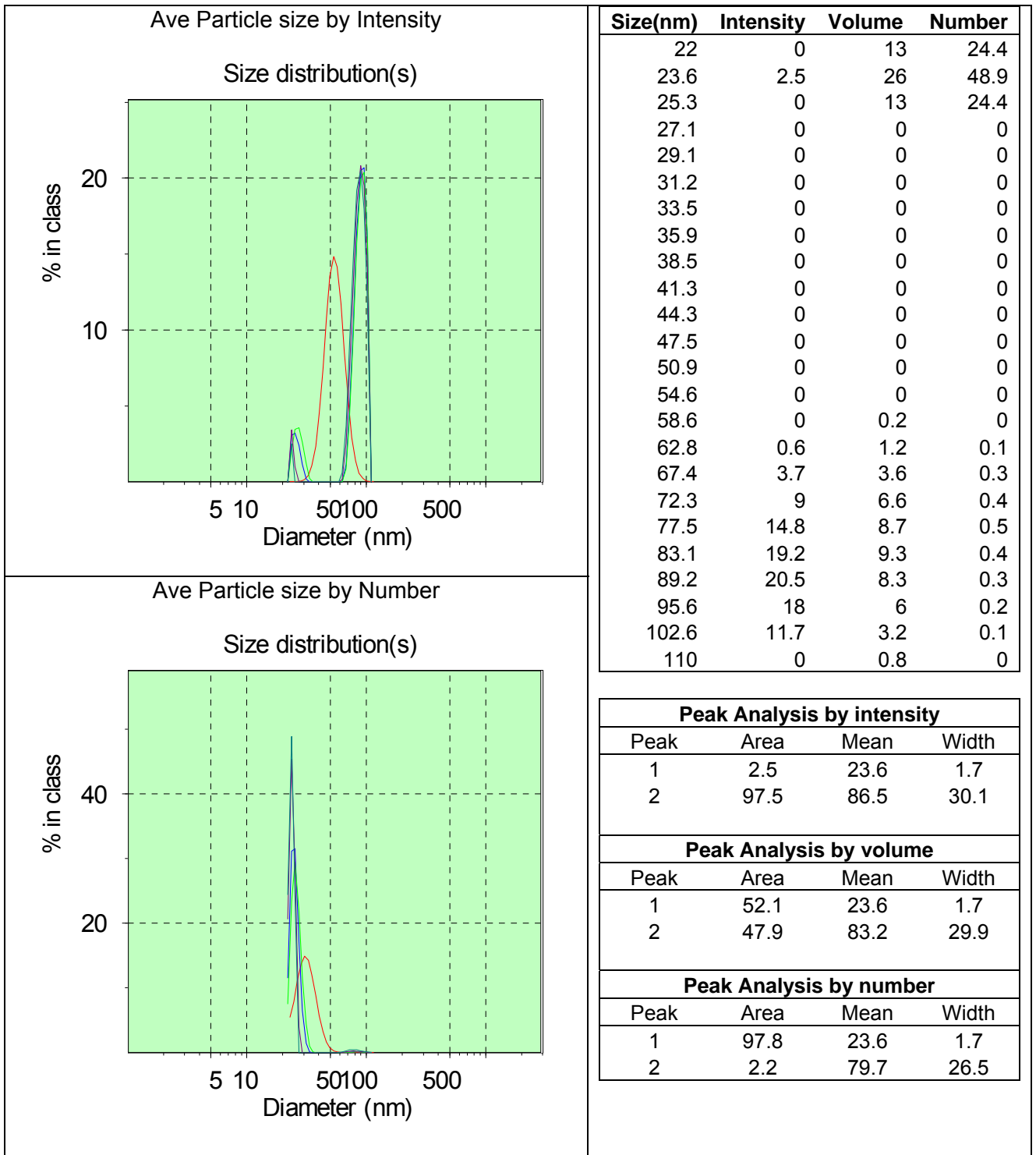


Figure A.7.5: Particle size analysis of PU dispersion at pH 7.42 at 20,3°C

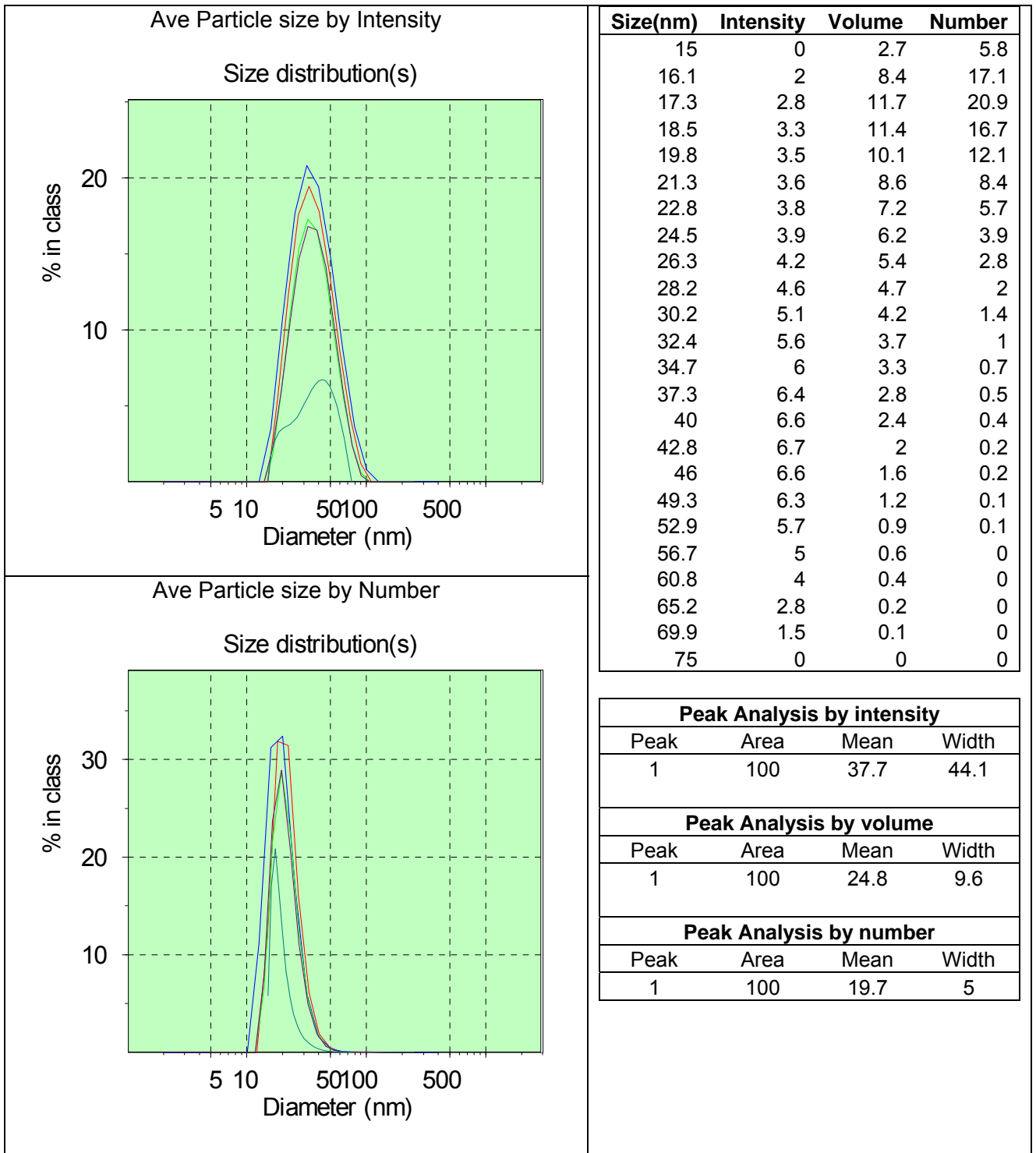


Figure A.7.6: Particle size analysis of PU dispersion at pH 7.60 at 20,3°C

A.7.2 Particle size analysis by TEM

The particle sizes of the polyurethane dispersions over a pH range of 6.90 to 7.60 are shown in Figures A.7.7 to A.7.11, as determined by TEM.

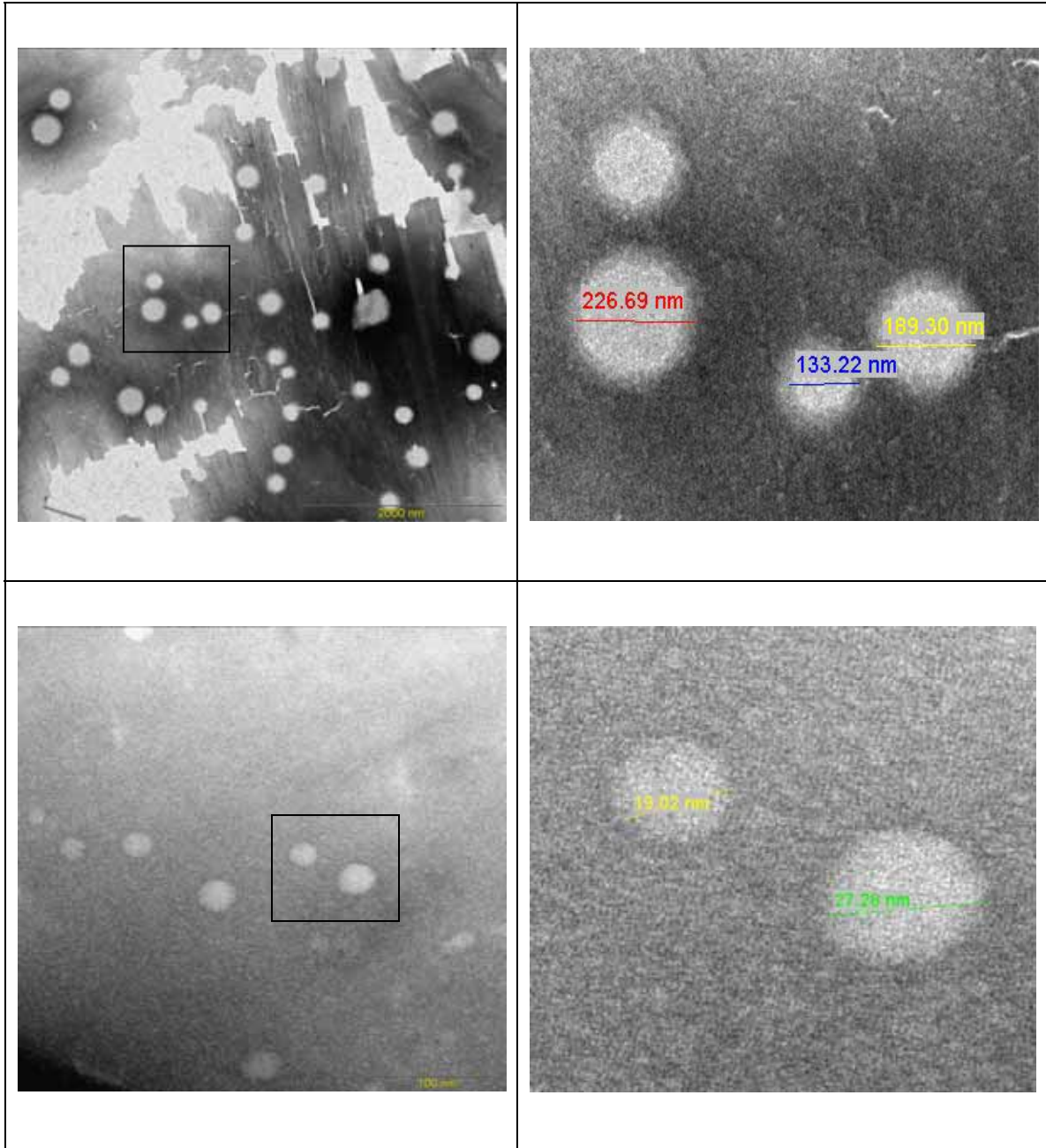


Figure A.7.7: Particle size analysis of PU dispersion as determined by TEM at pH 6.90

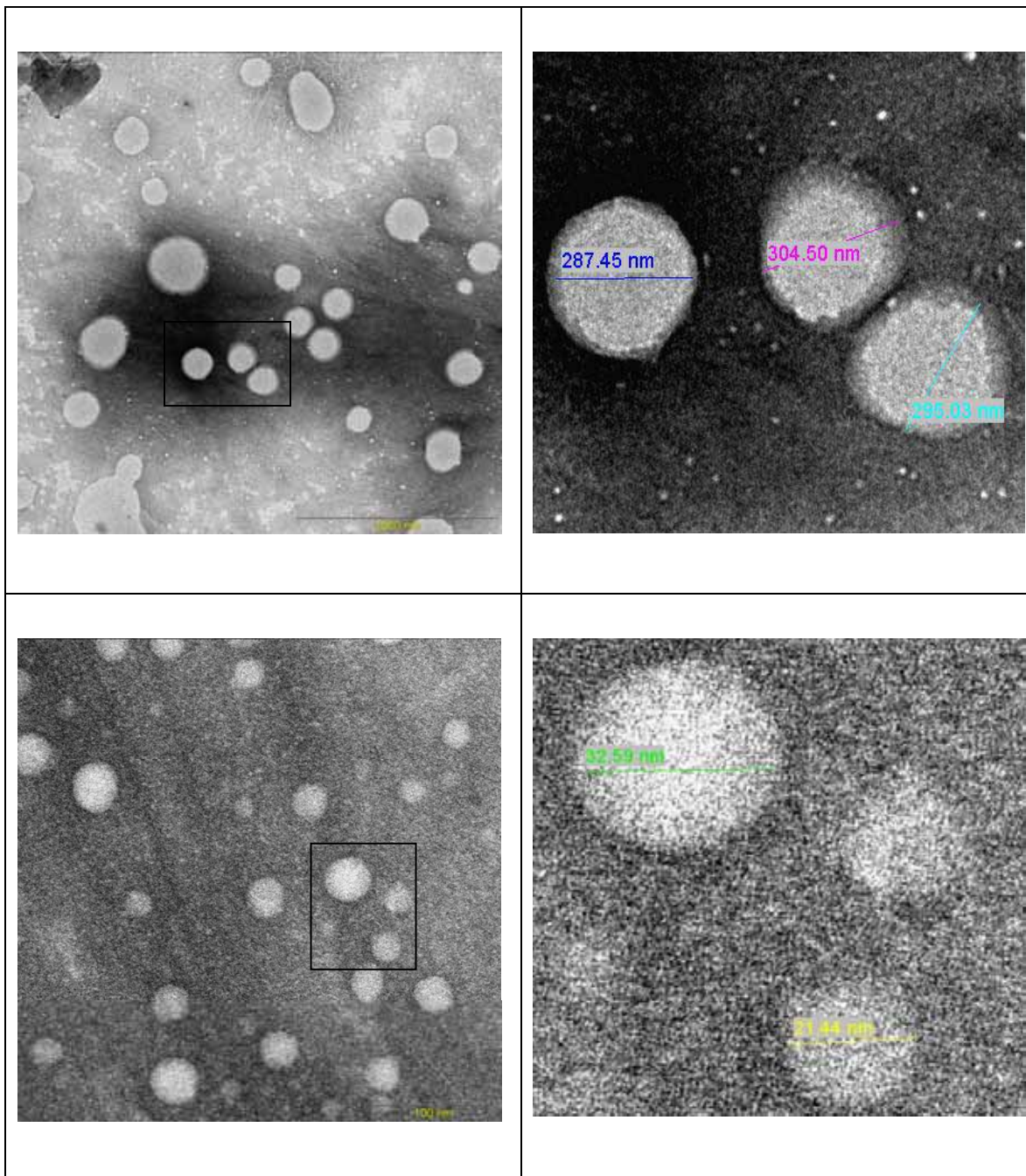


Figure A.7.8: Particle size analysis of PU dispersion as determined by TEM at pH 6.98

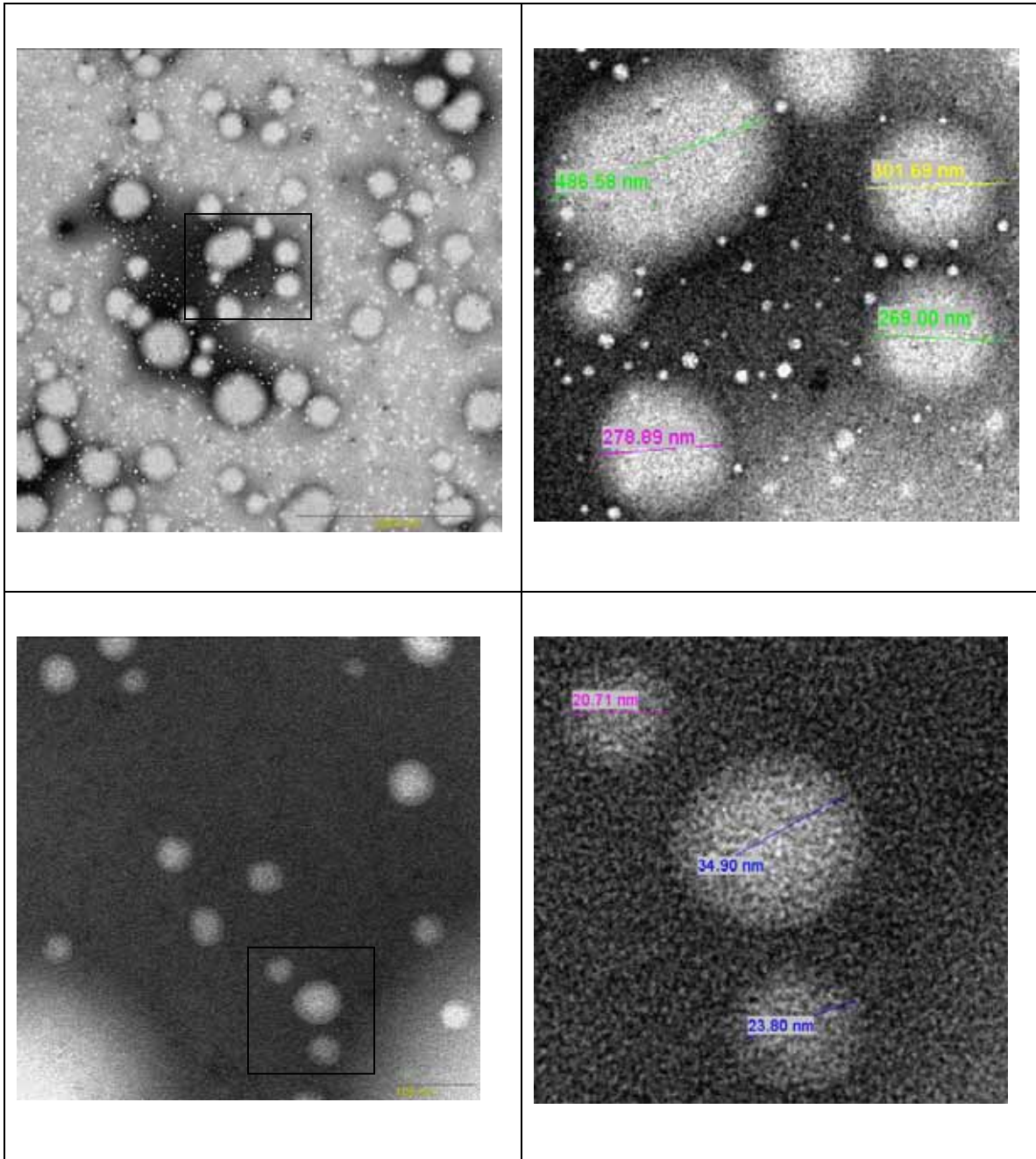


Figure A.7.9: Particle size analysis of PU dispersion as determined by TEM at pH 7.14

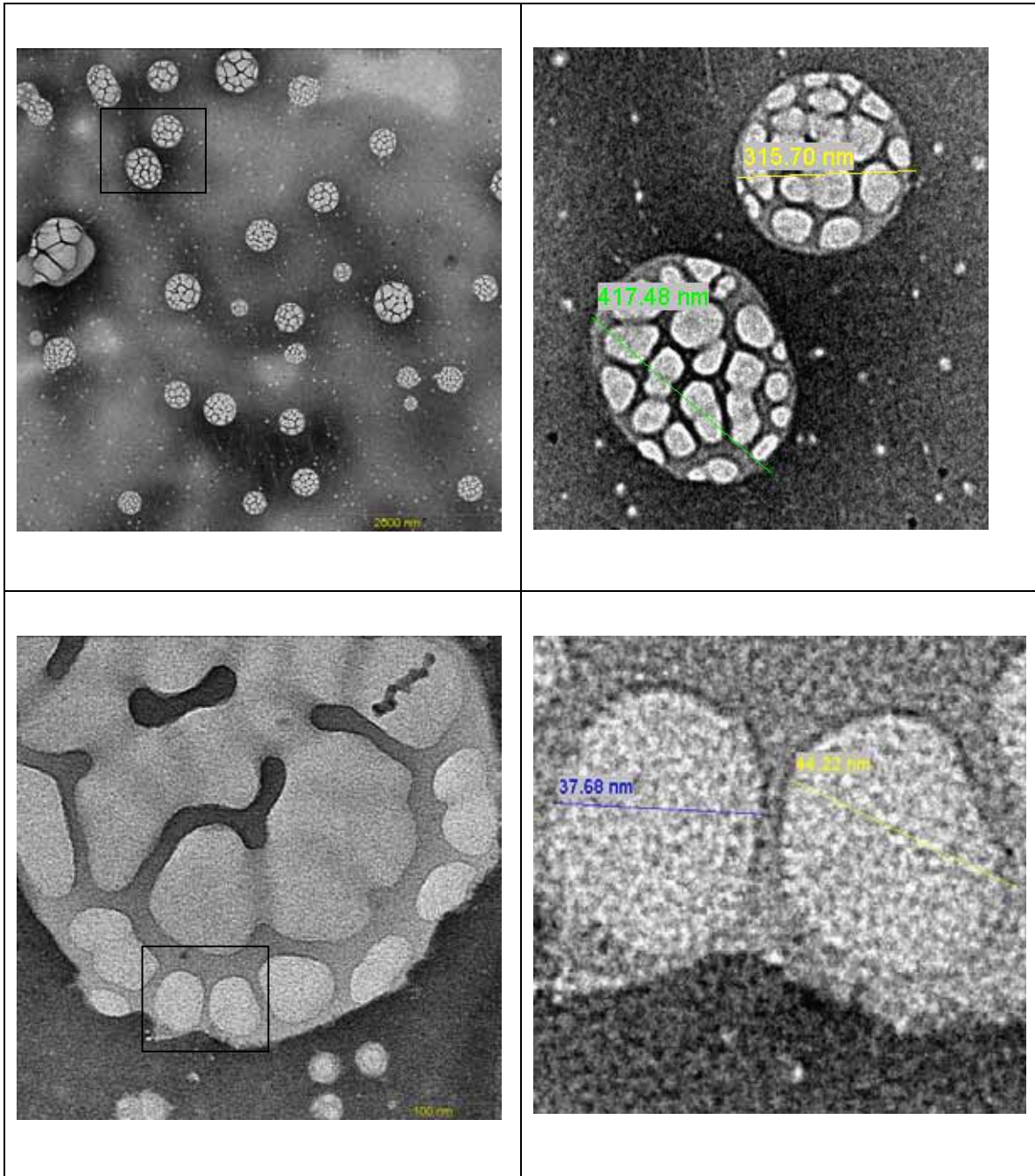


Figure A.7.10: Particle size analysis of PU dispersion as determined by TEM at pH 7.29

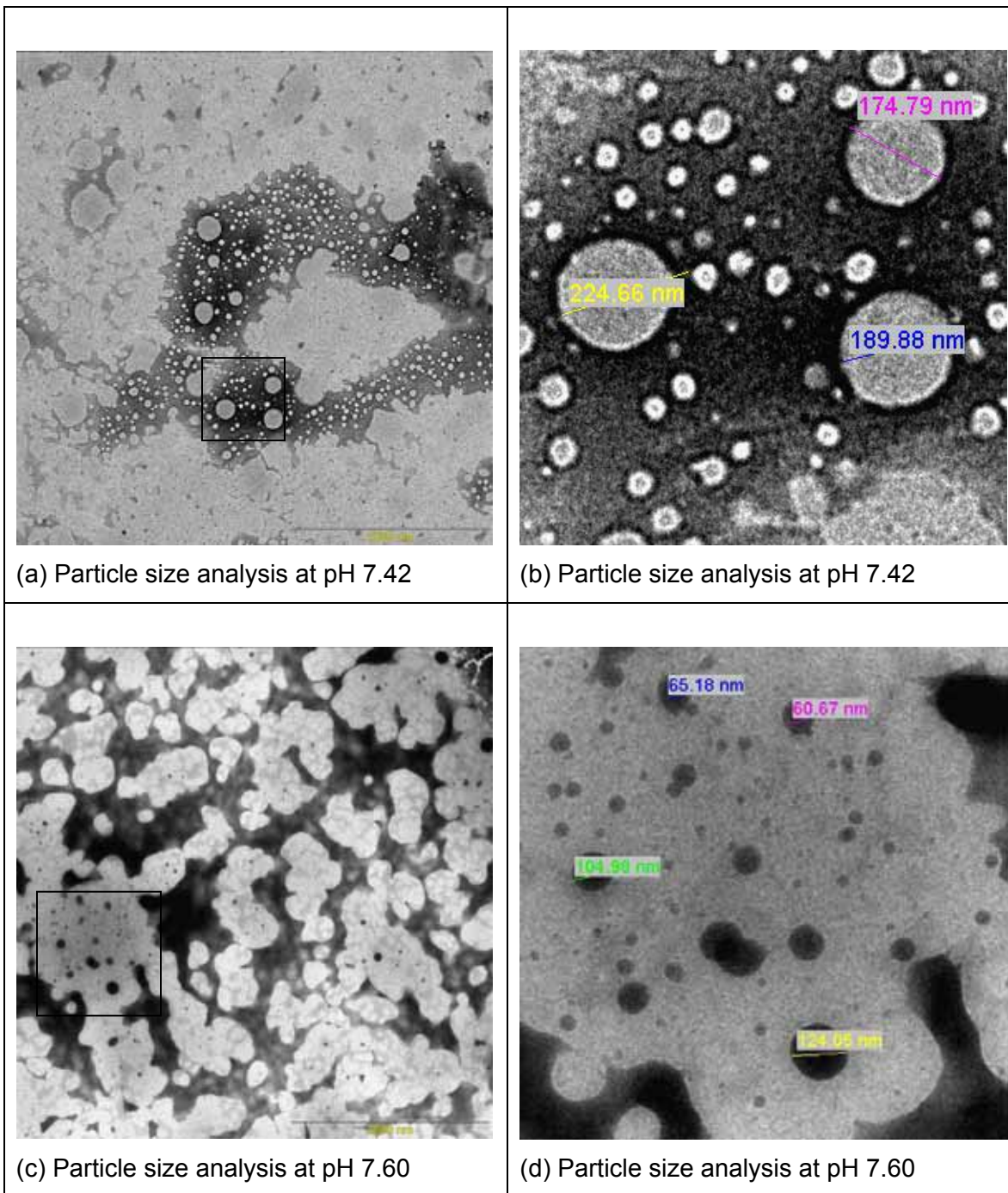


Figure A.7.11: Particle size analysis of PU dispersion as determined by TEM at pH 7.42 and pH 7.60 respectively

Appendix 8: Recyclability Evaluation

A. Methodology

Paper Pulping

Purpose: To break up the paperboard into a fine pulp.

Approximately 400 grams of paperboard is required for the current recyclability process used. The paperboard is shredded by hand and soaked in water before being pulped. It is then placed into a 25-liter container, half filled with water. An overhead stirrer, equipped with a shredder, is used to pulp the paperboard. A low speed setting is used for the initial 15 minutes, whereafter it is set at the high-speed setting and left for 30 minutes to pulp the paperboard. The quality of the paper pulp is tested by taking a small amount (spatula tip) of the pulp and dispersing it in a beaker of water. The completion of the pulping process is indicated by the absence of solid paperboard particles. Only the individual fibers should be visible.

Screening Test

Purpose: To separate the paper fibers from the coating and other additives.

A slit screening machine (a ±25-liter capacity cylinder with an interchangeable slit screen bottom) with 0.1 mm x 50 mm slits, is used to separate the fibers from other constituents in the coated paperboard. Constant water pressures in conjunction with a blender-type-mixing blade are used to ensure separation of the fibers by forcing the paper pulp fibers through the slits. The water is then guided through a sieve, with a mesh size smaller than the pulp fiber, in order to accumulate the raw fiber. The pulp fiber is collected and placed in a bag that allows water drainage. It is then put in an industrial spinning machine to get rid of excess water. The pulp fiber is later used in the making of the hand paper. The residue (everything too big to go through the slits) is then dried, weighed and expressed as a percentage waste solid to pulp fiber.

$$\% \text{ Waste Solid} = \frac{\text{Residue}}{\text{Fibre pulp}} \times 100$$

The consistency (solid content) of the fibers is then determined as follows:

- A small sample of the spin-dried fiber is placed in a glass beaker and weighed
- The beaker with fiber sample is placed in an oven to dry

$$\text{Consistency} = \frac{\text{Weight (after)}}{\text{Weight (before)}} \times 100$$

- After 48 hours the beaker is weighed again to determine the dry weight of the fiber
- The consistency of the fibers is required to accurately weigh off 42 g of fiber for the handpaper-making process.

Handpaper

42 g of fiber is required for the handpaper-making process. This is accurately weighed off by using the consistency as determined after the screening test.

$$\text{Sample weighed} = \frac{42}{\text{consistency}}$$

Dispersing the fibers

Purpose: To disperse fibers homogeneously in water.

Place the accurately weighed fiber sample into a 1-liter plastic beaker and add sufficient water to break up the fibers with a blender. Use an overhead blender to disintegrate the fibers and disperse it evenly. Place the contents of the beaker into a 20-liter container equipped with an overhead stirrer. Fill the container with 15-liters of water to obtain a 0.28% consistency of the fibers in the water.

Schopper-Riegler Test

Purpose: To determine the Schopper-Riegler (°SR) value of the dispersion

Method 1

Pour 1 litre of dispersed pulp into the Schopper-Riegler-Wert machine and allow the water to drain into the calibrated Schopper-Riegler measuring cylinder. Take the °SR reading from the top of the measuring cylinder. This value is an estimate of the °SR value and can now be verified by means of Method 2 below.

Method 2

The Schopper-Riegler-Wert machine is opened up and a disc with paperpulp is removed from it. The remaining water is pressed from it by first placing the paperpulp disc between two layers of cloth and placing it in a small press, followed by placing the paperpulp disc between two sheets of blotting paper and pressing it again between the press. The paperpulp with blotting paper is then placed on a hotplate to dry. The dry disc of paper is weighed and the weight compared to the Schopper-Riegler chart to determine the accurate °SR value.

Preparation of handpaper sheets

Ten sheets of handpaper are made to ensure a large enough sample for the testing of the paper afterwards. The procedure for the preparation is as follows:

- Cut 20 pieces of blotting paper (6" x 11.5") and wet them prior to making the handpaper, as each handpaper prepared must be covered on both sides with wet blotting paper
- Half fill the rectangular sheet-former with water (remembering to open the vacuum!)
- Pour 1 litre of dispersed pulp into the rectangular sheet-former
- Fill the rectangular sheet-former to the mark at the top
- Use the "mixer" to disperse the pulp further in the water (push it down twice)
- Turn the vacuum on and wait for the water to drain completely from the rectangular sheet former
- Lift the top part of the sheet-former and remove the base (which contains the pulp)
- Remove the handpaper from the base by placing a wet sheet of blotting paper onto the paperpulp, followed by five dry sheets of blotting paper

- Roll a heavy roller across the surface of the handpaper (once forward and once backward), to remove excess water
- Remove the dry blotting paper
- Carefully lift the wet blotting paper with the wet paperpulp from the base of the rectangular sheet former
- Place another wet sheet of blotting paper on top, thereby covering the paperpulp between two pieces of blotting paper. This is to ensure that the two sides of the paper exhibit the same physical properties. If this is not done, 2-sided paper is obtained.
- Place the wet handpaper on a hotplate to dry

Tests

The handpaper thus made is used to determine its characteristics, and to determine the effectiveness of the recycling process. The characteristics are calculated by means of the equations summarized below.

Grammage	$\text{Grammage (g/m}^2\text{)} = \frac{\text{Average weight (g)} \times 10\,000}{\text{Area (cm}^2\text{)} \times \text{No. of sheets}}$
Drainage	The drainage is determined during the handpaper making process.
Burst Strength	$\text{Burst Index (kPa.m}^2\text{/g)} = \frac{\text{Bursting Strength (kPa)}}{\text{Grammage (g/m}^2\text{)}}$
Tear Strength	$\text{Tearing Resistance (mN)} = \frac{\text{Average} \times 16 \times 9.807}{\text{No. of sheets}}$ $\text{Tear Index (mN.m}^2\text{/g)} = \frac{\text{Tearing Resistance (mN)}}{\text{Grammage (g/m}^2\text{)}}$
Tensile Strength	$\text{Tensile Strength (kN/m)} = \frac{\text{Graph reading from Instron (N)}}{\text{Width of strip (mm)}}$ $\text{Breaking Length (km)} = \frac{\text{Tensile Strength (kN/m)} \times 102}{\text{Grammage (g/m}^2\text{)}}$

The recyclability tests on the urethane-coated paperboard were done by the Forestry Department, University of Stellenbosch. The recyclability of coated paperboard, with a coating consisting of: synthesized polyurethane, wax 5, mica and amazon clay, was evaluated against the recyclability of uncoated paperboard. The purpose was to determine whether the coated paperboard would be recyclable.

B. Experimental Recyclability Evaluation

Sample 1: Uncoated paperboard; Sample 2: Coated paperboard (Blank)

Paper tests	Drainage	Tear Index
	Tensile strength	Grammage
	Tearing resistance	Breaking length
	Burst strength and burst Index	

400 grams of each sample were prepared for the recyclability tests. After the recycling process, the paper pulp was used to make handpaper. These sheets were used for a series of tests to determine whether the handpaper made from paper pulp from the coated paperboard displayed different characteristics to those of the blank sample.

Results and Discussion

The results are summarized in the Table A.8.1 below.

Table A.8.1: Recyclability test results

Test	Units	Sample 1	Sample 2
Grammage	g/m ²	81.36	78.24
Burst Strength	kPa	110.88	91.38
Burst Index	kPa.m ² /g	1.36	1.17
Tearing Resistance	mN	592.78	519.55
Tear Index	mN.m ² /g	7.29	6.64
Tensile Strength	kN/m	3.55	3.20
Breaking Length	km	4.45	4.17

These results indicate that the coated paperboard, sample 2, exhibited characteristics very similar to those of the blank sample, sample 1. The composite evaluated therefore did not significantly influence the recyclability of the paperboard.

Appendix 9: NMR spectra of polyester and polyurethane

Additional ^1H , ^{13}C , and ^{13}C Apt-NMR spectra of the polyester and polyurethane are shown in Figures A.9.1 to A.9.3.

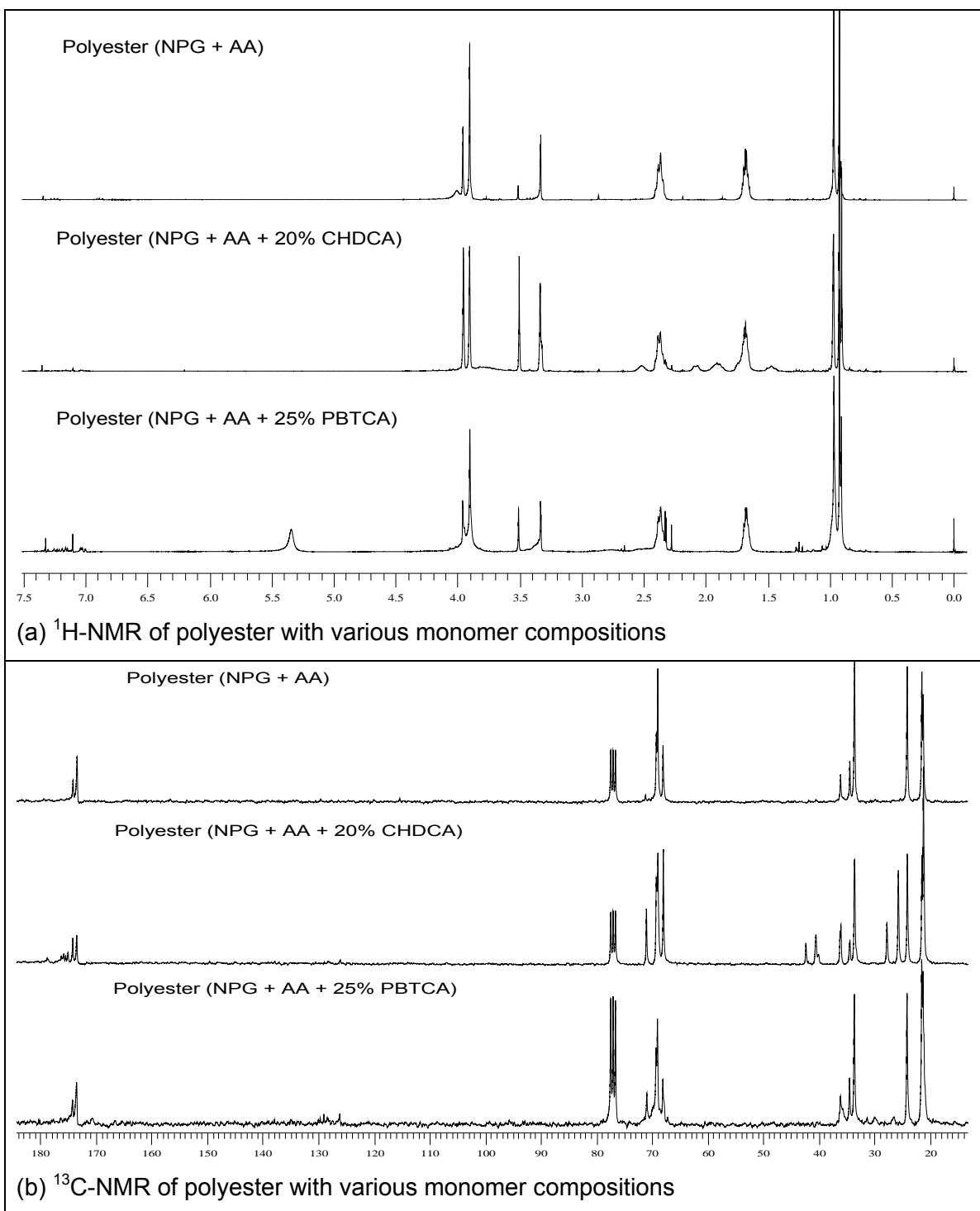


Figure A.9.1: ^1H and ^{13}C -NMR spectra of polyesters with various monomer compositions

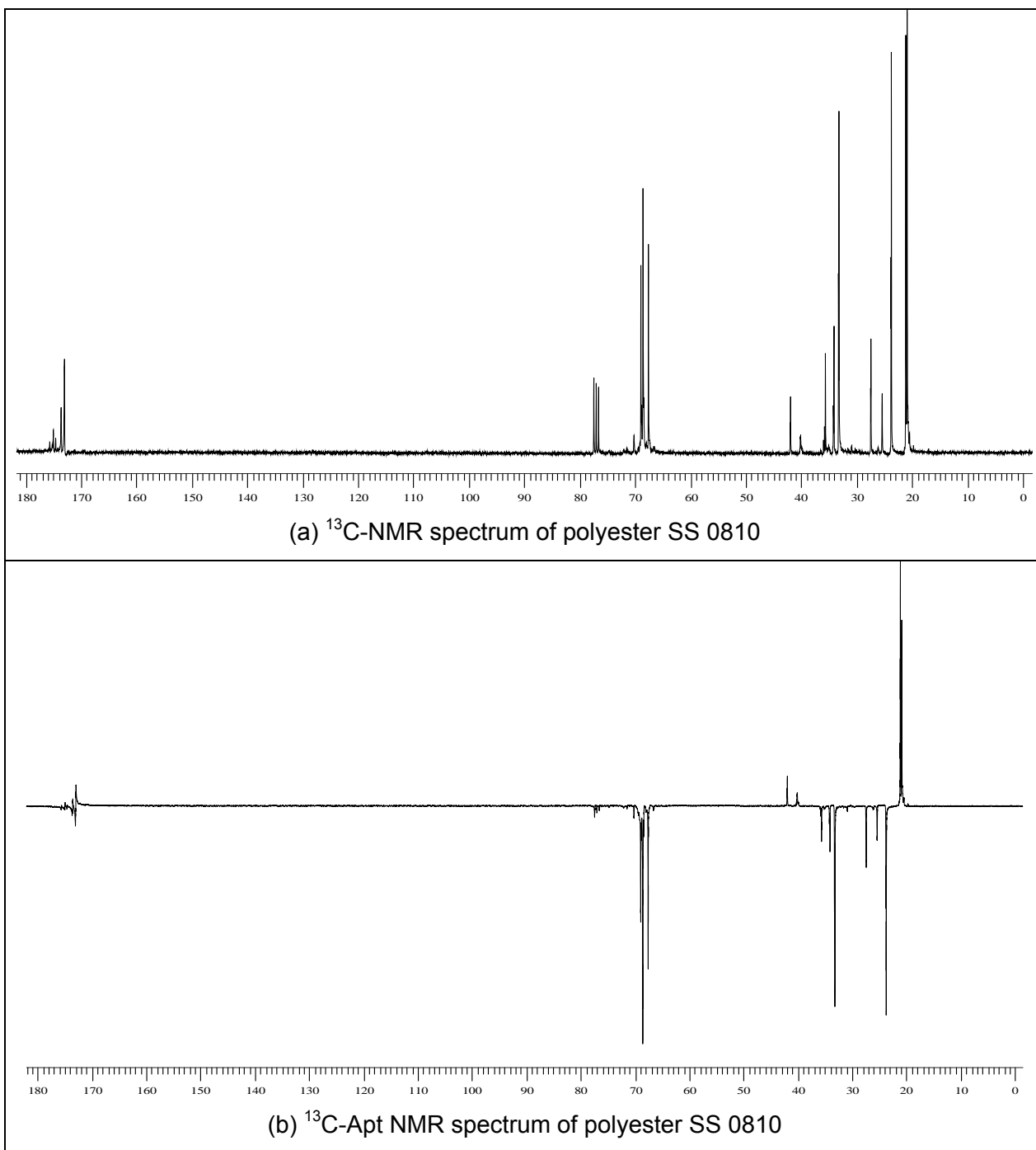
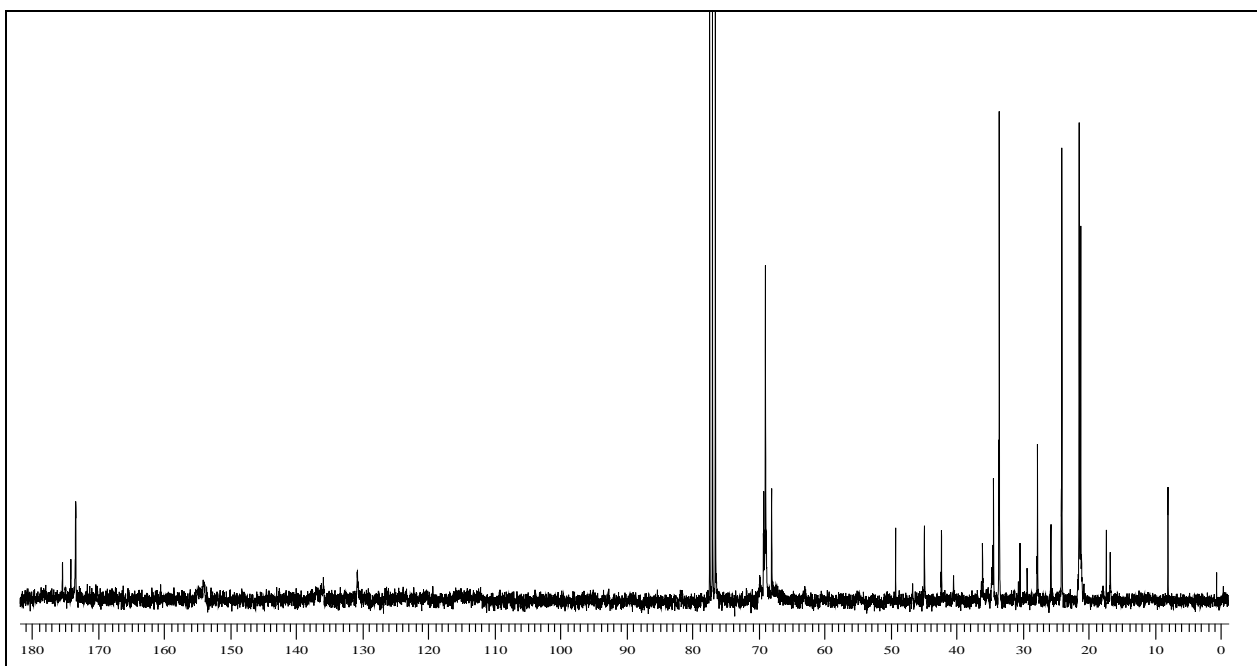
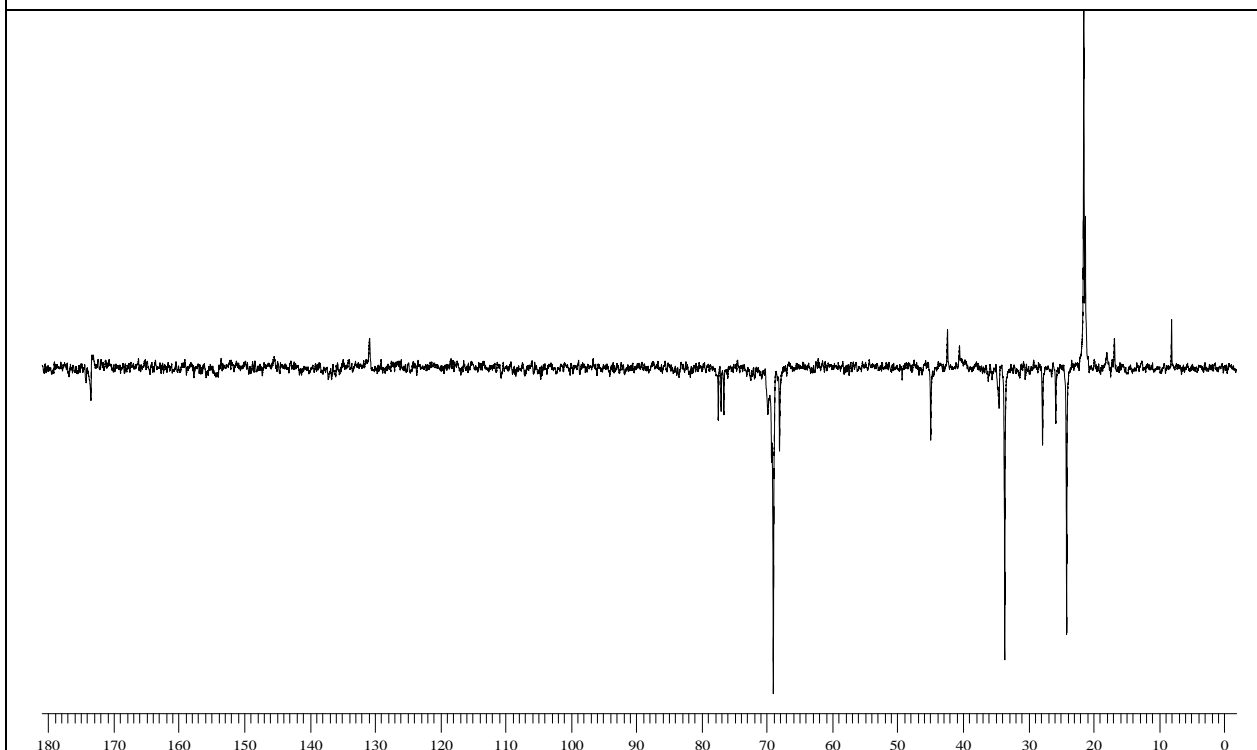


Figure A.9.2: ^{13}C and ^{13}C -Apt NMR spectra of polyester SS 0810

The ^{13}C -Apt NMR spectrum in Figure A.9.2 (b) presents uneven amount of protons on the carbon above the line, and the even amount of protons on the carbon below the line, so simplifying the interpretation of the carbon structures in Figure A.9.2 (a).



(a) ^{13}C -NMR spectrum of polyurethane (synthesized from polyester SS 0810)



(b) ^{13}C -Apt NMR spectrum of polyurethane (synthesized from polyester SS 0810)

Figure A.9.3: ^{13}C and ^{13}C -Apt NMR spectra of polyurethane (synthesized from polyester SS 0810)